HYDROLYTIC AND ASSOCIATED REACTIONS IN MOLTEN ZINC CHLORIDE-SODIUM CHLORIDE

BY

HUGH GAVIN CHARLES HAMILTON

A thesis submitted for the degree of Doctor of Philosophy of the University of London, and for the Diploma of Imperial College.

Department of Materials,
Royal School of Mines,
Imperial College of Science,
Technology and Medicine,
London.

JUNE 1989

ABSTRACT

The behaviour of hydrogen- and oxygen-containing compounds dissolved in molten mixtures of $ZnCl_2$-NaCl has been studied, with the aim of determining the species present in the melts which may be responsible for the catalytic nature of $ZnCl_2$ towards the hydrocracking of polynuclear hydrocarbons.

The extent to which the solubility of HCl gas in $ZnCl_2$-NaCl melts is dependent on temperature and melt composition was determined by an elution method. A chemical dissolution process was inferred, and a series of equilibria postulated for the behaviour of HCl within the melts. Cyclic voltammetric studies of HCl-saturated melts, using platinum electrodes, combined with the solubility results, yielded diffusion coefficients for the dissolved species. The Stokes-Einstein equation was obeyed in the acidic melts. A changeover from $H^+ZnCl_3^-$ to HCl_2^- in the species predominantly formed, with increasing melt basicity, accounts for the trends observed.

The individual dissolution of HCl and water in the $ZnCl_2$-NaCl melts resulted in opposing changes in the electrical conductivities of the melts. Using the a.c. impedance (F.R.A.) technique, HCl was found to cause a decrease in the melt conductivity, in contrast to water, with the effect strongest in the most acidic melts. It has been suggested that protons, formed by the dissociation of the HCl, act as bridging agents between the Zn-Cl entities.

Despite being unable to determine the solubility of water in the melts, the hydrolysis reaction was shown to occur to some extent, with the resultant hydroxide ions characterised by use of cyclic voltammetry. Comparison with voltammetric responses obtained for NaOH dissolved in the same melts confirmed that hydroxide ions undergo a single electron reduction which, in some cases, resulted in the formation of a ZnO layer on the electrode surface. Other voltammetric responses obtained upon dissolution of water in the melts could not be definitively identified, but it has been suggested that they arise from the reduction of water and the

oxide/oxygen couple, or are a result of peroxide formation.

A Raman spectroscopic investigation of quenched samples of $ZnCl_2$ saturated with either water, HCl or O_2, demonstrated the stabilising effect of the solutes on the amorphous form of the solvent, but was unable to confirm the presence of hydroxychloro- or oxychlorozincate species. The dissolution of O_2 in the melts resulted in an amber colouration which persisted faintly in the solid and resulted in a fluorescence response in the Raman spectrum. An e.s.r. spectrum exhibited one sharp response ($g = 2.008$) for the same sample, and it was concluded that the dissolution of O_2 results in superoxide ion formation. Voltammetric results for the individual dissolution of O_2 and Na_2O_2 indicated that a superoxide-peroxide-oxide ion equilibrium may occur within the melt systems.

Addition of NaOH to the melts resulted in the formation of a white precipitate. Quenching of the melts and removal of the $ZnCl_2$ left a solid identified as a mixture of NaCl, ZnO and $Zn_5(OH)_8Cl_2$. The hydroxychlorozincate was also isolated following saturation of the melts with water vapour, although no precipitation occurred. ZnO was found to be virtually insoluble in the $ZnCl_2$-NaCl melts, becoming yellow due to its non-stoichiometry at high temperatures. The addition of Na_2CO_3 to try to increase the oxide ion concentration merely resulted in the precipitation of ZnO as CO_2 was evolved.

ACKNOWLEDGEMENTS

I would like to thank my supervisor, Professor Douglas Inman, for his help and encouragement throughout the duration of this work, and for being so patient. I would also like to thank the members, past and present, of his research group; Dr. Nick Carthey, Ruth Wheeldon, Bhakti Thakur, Dr. Elzbieta Krasicka-Cydzik, Professor Duan, Professor Gu, Professor Qiao, Mr. Wu and Andrea Walker, his able secretary, for their friendship and help over the three years, and Bernard Henry and Jean Li Kan Tim for entertaining us through the long hot summers! My warmest thanks to all my colleagues and friends in the Nuffield Research Group who made me so welcome and who were always ready to help if problems arose.

Without technical help from the following people this work would have been immeasurably harder: Gordon Hicks (Glassblowing), Tim Mellor, Jim Wright, John Tipple and Richard Sweeney (X-ray diffraction) - thanks lads!! And to Mrs. S. Inada-Kim for taking such good care of me "Domo arigato gozaimashita". Without the typing skills of Jenny Bowring and Gill Hopkins I might still be bashing out my transfer report with one sore finger, so I am most grateful for their kind assistance.

The Raman and E.S.R. spectroscopic results were obtained with the help of Dr. W.P. Griffith, W. Ali and Dr. J.F. Gibson of the Department of Chemistry, Imperial College.

However, it hasn't been **all** work. I apologise to all the players in the W.U.S.S.I./Nuffield/R.D.R./Mining football squad who received my "personal touch" on the pitch, but who would still come out to play, regardless of conditions. Thanks for the games, boys - it was a pleasure to play with you all. My apologies also go to the ladies of I.C. Dance Club who received flattened toes over the years during my clumsy attempts at dancing. Thanks to all the members of the Dance Club, especially to Christine Norman and Shuko Noguchi, for making the classes so entertaining and enjoyable. Sadly, it is not

possible to individually mention all the people in the department and around the college who have been such good friends, but they are not forgotten.

I also wish to thank Pippa Stokes, Margaret Chapman and Desmond Eadon for their help with the proof-reading.

Last, but by no means least, I thank B.P./S.E.R.C. for providing the finance for the project and Dr. Keith Holder, my industrial supervisor, for his helpful discussions and interest.

CONTENTS

		Page
Abstract		*i*
Acknowledgements		*iii*
Contents		v
List of Figures		x
List of Tables		xv
CHAPTER 1	**INTRODUCTION**	1
1.1	Uses of Zinc Chloride Melts	2
1.2	Acidity - Basicity in Molten Salts	4
1.3	Complex Ions in Molten Salts	6
CHAPTER 2	**LITERATURE SURVEY**	7
2.1	Structure of Zinc Chloride and $ZnCl_2$-MCl Melts	7
2.2	Transport and Physico-Chemical Properties	12
2.2.1	Density	12
2.2.2	Electrical Conductivity	14
2.2.3	Viscosity	18
2.2.4	Vapour Pressure	18
2.2.5	Phase Diagrams	19
2.3	Solubility of Gases in Molten Salts	19
2.3.1	Solubility of HCl Gas in Chloride Melts	23
2.3.2	Solubility of H_2O in Chloride Melts	26
2.4	I.R. Spectroscopy of HCl and H_2O in Chloride Melts	27
2.5	Electrochemical Studies of HCl in Chloride Melts	28
2.6	Water in Chloride Melts	30
2.6.1	Electrochemical Studies of H_2O in Chloride Melts	31
2.7	Electrochemical Studies in Zinc Chloride Melts	34
2.8	Solute Studies in Zinc Chloride Melts	37
CHAPTER 3	**EXPERIMENTAL**	42
3.1	Melt Purification	42
3.2	Furnace and Temperature Control	44
3.3	Vacuum and Gas Supply System	45

			Page
CHAPTER 3	EXPERIMENTAL (continued ...)		
	3.4	Electrodes	45
	3.4.1	Platinum Electrodes	45
	3.4.2.	Tungsten Electrode	46
	3.4.3	Vitreous Carbon Electrode	46
	3.4.4	Graphite Electrode	47
	3.4.5	Silver/Silver Chloride Electrode	47
	3.4.6	Gold Electrode	50
	3.5	Electrochemical Cell	50
	3.6	Cyclic Voltammetry	52
	3.7	Solubility of HCl Gas in $ZnCl_2$-NaCl Melts	54
	3.8	Solubility of Oxy-Species in $ZnCl_2$-NaCl Melts	56
	3.9	Water Vapour Equilibration	58
	3.10	X-ray Diffraction	60
	3.11	Raman Spectroscopy	60
	3.12	Infra-red Spectroscopy	60
	3.13	Electron Spin Resonance Spectroscopy	61
	3.14	Atomic Absorption Spectrophotometry	61
	3.15	D.T.A./T.G.A. Analysis	61
	3.16	A.C. Impedance Spectroscopy	62
	3.17	Materials	63
CHAPTER 4	PURIFICATION OF $ZnCl_2$ MELTS		64
	4.1	Introduction	64
	4.2	Appearance of $ZnCl_2$ Melts	66
	4.3	Water Absorption Studies	68
	4.4	Voltammetric Investigation of Unpurified and Pure Melts	70
	4.4.1	Reference Electrodes	70
	4.4.2	Counter Electrode	71
	4.4.3	Working Electrodes	71
	4.4.3.1	Platinum Electrode	71
	4.4.3.2	Tungsten Electrode	74
	4.4.3.3	Vitreous Carbon Electrode	78
	4.4.3.4	Gold Electrode	78

(continued ...)

			Page
CHAPTER 5	BEHAVIOUR OF HCl IN $ZnCl_2$-NaCl MELTS		82
	5.1	Solubility of HCl in Molten $ZnCl_2$-NaCl	82
	5.2	Voltammetric Study of HCl in $ZnCl_2$-NaCl Melts	95
	5.2.1	Behaviour of the Platinum Quasi-Reference Electrode	97
	5.2.2	Reduction of HCl in $ZnCl_2$-NaCl Melts	99
	5.2.3	Diffusion Coefficients of HCl in $ZnCl_2$-NaCl Melts	128
	5.2.4	Stokes-Einstein Behaviour of HCl in $ZnCl_2$-NaCl Melts	132
	5.2.5	Possible Alloy Formation Between Zinc and Platinum	137
CHAPTER 6	ELECTRICAL CONDUCTIVITY OF $ZnCl_2$-NaCl MELTS CONTAINING HCl and H_2O		141
	6.1	Introduction	141
	6.2	The A.C. Impedance Technique	141
	6.3	Measurement of the Cell Constant	146
	6.4	Conductivity of $ZnCl_2$-NaCl Melts Containing HCl and H_2O	146
	6.5	Double Layer Capacitances Measured by A.C. Impedance	152
CHAPTER 7	BEHAVIOUR OF H_2O in $ZnCl_2$-NaCl MELTS		155
	7.1	Introduction	155
	7.2	Solubility of H_2O in $ZnCl_2$-NaCl Melts	156
	7.3	Extent of the Hydrolysis Reaction in $ZnCl_2$-NaCl Melts	157
	7.4	Voltammetric Study of H_2O in $ZnCl_2$-NaCl Melts	159
CHAPTER 8	SPECTROSCOPIC INVESTIGATION OF $ZnCl_2$ CONTAINING PROTONIC AND OXY-SPECIES		185
	8.1	Introduction	185
	8.2	Raman Spectrum of Pure $ZnCl_2$	185
	8.3	Raman Spectrum of $ZnCl_2$ Containing HCl	187
	8.4	Raman Spectrum of $ZnCl_2$ Containing H_2O	189
	8.5	Raman Spectrum of the Ar/H_2O Bubbler Deposit	191
	8.6	Raman Spectrum of $ZnCl_2$ Containing O_2	196
	8.7	Electron Spin Resonance Spectrum of $ZnCl_2$ Containing O_2	200

			Page
CHAPTER 9	BEHAVIOUR OF OXY-SPECIES IN $ZnCl_2$-NACl MELTS		203
	9.1	Behaviour of NaOH in $ZnCl_2$-NaCl Melts	203
	9.2	Behaviour of ZnO in $ZnCl_2$-NaCl Melts	213
	9.3	Behaviour of Oxygen in $ZnCl_2$-NaCl Melts	218
	9.4	Behaviour of Na_2O_2 in $ZnCl_2$-NaCl Melts	224
	9.5	Behaviour of Na_2CO_3 in $ZnCl_2$-NaCl Melts	231
CHAPTER 10	CONCLUSIONS		233
	Suggestions for Further Work		237
	REFERENCES		238
APPENDIX 1	METAL HALIDES IN THE HYDROCRACKING PROCESS		248
	A1.1	General	248
	A1.2	Zinc Chloride Hydrocracking Process	249
	A1.3	Process Chemistry	249
	A1.4	Structure of the Active Catalyst and Mechanistic Considerations	251
	A1.5	Effect of Addition of Transition Metal and Alkali Metal Chlorides to Zinc Chloride	253
	A1.5.1	Zinc Chloride - Alkali Metal Chloride ($ZnCl_2$-MCl) Catalysts	255
	A1.5.2	Zinc Chloride - Transition Metal Chloride ($ZnCl_2$-ACl_n) Catalysts	256
	REFERENCES		257

LIST OF FIGURES

		Page
Figure 2.1	The Structure of Crystalline Zinc Chloride	8
Figure 2.2	Liquid Structure Models of Zinc Chloride (Takagi and Nakamura, ref. 30)	11
Figure 2.3	Variation of the Density of Zinc Chloride with Temperature	13
Figure 2.4	Electrical Conductivity Isotherms for $ZnCl_2$-KCl (ref. 41)	15
Figure 2.5	Electrical Conductivity Isotherms for $CdCl_2$-KCl (ref. 204)	16
Figure 2.6	Electrical Conductivity Isotherms for $AlCl_3$-KCl (ref. 204)	17
Figure 2.7	Phase Diagram of $ZnCl_2$-LiCl (a) ref. 56 (b) Perry et al. ref. 58	20
Figure 2.8	Phase Diagram of $ZnCl_2$-NaCl	21
Figure 2.9	Phase Diagram of $ZnCl_2$-KCl	21
Figure 2.10	Phase Diagram of $ZnCl_2$-RbCl	22
Figure 2.11	Phase Diagram of $ZnCl_2$-CsCl	22
Figure 3.1	Melt Purification Apparatus	43
Figure 3.2	Electrodes	48
Figure 3.2.1	Platinum	48
Figure 3.2.2	Tungsten	48
Figure 3.2.3	Vitreous Carbon	48
Figure 3.2.4	Graphite	49
Figure 3.2.5	Ag/AgCl	49
Figure 3.2.6	Gold	49
Figure 3.3	Electrochemical Cell	51
Figure 3.4	Cyclic Voltammetry - Excitation and Response for the Reversible Deposition of a Soluble Product	53
Figure 3.5	Diagrammatic Representation of the Cyclic Sweep Circuit	53

		Page
Figure 3.6	Apparatus Used for the HCl Solubility Determination	55
Figure 3.7	Filtration Unit in the Electrochemical Cell	57
Figure 4.1	Water Absorption by $ZnCl_2$, Pure and Impure, and by 50 mol. % $ZnCl_2$-NaCl at Room Temperature	69
Figure 4.2	Typical Voltammogram Obtained With a Platinum Electrode in Impure 80 mol. % $ZnCl_2$-NaCl	72
Figure 4.3	Typical Voltammogram Obtained With a Platinum Electrode in Pure 80 mol. % $ZnCl_2$-NaCl	73
Figure 4.4	Typical Voltammogram Obtained With a Tungsten Electrode in Impure 80 mol. % $ZnCl_2$-NaCl	75
Figure 4.5	Typical Voltammogram Obtained With Tungsten Electrode in Pure 80 mol. % $ZnCl_2$-NaCl	76
Figure 4.6	Alloying Peaks on a Voltammogram Obtained With a Tungsten Electrode in Pure 80 mol. % $ZnCl_2$-NaCl	77
Figure 4.7	Typical Voltammogram Obtained With a Vitreous Carbon Electrode for Pure and Impure 80 mol. % $ZnCl_2$-NaCl	79
Figure 4.8	Typical Voltammogram Obtained With a Gold Electrode in Pure 80 mol. % $ZnCl_2$-NaCl	80
Figure 5.1	Solubility of HCl gas in $ZnCl_2$-NaCl Molten Mixtures	84
Figure 5.2	Solubility Isotherms of HCl gas in $ZnCl_2$-NaCl Molten Mixtures	88
Figure 5.3	Arrhenius Plot for HCl Solubility in $ZnCl_2$-NaCl Molten Mixtures	90
Figure 5.4	Equilibria Postulated to Exist in Solutions of HCl in Zinc Chloride Melts	94
Figure 5.5	Potential (E = F(t)) Between Pt and Ag/AgCl Electrodes in HCl-saturated 50 mol. % $ZnCl_2$-NaCl at 372°C	98
Figure 5.6	Voltammograms for the Reduction of HCl in 60 mol. % $ZnCl_2$-NaCl	100
Figure 5.7	Variation of i^I_{ads} With Scan Rate	107
Figure 5.8	Variation of the Peak Potential With Scan Rate for the Reduction of HCl in 80 mol. % $ZnCl_2$-NaCl	122

		Page
Figure 5.9	Variation of i_p With $\nu^{\frac{1}{2}}$ for the Reduction of HCl in 80 mol. % $ZnCl_2$-NaCl	124
Figure 5.10	"Corrected" Plot of i_p against $\nu^{\frac{1}{2}}$ for the Reduction of HCl in 70 mol. % $ZnCl_2$-NaCl	125
Figure 5.11	Variation of the Current Ratio With Scan Rate for Reduction of HCl in 60 mol. % $ZnCl_2$-NaCl	127
Figure 5.12	Arrhenius Plot for D_{HCl} in $ZnCl_2$-NaCl Melts	133
Figure 5.13	Voltammograms Showing Possible Zn-Pt Alloy Formation for 80 mol. % $ZnCl_2$-NaCl (317°C)	138
Figure 6.1	Complex Plane Impedance Spectra With Their Associated Equivalent Circuits	143
Figure 6.2	Randles - Type Equivalent Circuit and Response	144
Figure 6.3	Modified Equivalent Circuit Incorporating the Warburg Impedance Component	144
Figure 6.4	Complex Plane Impedance Spectra for 80 mol. % $ZnCl_2$-NaCl (357°C)	147
Figure 6.5	Complex Plane Impedance Spectra for Molten $ZnCl_2$+H_2O (355°C) Showing the Effect of Varying the A.C. Amplitude	149
Figure 6.6	Conductivities of $ZnCl_2$-NaCl Melts (620-640 K)	153
Figure 7.1	Voltammogram for Water in Pure Molten Zinc Chloride	160
Figure 7.2	Voltammogram Showing the Effect of Three Successive Scans for Water in Molten Zinc Chloride	165
Figure 7.3	Voltammogram Recorded at a Low Scan Rate for Water in Molten Zinc Chloride	166
Figure 7.4	Variation of i_p^I with $\nu^{\frac{1}{2}}$ for Water in Zinc Chloride	167
Figure 7.5	(a) Variation of i_p with $\nu^{\frac{1}{2}}$ for Peaks III and IV for Water in Zinc Chloride (Initial Scan)	169
	(b) Variation of i_p^{IV} with $\nu^{\frac{1}{2}}$ for Water in Zinc Chloride (Subsequent Scans)	170
Figure 7.6	Variation of i_p With $\nu^{\frac{1}{2}}$ for Peaks V and VI for Water in Zinc Chloride	171
Figure 7.7	Voltammogram Showing the Effect of Holding the Scan at Peak I for 30 Seconds	172

		Page
Figure 7.8	Voltammogram Obtained for Water in 80 mol. % $ZnCl_2$-NaCl	173
Figure 7.9	Variation of i_p^I with $\nu^{\frac{1}{2}}$ for Water in 80 mol. % $ZnCl_2$-NaCl	179
Figure 7.10	Variation of Peak I With Water Vapour Pressure for 80 mol. % $ZnCl_2$-NaCl	180
Figure 8.1	Raman Spectrum of Pure Zinc Chloride	186
Figure 8.2	Raman Spectrum of $ZnCl_2$ Containing HCl	188
Figure 8.3	Raman Spectrum of $ZnCl_2$ Containing H_2O - 20 Minutes Grinding	190
Figure 8.4	Raman Spectrum of $ZnCl_2$ Containing H_2O - 5 Minutes Grinding	192
Figure 8.5	Raman Spectrum of the Ar/H_2O Bubbler Deposit	193
Figure 8.6	Raman Spectrum of $ZnCl_2$ Containing O_2	197
Figure 8.7	E.s.r. Spectrum of $ZnCl_2$ Containing O_2	201
Figure 9.1	Voltammogram Obtained for NaOH in 80 mol. % $ZnCl_2$-NaCl	205
Figure 9.2	Voltammograms Showing Prepeaks Obtained for NaOH in 80 mol. % $ZnCl_2$-NaCl	205
Figure 9.3	I.R. Spectrum of NaCl-ZnO-$Zn_5(OH)_8Cl_2$ Mixture (as a Nujol Mull)	209
Figure 9.4	Thermogram for NaCl-ZnO-$Zn_5(OH)_8Cl_2$ Mixture	213
Figure 9.5	Temperature - Dependent Weight Loss of NaCl-ZnO-$Zn_5(OH)_8Cl_2$ Mixture	214
Figure 9.6	Voltammogram Obtained for ZnO in 80 mol. % $ZnCl_2$-NaCl	217
Figure 9.7	Voltammograms Obtained for O_2 in 80 mol. % $ZnCl_2$-NaCl (a) Scan rate > 10 mVs^{-1} (b) Scan rate < 10 mVs^{-1}	 219 210
Figure 9.8	Variation of i_p With $\nu^{\frac{1}{2}}$ for O_2 in 80 mol. % $ZnCl_2$-NaCl	223
Figure 9.9	Voltammogram Obtained for Na_2O_2 in 80 mol. % $ZnCl_2$-NaCl Immediately After Solute Addition	226
Figure 9.10	Voltammograms Obtained for Na_2O_2 in 80 mol. % $ZnCl_2$-NaCl Three Minutes After Solute Addition	226

		Page
Figure 9.11	Variation of i_p with $\nu^{\frac{1}{2}}$ for Na_2O_2 in 80 mol. % $ZnCl_2$-NaCl	229
Appendix 1		
A1.1	Conversion of n-butyl Benzene	254

LIST OF TABLES

		Page
TABLE 2.1	Solubilities of HCl in LiCl-KCl eutectic	24
TABLE 2.2	Solubilities of zinc metal in molten zinc chloride	35
TABLE 3.1	Water Vapour Pressures of Saturated Solutions of Various Salts	59
TABLE 3.2	Materials and Chemicals Used	63
TABLE 5.1	Solubility of HCl gas in $ZnCl_2$ Melts	87
TABLE 5.2	Heats of Solution for the Dissolution of HCl Gas in Various Molten Chlorides	92
TABLE 5.3	Voltammetric Parameters for the Hydrogen Adsorption Peaks (I, IV) in Pure $ZnCl_2$	102
TABLE 5.4	Voltammetric Parameters for the Hydrogen Adsorption Peaks (I, IV) in 80 mol. % $ZnCl_2$-NaCl	103
TABLE 5.5	Voltammetric Parameters for the Hydrogen Adsorption Peaks (I, IV) in 70 mol. % $ZnCl_2$-NaCl	104
TABLE 5.6	Voltammetric Parameters for the Hydrogen Adsorption Peaks (I, IV) in 60 mol. % $ZnCl_2$-NaCl	105
TABLE 5.7	Voltammetric Parameters for the Hydrogen Adsorption Peaks (I, IV) in 50 mol. % $ZnCl_2$-NaCl	106
TABLE 5.8	Voltammetric Parameters for the Diffusion-Controlled Reduction of HCl in Pure $ZnCl_2$	112
TABLE 5.9	Voltammetric Parameters for the Diffusion-Controlled Reduction of HCl in 90 mol. % $ZnCl_2$-NaCl	113
TABLE 5.10	Voltammetric Parameters for the Diffusion-Controlled Reduction of HCl in 80 mol. % $ZnCl_2$-NaCl	114
TABLE 5.11	Voltammetric Parameters for the Diffusion-Controlled Reduction of HCl in 70 mol. % $ZnCl_2$-NaCl	116
TABLE 5.12	Voltammetric Parameters for the Diffusion-Controlled Reduction of HCl in 60 mol. % $ZnCl_2$-NaCl	118
TABLE 5.13	Voltammetric Parameters for the Diffusion-Controlled Reduction of HCl in 50 mol. % $ZnCl_2$-NaCl	120
TABLE 5.14	Calculated Rate Constants for the Reaction Following the Reduction of HCl in $ZnCl_2$-NaCl Melts	129

		Page
TABLE 5.15	Diffusion Coefficients of HCl in $ZnCl_2$-NaCl Melts	131
TABLE 5.16	Activation Energies of the Diffusion Processes Present in Solutions of HCl in $ZnCl_2$-NaCl Melts	134
TABLE 5.17	Stokes-Einstein Radii of the Diffusing Species Present in Solutions of HCl in $ZnCl_2$-NaCl Melts	136
TABLE 6.1	Specific Conductivities of $ZnCl_2$-NaCl Melts Containing HCl and H_2O and of the Pure Melts	150
TABLE 7.1	Evolution of HCl by Addition of Water to Pure Molten Zinc Chloride	158
TABLE 7.2	Voltammetric Parameters of Peaks I and II for H_2O (v.p. = 19.8 torr) in Zinc Chloride	162
TABLE 7.3	Voltammetric Parameters of Peaks III and IV for H_2O (v.p. = 19.8 torr) in Zinc Chloride: (a) Initial Scan, (b) Subsequent Scans	163
TABLE 7.4	Voltammetric Parameters of Peaks V and VI for H_2O (v.p. = 19.8 torr) in Zinc Chloride	164
TABLE 7.5	Voltammetric Parameters of Peaks I and II for H_2O (v.p. = 19.1 torr) in 80 mol. % $ZnCl_2$-NaCl	175
TABLE 7.6	Voltammetric Parameters of Peaks I and II for H_2O (v.p. = 12.35 torr) in 80 mol. % $ZnCl_2$-NaCl	176
TABLE 7.7	Voltammetric Parameters of Peaks I and Ii for H_2O (v.p. = 7.84 torr) in 80 mol. % $ZnCl_2$-NaCl	177
TABLE 7.8	Voltammetric Parameters of Peak I for H_2O (v.p. = 2.61 torr) in 80 mol. % $ZnCl_2$-NaCl	178
TABLE 8.1	Peak Assignments for the Raman Spectrum of the Deposit Formed in the Ar/H_2O Bubbler	195
TABLE 9.1	Assignment and d-spacings of X-ray diffraction pattern for the precipitate from NaOH in 80 mol. % $ZnCl_2$-NaCl at 330°C	207
TABLE 9.2	Hydroxy- and Oxychlorides of Zinc	210

		Page
TABLE 9.3	Voltammetric Parameters for O_2 in 80 mol. % $ZnCl_2$-NaCl	222
TABLE 9.4	Voltammetric Parameters for Na_2O_2 in 80 mol. % $ZnCl_2$-NaCl	228

CHAPTER ONE

INTRODUCTION

The discovery that zinc chloride is a catalytic promoter of the hydrocracking of polynuclear hydrocarbons and has a good heteroatom removal capacity has led to a great deal of work being carried out to improve the process. Attempts to determine the mechanism of the process have centred around the use of organic compounds as models for the coal/oil. It is known that the presence of a small amount of water is necessary for the catalytic process to start, and since the zinc chloride used for the cracking experiments is rarely dried and purified, the necessary water is usually found in the salt as it comes from the suppliers. The species responsible for the catalysis is thought to be a complex formed by interaction of the zinc chloride with the water e.g. $H^+[ZnCl_2\ OH]^-$. Little work has been carried out on the behaviour of protonic or oxide species in purified zinc chloride melts to see if such a species might exist.

In the solid state, zinc chloride has a network structure which is maintained to a large extent in the molten state, leading to its high viscosity and low conductivity. This structure may be broken up to form complexes, such as $ZnCl_4^{2-}$, by increasing the temperature or by the addition of alkali metal chlorides which will donate Cl^- ions to the network. The alkali metal chlorides may be thought of as Lewis bases interacting with the acidic zinc chloride to form a binary mixture of lower Lewis acidity. Cl^- ion donation by the alkali metal chlorides increases with the heavier metal cations, since their polarizing power is lower than that of the lighter cations. Additions of MCl to $ZnCl_2$ makes the resultant melts easier to work with, mainly due to reduction of the high viscosity of $ZnCl_2$ in pure molten $ZnCl_2$.

Whilst the amount of work carried out on $ZnCl_2$ melts is small compared to that done, for example, on nitrate or LiCl-KCl melts, the

subject is by no means an unknown quantity. Structural studies are quite widespread (Section 2.1); the transport properties have been measured for several $ZnCl_2$-MCl melts (Section 2.2); solute behaviour has been fairly widely studied; electrochemical cells have been utilised to look at activities of the melt components for $ZnCl_2$-MCl[1]; glass formation by $ZnCl_2$ is well documented; phase diagrams are known for all $ZnCl_2$-MCl mixtures (Section 2.2) and as industrial uses are found so more work is carried out. Where gaps exist, analogies with the more extensively covered aluminium chloride-based melts provide at least an idea of what could occur in the $ZnCl_2$ melts. $AlCl_3$, like $ZnCl_2$, is a strong Lewis acid, an associated liquid in the pure state and is hygroscopic, probably more so than $ZnCl_2$. Similarly, experimental techniques used in the purification and handling of other chloride melts are often applicable to $ZnCl_2$ melts[2].

1.1 Uses of Zinc Chloride Melts

Apart from the ability of zinc chloride to catalyse the hydrocracking of heavy oils and coal, several other uses of zinc chloride melts have been found. The hydrocracking process is described in detail in Appendix 1, and so will not be further mentioned here. Rather, a brief survey of some of the other uses of zinc chloride melts will be given to show the diversity of areas in which the material is useful.

The exchange reaction between salt and metallic phases in molten salts has been put forward as a means of purifying some metals. In the recycling of plutonium residues it has been suggested that zinc chloride will be used to recover the plutonium using the Pyroredox reactions[3]:

$$2Pu + 3ZnCl_2/KCl \rightarrow 2PuCl_3/KCl + 3Zn \qquad [1.1]$$

$$2PuCl_3/KCl + 3Ca \rightarrow 2Pu + 3CaCl_2/KCl \qquad [1.2]$$

Impurities more noble than zinc are separated from the impure plutonium and remain in the zinc metal with the reaction moderated by dilution with potassium chloride.

Recent work by Delimarskii and Volkov[4] has shown that in the indium-molten zinc chloride equilibrium at 440°C, formation of a compound $2ZnCl_2$. InCl occurs on cooling the molten salt phase. The addition of MCl to the molten mixture shifts the equilibrium to the side of separation of the indium metal. This is put forward as a means of purifying indium metal. The reactivity to exchange with $ZnCl_2$ melts is found to decrease in the series In > Pb > Sn. Bismuth could not be purified by exchange reaction with $ZnCl_2$, but by reaction with its own chlorides.

Pez and Trotter[5] found an interesting use for molten $ZnCl_2$ in the area of gas separation. One gas can apparently be separated from a mixture of gases by selective permeation through a layer of molten salt immobilized in a thin rigid porous inert support. The separated gas undergoes a reversible reaction with the molten salt e.g. by formation of a co-ordination complex. Different salts can be used depending on which gas is to be removed from a mixture. Separation of the HCl and Cl_2 gases from various mixtures of gases was attempted using $ZnCl_2$ melts, a fair degree of success being achieved. This could possibly be tied in with work by Skudaev et al.[6] who have shown that using a molten mixture of $CuCl_2$ and $ZnCl_2$, it is possible to chlorinate methane. Their work was done under bubbling conditions, but it may be possible to use the same apparatus as that used by Pez and Trotter. The mechanism of the chlorination apparently involves the thermal dissociation of the $CuCl_2$ as the initiation step of the process.

Rapid quenching of molten zinc chloride can result in glass formation[7,8]. The structure of the glass is thought to be the same as that of the melt, with a random array of $ZnCl_4$ tetrahedra. Devitrification can occur in two ways- by heating the glass above the crystallization temperature (140-200°C) or by applying pressure to

the glass (e.g. by grinding). Like other chloride glasses, $ZnCl_2$ is highly transparent from the near U.V. region into the far I.R. region. However, the main problem with these glasses is their very hygroscopic nature, which has led workers to look for materials that are not as affected by water. Attempts to improve the stability of the $ZnCl_2$ glass by adding other chlorides or oxides have proved reasonably successful. Compounds that have been added include $AlCl_3$-H_2O[9] and $PbCl_2$, KCl, TeO_2 and various other MCl and MCl_2[10]. These glasses have become more technologically interesting with the development of optical fibres, waveguides and lasers where good optical properties are necessary.

Sundermeyer et al.[11,133-135] have investigated several recycling processes using molten salts as reaction media. Among processes discussed are those shown below which use zinc chloride melts as solvents:

$$(CH_3)_2SiCl_2 + 2CH_3OH \xrightarrow{ZnCl_2\text{-}KCl} [(CH_3)_2\ SiO]_n + H_2O + 2CH_3Cl \quad \ldots[1.3]$$

$$H_3COH + HCl \xrightarrow{ZnCl_2\text{-}KCl} H_3CCl + H_2O \quad [1.4]$$

$$H_3COCH_3 + 2HCl \rightarrow 2H_3CCl + H_2O \quad [1.5]$$

The first reaction results in environmentally safe silicon compounds whilst the latter two are the recycling of by-products from methylcellulosis manufacture into the starting reactant, CH_3Cl.

1.2 Acidity - Basicity in Molten Salts

Unlike aqueous solutions, where acidity is measured in terms of pH (= $-\log_{10}[H^+]$), the proton is a less important species in most

melts. It does, however, feature in molten bisulphates and hydroxides as well as in melts containing H_2O or HCl as solutes but in general the Lux-Flood[12] concept of acidity has been chosen in place of the Lowry-Bronsted proton scheme. A Lux-Flood acid is defined as an oxide ion acceptor leading to the formation of the conjugate base:

$$\text{Acid} + O^{2-} = \text{Base} \qquad [1.6]$$

e.g.

$$CO_2 + O^{2-} = CO_3^{2-} \qquad [1.7]$$

This system is especially applicable to the oxy-anionic melts, including those with polymeric or network structures. A scale analogous to that of pH may be set up to represent solutions of oxide ions in non-participating melts. The pO^{2-} scale ($=-\log_{10}[O^{2-}]$) is widely used in corrosion studies in molten salts but care must be taken since it is possible that O^{2-} is not the sole oxide ion present[13].

To a lesser extent the Lewis and the Pearson schemes are applied to molten salts since both are broad enough as to remain valid in these media. According to the Lewis electronic definition of acids and bases an acid is any species that is capable of accepting a pair of electrons in formation of a covalent bond, and a base is any species that can donate a pair of electrons to form a covalent bond. For example:

$$AlCl_3 + Cl^- = AlCl_4^- \qquad [1.8]$$

$$\underset{\text{(acid)}}{ZnCl_2} + \underset{\text{(base)}}{2Cl^-} = \underset{\text{(complex/conjugate)}}{ZnCl_4^{2-}} \qquad [1.9]$$

The Pearson[14] scheme uses the idea of 'soft' and 'hard' acids and bases where, for example, hard acids are characterised by ions of small size and high positive oxidation state.

Water can behave as a donor, an acceptor, or both, and the acid-base equilibria involved are shown below, according to the definition of acidity considered:

Brønsted-Lowry:

$$H_2O = H^+ + OH^- \qquad [1.10]$$

$$H_2O + H^+ = H_3O^+ \qquad [1.11]$$

Solvoacidity concept (i.e. $AX^- = A + X^-$)

$$H_2O + AX^- = A + H_2OX^- \qquad [1.12]$$

$$H_2O + 2AX^- = A_2O + 2X^- + 2H^+ \qquad [1.13]$$

Oxoacidity concept (Lux-Flood)

$$H_2O + O^{2-} = 2OH^- \qquad [1.14]$$

$$H_2O + 2X^- = 2HX + O^{2-} \qquad [1.15]$$

1.3 Complex Ions in Molten Salts

Defining a complex ion in a matrix consisting solely of anions and cations, each necessarily constituting the nearest neighbour to the other in order to preserve charge neutrality, is rather difficult. Flengas and Kucharski[15] have considered the problem in terms of bond lengths. Thus the anion-cation distance for the complexed state is shorter than that for the non-complexed state. However, Inman and Lovering[16] hold that instantaneous arrangements of anions around a "static" cation do not necessarily indicate formation of a discrete complex, and that one should go on to consider the lifetime of such a species. Observation times of the species should exceed the general quasi-lattice relaxation time of $\sim 10^{-11}$ sec. so that discrete kinetic entities may be separated from time-averaged assemblages of ions.

CHAPTER 2

LITERATURE SURVEY

2.1 Structure of Zinc Chloride and $ZnCl_2$-MCl Melts

Until the 1970's it was thought that solid zinc chloride existed in three crystalline forms, α, β, and γ[17]. The α-form, said to be obtained from solution or by rapid cooling of the melt, had a three-dimensional polymeric structure of linked $ZnCl_4$ tetrahedra with a cubic close-packed arrangement of chlorine atoms. Slow cooling of the melt was said to produce the β-form, with hexagonal close-packed chlorine atoms. The γ-form could be obtained from solution at about 75°C, and had a layer structure with zinc atoms in tetrahedral holes between alternate layers of cubic close-packed chlorine atoms. All three forms were well documented, with X-ray diffraction data provided[18]. However, there is little doubt that all three modifications were significantly contaminated by water. All three were prepared from hot concentrated aqueous solutions, and the material used for the melt preparations had been recrystallized from aqueous solutions, probably resulting in a high proportion of hydroxyl-ions substituting for chloride ions in the final product.

In 1978 Brynestad and Yakel[19,20] reported the structure of anhydrous zinc chloride having used material far more rigorously purified than that used previously. As seen in Figure 2.1 the structure approximates to a hexagonal sequence of close-packed chloride ion layers in which zinc ions occupy certain tetrahedral holes. Each chloride ion is common to two corner-sharing $ZnCl_4$ tetrahedra - there are no shared edges or faces. As its nearest neighbours each chloride ion has two zinc, six intratetrahedral chloride, and six intertetrahedral chloride ions.

There have been many investigations of the structure of molten zinc chloride and zinc chloride-alkali metal chloride (MCl) systems, mainly because they can be used as low temperature models of the glass-forming SiO_2 and BeF_2 systems. The structural pecularities of molten zinc chloride have been described variously as "polymers", "lattice

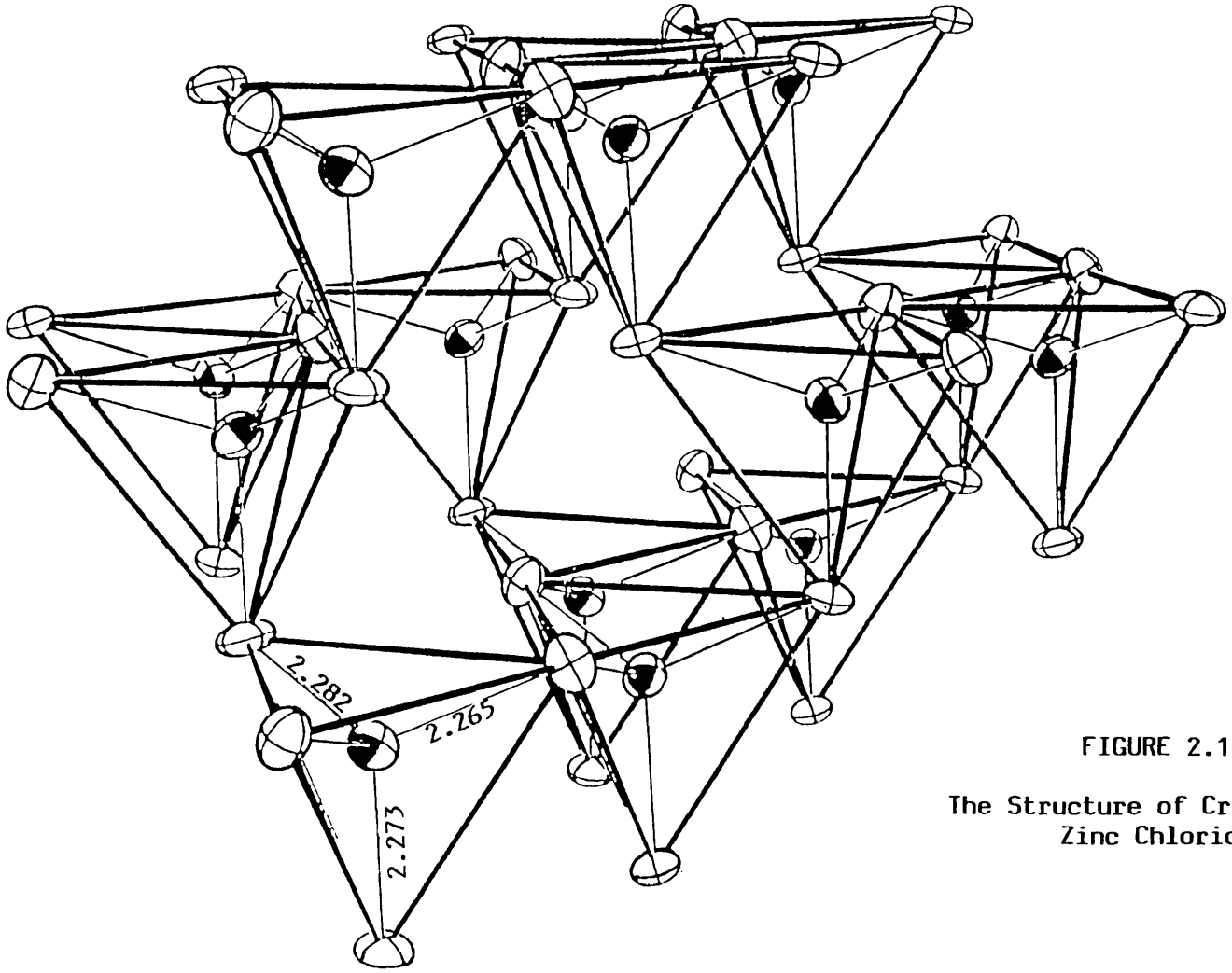


FIGURE 2.1

The Structure of Crystalline
Zinc Chloride

fragments", "layers", "ionic complexes" and "networks"[21]. In 1963, Wilmshurst[22], in his investigation of the I.R. spectra of molten $ZnCl_2$ + KCl/LiCl, eliminated the idea of complex species and stated that the observed bands were due to "lattice-like vibrations of the system", the added M^+ ions merely fitting into vacancies in the lattice. Two studies of the I.R. spectra of zinc chloride (liquid and glass) by Angell et al provided interesting results. In the earlier paper[23], data from work with nitrate, chloride and mixed nitrate-chloride systems seemed to indicate the existence of $Zn(Cl,NO_3)^{2-}$ "entities" with tetrahedrally co-ordinated Zn^{2+} ions, but no crystalline double salt of known geometry was available to confirm this. In the second paper[21], work on pure $ZnCl_2$ led to the idea that the melt has a weakened, continuous network structure, rather than network fragments co-existing in the liquid state. Other than this distinction, Angell et al. agree with earlier conclusions concerning the tetrahedrally co-ordinated polymeric nature of the liquid.

A large amount of the work on the structure of molten $ZnCl_2$ and $ZnCl_2$-MCl has involved Raman spectroscopy. Early Raman studies[7,21,24-27] all indicated that the network structure of the solid persists above the melting point, but with increasing temperature the degree of polymerization is lowered to form simpler species, including $(ZnCl_2)_n$ and $ZnCl_4^{2-}$. Progressive addition of an alkali halide (e.g. KCl) causes two reactions to occur. For small amounts of alkali chloride reaction [2.1] takes place, which is the depolymerization reaction:

$$(ZnCl_2)_n + Cl^- = (ZnCl)_{n-m} + (ZnCl_2)_m Cl^- \quad [2.1]$$

Additions of KCl beyond molar ratios of KCl:$ZnCl_2$ of 0.2 were said to cause a second process to predominate:

$$(ZnCl_2)_m Cl^- + Cl^- = ZnCl_4^{2-} + (ZnCl_2)_{m-1}$$

For the same compositions but varying MCl (M = Li,K,Rb,Cs) Ellis[26] hinted that the depolymerization increased with increase in cation size, but offered little explanation. Other units such as $ZnCl_3^-$, $ZnCl_6^{4-}$, monomeric $ZnCl_2$ and $ZnCl^+$ are all predicted to exist, supposedly being

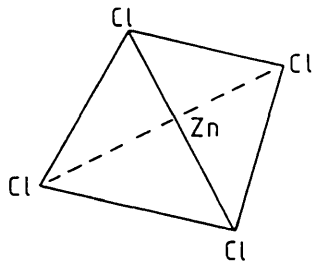
formed as the crystal structure breaks up. More recent work by Itoh et al.[28] on $ZnCl_2$-KCl molten systems agrees with the earlier results.

X-ray diffraction analysis of molten $ZnCl_2$ and $ZnCl_2$-KCl has been carried out. Triolo and Narten[29] state that molten zinc chloride "does not consist of $ZnCl_2$ molecules but of Zn^{2+} and Cl^- ions arranged as $ZnCl_4^{2-}$ tetrahedra". Takagi and Nakamura[30], who in 1985 were still talking about the α, β, γ and δ (Brynestad-Yakel structure) crystalline phases of solid $ZnCl_2$, used three models (Figure 2.2) involving $[ZnCl_4]$ and $[Zn_2Cl_7]$ species to account for behaviour in the $ZnCl_2$-KCl system. Their conclusion was that except for molten KZn_2Cl_5, no change is found in the nearest neighbour Zn-Cl distance and in the co-ordination number around the zinc atom with increasing KCl composition. This, they say, proves the existence of $[ZnCl_4]$ units in the systems, but a change in the long range order occurs with increasing KCl.

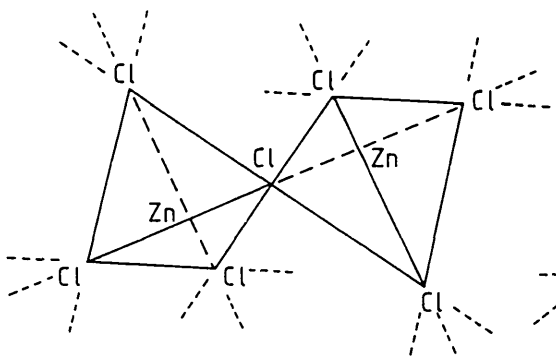
Susic and Mentus[31], drawing conclusions from work on the conductivity and viscosity of molten zinc chloride, suggest another structural model. Molten zinc chloride, at a temperature slightly above the melting point, is composed of fragments originating from the crystal structure of the solid, these fragments being "big, associated molecules, $(ZnCl_2)_x$". The Zn^{2+} and Cl^- ions, arising from the melting and dissociation of the salt, are mostly attached to the associates giving $[(ZnCl_2)_x\ Zn_p^{2+}]^{2p+}$ and $[(ZnCl_2)_xCl_q^-]^{q-}$, which are responsible for the electric conductance and viscosity.

Biggin and Enderby[32] broke with the idea of $ZnCl_4^{2-}$ species when, on the basis of neutron diffraction studies of molten zinc chloride, they concluded that the correct description of the melt is in terms of Zn^{2+} and Cl^- ions, the anomalous transport properties being due to restricted mobility of Zn^{2+} in close-packed Cl^- ions, rather than any degree of association. However, six years later Enderby[33] stated that molten zinc chloride shows structural features "not readily explained in a purely ionic framework".

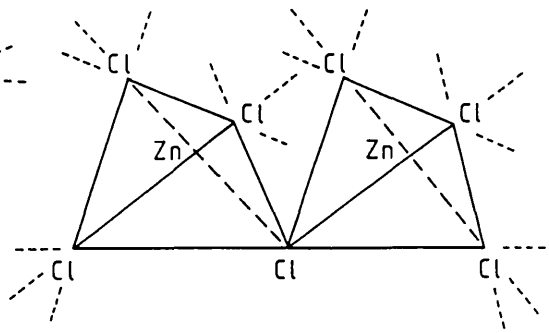
Early attempts[34,35] to simulate the liquid structure of zinc chloride used models taking into account coulombic interactions between



MODEL 1



MODEL 2



MODEL 3

FIGURE 2.2

Liquid Structure of Models of Zinc Chloride
(Takagi and Nakamura, ref. 30)

Zn^{2+} and Cl^- ions and short-range repulsive forces, with suitably chosen ionic radii for Zn^{2+} and Cl^-. The W.A.C. model (named after the authors of ref. 34) was found to give reasonable results for the Zn-Cl and Cl-Cl distances but failed completely for the Zn-Zn distance. The value for r_{Zn-Zn} found in the model was about 1Å greater than that found experimentally[32]. An enhanced model put forward by Ballone et al.[36] takes into account angular dependence of the interatomic forces, which have been simulated by screening effects and non-additivity of the ionic radii. The steric restrictions so introduced are said to account for the transport properties observed in molten $ZnCl_2$ near the freezing point.

2.2 Transport and Physico-Chemical Properties

A critical evaluation of the studies of these properties carried out prior to 1975 has been compiled by Janz et al.[37], the most reliable information being selected for display and the remainder being referenced. Since that time the number of such investigations has been few, with those by Ejima et al.[38-40] being the most interesting, relating changes in transport properties to change in composition of $ZnCl_2$-MCl mixtures.

2.2.1 Density

Duke and Fleming[41], working with the molten KCl-$ZnCl_2$ system, found that density vs. composition isotherms were approximately linear for the temperature range 475-650°C, slight deviations from additivity causing them to be rather "S-shaped". However, work on the same system by Angell and Wong[21] found that beyond 30 mol% KCl the density isotherms varied linearly with composition and had slightly higher values than those of Duke[41]. To give an idea of the magnitude, the densities of pure $ZnCl_2$ were around 2.4-2.5 gcm^{-3} (depending on temperature), dropping to 1.7-1.8gcm^{-3} at 80 mol% KCl-$ZnCl_2$. Bloom and Weeks[42] also worked on the KCl-$ZnCl_2$ system, as well as other $ZnCl_2$-MCl (M = Li, Na, Cs) systems, concentrating mainly on the $ZnCl_2$-rich compositions. The molten mixtures, except in very low X_{MCl} regions, were found to exhibit linear temperature dependence for the density. Bloom explains this as being due to the formation of $ZnCl_4^{2-}$ entities on the addition of alkali metal

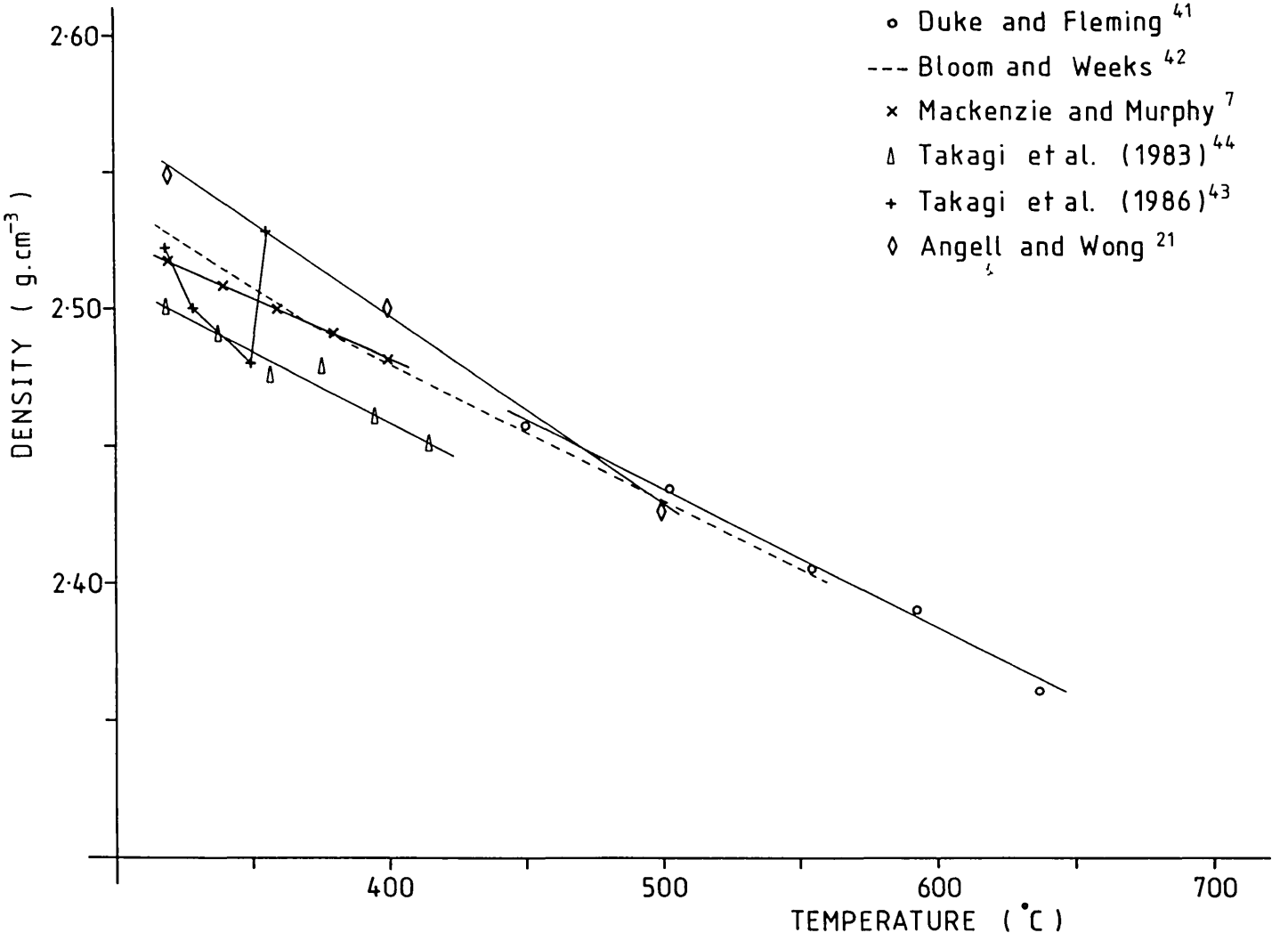


FIGURE 2.3: Variation of the Density of Zinc Chloride with Temperature

chloride. For the MCl-rich compositions the data of Ejima et al.[40] supplements that of Bloom very well, the combination of the two sets of results giving values for the whole composition range. From the initial marked increase (0-50 mol% MCl) in thermal expansion coefficients to a monotonous change for 50-100 mol% MCl, Ejima postulated a change from associated liquids to ionic species.

Working on pure $ZnCl_2$, Mackenzie and Murphy[7] found that between 320 and 400°C, the density had a linear temperature dependence, whereas Takagi et al.[43,44], using a novel X-ray transmission method, found a fair amount of non-linearity over the same temperature range. Figure 2.3 shows various published results for the behaviour of density with temperature for pure $ZnCl_2$.

2.2.2 Electrical Conductivity

Whilst several measurements of the conductivity of pure zinc chloride and its temperature dependence have been carried out[7,8,41,45,46], no two sets of data agree closely over a wide temperature range (e.g. 100°C). As Easteal and Angell[8] point out, at 336°C for example, the highest and lowest of the published specific conductances differ by almost 55% of the mean of the two values and at 400°C the difference is 49%. Published values for the specific conductance of pure $ZnCl_2$ show marked non-Arrhenius behaviour (lnK vs 1/T is curved), which may be due to melt impurities - small amounts of contaminants would produce marked changes in ion mobilities.

Electrical conductivity measurements in $ZnCl_2$-MCl mixtures have been carried out by Duke and Fleming[41] ($ZnCl_2$-KCl) and Bloom and Weeks[47] ($ZnCl_2$-MCl; M = Na, K, Cs). Conductance isotherms for $ZnCl_2$-KCl binary mixtures (Figure 2.4) show a reasonably smooth increase with increasing X_{KCl}, consistent with the continuous breakdown of the $ZnCl_2$ network by the alkali metal chloride. Deviation from additivity in similar systems, e.g. KCl + $CdCl_2$, KCl + $AlCl_3$, are much greater (Figures 2.5 and 2.6 respectively), for which work by Bloom and Heymann[48] could be used when looking for an explanation. Their findings showed that strong

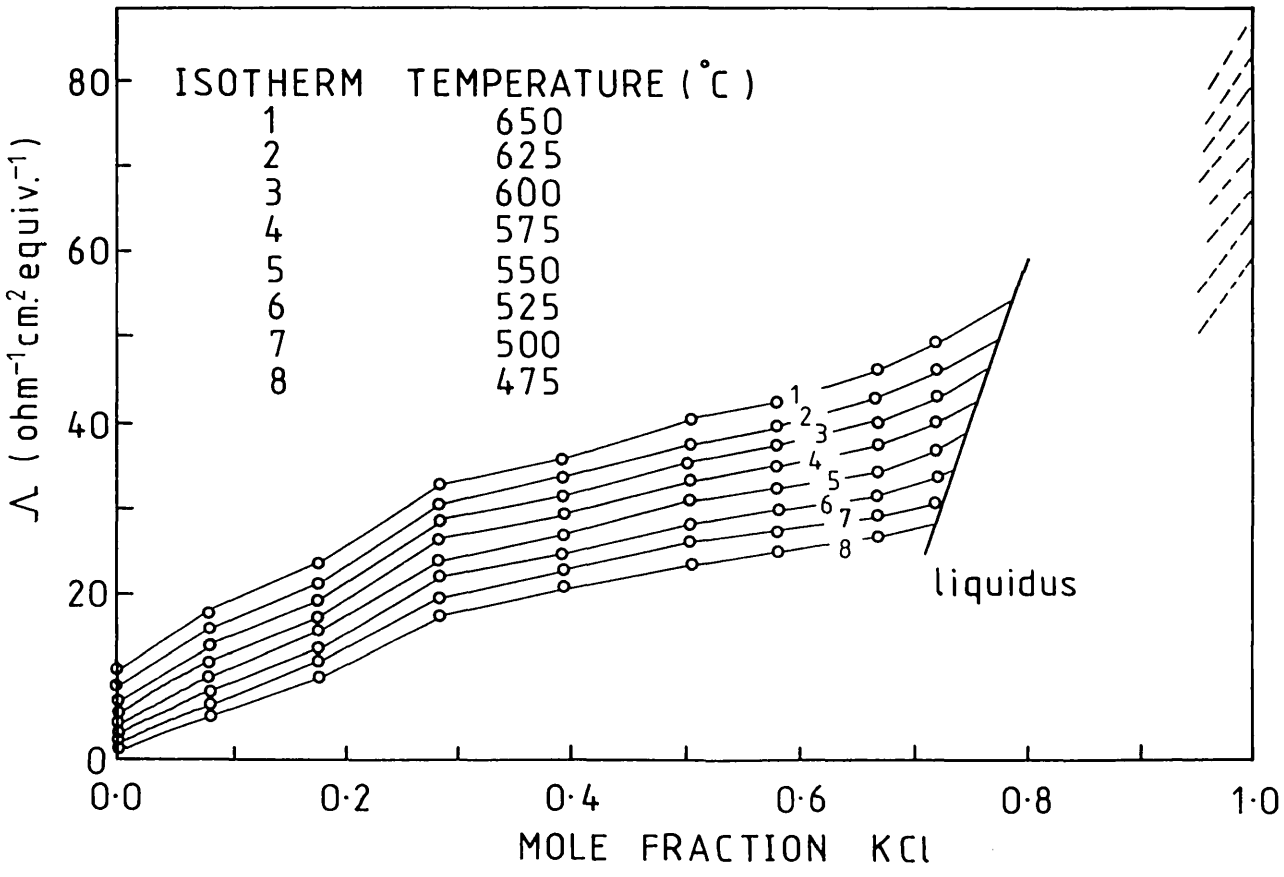


FIGURE 2.4: Electrical Conductivity Isotherms for $ZnCl_2$-KCl (ref. 41)

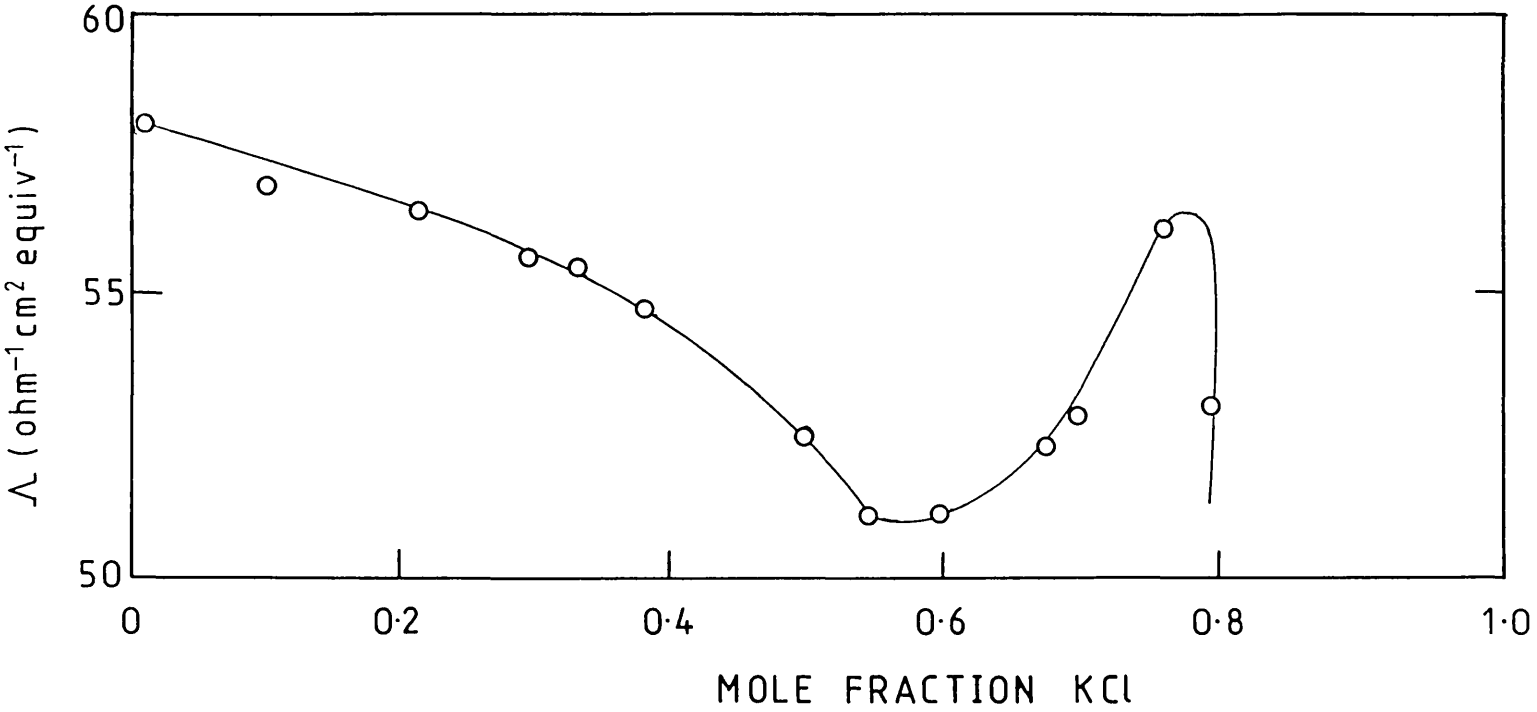


FIGURE 2.5: Electrical Conductivity Isotherms for $CdCl_2$-KCl (ref. 204)

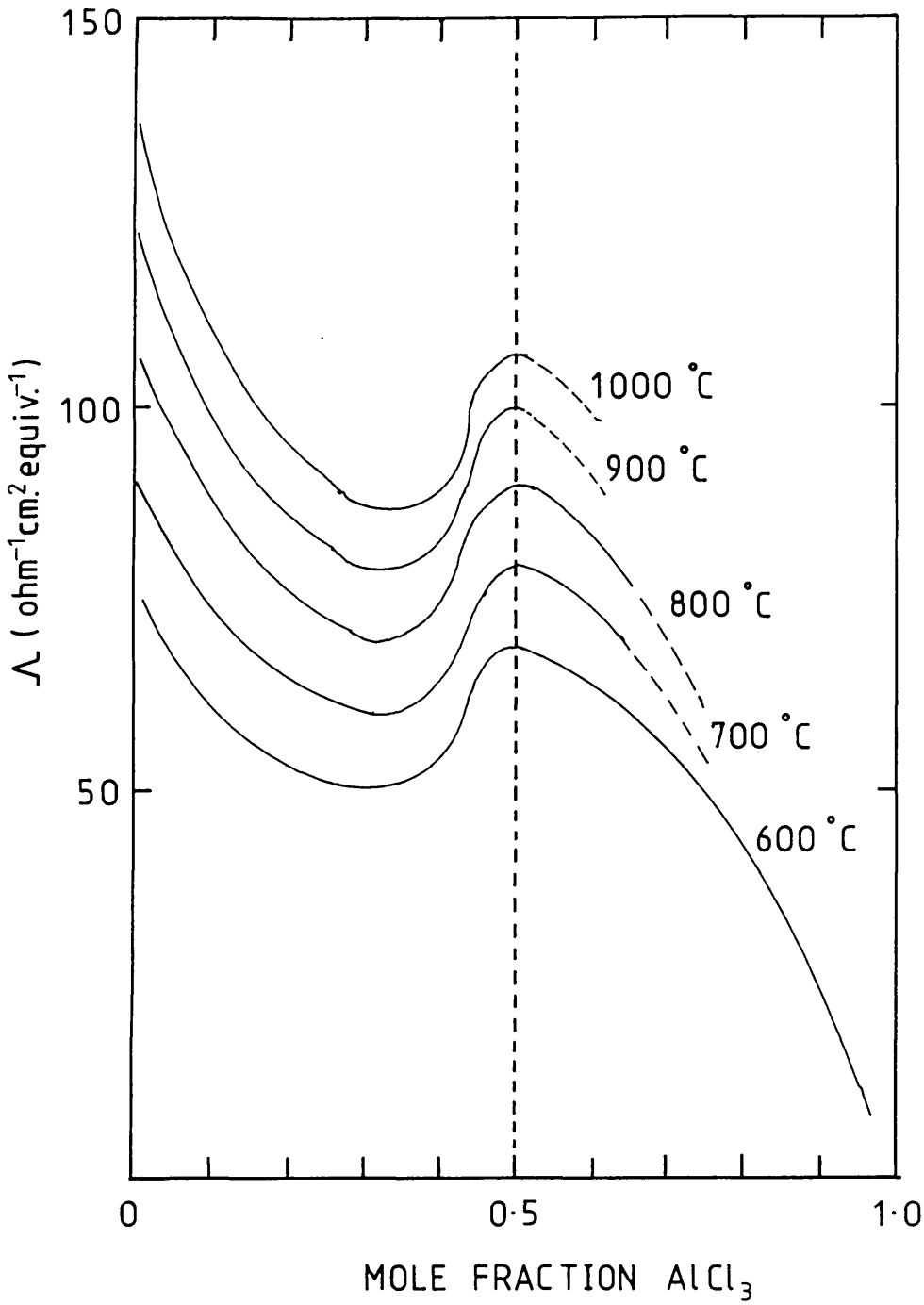


FIGURE 2.6

Electrical Conductivity Isotherms for $AlCl_3$-KCl (ref. 204)

negative deviations would be found to be associated with systems whose phase diagrams indicated the presence of congruently melting compounds, and could be explained on the basis of persistence in the liquid state of the complex known to be present in the solid state.

2.2.3 Viscosity

The viscosities of pure molten $ZnCl_2$ and of $ZnCl_2$-MCl systems (M = Li, Na, K, Cs) have been determined by various workers. Gruber and Litovitz[49] found that the viscosity of pure $ZnCl_2$ obeyed the Arrhenius equation above 325°C and drew the conclusion that there was little network behaviour present in the neighbourhood of the melting temperature and that "the dissociation process (into $ZnCl_4^{2-}$ units) is essentially complete within 20° above melting". Their results agree with those of Easteal and Angell[50] but not with those of Mackenzie and Murphy[7] who found marked non-Arrhenius behaviour over the same temperature range. Ejima et al.[39] found that the non-Arrhenius behaviour of the viscosity of $ZnCl_2$ could be divided into three stages for the temperature range 320-560°C, and postulated the constituent species in the melt corresponding to each stage. Susic and Mentus[31] obtained results agreeing with Mackenzie up to 360°C but deviating negatively at higher temperatures.

Addition of alkali metal chloride resulted in a drastic drop in viscosity, as found by all workers, the decrease being dependent on the M^+ cation size. Ejima[38,39] found that the $ZnCl_2$-KCl and $ZnCl_2$-CsCl systems exhibited maxima near the 66 mol % MCl region, which was attributed to greater Cl^- donor effects in KCl and CsCl, so forming more $ZnCl_4^{2-}$ complexes. However, Bloom[51] claims there is little or no relationship between complex formation and transport properties, since there is no correlation between conductivity and viscosity maxima/minima.

2.2.4 Vapour Pressure

Studies of the vapour pressure of pure molten $ZnCl_2$ in the temperature range 400-600°C[52-55] show that it exhibits Arrhenius behaviour but different workers have interpreted results in dissimilar

ways. Keneshea and Cubicciotti[52] discussed the existence of a proportion of zinc chloride dimers being present in the vapour over the liquid salt, the rest of the vapour being monomers. However, Bloom[54] seemed sceptical about this and assumed only the existence of monomers for his calculations. Addition of alkali metal chloride (NaCl[53]; NaCl and KCl[54]) causes a steady decrease in the vapour pressure with increase in X_{MCl}. KCl is found to cause a much larger decrease than NaCl for the same composition and temperature, especially where $X_{MCl} > 0.2$. Rice[53] mentioned the existence of Na_xZnCl_{2+x} species in the vapour phase, but the partial pressure of $NaZnCl_{3(g)}$ was said to be only 1% of that of $ZnCl_2$ at 600°C.

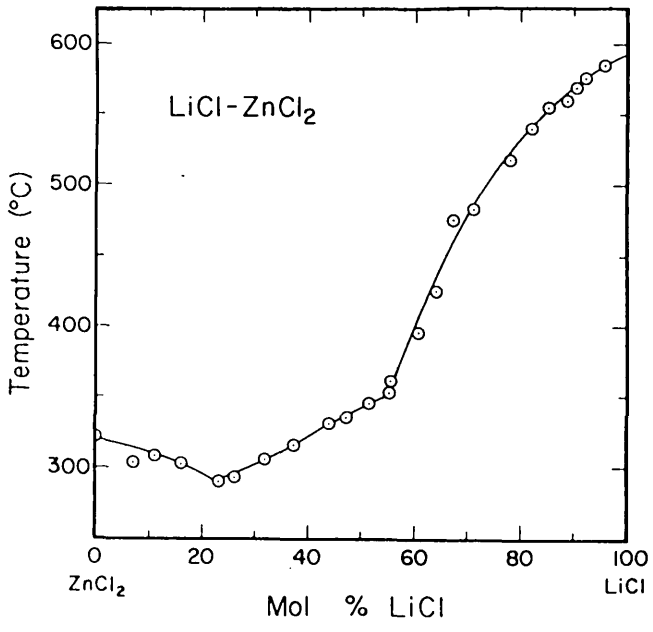
2.2.5 Phase Diagrams

For the $ZnCl_2$-MCl (M = Li, Na, K, Rb, Cs)[56] systems these are reproduced in Figures 2.7-2.11. The general trend seen is that as M^+ increases in size, so the complexity of the phase diagram increases, a feature that is probably due to the increasing Cl^- ion donor properties of the heavier alkali metal cations, which would cause break-up of the melt structure at lower X_{MCl} values than for the lighter M^+ cations.

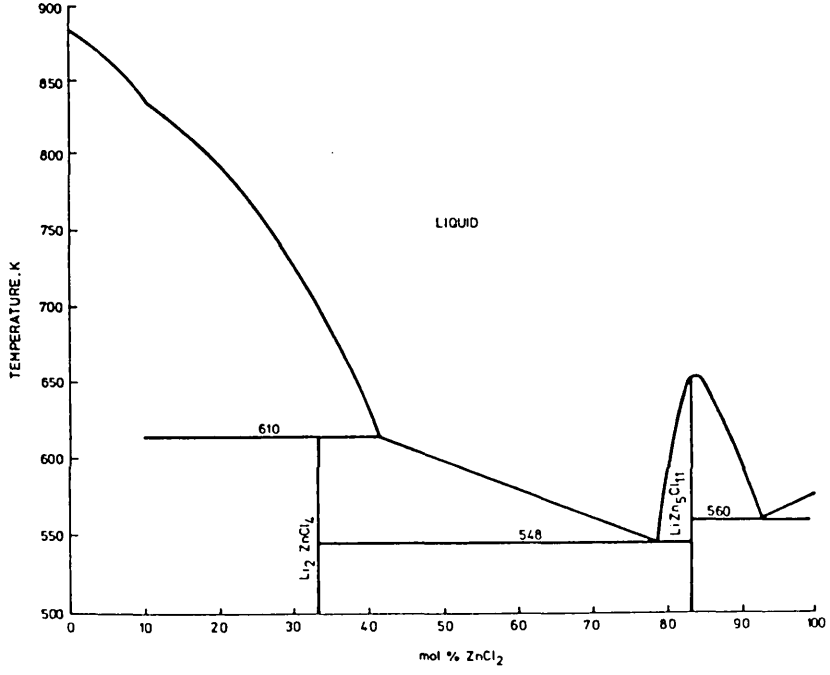
There is presently some controversy over the $ZnCl_2$-rich region of the LiCl-$ZnCl_2$ phase diagram. Evseeva and Bergman[56] reported for the LiCl-$ZnCl_2$ diagram, one eutectic, one peritectic and a LiCl phase change. Perry et al.[57,58] however, found two eutectics, one peritectic, the LiCl phase change and $LiZn_5Cl_{11}$, a congruently melting compound (m.pt. 659K). This compound, it is claimed, is only found when dried salts are used - the presence of moisture is apparently detrimental to its existence. No explanation of the effect of moisture is given, other than a suggestion that it may somehow catalyse the decomposition of the species.

2.3 Solubility of Gases in Molten Salts

Investigation into solubilities of gases in molten salts, and their effect on the physical and chemical properties of the melts, originated as a consequence of the gaseous fission products found in radiated molten



(a) ref. 56



(b) Perry et al. ref. 58

FIGURE 2.7

Phase Diagram of $ZnCl_2$-LiCl

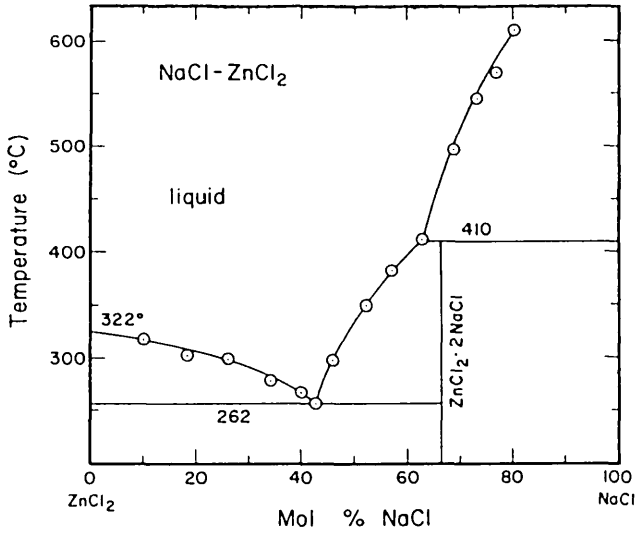


FIGURE 2.8

Phase Diagram of $ZnCl_2$-NaCl

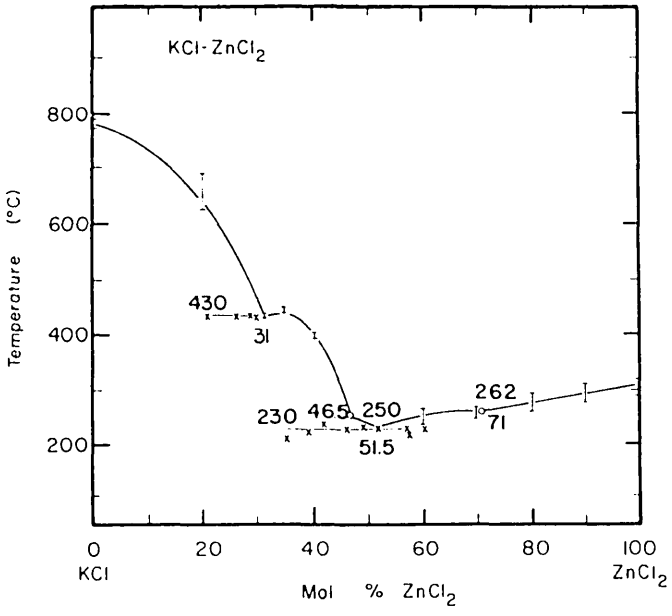


FIGURE 2.9

Phase Diagram of $ZnCl_2$-KCl

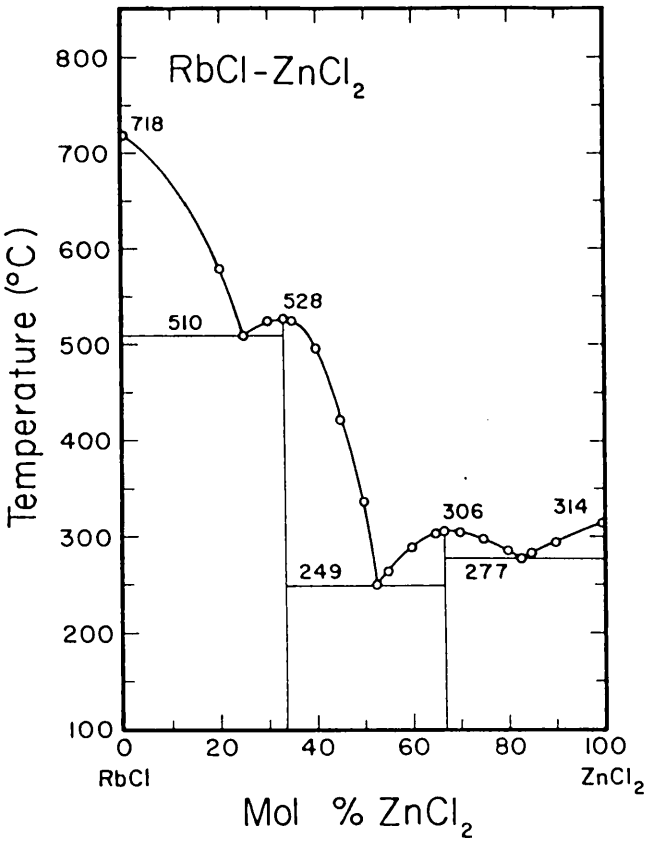


FIGURE 2.10

Phase Diagram of $ZnCl_2$-RbCl

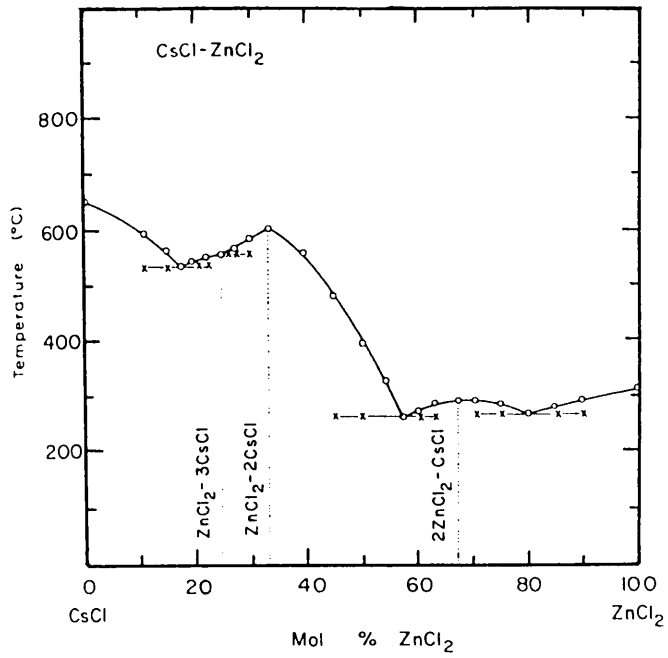


FIGURE 2.11

Phase Diagram of $ZnCl_2$-CsCl

salts and from the use of melts as heat treatment baths, electrolytes and metallurgical slags. Research into these gaseous solutions of molten salts lags far behind analogous studies in water and organic solvents, although theoretical studies can predict behaviour for the simpler molten salts.

Experimental methods employed for the determination of the gas solubilities in molten salts can be placed in three classes. A somewhat limited method is cryometry, utilizing the depression in the freezing point of the solvent caused by the gaseous solute. More widely used are the absorption and elution methods. In the former the solubility is determined by observing some property change in either the gas phase of the solute, a volumetric or manometric change, or the liquid phase of the solvent, a gravimetric or voltammetric change. In the latter, the solute is stripped from a saturated solution by means of displacement with a carrier gas, the resultant gas mixture then being analysed by physical or chemical methods.

2.3.1 Solubility of HCl Gas in Chloride Melts

An investigation of the solubility of HCl in the molten alkali metal chlorides was carried out by Ukshe and Devyatkin[59], who studied the solubility in molten LiCl, NaCl, KCl and RbCl by an elution method. In LiCl, NaCl and KCl the HCl solubility was found to increase with temperature whilst in RbCl it decreased as the temperature rose. It was suggested that the HCl is present in a dissociated form, with the free proton held in cationic holes formed by 3 or 4 chloride ions. This was said to represent the formation of chloro-complexes $H^+.xCl^-$ where $x = 3$ or 4, a conclusion reached in their electrochemical study of the same systems[60]. Other studies by Russian workers apparently gave contradictory results so Novozhilov et al.[61] devised a volumetric method which they used for all their solubility investigations. For pure molten NaCl[63] the solubility was found to increase slightly with temperature, but for KCl, RbCl and CsCl the HCl solubility decreased as the temperature was raised to over 1200K. The ln k vs.1/T plots were all S-shaped, which was explained as either being due to an interaction at the gas-melt interface or to structural changes in

the bulk of the melt. In this work, Novozhilov infers that interactions between the dissolved HCl molecules and Cl^- ions in the melts are occurring, becoming more intense with the presence of larger metal cations. The error given in the results is $\pm$1% which is significantly smaller than that of other workers[63].

A study of the HCl solubility in molten alkaline earth metal chlorides (MCl_2) using a volumetric method was also carried out by Novozhilov et al.[64]. For $CaCl_2$, $SrCl_2$ and $BaCl_2$ pure melts the solubility increased linearly with rise in temperature, for the temperature range studied, and it increased in the order $CaCl_2 > SrCl_2 > BaCl_2$. From the data it can be seen that the HCl solubility in each MCl_2 is an order of magnitude smaller than that in the neighbouring MCl melt at the same temperature. Solutions of HCl in the MCl_2 melts were all found to obey Henry's Law, as was the case in the MCl melts[62]. It is suggested that the dissolution of the HCl proceeds mainly through the formation of vacancies in the melt, and so is not accompanied by significant interaction with the melt, i.e. physical, rather than chemical, dissolution. Enthalpies of solution were all found to be endothermic.

The solubility of HCl in the LiCl-KCl eutectic (59:41 mol. %) has been studied by the Van Norman and Tivers[65] and Minh and Welch[66], their respective results summarised below in Table 2.1.

Temperature (^oC)	Minh and Welch	Van Norman and Tivers
404	1.04×10^{-6}	
462	1.27×10^{-6}	
490		$1.20 \pm 0.14 \times 10^{-6}$
520	1.56×10^{-6}	
570		$1.44 \pm 0.10 \times 10^{-6}$
675		$1.74 \pm 0.11 \times 10^{-6}$

TABLE 2.1

Solubilities of HCl in LiCl-KCl eutectic (mol. cm^{-3})

As can be seen, the values rise with increasing temperature and are of reasonable agreement, within experimental error. Minh and Welch gave their values an error of $\pm$10%. The data demonstrate the physical nature of the HCl dissolution in this molten mixture.

Ukshe and Devyatkin[67] determined the HCl solubility in NaCl-KCl molten mixtures; for all but the 1:1 mixture the solubility was seen to increase with temperature. This was explained by considering the symmetry of the chloride lattice, which is at its most distorted in the equimolar molten mixture. The distortion results in a change in the effective radii of the protons dissolved in the melt, which is linked to the heat of solution. The solubility, reported as X_{HCl}, of HCl was found to increase from pure NaCl, through the mixtures to pure KCl, for the same temperature.

For molten antimony trichloride the solubility of HCl has been investigated by Ryabov et al.[68]. It was shown that in the temperature range 80-120^{o}C the solute behaves in a manner characteristic of a chemical dissolution process, with the solubility decreasing from 0.809 mol. % at 80^{o}C to 0.619 mol. % at 120^{o}C. No attempt, however, was made to postulate the structure of any complex entity that may exist within the melt.

The solubility of HCl gas in zinc chloride - containing molten mixtures has been studied by Prasolov et al.[69] in KCl-$ZnCl_2$ (45 and 70 mol. % $ZnCl_2$) and Minh and Welch[70] in LiCl-KCl-$ZnCl_2$ ($0 < X_{ZnCl_2} < 0.174$). Both studies found solute behaviour characteristic of chemical solubility - the solubility of HCl decreased with increase in temperature and with decrease in X_{ZnCl_2} in the molten mixtures. However, the magnitudes of the solubilities determined by Prasolov are ~ 100 times larger than those of Minh and Welch. The latter workers employed an elution method of solubility determination, purging the dissolved HCl from the melt with argon, but the method of Prasolov is not described in the translation of the original paper, so it is not possible to see how such a large discrepancy could occur. Both studies have, on the basis of these results, postulated the existence of a complex species formed between the HCl molecules and the $ZnCl_2$ in the melt, although neither stated what the

complex structure might be.

A recent investigation[71] of the solubility of HCl in N-ethylpyridinium bromide-zinc chloride and in N-methylpyridinium chloride-zinc chloride molten mixtures at 393 and 443K respectively showed that increasing X_{ZnCl_2} resulted in a decrease in solubility to X_{ZnCl_2} = 0.33, after which the solubility values were approximately constant to X_{ZnCl_2} = 0.7. This behaviour has been interpreted as being due to the formation of bihalide ions (HX_2^-) in the melts, rather than any complexation with the aromatic ring or the $ZnCl_2$.

2.3.2 Solubility of H_2O in Chloride Melts

Studies of the solubility of water in molten chlorides are rare[72] and those carried out have nearly all been on LiCl-KCl mixtures. At higher temperatures and water vapour pressures hydrolysis of the LiCl was thought to occur[73], but linear relationships between solubility and vapour pressure were found in systems where the temperatures and vapour pressures were lower. "Considerable" amounts of HCl were formed as hydrolysis occurred. The tenacity with which lithium chloride molten mixtures retain water was noted, with solubilities of the order of 10-30 μmol. $torr^{-1}$ (mol. Li^+)$^{-1}$ at 390-480K and water vapour pressures of less than 18mm Hg. The data attributed by Combes[72] to Laitinen et al.[74] as the water solubility in LiCl-KCl eutectic is, on closer study, the amount of water removed from the solid components by evacuation. In the same survey(72) the data of Maricle and Hume[75] is in fact the amount of hydroxide found in an unpurified melt (NaCl-KCl) rather than the solubility of water.

Three other studies of water solubility are mentioned in Combes' survey[72], but they are not easily accessible. Two worked with at $MgCl_2$-50 mol. % KCl at 1008K and 853-873K, respectively, whilst the third studied NaCl at 1123K. The solubilities are given as 0.03 mol. %, 0.2 mol. % and 1.6×10^{-7} mol. cm^{-3} respectively.

2.4 I.R. Spectroscopy of HCl and H_2O in Chloride Melts

The infra-red absorption spectra of solutions of HCl in pure molten NaCl, KCl, RbCl, CsCl, $CaCl_2$ and $SrCl_2$ were recorded by Novozhilov, Gribova and Devyatkin[76]. The spectra suggested that the solute molecules are present as monomers in the alkaline-earth metal chlorides, whereas in the alkali-metal chlorides they are associated into complexes of the type Cl-H....Cl^-_{melt}. The stability of this hydrogen bond depends on the salt cation; for the larger, less polarising cations the hydrogen bond is stronger since the Cl^-_{melt} is not as strongly held by the large cations, e.g. Cs^+, as by the smaller cations. From the spectra the energies of the hydrogen bonds in the pure MCl melts were found to increase in the order NaCl (22kJ $mol.^{-1}$) < KCl< RbCl < CsCl (31 kJ $mol.^{-1}$).

Novozhilov et al. stated that in the MCl solutions of HCl are relatively free solute molecules as well as those associated in the Cl-H....Cl^-_{melt} complexes, the proportion of the free molecules decreasing from NaCl to CsCl. This implies that both physical and chemical dissolution processes are occurring.

Work by Mignonsin and Duyckaerts[77] on I.R. absorption by tablets prepared from molten NaCl-KCl eutectic treated with water vapour and sodium hydroxide at 800°C, indicated that OH^- ions were not present. The water solubility was very small, but reactions [2.3] and [2.4] were found to go to

$$H_2O + Cl^- = HCl_{(g)} + OH^- \qquad [2.3]$$

$$OH^- + Cl^- = HCl_{(g)} + O^{2-} \qquad [2.4]$$

completion i.e. only O^{2-} and HCl were detected. Introduction of NaOH was said to give rise to Na_2O and $H_2O_{(g)}$ or O_2^{2-}, Na_2^+ and $H_2O(g)$, depending on the amount added. Novozhilov and Pchelina[78,79], however, studied solutions of water in molten alkali metal chlorides using I.R. spectroscopy, rather than making tablets of treated melt. For molten NaCl + H_2O, two absorption bands were seen which broadened into one band for KCl, RbCl and CsCl. Moving along the series NaCl → CsCl, the band intensity

increased for the same melt temperature, but decreased with rise in temperature for all four metal halides. Novozhilov attributed this behaviour to the formation of hydrogen bonds between the dissolved H_2O molecules and the Cl^- ions of the melt. The strength of the hydrogen bond was found to increase with increasing cation size; said to be due to the availability of "freer chloride ions" in the melts of the larger cations. In addition, as well as dissolved H_2O molecules, it was suggested that OH^- groups are formed in the melts as a result of hydrolysis of the melt (reaction [2.3]). Other species postulated (O_2^-, O^{2-}, O_2^{2-}) could not be investigated since the range of vibrations of the M-O and O-O bonds lie outside the working range of the sapphire windows.

2.5 Electrochemical Studies of HCl in Chloride Melts

Relatively few investigations into the electrochemical behaviour of HCl gas dissolved in chloride melts could be found. Those carried out tended to be on widely used mixtures, like LiCl-KCl and $ZnCl_2$-KCl. Results obtained by the different workers exhibit a fair degree of discrepancy.

The earliest study found was that of Devyatkin and Ukshe [60]. Their chronopotentiometric investigation of HCl dissolved in pure molten LiCl, NaCl, KCl, RbCl and NaCl-KCl mixtures found diffusion coefficients of the order of 10^{-3}-10^4 $cm^2 sec.^{-1}$, decreasing in the order LiCl > NaCl > KCl > RbCl. With rising temperature the diffusion coefficients (D) in the lighter alkali metal chlorides were found to decrease, but in RbCl their values increased. Without a full translation their explanation is not clear but they postulate the existence of $HCl_n^{(n-1)-}$ complexes, which dissociate into H^+ and nCl^- in RbCl, presumably leading to the increase in D_{HCl} values with temperature. In the NaCl-KCl molten mixtures the diffusion coefficients were of the same magnitude as those for the pure salts, but for each mixture an increase in temperature resulted in an increase in the diffusion coefficient. No explanation of the difference in behaviour between the pure melts and the molten mixtures was given in the abridged translation.

Van Norman and Tivers[65] chronopotentiometrically studied the behaviour of HCl in the molten LiCl-KCl eutectic, utilizing a vitreous

carbon working electrode. Having determined the HCl solubility in this melt, values of the diffusion coefficients were found to be $2.4 \pm 0.5 \times 10^{-4}$ cm^2 $sec.^{-1}$ (490°C) and $2.3 \pm 0.5 \times 10^{-4}$ cm^2 $sec.^{-1}$ (570°C). For Cl_2 dissolved in molten chlorides similarly large diffusion coefficients were found, but in that case rationalized in terms of the formation of the trichloride ion, Cl_3^-, and a chain conduction mechanism[80]. A similar explanation for the D_{HCl} results seemed unlikely and Van Norman preferred to invoke the small size of the H^+ ion, formed by dissociation of HCl, as the cause of the high D_{HCl} values.

Minh and Welch, attempting to determine the mechanism of the cathodic reduction of HCl dissolved in LiCl-KCl eutectic, used cyclic voltammetry and chronopotentiometry at platinum[66] and vitreous carbon[81] working electrodes. On the platinum electrode the reduction was found to be a reversible, single-electron charge transfer step, giving a soluble product. Using their own solubility data, D_{HCl} values were of the same magnitude as those in Van Norman's less rigorous study. Minh and Welch also cite the existence of non-solvated protons as the cause of the large diffusion coefficients ($\sim 2 \times 10^{-4}$ cm^2 sec^{-1} at 500°C) and give weight to their assertion with low experimental values of the energy of activation of the diffusion process. Using the vitreous carbon electrode it was determined that the dissolved HCl is "completely dissociated into protons and chloride ions". The evolution of hydrogen was found to proceed via a two-step mechanism; reduction of H^+ to form H atoms followed by atom combination to form H_2, the latter being the slower step. Addition of zinc chloride to the LiCl-KCl melt[70] ($0 < X_{ZnCl_2} < 0.19$) followed by HCl saturation of the melt resulted in a decrease in the values of D_{HCl} compared to those measured in LiCl-KCl. On vitreous carbon the reduction was found to be a reversible, single-electron transfer step forming a soluble product, but on platinum adsorption of the solute species was inferred from the experimental data.

As part of a study of the hydrogen evolution reaction in LiCl-KCl, Kanzaki and Takahashi[82] voltammetrically investigated the behaviour of HCl-saturated LiCl-KCl at 450°C using a platinum working electrode. Their value for the diffusion coefficient of the hydrogen ions is similar

to that of Van Norman and Tivers[65] but "abnormal" adsorption of H^+ ions was observed when the electrode was allowed to stand. The effect was most marked at a gold electrode, but this phenomenon disappeared when the melt was stirred.

The behaviour of HCl in two $ZnCl_2$-KCl eutectic melts has been voltammetrically studied by Perry and MacDonald[83]. On platinum electrodes a reversible, one electron charge transfer process was inferred by the results but the magnitude of the diffusion coefficients ($\sim 10^{-8}$ cm^2 sec^{-1} at 500°C), calculated using the solubility data of Prasolov et al.[69], was much lower than expected, and led Perry to postulate the existence of a complex species in the melt. No indication of the nature of this species was given, though.

2.6 Water in Chloride Melts

For a compound that is so deleterious to molten salts, it is interesting to see how much work has been done on the behaviour and effect of water in these liquids. For example, at least six chapters are devoted to the subject in the book "Ionic Liquids" (1981)[84], listing several hundred references for work done with various media. Whilst nitrate melts have received most attention, the hydrolysis of molten and solid halides has been studied for a long time, the earliest reference found by this author having been published in 1922[85].

Solute water is a very reactive compound. Its properties interfere in several practical situations, such as corrosion of materials in the presence of melts and chemical transformations of either the solvent melt (hydrolysis), or of other solutes present. Included in the field of molten salts are liquids known as "molten salt hydrates". These solutions, melting at temperatures close to room temperature, are formed using hydrated salts such as $MgCl_2.6H_2O$ or $CaCl_2.6H_2O$. Much of the work on these systems has been carried out by Duffy and co-workers[86], who have looked at the acid-base behaviour of the solvents and the co-ordination behaviour of solutes within these very concentrated aqueous solutions.

With so many good reviews in existence[84], it is not necessary to attempt to cover every aspect of the field of water-containing molten salts here. One may approach from various angles; for example, by looking at the corrosive effects of aqueous contamination in molten salts, the industrial consequences of the same contamination or perhaps the solution chemistry of water and species that may be evolved within these molten solvents. More detail can be found in the reviews mentioned earlier. Elsewhere in this study, the solubility and I.R. spectroscopic studies of water in molten chlorides have been covered, (Sections 2.3 and 2.4 respectively), and a small review of melt purification techniques appears in the Section 4.1. In the next few pages, the electrochemical behaviour of water in a few chloride melts will be summarized.

2.6.1 Electrochemical Studies of H_2O in Chloride Melts

Some of the first work carried out on the electrochemical reduction of water in LiCl-KCl melts was by Laitinen et al.[74] and Delarue[87] who were in disagreement over the existence of a voltammetric wave for the reaction:

$$OH^- + e^- = O^{2-} + \tfrac{1}{2}H_2 \qquad [2.5]$$

More recently, an investigation of the hydrogen evolution reactions of H^+, H_2O and OH^- at a platinum electrode in molten LiCl-KCl[82] (450°C) showed all reactions to be reversible with a one-electron transfer process for each reaction. The electron transfer step for the evolution of hydrogen from water was assumed to be:

$$H_2O + e^- \rightarrow H + OH^- \qquad [2.6]$$

Without knowledge of the dissociation rate of water molecules into H^+ and OH^-, the workers hesitated to include the possibility of electron transfer to H^+ ions as a way of producing hydrogen.

Melendres et al.[88] also voltammetrically studied the behaviour of water in molten LiCl-KCl eutectic at 390°C, and observed two reversible

reduction peaks using platinum electrodes at $E_{\frac{1}{2}}$ of about 1.61V and 0.47V versus a LiAl reference electrode. These peaks were attributed to one electron transfer to H_2O and OH^- respectively. Values for D_{H_2O} obtained by this method averaged to $3.1 \pm 0.5 \times 10^{-5}$ $cm^2 sec.^{-1}$ at 390°C. After this work was carried out, Lysy and Combes[89] determined the equilibrium constants for the following reactions in molten LiCl-KCl eutectic:

$$2OH^- = O^{2-} + H_2O \quad (K_1) \qquad [2.7]$$

$$H_2O + 2Cl^- = O^{2-} + 2HCl \quad (K_2). \qquad [2.8]$$

Over the temperature range 642-742°C the constants were given by:

$$\log K_1 = 7.86 - 7.68 \times 10^3/T$$

$$\log K_2 = 2.29 - 10.03 \times 10^3/T.$$

The effect of moisture on the reduction of K_2CrO_4 and on the Cr(III)/Cr(II) electrode reaction in molten LiCl-KCl eutectic at 450° has been investigated by Uchida et al.[90,91]. In dry melts the reduction of chromate was found to involve consecutive electron transfer steps followed by a chemical reaction:

$$CrO_4^{2-} \xrightarrow{+2e^-} CrO_4^{4-} \xrightarrow{+e^-} CrO_4^{5-} \rightarrow CrO_3^{3-} + O^{2-} \qquad [2.9]$$

However, in the wet melt, the overall reduction process was found to be:

$$CrO_4^{2-} + 3e^- + 2H_2O \xrightarrow{Li^+} LiCrO_{2(s)} + 4OH^- \qquad [2.10]$$

Solutions of Cr^{3+} in LiCl-KCl eutectic at 450°C were found to undergo hydrolysis to form $[CrCl_5(OH)]^{3-}$, but raising the melt temperature caused a decrease in the extent of the hydrolytic reaction. A polymerization reaction to form $[CrCl_5\text{-}O\text{-}CrCl_5]^{6-}$ was invoked to explain the decrease in the current ratio, i_a/i_c, with decrease in voltammetric scan rate.

The reduction of water on platinum and gold electrodes in molten LiCl-KCl-CsCl at 300°C has been investigated voltammetrically[92], and

hydrogen atom adsorption processes were invoked to explain the presence of pre-peaks on the voltammograms. The phenomenon of adsorption of hydrogen atoms on metal electrodes appears to be quite sporadic: Minh and Welch observed it in LiCl-KCl-$ZnCl_2$[70] with HCl as the solute, but not in LiCl-KCl[66]. It is often observed in aqueous solutions, however, and White et al.[92] drew analogies with aqueous systems for their work in LiCl-KCl-CsCl.

Much of the work on NaCl-KCl systems has been carried out by Combes, Tremillon et al.[93-96], who have been concerned with the behaviour of stabilized zirconia electrodes in these solvents, using them to monitor the effect of addition of oxy-species to the melts. For reactions [2.7] and [2.8]given previously, the equilibrium constants in NaCl-KCl (1:1) over the temperature range 700-1000^{o}C were given by:

$$\log K_1 = 6.75 - 8.15 \times 10^3/T$$

$$\log K_2 = 40.2 - 55.3 \times 10^3/T$$

Comparing these results with those for LiCl-KCl at the same temperature, Lysy and Combes[89] point out that OH^- ions are about forty times more dissociated (i.e. into O^{2-} and H_2O) in LiCl-KCl than in NaCl-KCl (670-770^{o}C). Water behaves as a weaker oxoacid and a stronger oxobase in LiCl-KCl than in NaCl-KCl, a fact explained by Burkhard and Corbett[73] and Combes et al. as being due to the stronger acidity of Li^+ compared to Na^+, the KCl merely acting as a physical diluent.

By changing the partial pressures of HCl, H_2 and O_2 above molten NaCl-KCl (1:1) at 700^{o}C, or adding Na_2O, Littlewood and Argent[97] could look at the behaviour of the individual dissociation and hydrolysis products found in melts contaminated by water. Changes in O_2 partial pressure did not affect the activity of O^{2-} ions, but the H^+ activity did alter when the hydrogen partial pressure was changed.

The effects of moisture in $CaCl_2$-KCl (73:27 mol. %) at 700^{o}C were studied voltammetrically and potentiometrically by Brookes and Inman[98].

A series of redox and chemical equilibria were used to explain the results, with the assumption that the peroxide ion is stable in the melt. Additions of O^{2-}, O_2^{2-}, $O_{2(g)}$, H_2O and OH^- were made, the hydroxide and moisture apparently being rapidly converted to oxide in the melt.

The addition of moisture to molten $AlCl_3$-BuPyCl[99] resulted in the formation of HCl, which could be reduced electrochemically to H_2, and either $AlOCl_2^-$ or $AlOHCl_2$. The authors were unable to distinguish whether the oxy- or hydroxy- chloride were present, but Tremillon et al.[100] using $AlCl_3$-NaCl melts determined that O^{2-} ions were solvated in the forms $AlOCl_2^-$ and AlOCl in chlorobasic and chloroacidic melts, respectively.

Equilibrium constants for the reactions [2.7] and [2.8] were determined experimentally in molten NaCl-$ZnCl_2$ at 360°C, using yttria-stabilised zirconia as the oxide-sensitive electrode, by Ito et al.[101]. The values of the constants were $K_1 = 6.4 \times 10^{-1}$ (atm) and $K_2 = 1.91 \times 10^{-7}$ (atm). It can be seen that the value for the hydrolysis reaction, [2.8], is surprisingly low, indicating that the melt is relatively stable in the presence of water. This fits in well with work carried out by Gorre and Pastor[102], who found that above 90°C anhydrous $ZnCl_2$ is not deliquescent if the water vapour pressure is less than 10mm Hg. Neutron diffraction studies[103] of pure $ZnCl_2$ melts show that H_2O molecules only enter the first co-ordination sphere of zinc at relatively high H_2O:Cl^- ratios (2:1). This information indicates that the extent of hydrolysis of zinc chloride melts in the presence of water is actually fairly small.

2.7 Electrochemical Studies in Zinc Chloride Melts

Two chronopotentiometric investigations[104,105] of the solubility of zinc metal in molten zinc chloride both indicated that the solubility was very low, as shown in Table 2.2.

Temp/^{o}C	Solubility/mol. %	Reference
500	0.019	104
525	0.187	105
600	0.326	105
702	1.30	106
777	2.40	106

TABLE 2.2

Solubilities of Zinc Metal in Molten Zinc Chloride

As seen, the chronopotentiometric results seem to fit in with those of Bombi et al.[106] who dissolved their samples in standard aqueous iodine solution and determined the decrease of the iodine concentration. Both chronopotentiometric studies inferred interactions of the form:

$$Zn + ZnCl_2 = Zn_2Cl_2 \qquad [2.11]$$

with the formation of the Zn_2^{2+} ion. Formation of the Zn^{+} ion was ruled out by both groups, who went on to give values of diffusion coefficients for the Zn_2^{2+} species of the order of 10^{-5}-10^{-6} cm^2 $sec.^{-1}$. Interestingly, the third group, using chemical means, could only explain their results by assuming the existence of Zn^{+}.

The behaviour of $ZnCl_2$ in LiCl-KCl eutectic was studied voltammetrically[107] at 390^{o}C and 450^{o}C to take account of the fact that zinc could deposit as a solid or a liquid (m.pt. 419^{o}C). A limiting current plateau was seen on the polarogram for Zn deposition above 419^{o}C, but below this temperature no such plateau was observed. Problems occurred with the platinum electrode, however, when the solvent decomposition limits were reached, since alloy formation between Zn and Pt seemed to be occurring, and the Pt electrode dissolved before chlorine was evolved. Much later, work by Taoumi et al.[108] gave evidence of the presence of chlorozincate complexes in molten NaCl-KCl (1:1) at 700^{o}C.

The diffusion coefficient determined for Zn^{2+} ions in this solvent was 3.2 x 10^{-5} cm^2 sec^{-1}, the Zn/Zn^{2+} couple being reversible on both liquid zinc and tungsten micro-electrodes, with a diffusion-controlled two-electron charge transfer process. Some evidence was put forward for the reduction process involving adsorption of Zn^{2+} ions onto the electrode surface and a three-stage mechanism for the reduction was proposed.

The deposition of zinc from melts of $ZnCl_2$-LiCl-KCl has been studied by Koziol and Sadoway[109], who recorded the electrolyte flow patterns during the electrodeposition using a laser Schlieren technique. This method detects variations in the refractive index of the electrolyte, which are interpreted as changes in the fluid density or composition. By changing the orientation of the anode and cathode, dendrite formation could be controlled to prevent "shorting out" of the system. This was explained by discussing the changes in the concentration of zinc in the melt, and hence changes in the melt density and the effect on the convective flow of the electrolyte.

Using platinum and glassy carbon electrodes, the electrochemical decomposition of $ZnCl_2$ from $ZnCl_2$-LiCl-KCl and pure molten $ZnCl_2$ was investigated voltammetrically by Susic and Mentus[110]. The glassy carbon electrode proved to be inert and was used to determine the "electrochemical windows" of the melts. The platinum electrode, however, underwent anodic dissolution and passivation, forming a layer of $PtCl_2$, before the chlorine evolution reaction could occur. At cathodic potentials it was found that zinc-platinum alloys, of which several are known, would form, with any non-alloyed zinc separating as a powder. This behaviour ties in with the earlier work mentioned on $ZnCl_2$-LiCl-KCl[107], and the anodic formation of $PtCl_2$ in other chloride melts[110,111]. The electrochemical oxidation of Pt, Ni, Mo and W in $ZnCl_2$-KCl (49-51 mol.%) at 260 and 350°C investigated by Rubel and Gross[111], who compared the behaviour found in that solvent with that of the same metals in AgCl-KCl melts. Platinum could be oxidised to form a layer of $PtCl_2$ in both melts, whilst a Zn-Pt alloy formed at relatively cathodic potentials. The anodic dissolution of nickel and molybdenum formed Ni^{2+} and Mo^{3+} in both melts, and these metals could be deposited from their solutions. In AgCl-KCl

tungsten dissolved to form the W^{3+} oxidation state but formed the W^{6+} state in $ZnCl_2$-KCl, which was thought to have been stabilized as an oxychloro-complex arising from contamination of the melt. Tungsten metal could be electro-deposited, however. For the tungsten and molybdenum electrodes, the electrochemical corrosion was ten times greater in the $ZnCl_2$ melt than in the AgCl melt, indicating that users of tungsten as an inert electrode material should be cautious when dealing with some chloride melts.

The behaviour of the sodium Pyrex glass electrode in molten $ZnCl_2$-NaCl[112] (340-500°C) has also been determined. Its reversibility and responsivity to Na^+ ions were demonstrated, the activation energy for the conduction process being of the same magnitude as that usually found for small-ion conduction in glass (~ 88 kJ $mol.^{-1}$). Quantitive electrodeposition of sodium from the glass into indium confirmed that conduction through the glass is via sodium ions.

2.8 Solute Studies in Zinc Chloride Melts

The adopted co-ordination states of 3d ions in molten chlorides are the result of factors such as the formal charge of the 3d ion, the octahedral site preference energy and the polarizing power of the cations in the bulk solvent[113]. Octahedral co-ordination is favoured by highly charged 3d ions in molten chlorides whose cations are also highly charged with small radii. However, by varying the temperature and solvent composition, all of the M^{2+} and some of the M^{3+} 3d ions can be made to undergo octahedral-tetrahedral transformations. M^{2+} 3d ions are tetrahedrally co-ordinated in alkali chloride melts[114] but are octahedrally co-ordinated in molten aluminium chloride[115]. The explanation put forward for this is as follows. The alkali metal cations have low polarizing powers compared to the aluminium cations, which are far more strongly polarizing. As a result of this, the Cl^- ions in the molten alkali chlorides have much higher negative charge densities than those in the molten $AlCl_3$. The greater electrostatic repulsion forces, in the alkali chlorides, between nearest neighbour chloride ions surrounding a 3d ion favour low (four) rather than high (six) co-ordination numbers. Octahedral co-ordination is possible in molten $AlCl_3$ presumably because

the reduction of the negative charge density on the Cl^- ions by the Al^{3+} cation causes a decrease in the electrostatic repulsion forces between the Cl^- ions, allowing them to adopt the higher co-ordination number around the 3d cation. These effects can be modified by mixing the two types of chloride solvents, so that tetrahedral-octahedral equilibria can be set up. The position of these equilibria may be altered by varying the solvent composition, as is discussed below.

For a good review of the work carried out on the behaviour of transition metal ions in chloride melts up to 1963, the paper of Gruen and McBeth[114] is recommended, but LiCl-KCl melts were the solvents used by most of the workers, and little had been carried out specifically in $ZnCl_2$ melts. The VCl_4^{2-} ion was shown to exist in a distorted tetrahedral configuration in $ZnCl_2$-CsCl (33-67 mol. %) at 900°C, whilst much of the other work used crystal spectra of transition metal ions held within the Cs_2ZnCl_4 host lattice.

The spectroscopic and co-ordination behaviour of Ni^{2+} ions "have studied" in $ZnCl_2$-KCl and $ZnCl_2$-CsCl molten mixtures. Ni^{2+} in $ZnCl_2$-KCl[116] (250-900°C) was found to exist in a two-species equilibrium involving the Ni^{2+} in octahedral and distorted tetrahedral sites, with a "continuous distortion mechanism" responsible for transformation between the two extremes. Two of a series of papers by Smith et al.[117-120] on the behaviour of Ni^{2+} in chloride melts looked at the co-ordination of Ni^{2+} in molten $ZnCl_2$-CsCl melts, at temperatures between 260-1000°C and for the full composition range[117]. An equilibrium between octahedral and tetrahedral centres occurred between 0-8 mol. % CsCl, the octahedral form being favoured with increasing CsCl content. Between 20-50 mol. % CsCl a different octahedral-tetrahedral pair occurred, this time with the tetrahedral form favoured by increasing CsCl content and temperature. The tetrahedral form was predominant in CsCl-rich melts, with species such as $Cl_3NiClZnCl_3^{3-}$ and $NiCl_4^{2-}$. A polarographic study[121] of Ni^{2+} in molten $ZnCl_2$-NaCl-KCl (41-33-26 mol. %) has been carried out, but whilst the authors carefully described the methods used, they neglected to give many results, other than to say that the reduction process involved a two-electron transfer which exhibited "certain deviations" from

reversibility.

Absorption spectra of Co^{2+} in $ZnCl_2$-$AlCl_3$[113] molten mixtures showed that increasing temperature favours the formation of tetrahedrally co-ordinated Co^{2+} from octahedral Co^{2+} via an octahedral-tetrahedral equilibrium similar to that of Ni^{2+} in $ZnCl_2$-KCl[116]. However, in $ZnCl_2$-KCl melts, Co^{2+} exhibited tetrahedral co-ordination over the whole composition range[113]. The difference between the two systems was thought to arise from the strong competition between the Al^{3+} and Zn^{2+} cations for the available chloride ions. $CoCl_2$, which can be precipitated out of $AlCl_3$-KCl melts, was not seen in the $ZnCl_2$-$AlCl_3$ melts. It was suggested that Zn^{2+} and Al^{3+} are similar in their complexing power with respect to Cl^-. With the absence of any well characterized compounds in the $ZnCl_2$-$AlCl_3$ system (c.f. $NaAlCl_4$ in NaCl-$AlCl_3$), discrete complex chloroaluminate species are unlikely to exist in these molten mixtures. The same conclusion was reached by Begun et al.[122] in their Raman study of the $AlCl_3$-$ZnCl_2$ system.

Duffy et al.[123,124] have carried out a lot of work on the behaviour of metal cations in zinc chloride hydrate melts. These "melts", elsewhere termed "ionic liquids", are composed of $ZnCl_2$ and water, with salt: water ratios ranging from 1:3 to 1:108. The "silica-type" structure of $ZnCl_2$ is only partially disrupted by water, and even in dilute solution fragments of the $Zn(\mu\text{-}Cl)_2\,Zn$ structure remain[124]. The consequence of this can be seen on addition of metal cations to the $ZnCl_2$-H_2O ionic liquids. In aqueous solution, Co^{2+} exists as the pink $[Co(H_2O)_6]^{2+}$ complex, and addition of chloride ions converts this to the blue $[CoCl_4]^{2-}$ complex, the H_2O ligands being gradually replaced by Cl^-. This is the case for systems such as $CaCl_2.12H_2O$, but for the $ZnCl_2$-H_2O system the Co^{2+} remains octahedrally co-ordinated even for the mixture $ZnCl_2.3H_2O$[23]. Virtually no $[CoCl_4]^{2-}$ complexes are produced, suggesting that there are insufficient Cl^- ions for complexation with the Co^{2+}. Any chloride co-ordinating to solute metal ions was found to be part of a chlorozincate group. The same group have also looked at the behaviour of Tl^+, Pb^{2+}, Ni^{2+}, VO^{2+} and Fe^{3+} in these ionic liquids and found the same effect as seen for Co^{2+}.

The reduction of K_2CrO_4 in equimolar $ZnCl_2$-KCl at 300°C was found to occur as a single, irreversible, diffusion-controlled step yielding an insoluble electrode deposit that had the general form $K_xZn_yCrO_z$ [125]. The values of x, y and z depended upon the conditions of the electrolysis. In LiCl-KCl containing $ZnCl_2$, a similar product $LiZn_2CrO_4$ was found, except this remained stoichiometric over a wide range of conditions. In both cases a Cr^{4+} species, CrO_4^{4-}, was postulated to be the transitory intermediate. In $ZnCl_2$-KCl it was found that the Cr^{4+} was sufficiently stable so as to prevent complete reduction to Cr^{3+} unless high current densities were used.

The same authors [125(1)-(3)] investigated the behaviour of $HgCl_2$ and $CdCl_2$ in the $ZnCl_2$-KCl solvent. The reduction of Hg^{2+} involved a reversible, two-electron process; no evidence was observed for the formation of Hg^{+}. A diffusion coefficient of 2.17×10^{-6} cm^2 $sec.^{-1}$ was found for $HgCl_4^{2-}$ at 300°C. Strong adsorption of Hg on the Pt cathode was observed, and further complications arose from the reaction of metallic mercury with the electrode to form $PtHg_4$. The reduction of $CdCl_2$, however, involved a two-step process; the first being a two-electron transfer to form Cd_2^{2+}, the second an ill-defined process with a chemical reaction between Cd and Cd^{2+} to form Cd_2^{2+} coupled to the reduction mechanism.

Voltammetric studies of a wide range of solute species in molten $ZnCl_2$-NaCl-KCl (60-20-20 mol. %) have been carried out by Topol et al. [126]. Various oxidation states of silver, copper, nickel, bismuth, antimony, chromium and iron were stable within the voltammetric range of the solvent. The study is quite exhaustive, over 200 pages in length, and goes on to compare the behaviour in the $ZnCl_2$ solvent with that seen in $AlCl_3$-NaCl and NaOH-KOH melts. The electrochemical reactions of Fe^{3+}/Fe^{2+}, Fe^{2+}/Fe and Cr^{3+}/Cr^{2+} in molten $ZnCl_2$-NaCl eutectic have also been investigated [127]. The diffusion coefficients of Cr^{3+} and Fe^{3+} ions at 300°C were 1.7×10^{-6} and 1.2×10^{-6} cm^2 $sec.^{-1}$ respectively. Both were found to increase with temperature, the voltammetry having been carried out with Pt and W electrodes.

Studies[128,129] of oxidation states of bismuth in $ZnCl_2$-KCl and $AlCl_3$-NaCl molten mixtures, carried out by adding $BiCl_3$ to the melts, showed that Bi^+ and $[Bi_5]^{3+}$ entities existed in both melts but $[Bi_8]^{2+}$ was present only in the chloroaluminate melt. No information on the ligands attached to these three species was obtainable, and hence the molecular units and overall charges of the $[Bi_n^{m+}$ + ligands] systems were unknown.

Voltammetric studies of Cr^{2+}, Ga^{3+} and Ti^{3+} in molten $ZnCl_2$-MCl (M = Na, K) were carried out by Carthey[1]. In acidic molten mixtures an electrode deposit of pure $CrCl_3$ was obtained, and in the same melt compositions the Ga^+ state could be stabilised. However, as the melts were made more basic the Ga^+ disproportionated to Ga^{3+} and gallium metal, which could be co-deposited with zinc. Oxidation of Ti^{3+} to Ti^{4+} caused the formation of $TiCl_4$ which was lost from the electrode surface as bubbles.

CHAPTER 3

EXPERIMENTAL

3.1 Melt Purification

A rigorous purification procedure is required to remove hydrolysis products and water, as well as any trace heavy metal impurities. The zinc chloride used was purified by vacuum drying, bubbling with dry hydrogen chloride gas and pre-electrolysis followed by vacuum filtration.

The apparatus used, mainly constructed from Pyrex glass, is shown in Figure 3.1. All glassware that was to come into contact with the melt was kept in a 1:1 mixture of concentrated sulphuric and nitric acids for 24 hours, washed with distilled water and dried overnight at 150^{o}C. AnalaR zinc chloride (500g) was placed in the inner tube of the system and vacuum-dried at room temperature for 4-5 days until the pressure fell to about 5 x 10^{-3} torr. A gradual increase in temperature to 250^{o}C was carried out over several days until the pressure returned to its level at room temperature. Hydrogen chloride gas, dried over activated charcoal and AW500 molecular sieve, was passed over the solid salt and the temperature raised to 350^{o}C, by which time the zinc chloride was molten. HCl gas was vigorously bubbled through the melt for five hours, followed by dry argon for five hours to purge the melt of the HCl dissolved in it. The effect of bubbling HCl gas was to produce water on the cell cap, and the bubbling was continued until this condensation was swept from the system.

Following the argon purge, a stainless steel cathode and a graphite anode were inserted into the melt via two of the SQ13 vacuum seals on the cell cap. The pre-electrolysis was carried out overnight, with an applied potential of 1.6V, during which time the current dropped to about 0.3mA. Problems could occur with condensation of the volatile zinc chloride blocking the gas outlet tube, and care had to be taken to ensure that this did not occur. Holding the system under a positive argon pressure went some way to eliminating this trouble.

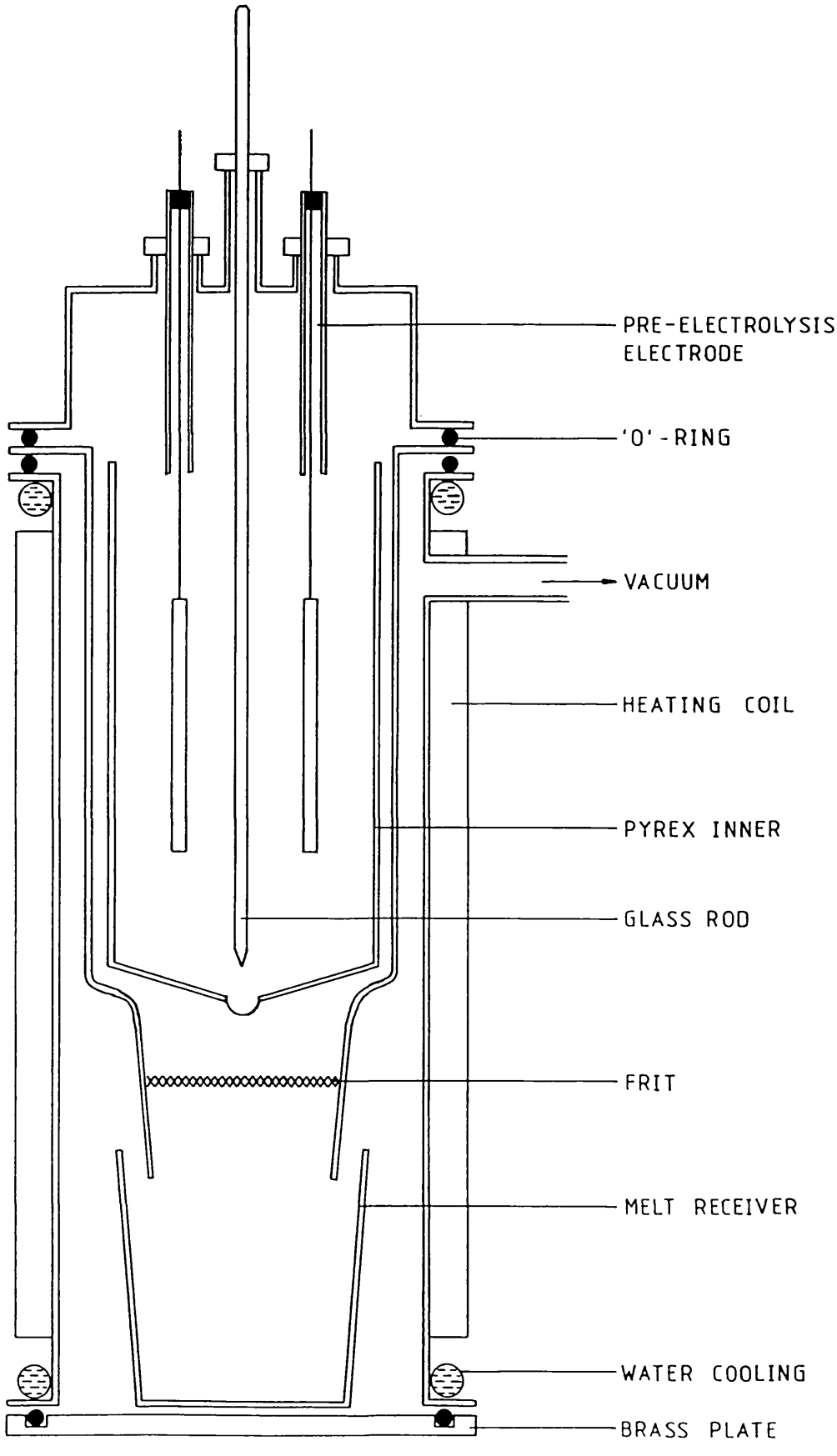


FIGURE 3.1: Melt Purification Apparatus

The melt was again purged with argon gas for a further thirty minutes and then, by breaking the thin glass bubble at the bottom of the melt container, filtered through a Pyrex No. 2 glass frit. Applying a vacuum to the bottom part of the system served to draw the melt through the frit more quickly, application of a positive argon pressure to the top of the cell having the same effect. The melt was collected in a Pyrex beaker and cooled. The solid was transferred to an argon-filled dry box, broken into lumps and stored in a glass bottle.

The sodium chloride used was prepared simply by vacuum drying 300g samples up to a temperature of 400^{o}C, and then storing it in the dry-box. The required melt compositions could then be produced by mixing the solids, rather than by the alternative method of making the solid mixture from impure components and then purifying that. Melts produced in this way were invariably clear liquids, but suffered from contamination by black flecks of carbon.

3.2 Furnace and Temperature Control

Two furnaces were used for the various experiments described here. For much of the work a Grant 400^{o}C aluminium block heater, into which the electrochemical cell (Section 3.5) could be snugly fitted, was used. The temperature here was monitored with a chromel-alumel thermocouple in the melt, since the temperature dial on the front of the heater only gave a rough guide to the block temperature.

A larger diameter furnace was required for the HCl solubility work (Section 3.7) and this was constructed using a 6.7cm diameter alumina tube, wound with 18 s.w.g. Kanthal wire, which was held vertically in a thermally insulated "Sindanyo" box. The furnace temperature was controlled with a PID/SCR.25A. Eurotherm unit and monitored with a Pt/Pt-13%Rh thermocouple located next to the furnace tube, within the hot zone. The hot zone was roughly determined by holding the furnace at one setting on the Eurotherm, and measuring the temperature inside the furnace from the top to

the bottom using a chromel-alumel thermocouple. Cell temperature was measured with a chromel-alumel thermocouple, and could be controlled to about $\pm 2^{o}C$.

3.3 Vacuum and Gas Supply System

A combined gas and vacuum glass line was used for the melt purification and the electrochemical cell. Evacuation was carried out with an Edwards ED200 rotary pump, the pressures inside the system being monitored with a mercury manometer and an Edwards GSC-2 Pirani gauge. High purity argon could be introduced into the cell, and controlled by means of a needle valve. It was further dried by passing it over molecular sieves.

Two types of grease were used. For taps and ball-joints that would come in contact with corrosive gases such as HCl, "Voltalef 90" grease was used. For most of the taps in the vacuum line, through which only argon would be passed, a high-vacuum grease such as Apiezon 'T' grease was more suitable.

3.4 Electrodes

Various electrodes were made to be used in the electrochemical operations. The melt purification electrodes were simply constructed by attaching lengths of graphite and stainless steel rods (10 cm, 0.5 cm dia.) to thin stainless steel rods (1m, 0.1 cm dia.) and fixing glass sheaths (0.6 cm o.d., Pyrex) to the other ends of the electrodes so that they could be held in SQ13 vacuum seals. The other electrodes used will be described in turn, with corresponding diagrams.

3.4.1 Platinum electrodes

Four types of platinum electrode were used during the various experiments; platinum wire, disc, flag and reference electrodes. For the wire electrode, Figure 3.2.1, a length of platinum wire (2 cm, 0.5mm dia.) was spot-welded to a length of copper wire, and a thin sleeve of glass was

sealed onto the section of platinum near the copper. This sleeve was then sealed inside a Pyrex tube (0.6 cm o.d.) so that about 1 cm of wire was left exposed below the seal. The electrode was filled with argon and sealed with epoxy resin. The flag electrode was made by spot-welding a piece of platinum foil (approximately 1 cm x 1 cm) to a wire electrode. These electrodes were cleaned either by flame-polishing or by treatment in concentrated hydrochloric acid.

The platinum disc electrode was made in the same way as the tungsten electrode (Section 3.4.2) with a length of platinum rod (1.5 cm, 0.15 cm dia.) being used. The platinum rod was joined to a short length of platinum wire, which was spot-welded to the copper wire. Before use the end of the electrode was polished with a 1 μ diamond polishing solution until the metal had a mirror-like surface.

The reference electrode used the same glassware as that used in the silver/silver chloride reference electrode (Section 3.4.5), but a platinum wire electrode was constructed at the end of the glass tube, instead of the glass bulb. Again copper wire was used to make electrical contact, and the electrode was sealed under argon.

3.4.2 Tungsten electrode (Figure 3.2.2)

A length of tungsten rod (2 cm, 0.15 cm dia.) was spot-welded to copper wire, as for the platinum wire electrode, but the whole of the tungsten was then sealed into a thin sleeve of glass. This was sealed into the end of a Pyrex glass tube (0.6 cm o.d.) and the electrode filled with argon and sealed with epoxy resin. Before use the end of the electrode was polished, first with differing grades of silicon carbide paper and finally with 1μ diamond polishing solution, to a mirror-like finish.

3.4.3 Vitreous carbon electrode (Figure 3.2.3)

The construction of this was similar to the tungsten electrode. A length of vitreous carbon rod (2 cm, 0.3 cm dia.) was vacuum-sealed into

Pyrex tube (0.6 cm o.d.). Stiff copper wire was pressed against the end of the vitreous carbon inside the glass tube, and a layer of graphite powder added to provide good electrical contact between the copper and vitreous carbon. The electrode was sealed as before and the end polished with the diamond polishing solution.

3.4.4 Graphite electrode (Figure 3.2.4)

This consisted of a Pyrex tube (0.6 cm o.d.) with a fritted compartment at one end, into which a graphite rod (0.3 cm dia.) could be inserted. The purpose of the fritted compartment was to ensure that any reaction products formed at the graphite electrode could not mix with the bulk melt, and so change its properties. At the other end the electrode was sealed by means of a glass tube (0.8 cm o.d.) with a SQ13 vacuum seal at each end. One vacuum seal was fitted over the Pyrex tube, the other, with a silicone rubber washer inside, was fitted over the end of the graphite rod. This meant that the graphite rods could be changed in the event of breakage. Electrical contact was made directly to the graphite rod.

3.4.5 Silver/Silver Chloride electrode (Figure 3.2.5)

A length of Pyrex tube (30 cm, 0.8 cm o.d.) was fitted with a SQ 10/19 ground glass joint in the middle, and had a thin bulb blown at one end, into which the silver chloride - containing mixture could be placed. The mixture used was 0.4m AgCl in LiCl-NaCl-KCl eutectic. A silver wire was dipped into the powder and the electrode filled with argon and sealed. The purpose of the ground glass joint was to allow a fritted compartment to be easily fitted, using a P.T.F.E. sleeve to prevent jamming. This meant that the environment around the electrode remained constant, and that should the electrode happen to fall to the bottom of the cell, there was a good chance that the bulb would not break. The same design was used on occasion with the platinum quasi-reference electrode.

The silver chloride electrode was not used extensively however, because the platinum q.r.e. was found to hold a reasonably stable potential in the melts and was much easier to use since it was more durable. The bulb

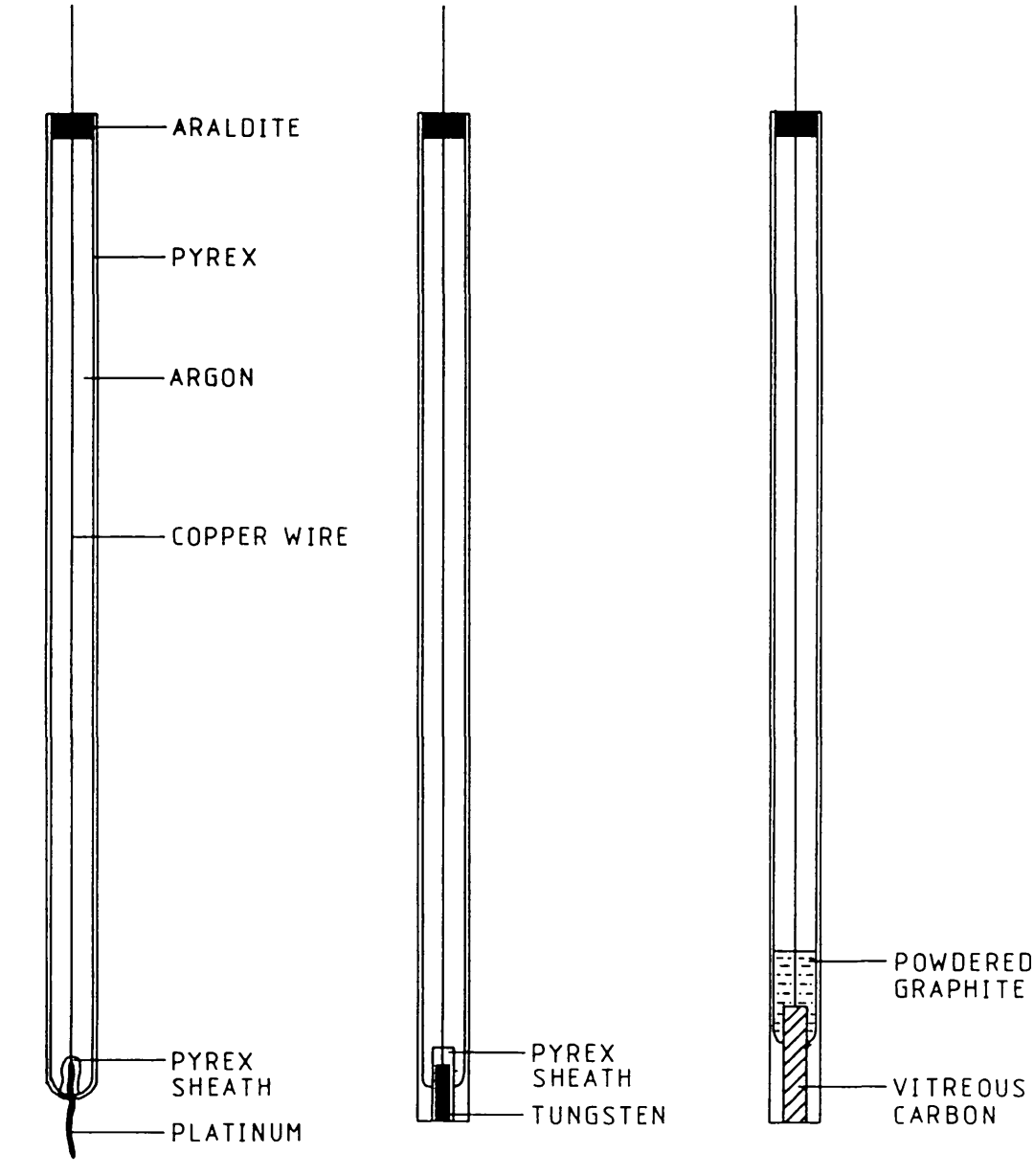


FIGURE 3.2

Electrodes

(continued ...)

(continuation ...)

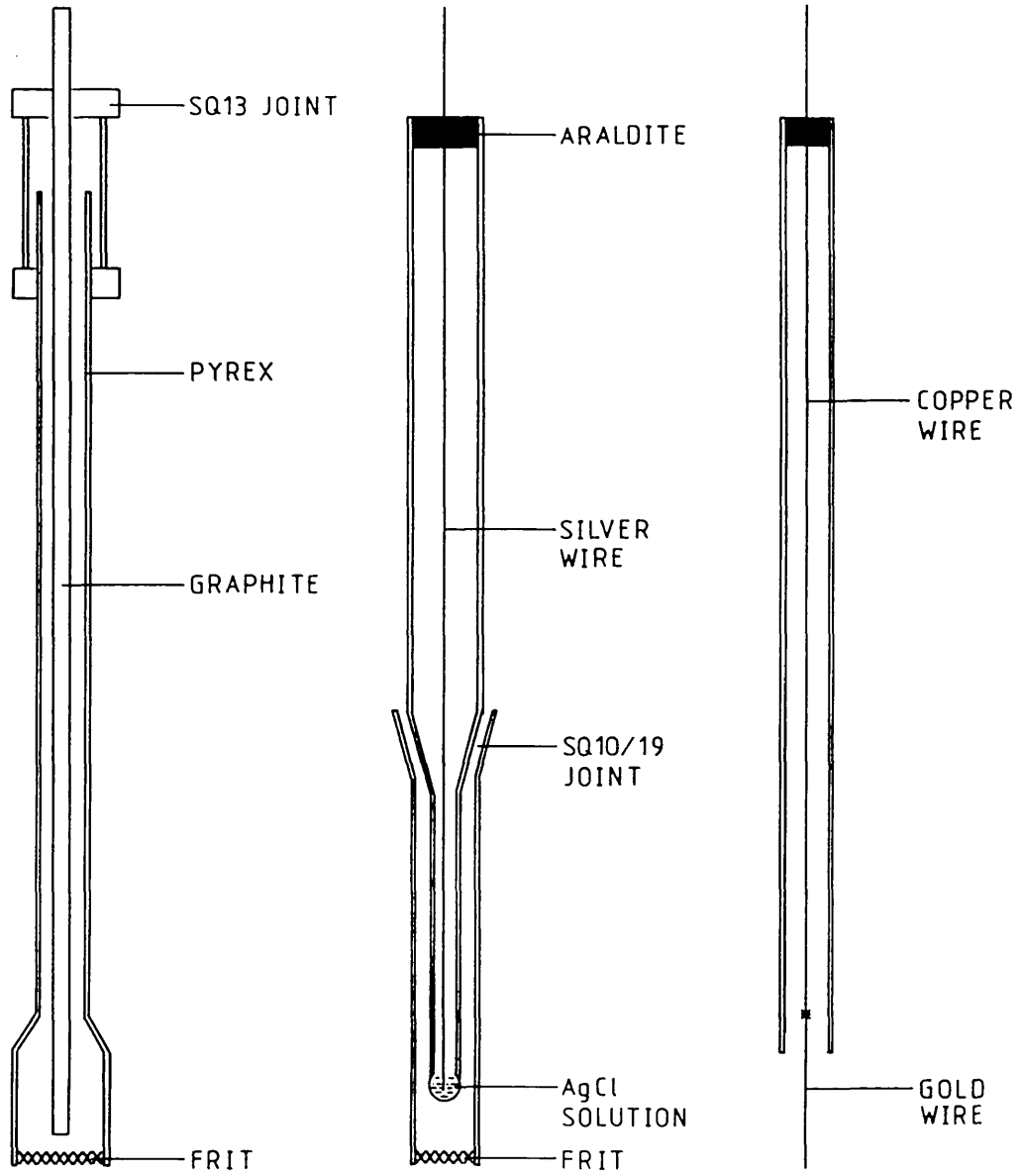


FIGURE 3.2

Electrodes

on the silver electrode, even though protected in the fritted compartment, often broke after 2 or 3 experiments. This may well have been due to thermal shock effects on the glass membrane, or the melt in the compartment cracking the glass as it solidified. Once a bulb had broken, the electrode was useless and the melt was contaminated with small amounts of silver and alkali metal cations.

3.4.6 Gold electrode (Figure 3.2.6)

A length of gold wire (4 cm, 0.25 mm dia.) was joined to copper wire by winding the two together to make a continuous length. This was placed inside a length of Pyrex tube (40 cm, 0.6 cm o.d.) so that the gold wire protruded from one end, the copper wire from the other. The electrode was sealed at one end with epoxy resin, holding the copper wire in place and allowing electrical contact to be made to the copper. The end at which the gold wire protruded was not sealed, so care had to be taken not to push the electrode all the way into the melt.

3.5 Electrochemical Cell

Previous workers in the research group had often used large, cumbersome electrochemical cells, since most of the studies were of electroplating of metals from molten salt solutions which required more melt volume. For this work, however, it was decided that a smaller cell could be used, which would fit in the Grant aluminium block heater (Section 3.2). The cell, shown in Figure 3.3, was made up of a flat-bottomed Pyrex glass beaker, (12 cm long, 5 cm o.d.), which was fitted with a 5 cm glass flange on the top. The Pyrex melt container would fit snugly inside the outer jacket.

The cell-head, again made of Pyrex, had a matching 5 cm flange fitted, the two flanges being separated by a P.T.F.E. washer when the cell was in use. On opposite sides of the cell head were two spherical ball-joints to act as inlet and outlet for gases. Incorporated into the top of the cell head were three SQ13 and one

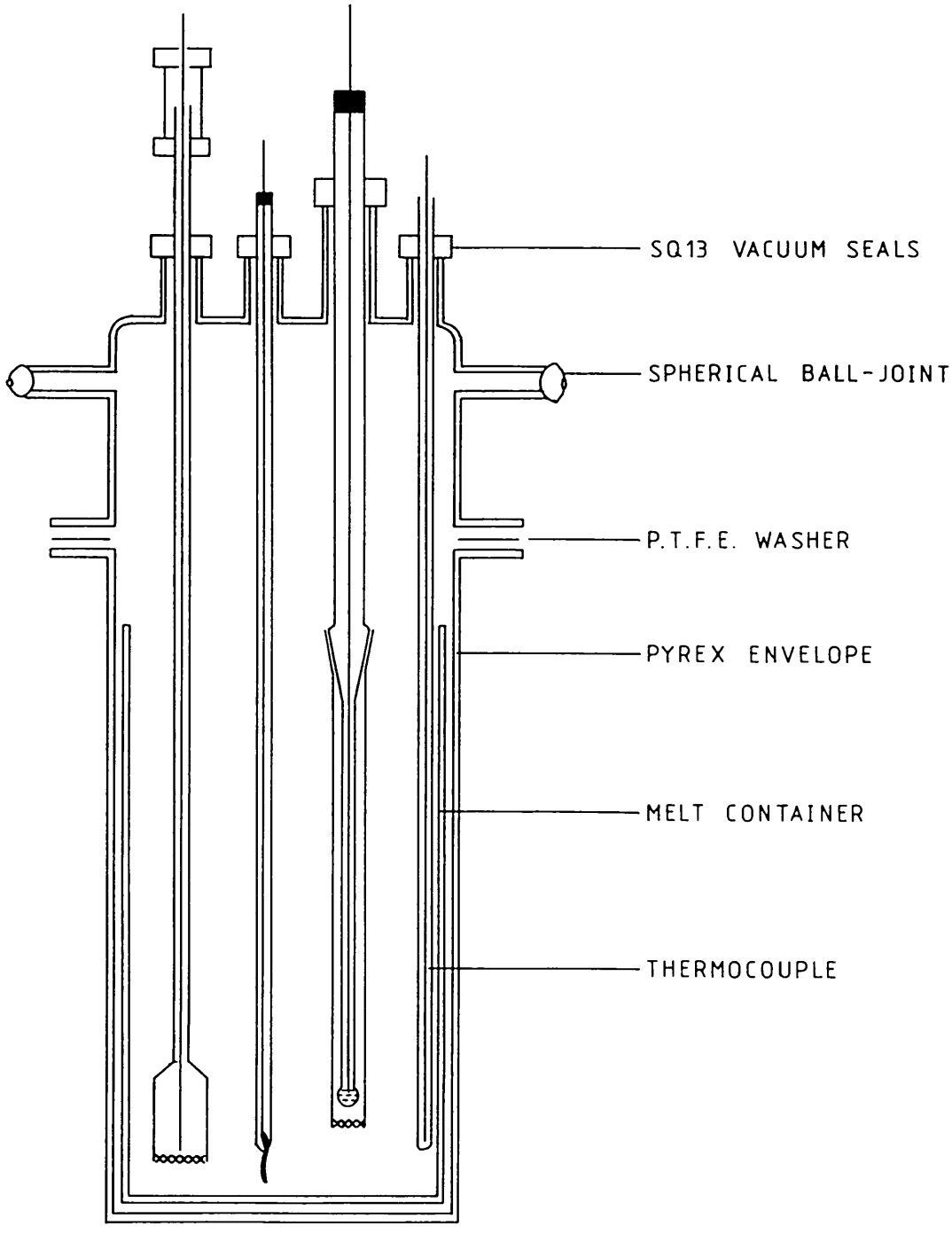


FIGURE 3.3: Electrochemical Cell

Sovirel 15 screw thread vacuum seals, through which the electrodes, thermocouple or bubbler could be passed. Vacuum tight seals could be obtained by using the matching screw caps, with fitted silicone rubber and P.T.F.E. washers. When in use, the silver/silver chloride and graphite electrodes were semi-permanent fixtures since they would not fit through the seals, but the other two seals could be used as required by exchanging the thermocouple for an electrode, say, all the time keeping a fast flow of argon through the cell.

Before use, all glass components that would come into contact with the melt were kept in a 1:1 mixture of concentrated sulphuric and nitric acids for 24 hours, after which they were rinsed with distilled water and dried at 150^{o}C. The glass components were then transferred to the dry box where the cell was assembled, the solid melt components being weighed into the melt container and put inside the cell. A little of the solid mixture was sometimes put in the fritted compartment of the reference electrode to help the flow of melt through the frit. When complete, the cell was transferred to the Grant aluminium block heater and heated under a continuous flow of dry argon.

3.6 Cyclic Voltammetry

Cyclic voltammograms were obtained by applying a linearly varying potential ramp to the working electrode and measuring the resultant current flowing between the working and counter electrodes as a function of the potential ramp. A diagrammatic representation of the applied potential and measured response is shown in Figure 3.4 and the block circuit diagram in Figure 3.5.

A Princeton Applied Research Model 175 sweep generator and a Thompson Ministat Model 251 provided the linearly varying potential, at sweep rates between 5 and 1000 mVs^{-1}. The resultant current potential curves were recorded on a Bryans 29000 A4 X-Y recorder. The electrodes used for the different experiments will be given in the the sections dealing with those experiments. A three electrode system was used for all voltammetric experiments.

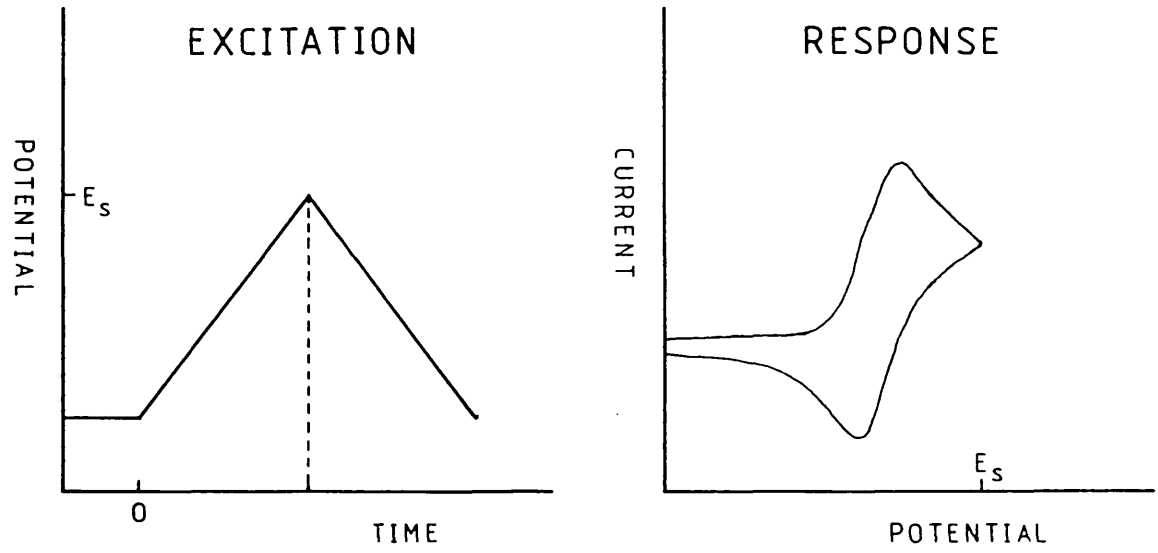


FIGURE 3.4

Cyclic Voltammetry - Excitation and Response for the Reversible Deposition of a Soluble Product

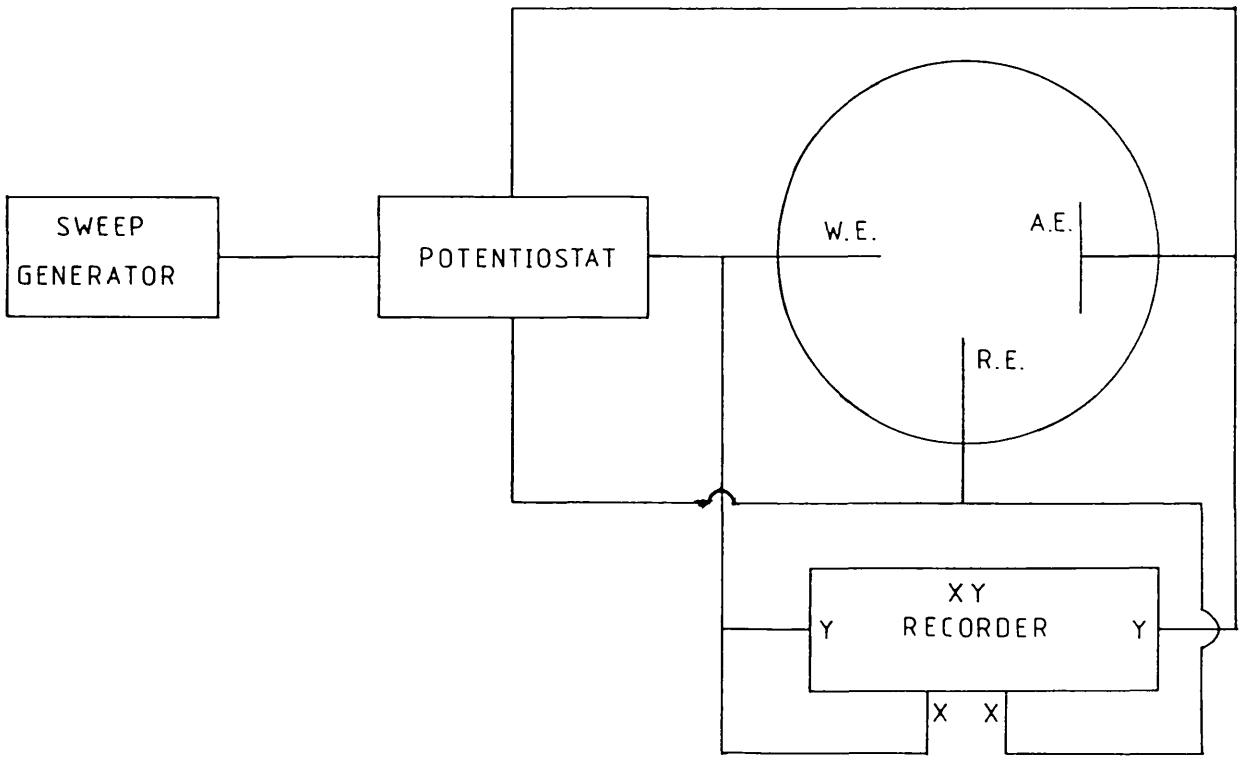


FIGURE 3.5

Diagrammatic Representation of the Cyclic Sweep Circuit

3.7 Solubility of HCl gas in $ZnCl_2$-NaCl melts

The apparatus employed for the determination of solubility of hydrogen chloride gas in $ZnCl_2$-NaCl melts of varying compositions is shown in Figure 3.6. The Pyrex outer container was 38 cm long and 6.5 cm o.d., with a 7.5 cm flange fitted on the open end. The melt container, also Pyrex, fitted inside this. The cell-head, with matching 7.5 cm flange, was fitted with several SQ13 vacuum seals through which the glass thermocouple tube, gas bubbler and gas outlet could be lowered into the cell. Before use all glassware in contact with the melt was kept in a bath of concentrated nitric and sulphuric acids (1:1 by volume), washed with distilled water and dried at 140^{o}C.

The preparation of the melt components has been outlined elsewhere (Section 3.1). Melts of varying compositions, but each totalling about 250g, were prepared in the argon filled dry-box and the filled cell transferred to the large furnace (Section 3.2). The temperature inside the cell was monitored with a chromel-alumel thermocouple linked to a D.V.M.

The $ZnCl_2$-NaCl mixtures were heated to the required temperatures under an HCl atmosphere, and then the HCl gas was bubbled through the melt for four hours to allow equilibrium to be reached. A glass-fritted bubbler was used for better dispersion of the gas. At the end of this period the bubbler was removed from the melt and a fast stream of dry argon was blown through the cell for thirty minutes to change the atmosphere above the melt. Having achieved this change in atmosphere the cell gas outlet was attached to the Dreschel bottles that contained known volumes of distilled water, and when a reasonable gas flow rate was reached, the bubbler was pushed back into the melt. Argon was bubbled through the melt for four hours, displacing the dissolved HCl. The HCl-carrying argon passed through the Dreschel bottles where the HCl dissolved in the distilled water. The resulting acidic solution was titrated against standard sodium hydroxide solution (0.02 M), using phenolphthalein as an indicator.

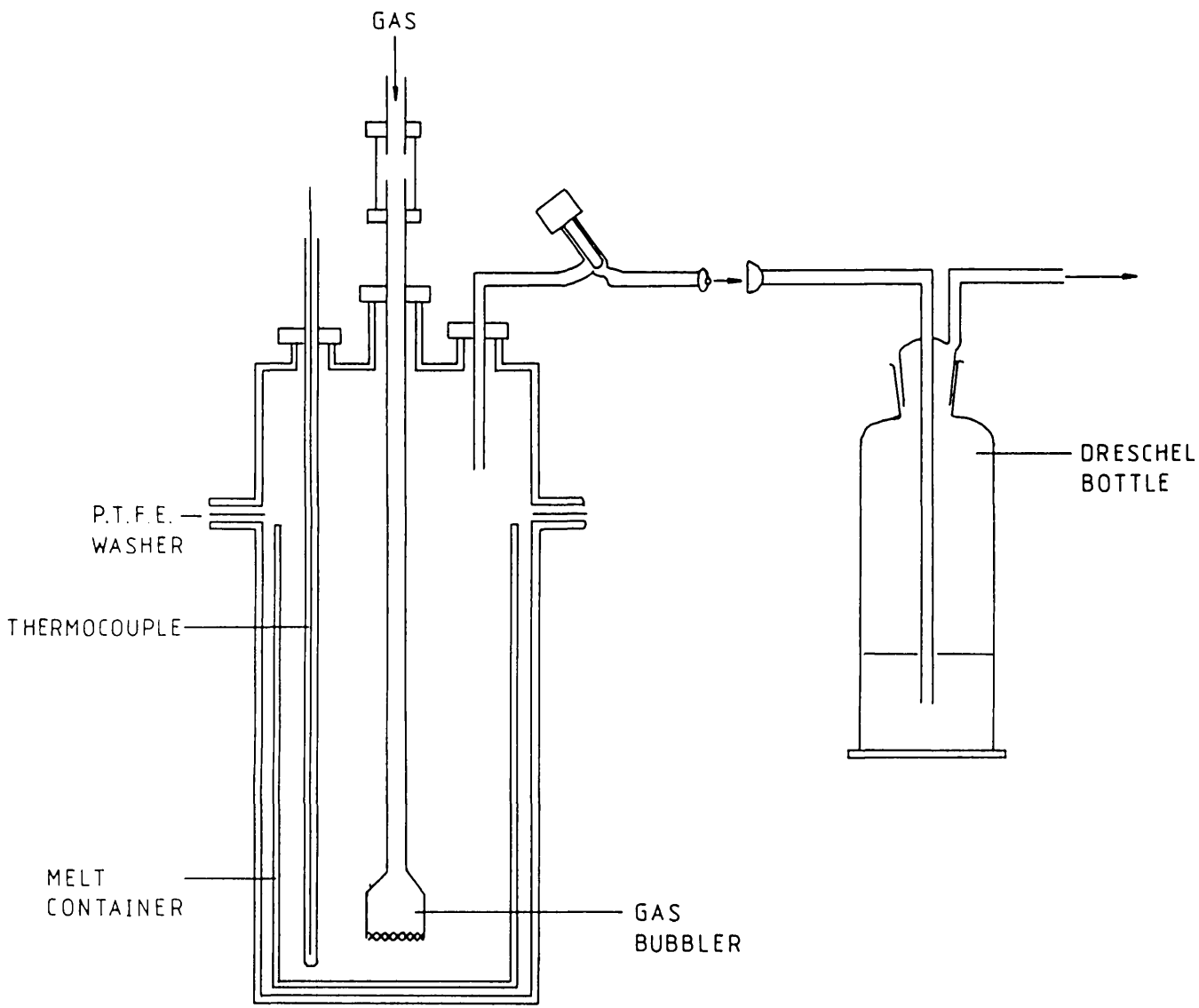


FIGURE 3.6

Apparatus Used for the HCl
Solubility Determination

From this the amount of hydrogen chloride dissolved in the known mass of melt could be determined.

This procedure was carried out three times at each temperature before the temperature was raised, the average value of the solubility being taken as the final result. Errors are discussed in the relevant section in the Results chapter (Section 5.1).

The molten mixtures were found to be clear and colourless but slightly contaminated by black flecks of carbon. Sublimation of the zinc chloride onto the cell cap was minimal until temperatures rose above 450^{o}C, when a build-up of white, solid zinc chloride slowly occurred. A correction for this has not been made.

3.8 Solubility of Oxy-Species in $ZnCl_2$-NaCl Melts

Attempts were made to measure the solubilities of zinc oxide and water in the molten mixtures of $ZnCl_2$-NaCl. The apparatus used for these experiments was the electrochemical cell glassware (Section 3.5), minus the electrodes, and a glass column packed with AW500 molecular sieve. In order to determine the solubility of zinc oxide, a small Pyrex filtration set was designed and constructed, shown in Figure 3.7, which fitted inside the outer sleeve of the electrochemical cell. Once the $ZnCl_2$-NaCl mixture held in the top container was molten, excess zinc oxide was added and stirred into the solvent by bubbling argon through the liquid. The thin bubble at the bottom of the container was broken with a glass rod, allowing the melt to fall through onto the frit. This was to filter out undissolved zinc oxide from the solution, which was collected in the bottom container.

After the filtration, the top two pieces of glassware were quickly removed from the cell, and the gas outlet on the cell head connected to a glass column packed with AW500 molecular sieve. Hydrogen chloride gas was bubbled through the melt, forming water by reaction with the dissolved oxide, which was carried out of the cell

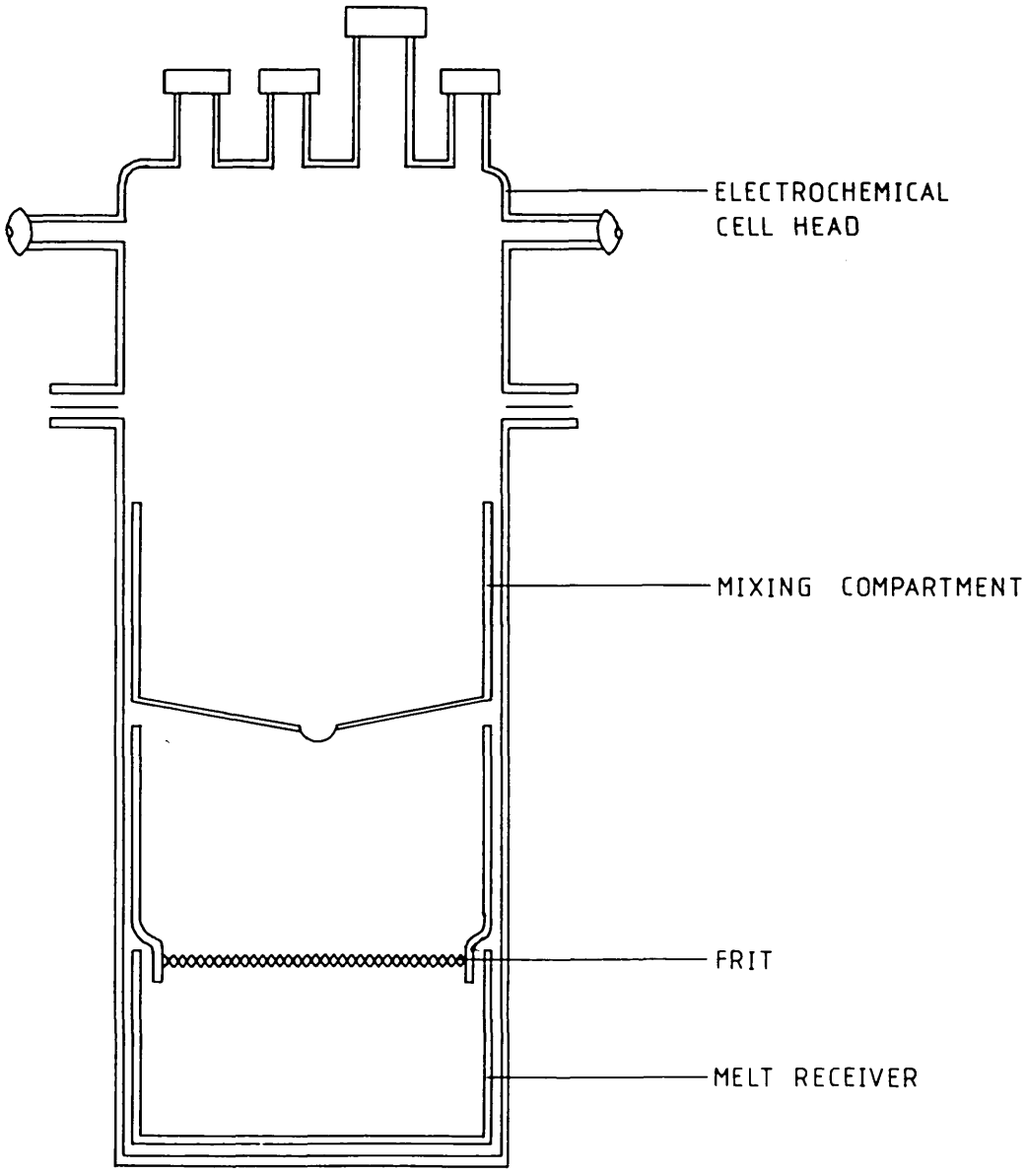


FIGURE 3.7: Filtration Unit in the Electrochemical Cell

and onto the drying column. The amount of water so formed could be determined by weighing the column before and after the experiment, and hence the amount of zinc oxide dissolved in the known amount of melt could be found.

For the attempts to determine the solubility of water in these melts, the melts were first saturated with water vapour using the equilibration apparatus described in Section 3.9. HCl gas was then used to purge the water from the melt and to carry it onto the AW500 molecular sieve drying column. Knowing the initial amount of melt, it should have been possible to determine the solubility of water in the melt, having weighed the column to find how much water had been carried over.

These experiments were carried out on pure $ZnCl_2$ and 80 mol. % $ZnCl_2$-NaCl, at temperatures between 340-380^{o}C with about 70g of melt being used each time. Once again contamination of the melts by carbon was evident.

3.9 Water Vapour Equilibration

For the experiments involving addition of water to the melts, the means by which the water could be added required some investigation. Injecting liquid water into the melt using a syringe, a method used by some workers dealing with the low temperature aluminium chloride melts, was felt to be unsuitable for these higher temperature liquids, since in all likelihood most of the water would boil off before it had had a chance to interact with the melt. Adding water in the form of pellets of zinc chloride hydrate also seemed somewhat complicated, especially trying to manufacture these pellets which had to have a known amount of water in them. Probably the simplest method of adding water to the melts, and the one chosen to be used here, was by equilibrating the melts with various vapour pressures of water. Melendres et al.[88] have given details of saturated aqueous solutions of various salts which will produce different water vapour pressures. These salts, and their water

vapour pressures, are given in Table 3.1.

Salt	Solubility in Water (g per 100g at 25°C)	Vapour Pressure of Saturated Solution at 25°C torr
LiCl	63.7	2.61
$MgCl_2$	54.25	7.84
$Mg(NO_3)_2$	125 (for $Mg(NO_3)_2.6H_2O$)	12.35

TABLE 3.1

Water vapour pressures of saturated solutions of various salts

The apparatus used for introducing the water vapour into the melt simply consisted of two Dreschel bottles containing the saturated solution being used, held in a constant temperature water bath. Argon was passed through the saturated solutions, using glass frits for better gas dispersion in the liquid, and on into the melt. The water bath temperature was regularly monitored, being held at 25°C by using a heater through which the water was constantly circulated. The moist argon was bubbled through the $ZnCl_2$-NaCl melts for 3-4 hours, to allow the system to equilibrate before the electrochemical experiments were carried out. During these experiments the gas bubbler was lifted out of the melt, but the moist argon continued to be passed through the cell.

3.10 X-ray Diffraction

Solid samples to be examined by X-ray powder diffraction were finely ground, and dispersed on a silicon crystal slide using acetone as the dispersant. A Phillips PW-1050 X-ray diffractometer fitted with a graphite monochromator was used, with CuK_α radiation (λ = 1.542 Å) as the incident radiation. The resulting diffraction patterns were recorded on chart paper and analysed using data from the Powder Diffraction File (pub. J.C.P.D.S. International Centre for Diffraction Data).

3.11 Raman Spectroscopy

Raman spectra of solid samples were recorded using an argon laser, a SPEX RAMALOG 5 Raman spectrometer and a "Datamate" data acquisition unit. Samples were prepared by melting batches of pure zinc chloride in the electrochemical cell glassware (Section 3.5), then saturating the liquids with various gases e.g. HCl, O_2, H_2O vapour or making additions of solid materials. The melts were then air-quenched and transferred to the dry-box, where they were ground to fine powders. Samples were held in glass tubes (15 cm, 0.6 cm o.d.), which were sealed under vacuum after having been half-filled in the dry-box. The wavelength of the radiation used was 514 nm, with the spectra being recorded in the range 50-4000 wavenumbers. The advantage of this method over I.R. spectroscopy was that deliquescent samples could be more easily handled, and would remain dry since they were sealed under vacuum.

3.12 Infra-Red Spectroscopy

Infra-red absorption spectra were recorded on a Perkin Elmer 237 grating infra-red spectrophotometer. The samples were prepared as Nujol mulls, held between potassium bromide discs. Deliquescent materials were handled in the dry box, and the mulls prepared under argon before being transferred to the spectrophotometer. Without a high temperature I.R. cell, it was not possible to record spectra of molten samples, which might have provided more information.

3.13 Electron Spin Resonance Spectroscopy

Samples for these experiments were prepared in the same way as those for the Raman spectroscopic experiments (Section 3.11), but this time were held in glass tubes designed specifically for the measuring instrument, rather than in the home-made tubes used for the Raman work. The E.S.R. spectra were recorded on a Varian E9 E.P.R. Spectrometer, and were run at room temperature. A spectrum of the glass tube was recorded first, so that peaks due to the glass could be separated from those due to the sample.

3.14 Atomic Absorption Spectrophotometry

Measurements of the atomic absorption of aqueous solutions of zinc chloride were carried out on a Perkin Elmer 2280 Atomic Absorption Spectrophotometer. Incident radiation was produced using a lamp which emitted radiation characteristic of zinc, magnesium and calcium ionization. Samples were vaporized in an acetylene flame, the flame being in the path of the incident radiation. Absorption of the incident radiation by the sample was recorded at a wavelength of 213.9 nm, which is the most sensitive for zinc absorption measurements. Comparison of the absorbances of standard zinc solutions with those of the unknown samples allowed the spectrophotometer to give a value for the zinc content of the sample in ppm, and hence the concentration of zinc could be determined. Care had to be taken to remember to take into account dilutions of the samples that were made to bring the zinc concentrations down to levels comparable with those of the standard solutions.

3.15 D.T.A./T.G.A. Analysis

The simultaneous differential thermal analysis/thermogravimetric analysis study was carried out using a Stanton-Redcroft STA 780 Analysis machine. Platinum crucibles (o.d. 0.5 cm) were used to hold the finely ground samples and the reference material, aluminium oxide. The amount of sample used was approximately 10 mg, the exact weight being taken each time to calculate the percentage weight loss.

Temperatures were measured with Pt-Pt 13% Rh thermocouples attached to the bases of the sample and reference material holders. The rate of heating was $10^{o}C$ $min.^{-1}$, with a dried air atmosphere, flow rate 50 cm^{3} $min.^{-1}$, being maintained throughout the system. Data was recorded on a Commodore PET computer and analysed using software provided.

3.16 A.C. Impedance Spectroscopy

A Hewlett Packard 4192 A LF Impedance Analyzer (5 Hz- 13 MHz) was used to impose fixed amplitude, variable frequency a.c. between two platinum electrodes held in molten zinc chloride-sodium chloride mixtures. The electrochemical cell described before (Section 3.5) was used, with a platinum wire working electrode, a platinum flag counter electrode, a gas bubbler and a thermocouple fitted in the SQ13 joints on the cell cap. The electrodes were stored in concentrated hydrochloric acid, and washed and dried prior to being placed in the cell. All glassware in contact with the melt was treated as described earlier (Section 3.1).

Impedance measurements were carried out on various melt compositions, the melts being saturated with HCl gas, purged with argon and then saturated with water vapour by bubbling argon through distilled water and into the melt. The effect of the solutes on the melt conductivity could then be seen. The whole cycle was repeated four or five times for each melt composition, the temperature being held constant at about $355^{o}C$. The order of solute addition was occasionally varied to see if any difference in response occurred. The amplitude of the alternating current used was 10 mV, the Impedance Analyzer being capable of producing alternating currents with amplitudes up to 1.5 V.

3.17 Materials and Chemicals Used

The sources and quoted purities of the materials used during this work are listed in Table 3.2.

Material	Source	Purity/Grade
$ZnCl_2$	B.D.H.	AnalaR
NaCl	B.D.H.	AnalaR
Platinum	B.D.H.	99.9%
Tungsten	Jencons	--
Gold	Johnson-Matthey	"Puratronic" (20 ppm T.M.I.)
Copper	B.D.H.	--
Vitreous Carbon	Sigri-Hoechst	Sigradur-G
Graphite	Johnson Matthey	"Spectro-tech"
Epoxy Resin	--	Araldite 'Rapide'
$MgCl_2$	B.D.H.	G.P.R.
$Mg(NO_3)_2.6H_2O$	B.D.H.	G.P.R.
LiCl	B.D.H.	G.P.R.
NaOH	B.D.H	AnalaR
Na_2CO_3	B.D.H.	AnalaR
ZnO	B.D.H.	AnalaR
Na_2O_2	Aldrich	~95%
HCl gas	B.O.C.	High purity - 99.9%
O_2	B.O.C.	High purity - 99.9%
Ar	B.O.C.	High purity - 99.9%
Voltalef 90 grease	B.D.H.	--
Apiezon T grease	B.D.H	--
AW500 molecular sieve	Union Carbide	--

TABLE 3.2

Materials and Chemicals Used

CHAPTER 4

PURIFICATION OF $ZnCl_2$ MELTS

4.1 Introduction

Up until the mid-1970's many of the techniques used for melt purification were particular to those groups that had formulated them or who had learnt about them by word of mouth. A series of books by Lovering and Gale[2] and a large chapter by White[144] in the book "Ionic Liquids"[84] have gone a long way to cataloging the different methods used for melt purification, giving details of the processes and equipment used by various workers.

Moisture is the most troublesome impurity in chloride melts and the hardest to remove, especially from those melts where the components include deliquescent salts like LiCl or $ZnCl_2$. Laitinen et al.[74] were amongst the first to experiment with methods for drying LiCl-KCl mixtures. They found that vacuum-drying of the salts to remove surface water, followed by fusion under anhydrous HCl which was then bubbled through the melts, resulted in liquids which to a large extent were found to be oxide free. Introduction of the HCl into the melts was found to drive equilibria [4.1] and [4.2] to the right converting impurity oxy-species to water which

$$HCl + OH^- = Cl^- + H_2O_{(g)} \qquad [4.1]$$

$$2HCl + O^{2-} = 2Cl^- + H_2O_{(g)} \qquad [4.2]$$

was driven off. Subsequent argon-purging of the HCl from the melts gave liquids with much lower polarographic residual currents than those found for unpurified melts. Maricle and Hume[75], working with NaCl-KCl melts, found that by bubbling chlorine gas through the melts, it was possible to

dispense with the vacuum-drying step and to purify undried melts in one step, shown in equilibrium [4.3]. This took about one hour, instead of the several days needed previously.

$$2OH^- + 2Cl_2 = O_{2(g)} + 2HCl + 2Cl^- \qquad [4.3]$$

Different groups of workers all have their own favourite purification recipes, which are usually made up of a few standard steps. Popular steps for the purification or preparation of anhydrous zinc chloride melts[37] are listed below:

- vacuum drying of the salt to temperatures just below the melting point,
- fusion of the salt under HCl or Cl_2, followed by periods of saturation of the melt with one or other of the two gases,
- argon or nitrogen purging of the melt to remove dissolved HCl or Cl_2,
- filtration of the melt,
- distillation; often used by spectroscopists who only require small amounts of melt,
- addition of metallic zinc to the melt, followed by decanting of the liquid,
- reaction of pure zinc metal and gaseous HCl or Cl_2, again popular with spectroscopists,
- recrystallisation of $ZnCl_2$ from aqueous solution followed by HCl saturation of melt (this may only introduce more hydroxide impurity[19,20])
- electrolysis between inert electrodes to remove heavy metal cation impurities.

A series of papers by Monk and Fray[145-7] is concerned with the purification of zinc chloride produced by chlorination of zinc sulphide ores, and deals with the removal of iron, the precipitation of impurities by zinc addition and the treatment of concentrated aqueous solutions of $ZnCl_2$. The recovery of $ZnCl_2$ from zinc materials contaminated with chlorine has been investigated by Hager and Lemons[148], who looked at the behaviour of $ZnCl_2/FeCl_3$ complexes and how the vapour pressure of $ZnCl_2$ might be enhanced by formation of these species.

A rather more hazardous method of removing oxide impurities from chloride melts has been proposed by Abdul-Sada et al.[149], who have experimented with the use of phosgene on room temperature chloroaluminate melts. Oxide ions were removed from the melts by reaction with the gaseous phosgene to produce carbon dioxide (reaction [4.4]), with both reagent and product finally removed from the melt by continuous evacuation. Alkali

$$O^{2-} + COCl_2 \rightarrow CO_2 + 2Cl^- \qquad [4.4]$$

halides have been purified by reaction with carbon tetrachloride and chloroform transported in an inert carrier gas or by refluxing with $SOCl_2$[144]. The advantage with these reagents is that HCl and CO_2 are the products rather than water, thus eliminating hydrolysis, but carbon impurities may be introduced if the organic halides undergo pyrolysis.

4.2 Appearance of $ZnCl_2$ Melts

Solid $ZnCl_2$, as bought from the suppliers (Section 3.17) was in the form of white granules. At the end of the purification process the $ZnCl_2$ had collected as a grey lump in the melt receiver, the grey colour presumably a result of partial glass formation. Grinding of this material in the dry-box resulted in a white powder, but the $ZnCl_2$ was stored in coarse lumps to reduce the extent of any deliquescence that may occur in the dry-box.

Heating unpurified zinc chloride, regardless of the atmosphere, caused a large amount of water to be evolved which condensed on the cell cap and was eventually transported out of the cell if a carrier gas was used. Upon melting, the impure zinc chloride was a viscous liquid, but almost invariably clear: no sign of cloudiness was observed. However, many of the melts used during this work, both pure and impure, were contaminated by black flecks of carbon. The origin of this impurity is still unknown, despite several attempts to clear up the problem. Other workers[10,150,151] have suffered the same contamination, and the general conclusion was that it is present in the supplied material. Even the filtration step used during the purification failed to completely remove the carbon. It was surprising how little carbon was needed to produce a completely black melt. Similarly, in chloroaluminate melts, milligrammes of carbon will cause the melt to appear black[152]. Allowing the melts to stand resulted in the carbon coagulating to form large agglomerates.

Etching of the Pyrex melt containers occurred with melts contaminated with moisture, but it took many hours before this etching became visible. Carthey[1] has stated that upon cooling a $ZnCl_2$ melt contaminated with water, the Pyrex melt container cracked. The explanation given for this was that as water-contaminated melts are cooled they adhere to the glass surface, causing the glass to crack under the strain as the cooling melt contracts. Moisture-free melts do not adhere to the glass, and hence cracking is not observed. However, no cracking of the melt container, caused by adherence of the melt to the glass, was ever observed during this project, from which it is concluded that the container used by Carthey may have been flawed. It was noticed that purified melts, upon cooling, shrank away from the container to a much greater degree than moisture-contaminated melts, and that the former would easily slide out of the container if it was inverted in the dry-box, whereas the latter would often stick.

4.3 Water Absorption Studies

Zinc chloride is a very hygroscopic material, and if left for long enough in the open atmosphere will dissolve in the moisture it attracts to form a clear liquid. As an interesting, but simple, experiment it was decided to compare the water absorption behaviour of purified $ZnCl_2$ with that of the impure material to get an idea of the amount of moisture present in the supplied $ZnCl_2$ before it is purified. The addition of sodium chloride to molten zinc chloride has an effect on the viscosity and conductivity of the melt, but it was not known to what extent it would affect the deliquescent nature of solid $ZnCl_2$. If it was found that the extent and rate of deliquescence of $ZnCl_2$ fell when NaCl was present in the solid material then this would mean that it would be better to store the $ZnCl_2$ and NaCl as mixtures rather than individually.

Samples of pure and impure $ZnCl_2$ and of 50 mol. % $ZnCl_2$-NaCl were placed in turn on a watch glass on a micro-balance open to the atmosphere, and their weights recorded at various intervals. The experiment was carried out within one day so that atmospheric humidity would remain reasonably constant. The 50 mol. % $ZnCl_2$-NaCl mixture had been melted beforehand to ensure complete mixing of the components, then cooled and crushed. All three samples were in rough granular form and had about the same starting weight. Obviously the rate of deliquescence would depend on the size of the granules, so the samples were made reasonably similar.

The variation in the weight of the samples with time is shown in Figure 4.1. The measurements were continued until the weights had stabilized. It can be seen that the initial rates of water absorption were the same for the samples, but the percentage increases in their weights were quite different. Unsurprisingly, the pure $ZnCl_2$ absorbed most water, undergoing a 65% weight increase to form a clear liquid which became less viscous as time progressed. Calculating the molar amounts of $ZnCl_2$ and water absorbed showed that a mole of pure $ZnCl_2$ would absorb almost 5 moles of water. The undried $ZnCl_2$ was found to increase weight by around 61%, showing that there is a non-negligible amount of moisture present in the material purchased from suppliers, but the rates of deliquescence of the two samples were very similar. For the 50 mol. % $ZnCl_2$-NaCl mixture a 38%

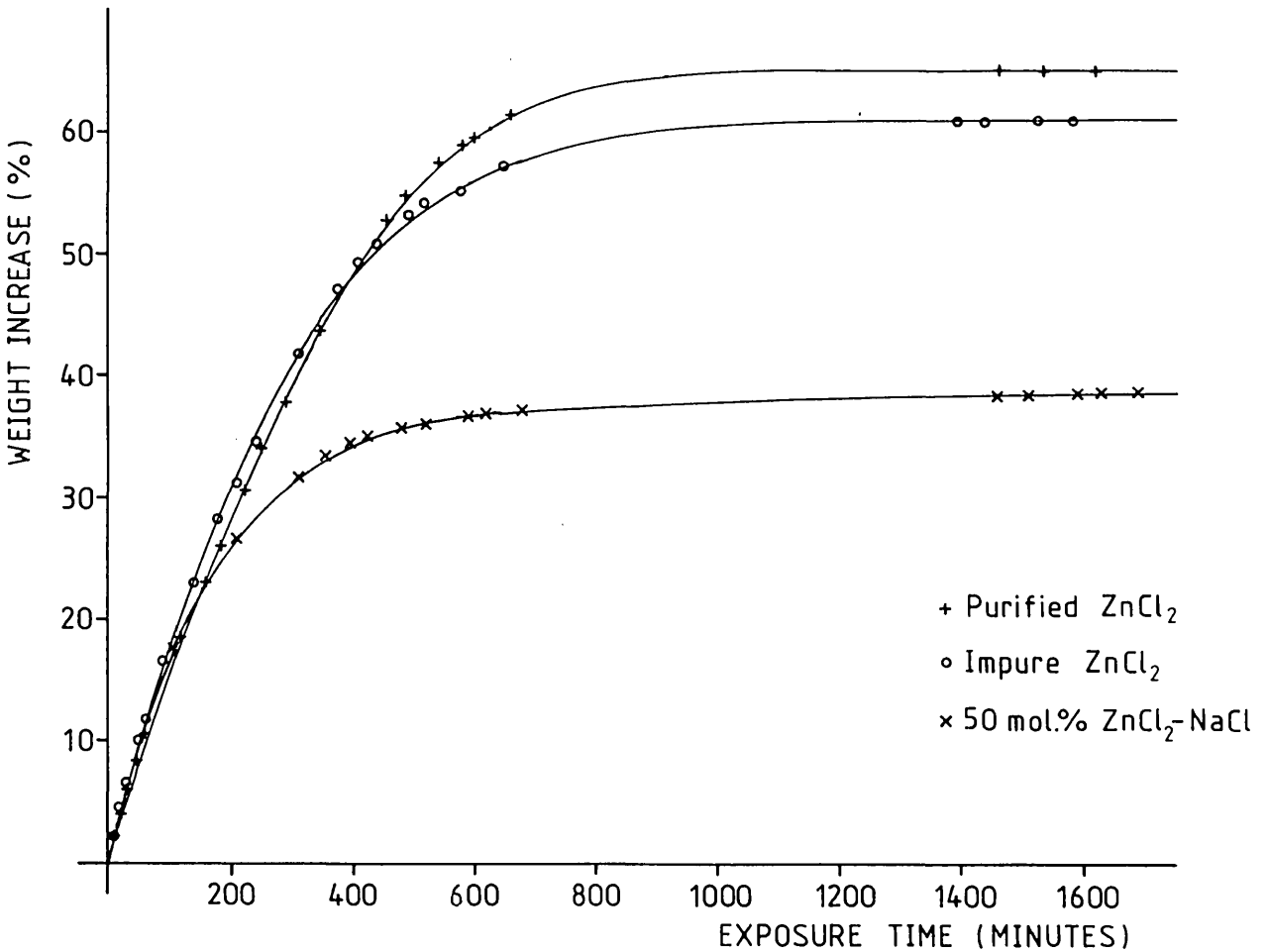


FIGURE 4.1: Water Absorption by $ZnCl_2$, Pure and Impure, and by 50 mol. % $ZnCl_2$-NaCl at Room Temperature

increase in the weight of the sample was recorded, showing that the presence of the alkali metal chloride does diminish the extent of the water absorption process, but not the initial rate of that process.

Similar studies have been carried out by Perry et al.[153] using solid $ZnCl_2$-KCl eutectic mixtures (31.5 and 72 mol. % $ZnCl_2$). The $ZnCl_2$-rich mixture was found to increase its weight by 10% in 200 hours to form a saturated solution, whilst the KCl-rich mixture underwent a weight increase of only 0.3% over 100 hours and no change over the next 700 hours. So there is a marked difference between the behaviour of $ZnCl_2$-NaCl and $ZnCl_2$-KCl mixtures. The extent of deliquescence has been linked to the ease with which the water molecules may co-ordinate to the zinc ions[103,153], which decreases upon changing from $ZnCl_2$-NaCl to $ZnCl_2$-KCl. KCl is known to act as a better Cl^- ion donor in the melt, enhancing the formation of $ZnCl_4^{2-}$ species which presumably then persist in the solid. Even so, the difference in behaviour between the two mixtures is quite remarkable.

Since the initial rates of water absorption by pure $ZnCl_2$ and $ZnCl_2$-NaCl were very similar it was decided to store the melt components individually. This had the added advantage that any composition could be made quite quickly, rather than having to work with the compositions in storage or having to purify more material.

4.4 Voltammetric Examination of Unpurified and Pure Melts

Different electrodes were tried in various melts to investigate their response under different conditions and ascertain which type would be best employed for the voltammetric experiments. All electrodes have been described in Section 3.4.

4.4.1 Reference electrodes

Two different electrodes were tested - the silver/silver chloride reference electrode and the platinum quasi-reference electrode. Whilst the Ag/AgCl electrode held a constant potential in all melts, the bulb was

susceptible to cracking after two or three experiments, contaminating the bulk melt with silver ions. Since the platinum quasi-reference electrode was much more durable and was found to maintain a reasonably steady potential (Section 5.2.1) in $ZnCl_2$-NaCl melts, it was chosen as the electrode to be used for the voltammetric studies. Carthey[1] found that by depositing zinc onto a vitreous carbon electrode a stable reference electrode could be produced. However, it was felt that this could not be used here since the presence of HCl in the melt would cause the zinc metal to react to form $ZnCl_2$. The presence of oxy-species (e.g. by addition of NaOH, H_2O, ZnO) would probably result in formation of a ZnO layer on the electrode which might adversely affect the electrode potential.

4.4.2 Counter electrode

For the voltammetric experiments the graphite electrode was employed. This had to be lowered into the melt in advance of the other electrodes to allow melt to seep into the electrode compartment. The electrode was extremely durable, being used for numerous experiments with no noticeable disintegration of the graphite rod. It had been suggested[1] that evolution of chlorine at the graphite rod caused swelling and crumbling of the rod, but this was not noticed here.

4.4.3 Working electrodes

Four different materials were tried as working electrodes - platinum tungsten, vitreous carbon and gold. The behaviour of each in unpurified and pure melts will be described in turn.

4.4.3.1 Platinum electrode

Both wire and disc electrodes were used during the voltammetric experiments, but the behaviour of platinum in unpurified and pure melts was investigated using wire electrodes. A typical voltammogram obtained with the Pt electrode in an impure melt is shown in Figure 4.2, and this may be compared with voltammogram obtained in a pure melt, shown in Figure 4.3. Within the working range of the electrode, around 1.1-1.2 V, at least six

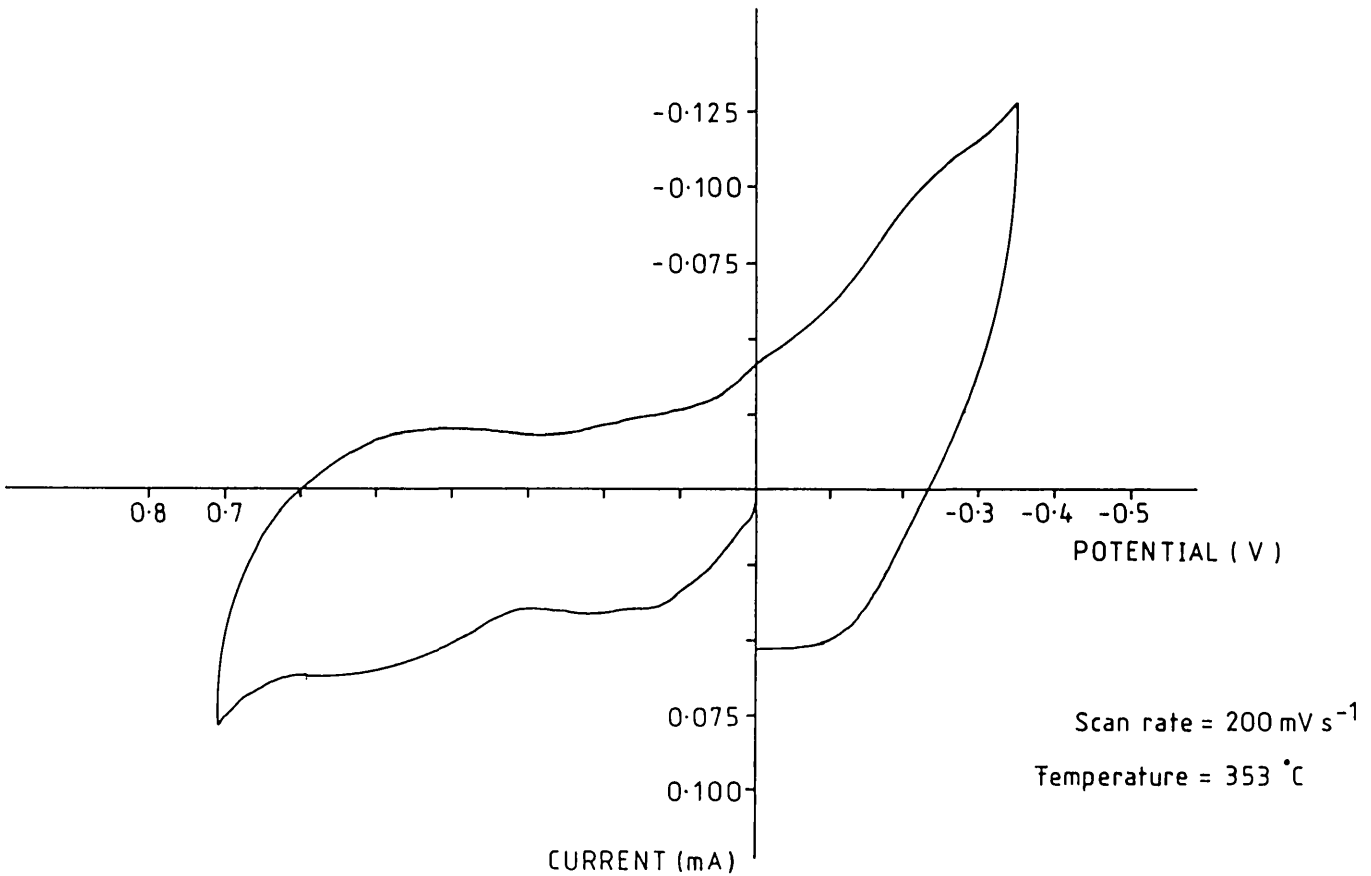


FIGURE 4.2: Typical Voltammogram Obtained with a Platinum Electrode in Impure 80 mol. % $ZnCl_2$-NaCl

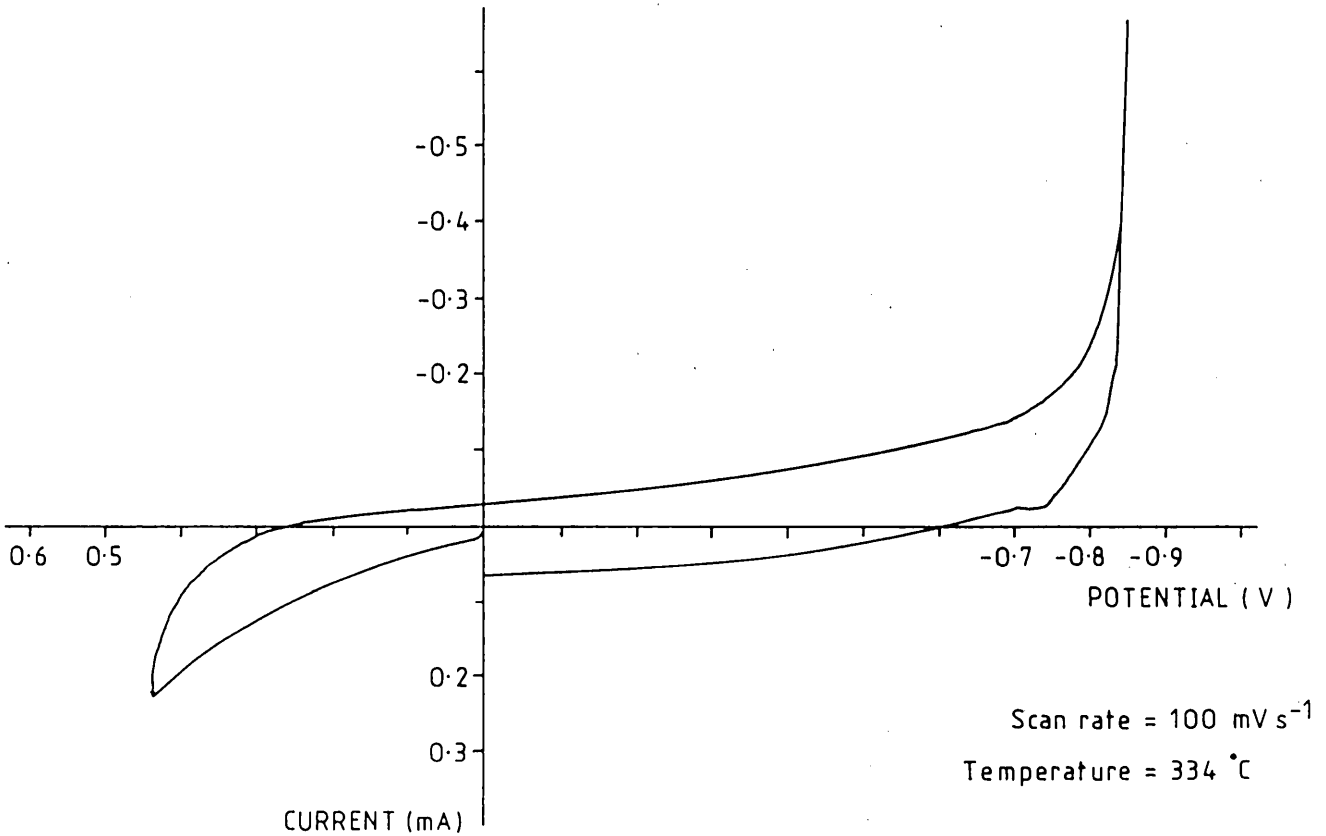


FIGURE 4.3: Typical Voltammogram Obtained with a Platinum Electrode in Pure 80 mol. % $ZnCl_2$-NaCl

waves can be seen on the voltammogram from the impure melt. Since moisture is the major impurity it is almost certain that these waves are related to whatever species are formed in the melts when water is present. Possibilities include hydroxy-, oxy-, and oxychloro- species, all of which are probably electroactive within the range of platinum.

In comparison, the voltammogram obtained in a pure melt using the Pt electrode shows no waves within the working range, otherwise called the "electrochemical window". At sufficiently negative (cathodic) potentials a sharp peak is seen, which is caused by zinc depositing on the platinum. The lack of sharp stripping peak on the reverse scan infers that the zinc is alloying with the platinum[111]. In the positive (anodic) direction a reaction is occurring, which is probably the dissolution of platinum[111], rather than chlorine evolution which normally gives rise to the anodic limit.

4.4.3.2 Tungsten electrode

The tungsten electrode was tried in both unpurified and pure melts, with some degree of irreproducibility in the voltammograms obtained. Figure 4.4 shows a typical voltammogram obtained in an unpurified melt. Several waves can be seen within the working range of the electrode, the range being about the same size as that of platinum, but these waves lack the definition of those seen with the Pt electrode. The waves are probably due to formation of oxides on the tungsten surface, which has been reported by other workers[1,88,154]. The increasing anodic current could be caused by the dissolution of tungsten, which is known to form several chloro-species[154], so exhibiting behaviour similar to that of platinum. After the purification process, voltammograms obtained with the W electrode no longer exhibited these "extraneous" peaks[88], leaving a clear electrochemical window between the melt limits (Figure 4.5).

As mentioned, the anodic melt limit is governed by the onset of dissolution of the tungsten. In the cathodic direction, if the limit was reached then occasionally some small, sharp pre-peaks occurred before the

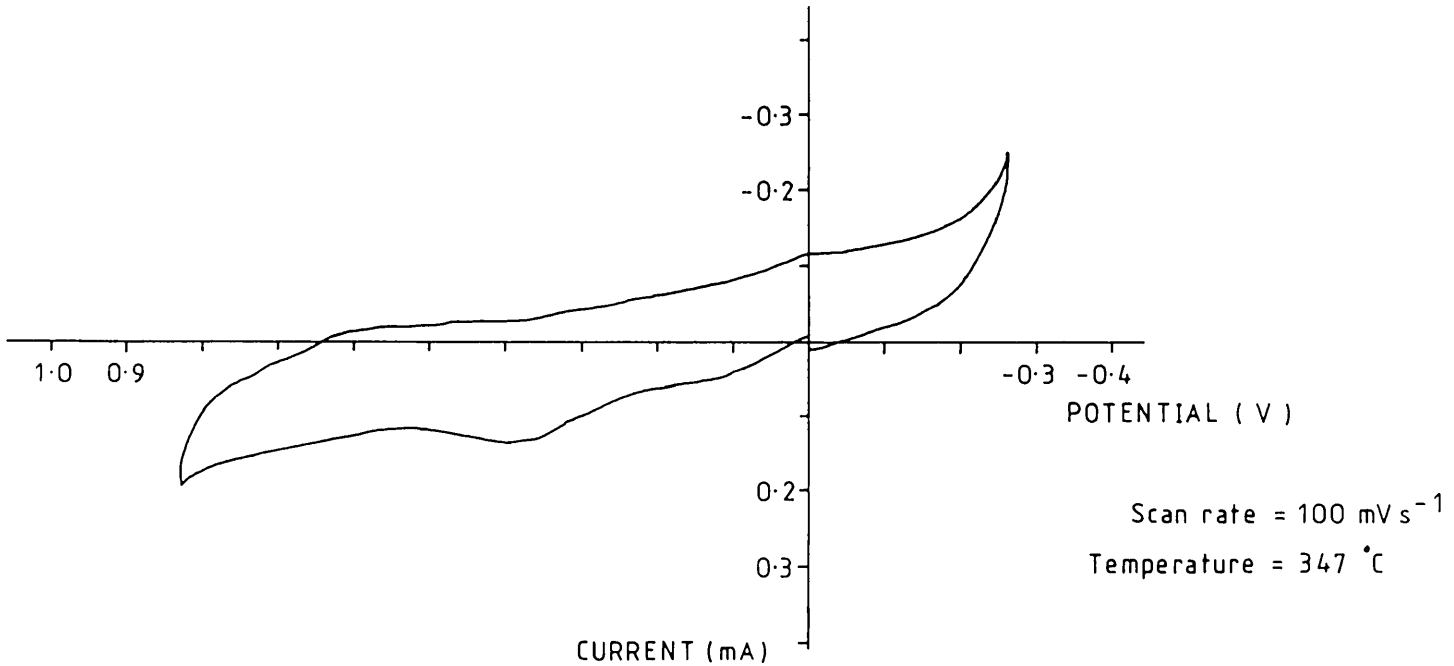


FIGURE 4.4: Typical Voltammogram Obtained with a Tungsten Electrode in Impure 80 mol. % $ZnCl_2$-NaCl

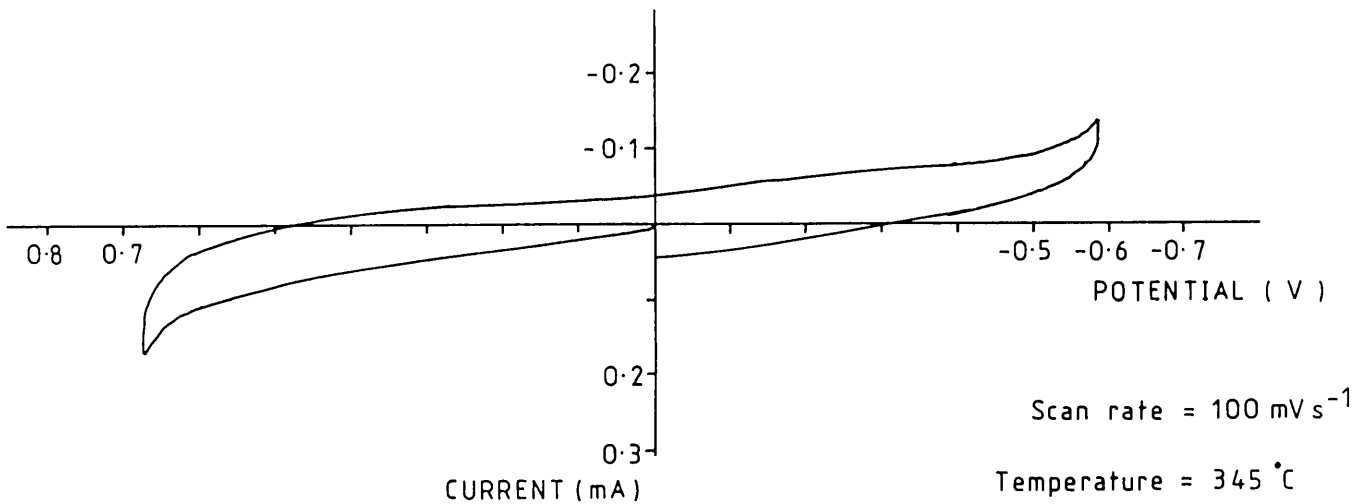


FIGURE 4.5: Typical Voltammogram Obtained with Tungsten Electrode in Pure 80 mol. % $ZnCl_2$-NaCl

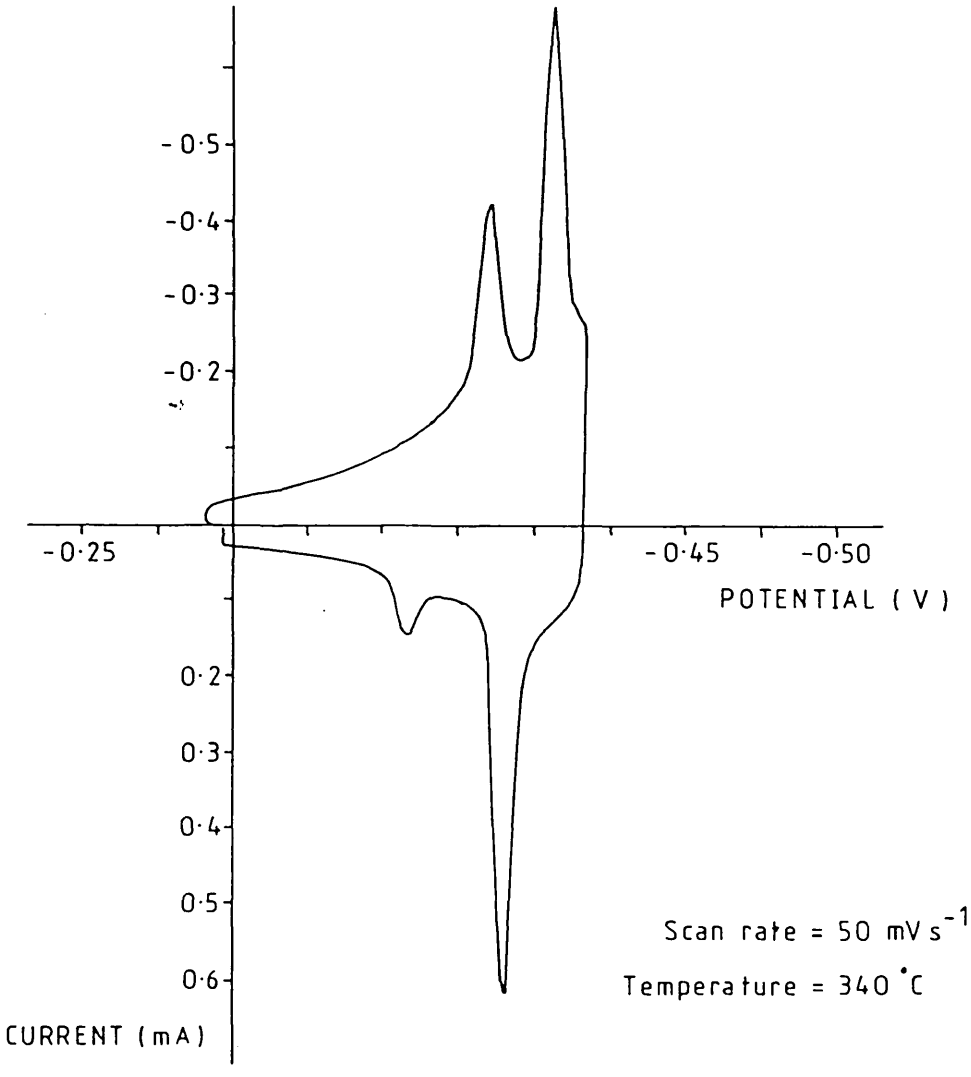


FIGURE 4.6: Alloying Peaks on a Voltammogram Obtained With a Tungsten Electrode in Pure 80 mol. % $ZnCl_2$-NaCl

Zn deposition peak (Figure 4.6). These peaks are thought to be due to an alloying process occurring between deposited Zn and the W substrate. The cause of such pre-peaks is discussed in Section 5.2.5 and will not be reiterated here. These peaks were not always observed, but no pattern in their appearance could be found.

4.4.3.3 Vitreous carbon electrode

In contrast to the other electrode materials, vitreous carbon was found to give the same voltammograms in unpurified and pure melts. Even in water-saturated melts no peaks other than the melt limits were observed. A typical voltammogram is shown in Figure 4.7. The electrochemical window, around 1.7 V, with this electrode was larger than those seen with W and Pt, since here the anodic limit was the evolution of chlorine rather than the dissolution of the electrode substrate.

As discussed in Section 5.2, many other workers have been unable to obtain voltammetric waves corresponding to electrode processes involving aqueous or protonic contaminants in chloride melts using vitreous carbon electrodes, so limiting the use of this electrode in that area.

4.4.3.4 Gold electrode

This was only tested in purified melts, a typical voltammogram being shown in Figure 4.8. The electrochemical window for this material, about 0.8V, was less than those for Pt and W. At the cathodic limit zinc is deposited, whilst at the anodic limit gold is anodically dissolved before chlorine is evolved. It has been found[1] that prolonged use leads to a brown colouration around the gold electrode, presumably a result of the dissolution process. The lack of a sharp stripping peak infers the formation of an alloy between deposited Zn and the Au substrate, between which at least six alloys are known[155].

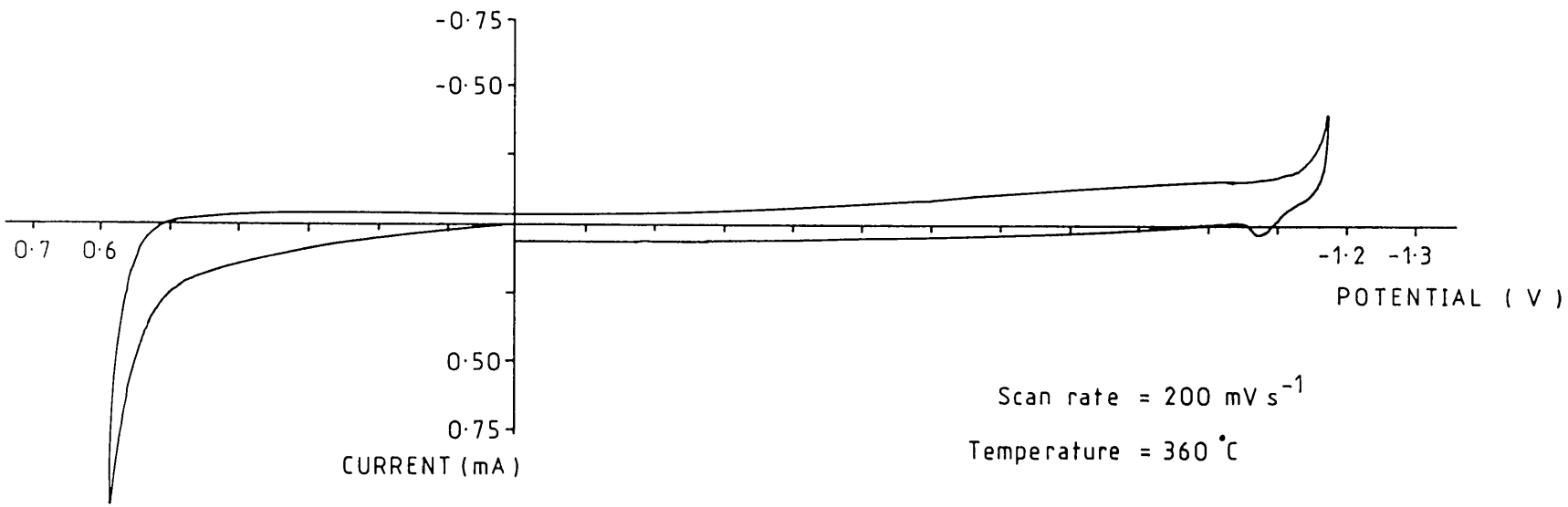


FIGURE 4.7: Typical Voltammogram Obtained With a Vitreous Carbon Electrode for Pure and Impure 80 mol. % $ZnCl_2$-NaCl

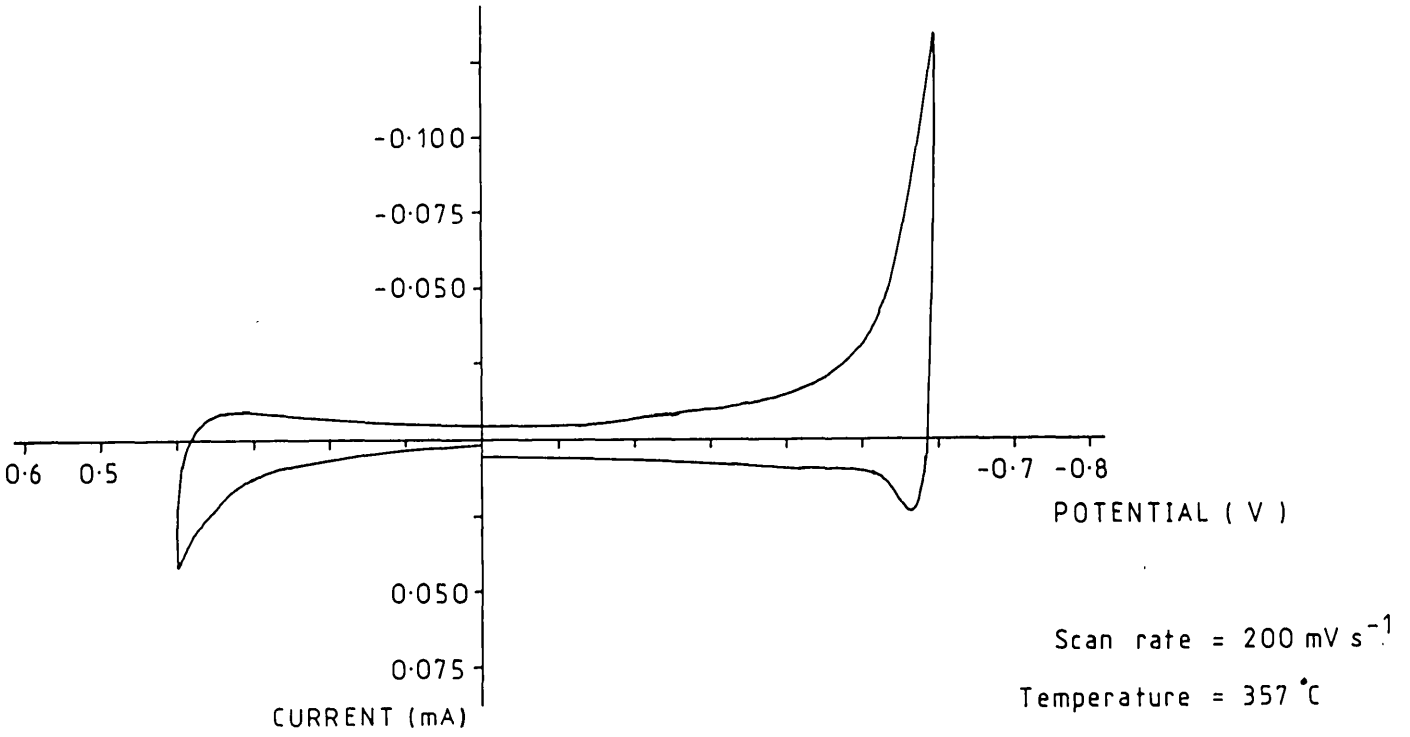


FIGURE 4.8: Typical Voltammogram Obtained With a Gold Electrode in Pure 80 mol. % $ZnCl_2$-NaCl

These results were used to determine which electrode material should be used for voltammetric experiments involving protonic and oxy-species dissolved in the $ZnCl_2$-NaCl melts. The lack of responsivity of vitreous carbon to the presence of aqueous contaminants made that material unsuitable for this project. The small electrochemical window of gold, and the ease with which it dissolved, also rendered this metal unsuitable as a working electrode. Of the other two melts, both of which undergo anodic dissolution and possible alloy formation, platinum was chosen as the working electrode material to be used for subsequent work. Many other workers[1,88,99,111] have advised against the use of tungsten for monitoring aqueous and protonic solutes, and this, coupled with the irreproducible results found during this work, indicated the unsuitability of tungsten as a working electrode for this project. So many groups have used Pt for their work, e.g. references 60, 66, 74, 82, 92, 97, 99, 110, 131, that it was decided to use Pt so that comparisons could be made between these results and those of other groups.

CHAPTER 5

BEHAVIOUR OF HCl IN $ZnCl_2$-NaCl MELTS

5.1 Solubility of HCl in molten $ZnCl_2$-NaCl

Studies of the solubility of HCl gas in various molten chlorides have been briefly outlined in Section 2.3.1. Much of the work has been carried out by Novozhilov et al.[61,62,64,76,78,79], who have tried to couple the results of I.R. spectroscopic investigations with the solubility behaviour of HCl in molten chlorides. By considering the existence of $ClH...Cl_{melt}$ hydrogen bonds in these solutions, it was possible to account for the different effects observed in the alkali metal chloride and alkaline earth chloride melts. The existence of such "complexes" in zinc chloride melts has been mentioned by several people[64,70,83] but little work has been carried out to determine the structure of these species, or even if they actually exist. It was hoped that this solubility study might provide an indication of the nature of the dissolution process, be it chemical or physical, which could infer the existence or non-existence of any complex species.

The method used in this determination of the solubility of HCl gas in $ZnCl_2$-NaCl melts was a rather simplified version of the elution method, the apparatus here, shown in Figure 3.6, being somewhat more basic than that used for previous studies[63]. Some workers have evacuated the chamber containing the melt after the melt has been saturated with the solute gas[61], whilst others have isolated known volumes of the gas-saturated melt and eluted the dissolved gas from these samples, ruling out the necessity of density data[59,67]. The former step was deemed impractical for the molten $ZnCl_2$-NaCl mixtures used here, since the high vapour pressure of zinc chloride at these temperatures would probably have meant a non-negligible loss of that component from the melts. This evacuation step also relies upon the hope that the solute gas will remain in the melt whilst the evacuation of the chamber is occurring, which may well not be the case here. The rapid stream of argon passed for 30 minutes between the

dissolution and elution stages was expected to have replaced the HCl atmosphere with one of argon in the melt chamber. Since the densities of $ZnCl_2$-NaCl melts have been determined (Section 2.2.1), the masses of the mixtures were recorded and their corresponding volumes calculated using the density data. This, unfortunately, will introduce an extra error into the solubility values, which will be reported in $mol.cm^{-3}$ units, as is usually the case.

An attempt was made to measure the solubility of HCl gas in pure molten zinc chloride using the same apparatus, but it was found that upon bubbling the gas through the melt a multitude of minute bubbles formed in the melt. Due to the high viscosity of molten zinc chloride these bubbles could not be removed by any mechanical means, and prolonged attempts only resulted in changes in the melt temperature. The idea, outlined earlier, of evacuating the melt chamber was thought to remove this problem for less volatile melts since some melts can be vacuum degassed, but this was not practicable here. Replacing the fritted gas bubbler with a straight glass-tube bubbler did nothing to improve the situation, merely lengthening the time for this suspension of bubbles to form. Consequently, no data are available for the solubility of HCl in pure molten zinc chloride, and none could be found in the literature.

The solubility of HCl gas in molten mixtures of $ZnCl_2$-NaCl was determined in melts with mole fractions of zinc chloride of 0.80, 0.65 and 0.50, over a range of temperatures between about 320-460^{o}C. The results are displayed graphically in Figure 5.1, with a plot of solubility ($mol.cm^{-3}$) versus the melt temperature (^{o}C). The actual temperatures at which the solubilities were determined varied for each melt, but in general the measurements were carried out with increments of approximately 50^{o}C between each reading, so that values of the solubility were obtained at four temperatures for each melt composition. Each measurement was repeated three times, which gave an opportunity to observe the deviation in the measurement of each point and to assess the error inherent in this simplified method. Ideally, each determination should have been carried out 6-8 times, but for such a rigorous determination much more precise experimental equipment would have to be constructed.

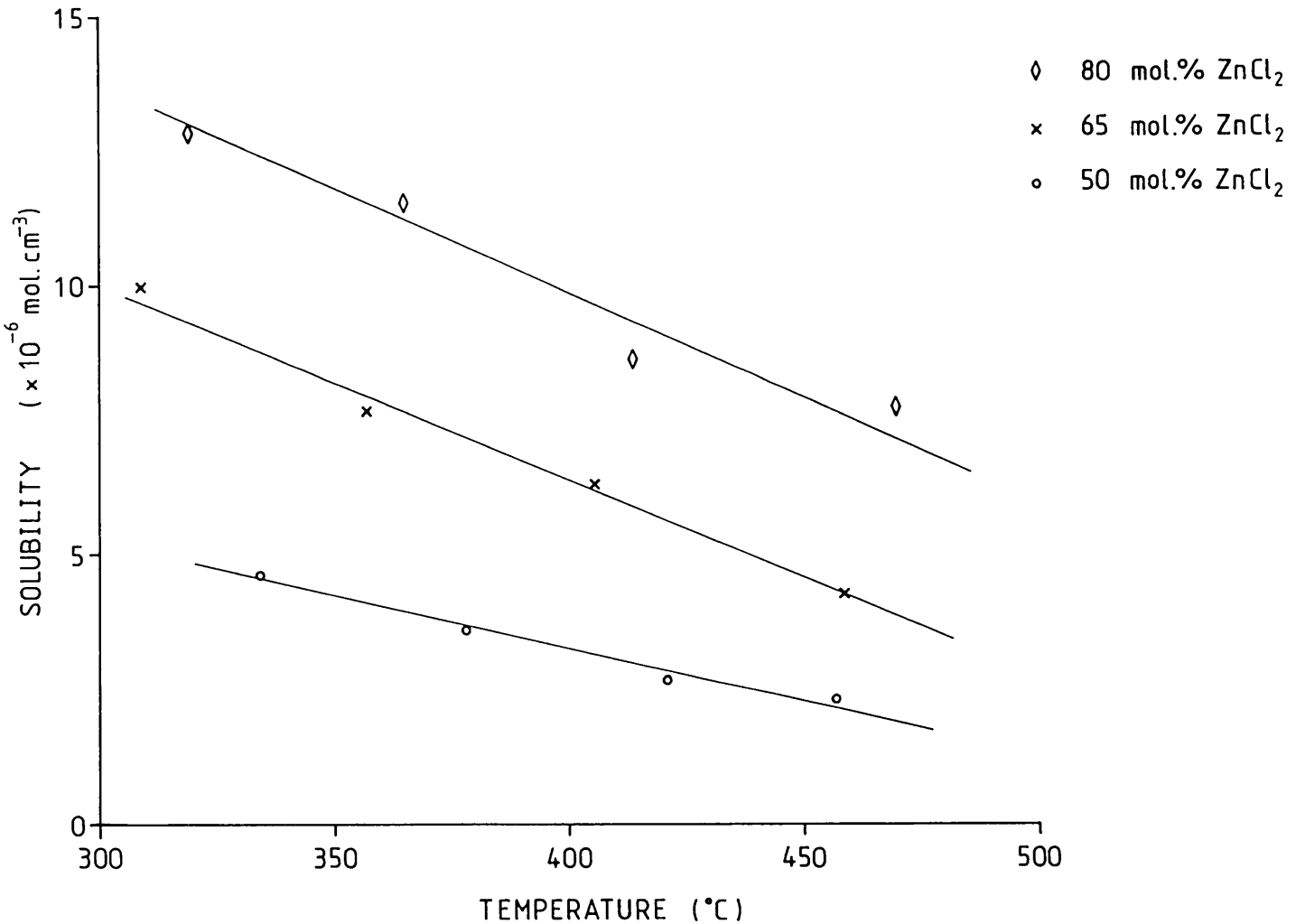


FIGURE 5.1: Solubility of HCl gas in $ZnCl_2$-NaCl Molten Mixtures

From Figure 5.1 the pattern of the solubility behaviour of HCl in these melts can be seen. As the mole fraction of zinc chloride in the melts is decreased, so the HCl solubility is found to decrease for a specific temperature. Maintaining the same melt composition and increasing its temperature also resulted in a decrease in the HCl solubility. The rate of decrease in the gas solubility with rise in melt temperature was found to be smaller as the mole fraction of zinc chloride in the melts was lowered. This would seem to imply that in the alkali metal chloride-rich melts the solubility behaviour of HCl would tend towards its behaviour in the pure molten alkali metal chloride, although there is some controversy over that matter for the case of NaCl. One study[61] has found that the HCl solubility in molten NaCl decreases very slightly with increase in melt temperature, whereas three others[59,62,67] have indicated a slight increase in solubility with temperature.

Two mechanisms of gas dissolution in molten salts have been suggested; those of chemical and physical dissolution. The former can be thought of by considering interactions between the solute and solvent molecules, resulting in the formation of one or more complex ionic species, which could be assumed to exist in the solvent phase. Solubilities in this case are found to be relatively high, and to decrease in value with increasing solvent temperature. Characteristics of physical dissolution are shown by solutes that do not interact with the solvent, leading to lower magnitudes of the solubility values which increase with increasing solvent temperature. Heats of solution determined for systems exhibiting physical solubility are found to be endothermic.

From this outline of the two types of solubility, it would appear that HCl dissolved in molten $ZnCl_2$-NaCl mixtures follows the trends characteristic of a chemical dissolution process. Only two other studies of HCl solubility in zinc chloride-alkali chloride melts could be found, but they provide an interesting comparison. For molten $ZnCl_2$-KCl mixtures (X_{ZnCl_2} = 0.45 and 0.70) it was found[69] that increasing the melt temperature from the melting point gave rise to an initial increase in HCl solubility, which, at about 400^{o}C, suddenly changed to the opposite

behaviour, and the HCl solubility began to decrease as the temperature was increased to 550°C. A decrease in the mole fraction of zinc chloride in the melt caused a decrease in the HCl solubility, as found in $ZnCl_2$-NaCl melts. Those workers, Prasolov et al.[69], used "an isobaric variant of Sievert's well-known method" but the method is not described in the English translation of the original Russian paper. However, their values of the HCl solubility, when calculated by Perry[83] in units of mol. cm^{-3}, can be seen to be up to 100 times larger than the values found in this work in $ZnCl_2$-NaCl, which are of the order of 10^{-6} mol. cm^{-3}. The only other values of HCl solubility in zinc chloride melts are those of Minh and Welch[70], in LiCl-KCl-$ZnCl_2$ molten mixtures ($0 < X_{ZnCl_2} < 17.4$), who obtained values of a similar magnitude to those obtained in this study. Table 5.1 shows the results for this study, and those for the work in $ZnCl_2$-KCl and $ZnCl_2$-LiCl-KCl so that a visual comparison may be made. Without knowledge of the method used by Prasolov[69] it is difficult to see how such a large discrepancy between the sets of results could occur.

For later work it was necessary to estimate the solubility of HCl in $ZnCl_2$-NaCl melts at melt compositions other than those used here. To do this, the decrease in solubility with temperature, shown in Figure 5.1, was taken to be linear. This may be an over-simplification of the true case, but the plots of the data approximated to linear behaviour more than any other function. In one paper by Novozhilov et al.[62] on the HCl solubility in molten alkali metal chlorides, great significance was read into the S-shape of their plots, which was said to be indicative of the temperature dependence of the heats of solution. Most workers, however, have assumed a linear relationship between solubility and temperature. From Figure 5.1 it was possible to construct a plot of X_{ZnCl_2} against HCl solubility, this time keeping the temperature constant, shown in Figure 5.2. In increments of 25°C from 350-450°C a series of solubility isotherms have been created. Knowing the mole fraction of zinc chloride in a melt and the melt temperature, an estimate of the HCl solubility in that melt may be obtained.

As previously mentioned, each solubility measurement was carried out three times in order to estimate the errors. It was found that for all

Mol.% $ZnCl_2$-MCl		Temp.(^oC)	HCl solubility (mol. cm^{-3})	Reference
80	(+NaCl)	319	12.83×10^{-6}	This work
	(+NaCl)	365	11.53×10^{-6}	
	(+NaCl)	414	8.62×10^{-6}	
	(+NaCl)	470	7.73×10^{-6}	
65	(+NaCl)	309	9.98×10^{-6}	This work
	(+NaCl)	357	7.67×10^{-6}	
	(+NaCl)	406	6.32×10^{-6}	
	(+NaCl)	459	4.29×10^{-6}	
50	(+NaCl)	334	4.60×10^{-6}	This work
	(+NaCl)	378	3.56×10^{-6}	
	(+NaCl)	421	2.66×10^{-6}	
	(+NaCl)	457	2.30×10^{-6}	
70	(+KCl)	310	2.7×10^{-4}	83 (Taken from 69)
	(+KCl)	350	2.8×10^{-4}	
	(+KCl)	400	2.9×10^{-4}	
	(+KCl)	450	2.4×10^{-4}	
	(+KCl)	500	2.2×10^{-4}	
45	(+KCl)	350	1.9×10^{-4}	83 (Taken from 69)
	(+KCl)	400	2.4×10^{-4}	
	(+KCl)	450	1.8×10^{-4}	
	(+KCl)	500	1.4×10^{-4}	
	(+KCl)	550	1.2×10^{-4}	
11.9	(+LiCl-KCl eutectic)	395	2.14×10^{-6}	70
		450	2.03×10^{-6}	
		500	1.83×10^{-6}	

TABLE 5.1

Solubility of HCl gas in zinc chloride melts

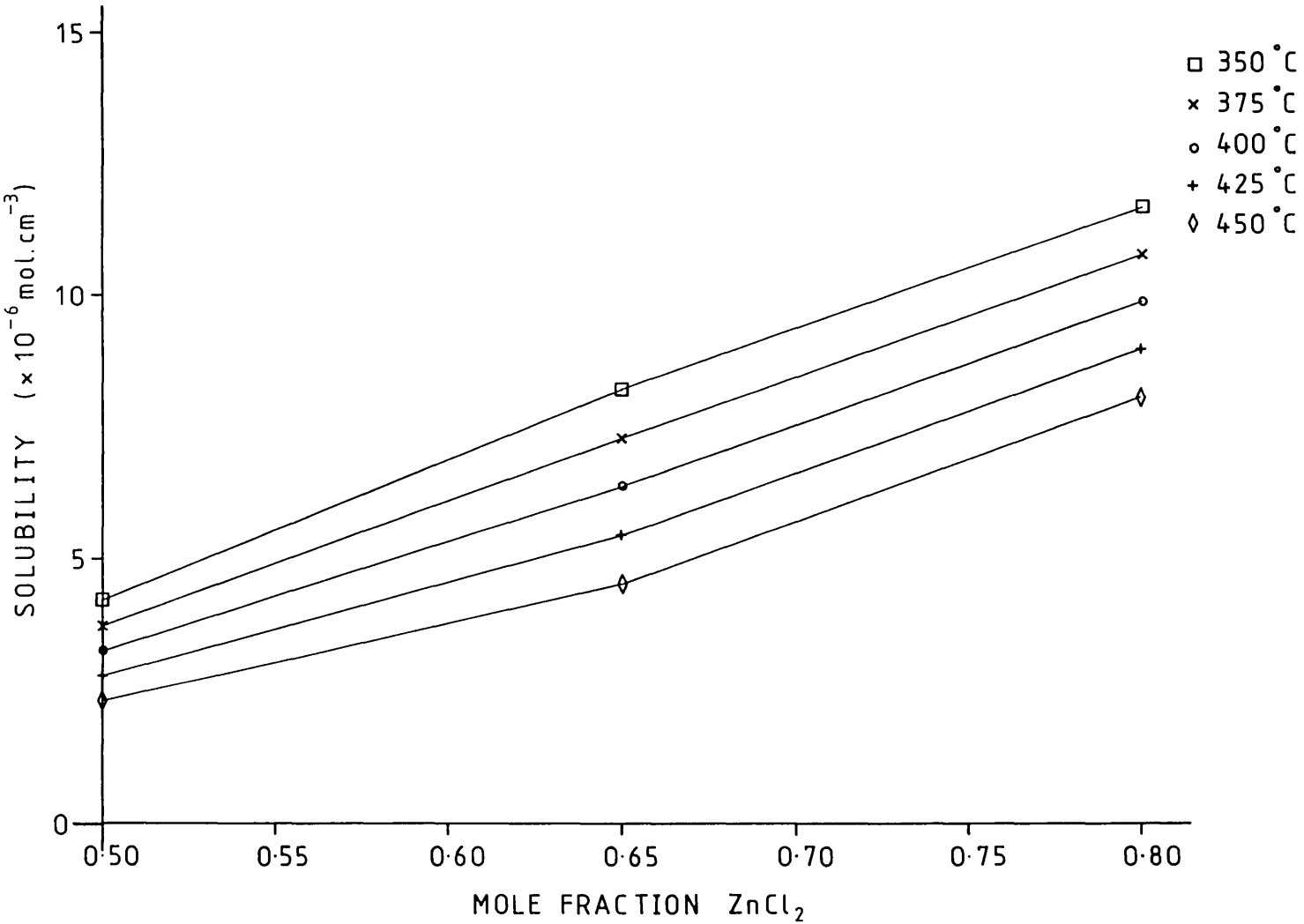


FIGURE 5.2: Solubility Isotherms of HCl gas in $ZnCl_2$-NaCl Molten Mixtures

of the points measured, the error in the value obtained was lower than $\pm$15%, the lowest error being $\pm$10%, but Novozhilov and his co-workers(62) claim an accuracy of $\pm$1% for their work, perhaps a rather optimistic value. Most workers in the gas solubility field give an error $\pm$5% or greater[63].

From the experimental results it is possible to obtain estimated values of the heat of solution for HCl in these melts[65,130]. The process being studied is:

$$HCl\ (gas) = HCl\ (dissolved) \qquad [5.1]$$

with an equilibrium constant given by:

$$K = \frac{a_{HCl\ (d)}}{a_{HCl}(g)} \qquad [5.2]$$

Taking the traditional standard states for the gas and liquid components; HCl gas at 1 atm. and dissolved HCl at 1 mol. cm^{-3}, and assuming Henry's Law and ideal gas behaviour, the equilibrium constant is equal to the Henry's Law constant:

$$K_H = C_{HCl}(d)/p_{HCl}(g) \qquad [5.3]$$

At 1 atm. of HCl pressure the Henry's Law constant is equal to the solubility of HCl. The standard enthalpy change for the dissolution process is:

$$\Delta H_d^o = - R \frac{d \ln K_H}{d(1/T)} \qquad [5.4]$$

A plot of log X_{HCl} versus 1/T should be linear, with a slope equal to $-\Delta H_d^o/2.303\ R$. This plot was constructed, taking

$$X_{HCl} = n_{HCl}/(n_{HCl} + n_{melt})$$

and is shown in Figure 5.3 for the three melt compositions studied.

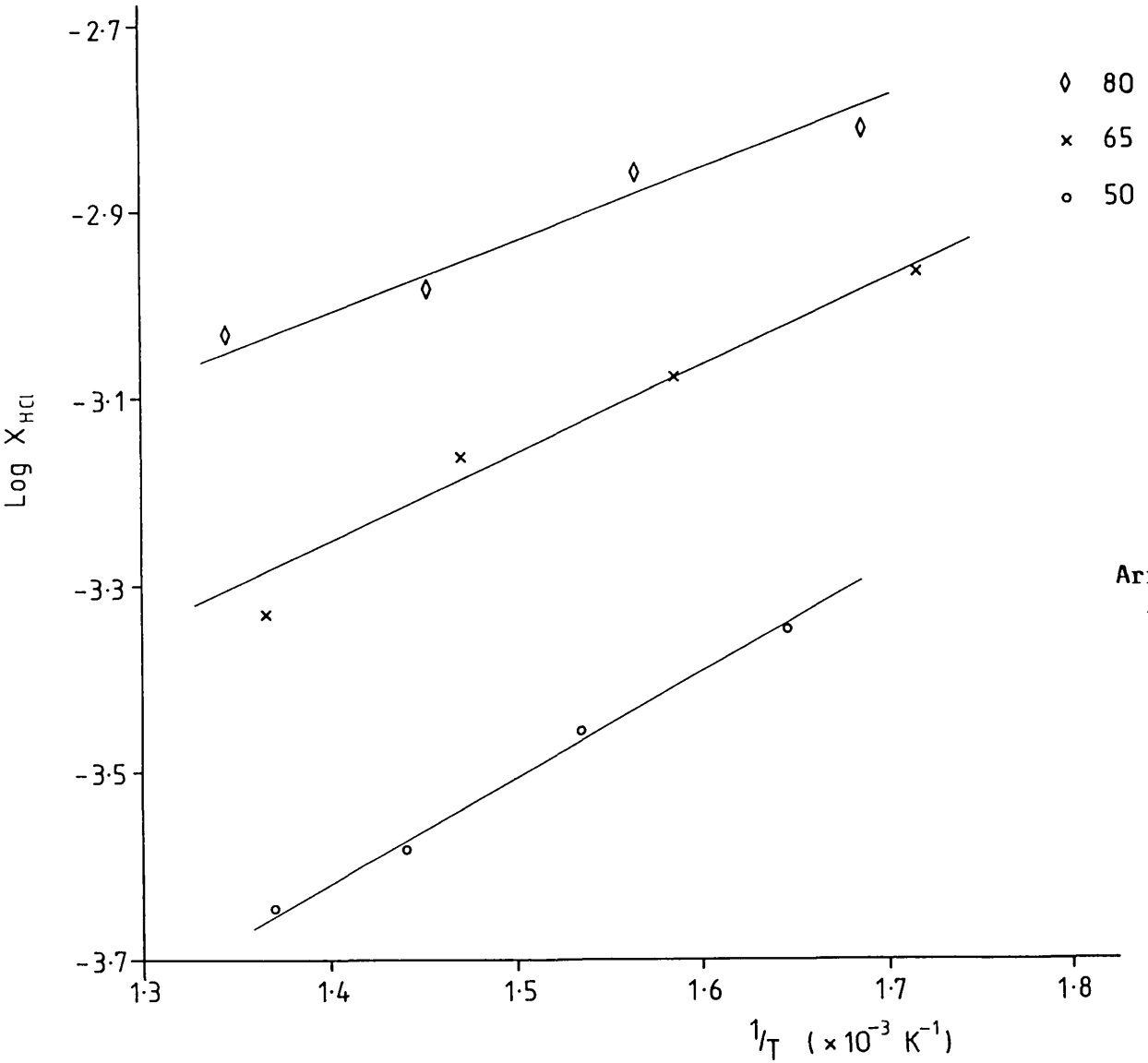


FIGURE 5.3

Arrhenius Plot for HCl Solubility in $ZnCl_2$-NaCl Molten Mixtures

Although they are by no means perfectly linear, it is reasonable to assume a linear relationship for the sake of the calculations. The heats of solution were calculated and are shown in Table 5.2, along with those calculated for other molten chlorides. It can be seen that as the $ZnCl_2$-NaCl melts are made more basic, so the heat of solution increases, but one should perhaps not attach too much importance to this since the errors are larger than the gaps between the values. More importantly, the heats are seen to be exothermic, indicating the chemical nature of the dissolution process. Similarly, the alkali metal chlorides and $SbCl_3$ have exothermic ΔH_d values, whereas the alkaline earth chlorides do not, indicating a physical dissolution process is occurring. This can be tied in with I.R. spectroscopic studies[76], which showed that HCl is present as monomers in MCl_2 melts, whereas it is associated into complexes of the type $Cl\text{-}H....Cl^-_{melt}$ in the MCl melts. It would be interesting to study HCl dissolved in the $ZnCl_2$ melts using I.R. spectroscopy, but this work has not yet been carried out. The ΔH_d values for the $ZnCl_2$-KCl melts have been asterisked because the data were treated as a whole, rather than treating the two parts of solubility/temperature plots individually.

Having indicated that a chemical dissolution process is occurring in the $ZnCl_2$-NaCl melts, it would be useful to consider possible complex species that might be formed. A variety of species can be thought of, but the two that most people concentrate on are $H^+ ZnCl_3^-$ and the bihalide, HCl_2^-. The former species is popularly invoked by those interested in hydrocracking as being the entity responsible for the catalytic activity of $ZnCl_2$ (see Appendix 1), whilst the latter is that usually invoked by those measuring HCl solubilities (Section 2.3.1). For the two complexes one may consider their effect on the solubility behaviour of HCl in $ZnCl_2$ melts.

If $H^+ ZnCl_3^-$ is the species formed, then one could imagine the HCl molecule acting in the same way as MCl; enhancing the formation of four-co-ordinate zinc species, c.f. $ZnCl_4^{2-}$, and breaking down the $ZnCl_2$ polymeric structure. In $ZnCl_2$-KCl melts, the weak polarizing nature of K^+ ions means that there is a greater availability of Cl^- ions than in the $ZnCl_2$-NaCl melts, and more $ZnCl_4^{2-}$ can be formed. So the potential for formation

Solvent	Temp. Range (^{o}C)	ΔH_d (kJ $mol.^{-1}$)	Reference
80 mol% $ZnCl_2$-NaCl	319- 470	-13.15± 8.41	This work
65 mol% $ZnCl_2$-NaCl	309- 459	-19.20±10.28	This work
50 mol% $ZnCl_2$-NaCl	334- 457	-21.25± 4.54	This work
NaCl	820-1020	-0.46± 1.60	61,62
KCl	789- 987	-4.03± 0.55	62
RbCl	722- 972	-9.37± 1.55	62
CsCl	669- 945	-21.00± 1.30	62
$CaCl_2$	820-1000	28.01± 2.86	64
$SrCl_2$	890-1022	38.05± 1.18	64
$BaCl_2$	980-1078	42.25± 3.74	64
$SbCl_3$	80- 120	-7.64	68
*70 mol% $ZnCl_2$-KCl	310- 500	-4.20± 6.80	83 (from 69)
*45 mol% $ZnCl_2$-KCl	350- 550	-11.63±15.16	83 (from 69)
LiCl-KCl (eut.)	499- 675	14.70± 1.50	65

TABLE 5.2

Heats of Solution for the Dissolution of HCl gas in Various Molten Chlorides

of $H^+ZnCl_3^-$ in the $ZnCl_2$-KCl melts would seem to be lower than in $ZnCl_2$-NaCl, and it would depend on the ability of HCl to displace a Cl^- ion from the $ZnCl_4^{2-}$ by some equilibrium, say:

$$ZnCl_4^{2-} + HCl = H^+ZnCl_3^- + 2Cl^- \qquad [5.5]$$

In the pure molten $ZnCl_2$ used by the hydrocracking researchers much of the $ZnCl_2$ would still be in the polymeric state, and the HCl may well form $H^+ZnCl_3^-$, but this seems increasingly unlikely as more MCl is added. From the arguments above, if $H^+ZnCl_3^-$ is the only species formed, then one would expect the HCl solubility to be lower in $ZnCl_2$-KCl than in $ZnCl_2$-NaCl melts.

If HCl_2^- is the only species formed, than its formation would be enhanced in $ZnCl_2$-KCl, due to the greater availability of Cl^- ions which could "complex" to the HCl, as has been mentioned earlier. Now the HCl would be acting as a Lewis acid, and would be in competition with the $ZnCl_2$ for the available Cl^-. In this case it could be argued that the HCl solubility would be greater in $ZnCl_2$-KCl melts than in $ZnCl_2$-NaCl, as is found experimentally (Table 5.1). However, the fact that the HCl solubility increases as X_{ZnCl_2} increases points to the formation of $H^+ZnCl_3^-$.

As can be seen, the situation is rather complicated: one may postulate many equilibria that could theoretically be present in these solutions of HCl in $ZnCl_2$ melts, and some of these are shown in Figure 5.4. The position of these equilibria would undoubtedly be dependent on factors such as melt composition and temperature and possibly on the pressure of HCl over the melt. Other workers[70,83], whilst postulating the existence of complex species in $ZnCl_2$ melts, have hesitated to indicate what these species might be. Similarly, in $SbCl_3$[68], which is also known for its catalytic nature in the hydrocracking process, one could imagine the existence of species like $H^+SbCl_4^-$ (c.f. $H^+ZnCl_3^-$) which are responsible for enhancing the hydrocracking. To explain their results for the HCl solubility in $ZnCl_2$-KCl melts, Prasolov et al.[69] considered "the existence of two zones of structure in the melt" with " complex structures involving KCl as well as $ZnCl_2$".

$$HCl\ (gas) = HCl\ (dissolved)$$

$$HCl\ (physically\ dissolved) = HCl\ (chemically\ dissolved)$$

$$HCl\ (c.d.) = H^+ + Cl^-$$

$$HCl + nCl^- = HCl_{n+1}^{n-}$$

$$HCl + ZnCl_2 = H^+ZnCl_3^-$$

$$HCl + H^+ZnCl_3^- = H_2^{2+}ZnCl_4^{2-}$$

$$HCl + ZnCl_4^{2-} = H^+ZnCl_3^- + 2Cl^-$$

$$H^+ + mCl^- = HCl_m^{m-}$$

$$H^+ + 2\,ZnCl_4^{2-} = Cl_3ZnCl^{\delta-}\cdots H^{\delta+}\cdots ClZnCl_3^{\delta-}$$

FIGURE 5.4

Equilibria Postulated to Exist in Solutions of HCl in Zinc Chloride Melts

An explanation that could account for the solubility behaviour is as follows. In $ZnCl_2$-MCl melts with low amounts of alkali metal chloride, the HCl dissolves to form the species $H^+ZnCl_3^-$. As more alkali metal chloride is added, so this species becomes unfavourable, and HCl_2^- is formed in preference. As the melts are made more basic so HCl_2^- becomes the predominant species, and the solubility behaviour tends towards that seen in the pure alkali metal chlorides, as is found experimentally. The prospect of a bare proton existing in these chloride melts is most unlikely; a highly polarizing species like H^+ is almost sure to attract negatively charged species to it. The explanation outlined above would account for most of the phenomena observed experimentally; the increase of solubility with X_{ZnCl_2}, the lower solubility of HCl in $ZnCl_2$-NaCl than in $ZnCl_2$-KCl, the exothermic heats of solution and the decrease in solubility with increasing temperature for the same melt composition. The fact that the HCl solubility is lower in the MCl-rich melts indicates that $H^+ZnCl_3^-$ might be formed to a greater extent in the $ZnCl_2$-rich melts than HCl_2^- is formed in the MCl-rich melts. If this is so then $ZnCl_2$ would appear to be a stronger Lewis acid than HCl.

5.2 Voltammetric Study of HCl in $ZnCl_2$-NaCl Melts

As indicated in Section 2.5 there have already been various investigations into the voltammetric behaviour of HCl in chloride melts, but only two have involved the use of zinc chloride-containing melts; those of Minh and Welch[70] and Perry and MacDonald[83] working with $ZnCl_2$-LiCl-KCl and $ZnCl_2$-KCl respectively. However, the validity of some of the results obtained has been brought into question following controversy over the use of vitreous carbon as a working electrode material. Two groups of workers, using vitreous carbon electrodes, claim to have observed electrode reactions attributable to the reduction of HCl, and from these have calculated diffusion coefficients for the diffusing species[65,70,81]. In this case the D_{HCl} values were larger than expected, and caused those authors to invoke the existence of bare H^+ ions in order to explain their results.

However, in this work and in that of many other workers such reactions have not been observed, either voltammetrically or chronopotentiometrically[82,83,99,100,132]. The cathodic limit of the melt is reached before hydrogen is evolved on the vitreous carbon, indicating that the overpotential for reduction of H^+ to H atoms is too high for that process to be observed. Even results of those studies not using vitreous carbon electrodes are quite widely differing. In the two investigations of HCl dissolved in $ZnCl_2$ melts[70,83] the calculated diffusion coefficients differ by a factor of up to 10^4, which can not be solely accounted for by the fact that one set of results is for $ZnCl_2$-rich melts[83] whilst the other is for MCl-rich melts[70]. It was the purpose of this investigation to try to determine the behaviour of HCl in $ZnCl_2$ melts over a range of compositions and temperatures, by coupling the voltammetric results with those of the solubility determination (Section 5.1).

In passing, the use of iron as a working electrode in $MgCl_2$ melts by a Norwegian group[132] should also be mentioned. During their investigation of the behaviour of hydrogen- and oxygen -containing species in $MgCl_2$ melts, it was found that iron gave a better voltammetric response than vitreous carbon or platinum. However, iron is not noted for its inert nature, and it is quite likely that oxides or chlorides may have formed on the electrode surface, so interfering with the voltammetric response.

In this work the behaviour of solutions of HCl gas in molten $ZnCl_2$-NaCl mixtures has been investigated using cyclic voltammetry. The melt components had been prepared as outlined previously (Section 3.1) and were mixed in the required compositions in the dry-box. The compositions used are listed below:

Pure $ZnCl_2$
90 mol. % $ZnCl_2$ - 10 mol. % NaCl
80 mol. % $ZnCl_2$ - 20 mol. % NaCl
70 mol. % $ZnCl_2$ - 30 mol. % NaCl
60 mol. % $ZnCl_2$ - 40 mol. % NaCl
50 mol. % $ZnCl_2$ - 50 mol. % NaCl

A three electrode system was used; platinum wire working and quasi-reference electrodes and a graphite counter electrode, the description of each having been given earlier (Section 3.4). Vitreous carbon working electrodes were tested in the HCl-saturated melts, but no response other than the melt decomposition peaks was observed on the voltammograms. The platinum electrodes were cleaned either by flame-polishing or by immersion in concentrated hydrochloric acid, to see if the method of cleaning had any effect on the shape of the voltammograms. No difference could be seen, so it would appear that both are applicable to these electrodes. Mechanical polishing, which may be better than the other cleaning methods, is difficult to carry out on the wire electrodes but can be used for disc electrodes.

Cyclic voltammetry was used to estimate the time for saturation of the melt with the solute HCl gas, by recording the time at which the reduction peak reached its maximum value. For the less viscous melts, saturation was achieved within thirty minutes, taking slightly longer as the melts became more $ZnCl_2$-rich. However, for the voltammetric experiments the HCl was bubbled through the melts for 2-3 hours to be sure that equilibrium had been reached. The melts were water-clear but contained black flecks of carbon (Section 4.2).

5.2.1 Behaviour of the platinum quasi-reference electrode

To check the stability of the platinum quasi-reference electrode (q.r.e.) used in the HCl- saturated melts the potential between a platinum wire electrode and a silver/silver chloride reference electrode was recorded as a function of time. A 50 mol. % $ZnCl_2$-NaCl mixture, chosen arbitrarily, was heated to about $370^{o}C$, saturated with HCl gas, and the platinum electrode introduced. The Ag/AgCl electrode was put in the melt earlier to allow the reference mixture to be come molten. The potential between the electrodes was measured on a Fluke 8860A D.V.M., and noted at 60 sec. intervals.

The plot of potential against time is shown in Figure 5.5. From the introduction of the electrode to the melt (time = 0 sec) an initial

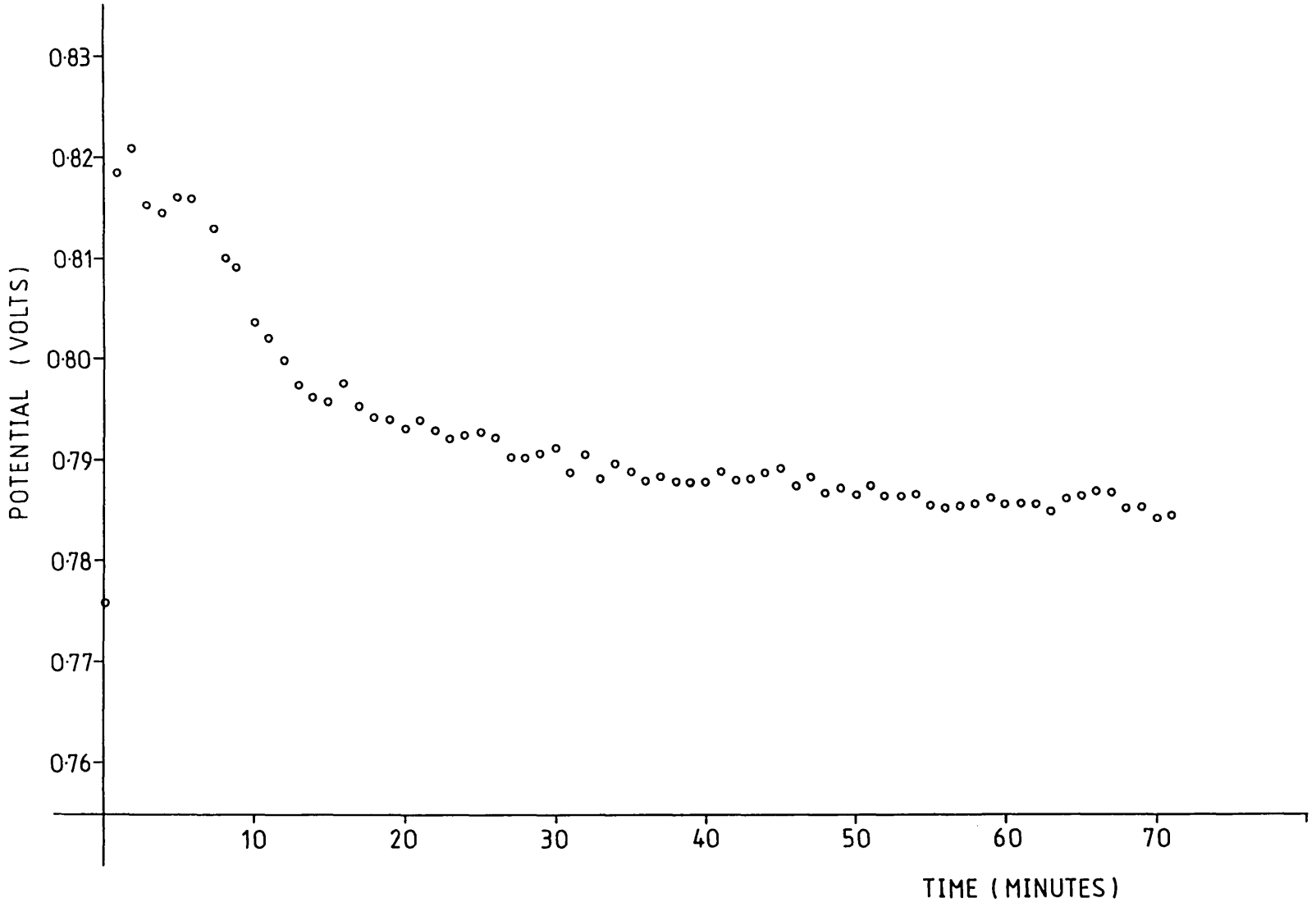


FIGURE 5.5: Potential (E = F(t)) Between Pt and Ag/AgCl Electrodes in HCl-saturated 50 mol. % $ZnCl_2$-NaCl at 372°C

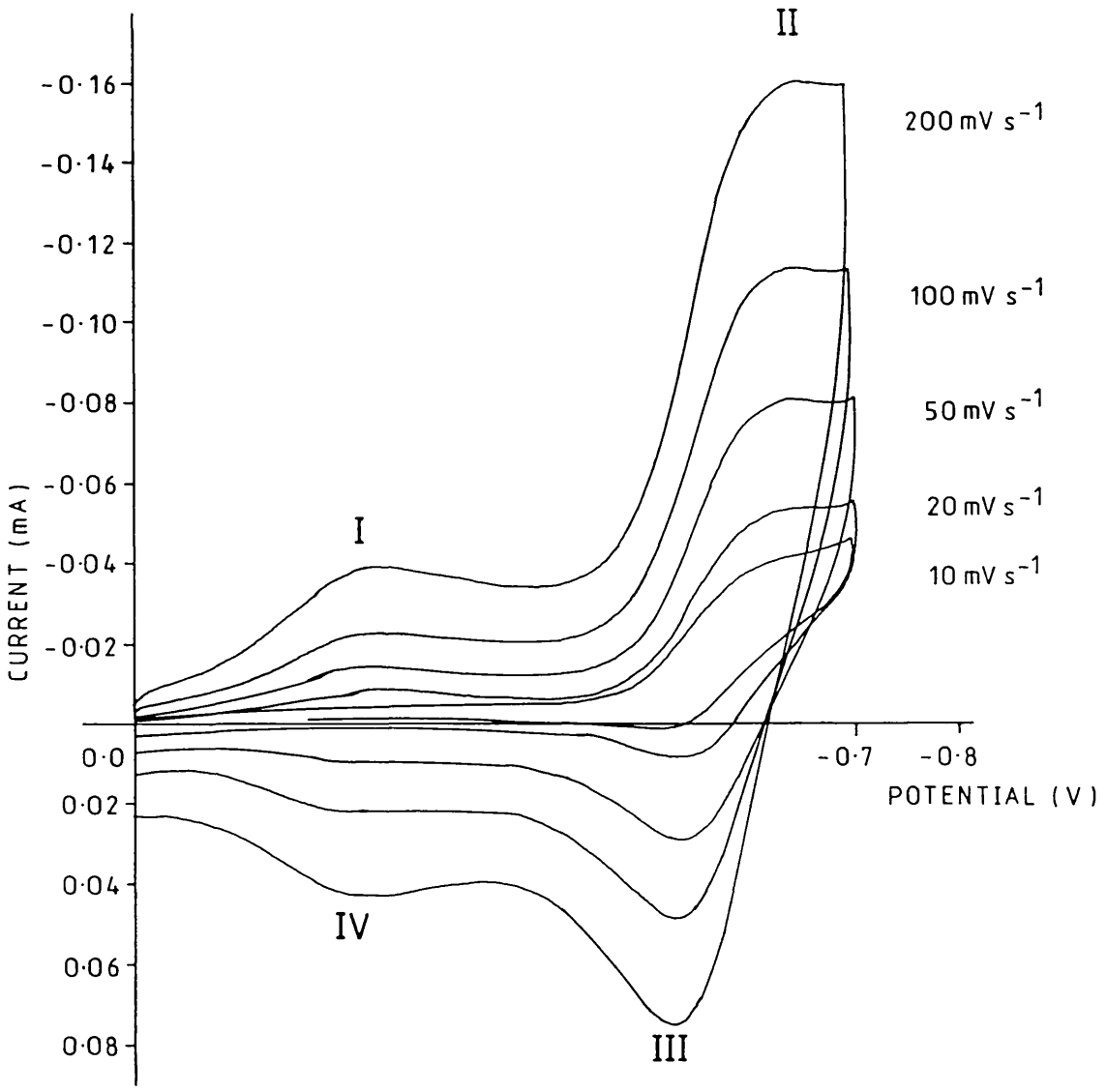
rise and fall in the potential between the two electrodes is seen to level out after 10-15 minutes and remain fairly constant from then onwards. Measurement was stopped after 70 minutes since the voltammetric experiments, in which the platinum q.r.e. was to be used, could be carried out in 30-40 minutes. The initial change in potential is probably due to the rapid heating of the electrode as it enters the melt and settles at the melt temperature. This experiment was carried out three times, and each time the potential difference settled at 0.78-0.79 V, the platinum electrode assuming a potential anodic to that of the Ag/AgCl electrode.

5.2.2 Reduction of HCl in $ZnCl_2$-NaCl melts

Cyclic voltammograms were obtained for the reduction of HCl dissolved in these melts over a range of temperatures for the compositions listed earlier. The voltage scans were started at the equilibrium position, and swept cathodically with respect to the quasi-reference electrode. Reversal of the scans was carried out at different potentials, depending on where the responses appeared, but in general took place at around -0.7V with respect to the q.r.e. Scans carried out in the anodic direction showed no peaks before the anodic limit of the system was reached.

A set of typical voltammograms for the reduction of $ZnCl_2$-NaCl melts is shown in Figure 5.6. Scan rates between 10 and 1000 mVs^{-1} were used for virtually all the melt compositions, with the voltammograms all resembling each other except for those recorded at higher melt temperatures where reduction peak (II) became rather less well defined.

Moving cathodically from the rest position two peaks (I, II) are observed before the reversal occurs, when two more peaks (III, IV) appear before returning to the rest position. The difference between the two pairs of peaks can be immediately seen. Peaks I and IV are virtually symmetrical about the potential axis, and only really begin to appear at the higher scan rates. On the other hand, peaks II and III are in no way symmetrical, being more like those



Working electrode = Platinum

Temperature = 319 °C

FIGURE 5.6

Voltammograms for the Reduction of HCl in 60 mol. % $ZnCl_2$-NaCl

resulting from a diffusion-controlled process. At low scan rates peak III, the anodic response of peak II, almost disappears, only becoming sharp at the higher scan rates. The two pairs of peaks will be treated separately to avoid confusion, and rather than plot all the possible graphs, data will be tabulated and example graphs given.

The symmetry of peaks I and IV indicates that, rather than being caused by a diffusion-controlled process, they are the result of a process that is affecting the electrode material. If it is recalled that the reduction of H^+ ions yields hydrogen atoms, then a process that suggests itself is that of adsorption of hydrogen atoms onto the platinum electrode. Platinum is well known for its adsorption of hydrogen in aqueous electrochemistry[136], and this phenomenon has also been reported by other molten salt workers[70,92]. Under conditions in which both adsorption and diffusion control are significant, a peak prior to the diffusion-controlled voltammetric peak is obtained for the reduction to the adsorbed state. The reverse potential scan contains a peak related to the desorption process, following the diffusion- controlled peak[137]. Observation of both responses is necessary for characterization of the process as the sequence:

$$O + ne = R$$

$$R = R_{(ads)}$$

Both peaks can be seen in Figure 5.6. The voltammetric parameters for peak I are given in Tables 5.3-5.7 for a range of melt compositions and temperatures.

The peak current of the adsorption peak, i_{ads}, can be seen to vary linearly with ν, the scan rate, (Figure 5.7) rather than with $\nu^{\frac{1}{2}}$ as in the case of a diffusion-controlled process. At low scan rates the adsorption peaks are not seen on the voltammograms (Figure 5.6), whilst the width of the responses indicate that the solute concentration was low. The sharpness of the response is

working electrode: platinum

$\nu(Vs^{-1})$	T (K)	$-Ep^{II}(V)$	$-E_{ads}{}^{I}(V)$	$\lvert Ep^{II}-E_{ads}{}^{I}\rvert$ (V)	$i_{ads}{}^{I}$ (mA)
0.20	620	0.540	0.180	0.360	0.025
0.50	620	0.535	0.190	0.345	0.056
1.00	620	0.540	0.210	0.330	0.100

TABLE 5.3

Voltammetric Parameters for Adsorption Peak (I) in pure $ZnCl_2$

working electrode: platinum

$\nu(Vs^{-1})$	T (K)	$-Ep^{II}(V)$	$-E^{I}_{ads}$ (V)	$\lvert Ep^{II} - E^{I}_{ads} \rvert$ (V)	i^{I}_{ads} (mA)
0.20	590	0.530	0.150	0.380	0.023
0.50	590	0.534	0.155	0.379	0.054
1.00	590	0.540	0.155	0.385	0.103
0.20	617	0.520	0.115	0.405	0.024
0.50	617	0.528	0.130	0.392	0.055
1.00	617	0.530	0.125	0.405	0.105
0.20	649	0.455	0.035	0.420	0.027
0.50	649	0.460	0.045	0.415	0.063
1.00	649	0.460	0.055	0.405	0.120
0.20	682	0.540	0.150	0.390	0.030
0.50	682	0.548	0.143	0.405	0.062
1.00	682	0.547	0.147	0.400	0.122

TABLE 5.4

Voltammetric Parameters for Adsorption Peak (I) in 80 mol. % $ZnCl_2$-NaCl

working electrode: platinum

$\nu(Vs^{-1})$	T (K)	$-Ep^{II}$(V)	$-E^{I}_{ads}$ (V)	$\lvert Ep^{II} - E^{I}_{ads} \rvert$ (V)	i^{I}_{ads} (mA)
0.20	586	0.650	0.230	0.420	0.030
0.50	586	0.645	0.225	0.420	0.067
1.00	586	0.655	0.230	0.425	0.130
0.20	619	0.490	0.060	0.430	0.033
0.50	619	0.505	0.070	0.435	0.070
1.00	619	0.510	0.075	0.435	0.143
0.20	654	0.700	0.260	0.440	0.038
0.50	654	0.690	0.250	0.440	0.075
1.00	654	0.685	0.250	0.435	0.145
0.20	680	0.617	0.182	0.435	0.040
0.50	680	0.610	0.170	0.440	0.076
1.00	680	0.620	0.185	0.435	0.150

TABLE 5.5

Voltammetric Parametes for Adsorption Peak (I)
in 70 mol. % $ZnCl_2$-NaCl

working electrode: platinum

ν (Vs^{-1})	T (K)	$-Ep^{II}$ (V)	$-E^{I}_{ads}$ (V)	$\lvert Ep^{II} - E^{I}_{ads} \rvert$ (V)	i^{I}_{ads} (mA)
0.20	592	0.650	0.240	0.410	0.036
0.50	592	0.660	0.235	0.425	0.078
1.00	592	0.665	0.240	0.425	0.145
0.20	623	0.620	0.190	0.430	0.040
0.50	623	0.630	0.195	0.435	0.085
1.00	623	0.635	0.195	0.440	0.157
0.20	651	0.520	0.090	0.430	0.045
0.50	651	0.525	0.090	0.435	0.090
1.00	651	0.520	0.100	0.420	0.165
0.20	685	0.610	0.185	0.425	0.047
0.50	685	0.605	0.180	0.425	0.098
1.00	685	0.615	0.185	0.430	0.182

TABLE 5.6

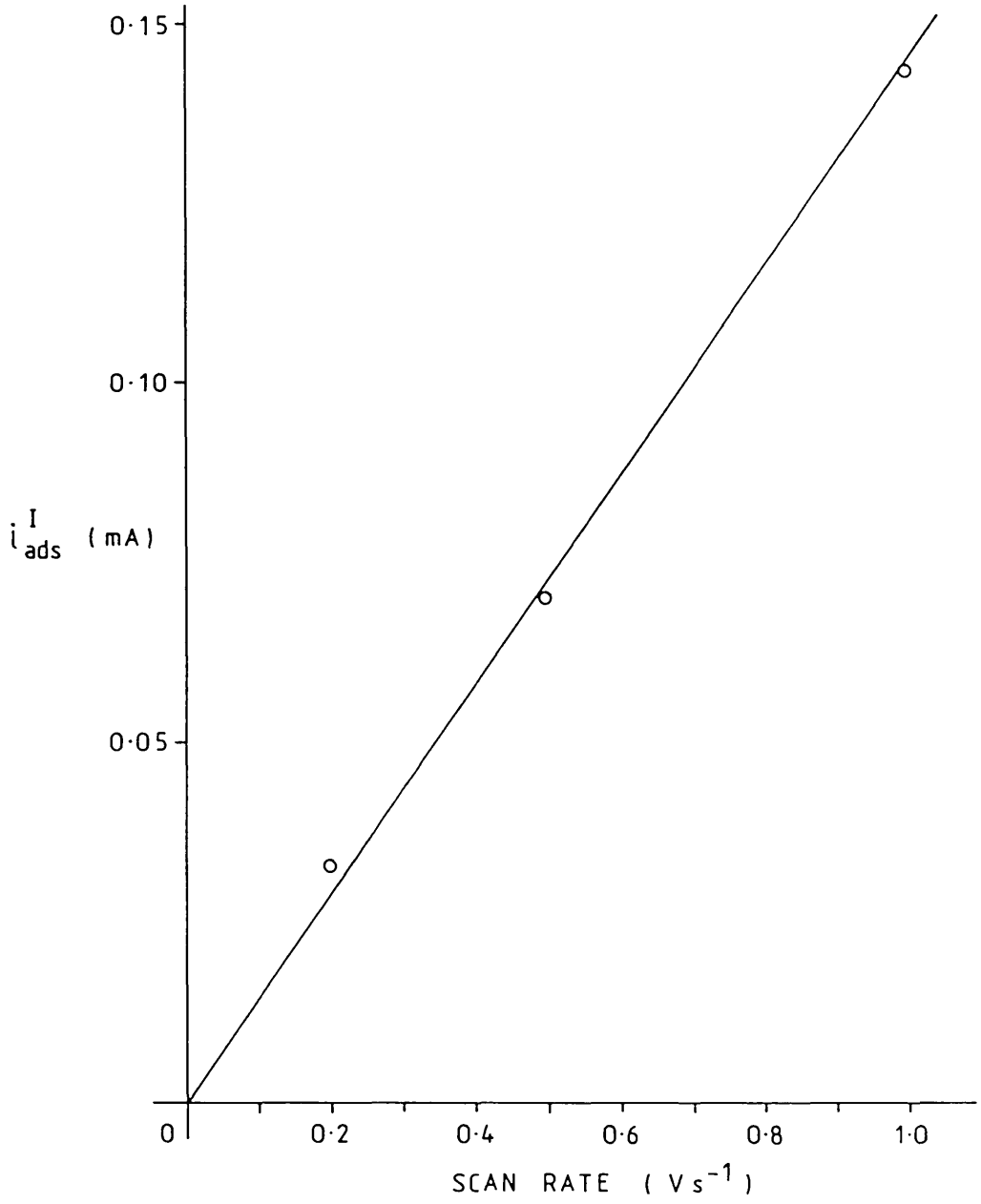
Voltammetric Parameters for Adsorption Peak (I)
in 60 mol. % $ZnCl_2$-NaCl

working electrode: platinum

$\nu(Vs^{-1})$	T (K)	$-Ep^{II}(V)$	$-E^{I}_{ads}$ (V)	$\lvert Ep^{II} - E^{I}_{ads} \rvert$ (V)	i^{I}_{ads} (mA)
0.20	604	0.640	0.225	0.415	0.040
0.50	604	0.652	0.230	0.422	0.090
1.00	604	0.655	0.235	0.420	0.160
0.20	628	0.650	0.220	0.430	0.044
0.50	628	0.650	0.215	0.435	0.095
1.00	628	0.650	0.220	0.430	0.170
0.20	657	0.650	0.220	0.430	0.045
0.50	657	0.640	0.220	0.420	0.098
1.00	657	0.645	0.220	0.425	0.183
0.20	687	0.635	0.200	0.435	0.048
0.50	687	0.640	0.210	0.430	0.095
1.00	687	0.640	0.210	0.430	0.173

TABLE 5.7

Voltammetric Parameters for Adsorption Peak (I)
in 50 mol. % $ZnCl_2$-NaCl



Melt = 70 mol.% $ZnCl_2$ - NaCl

Temperature = 346 °C

FIGURE 5.7

Variation of i^{I}_{ads} With Scan Rate

concentration dependent, with the width of the peak increasing at low concentrations of the adsorbed species, which was the case here. The rate of diffusion is not sufficient to maintain the surface concentrations in complete equilibrium with the solution concentration. As the scan rate is increased the adsorption response increases relative to the diffusion-controlled response until at very rapid scan rates only the adsorption response is seen. Such rapid scan rates were not measurable on the XY recorder used (Section 3.6).

The position of the adsorption pre-peak with respect to the diffusion-controlled peak is governed mainly by the free energy of adsorption in the absence of an applied field, ΔG_{ads}, but this does not have much influence on either the shape or height of the peaks[137]. As the free energy of adsorption is increased, the energy required for reduction to the adsorbed state is decreased and the reduction potential need not be as cathodic. While the peak separation is determined primarily by the value of ΔG_{ads}, the bulk concentration also has an effect, so it is not possible to use measured values of ΔE_p to determine ΔG_{ads} directly. However, a qualitative picture may be given. Adsorption processes are often described as being "strong" or "weak", each having different voltammetric characteristics. The type of process observed depends on a range of variables including electrode material, solute concentration and the oxidised and reduced species. From the results obtained in experimental work (Tables 5.3-5.7), the adsorption process in this work may be classified as being of the "strong" class. The peak separation $\Delta E_p = |E_p^{II} - E_{ads}^{I}|$ is greater than 120 mV, the value given in the literature as being the minimum peak separation distance for a "strong" adsorption process[138].

Other trends noticeable in the results are the slight increase in peak separation, ΔE_p, with decrease in mole fraction of zinc chloride in the melts, and an even slighter increase with increase in melt temperature. The main causes are the changing diffusion

coefficients of the oxidised and reduced species (H^+ and H respectively) as the melt system is changed, and the temperature changes which alter the free energy of adsorption. Since this project is more concerned with the species present in the melts the complex mathematical treatment necessary to fully describe the adsorption system is outside the scope of this work, but can be found in reference 138.

Having considered the adsorption peaks I and IV (Figure 5.6), the peaks due to the diffusion-controlled reduction process, II and III, may now be examined. A preliminary visual inspection of these peaks points to the reversibility of the electrode process. The peaks all lie at approximately the same potentials and increase fairly regularly with increasing scan rate. Deviation starts to occur at low scan rates ($< 10\ mVs^{-1}$) where the anodic current (peak III) has dropped to almost zero.

A brief survey of the parameters measured in the cyclic voltammetric experiment, and how they are related, would be helpful here. For cyclic (linear sweep) voltammetry the equation for a simple reversible charge transfer involving a soluble product is:

$$i_p = 0.4463\ nFAC_o \left(\frac{nF}{RT}\right)^{\frac{1}{2}} \nu^{\frac{1}{2}} D_o^{\frac{1}{2}} \qquad [5.8]$$

where i_p is the peak current (A), n is the number of electrons involved in the charge transfer step, F is the Faraday constant (JV^{-1} $mol.^{-1}$), R is the universal gas constant (J $mol.^{-1}$ K^{-1}), T is the absolute temperature, A is the area of the electrode (cm^2), C_o is the concentration of the diffusing species (mol. cm^{-3}), ν is the voltage scan rate (Vs^{-1}) and D_o is the diffusion coefficient of the diffusing species ($cm^2\ s^{-1}$). A knowledge of the voltammetric parameter i_p and the concentration allows calculation of the diffusion coefficient.

The precise measurement of E_p, the peak potential, can often be hampered if the peak is broad which leads to inaccuracies in the ΔE_p

measurement. Here ΔE_p is the difference between the anodic and cathodic peak potentials for a reversible process, and is related to the number of electrons involved in the charge transfer process by the equation:

$$\Delta E_p = 2.3\ RT/nF \qquad [5.9]$$

However, $E_{p/2}$, the potential where $i = \frac{1}{2}\ i_p$, and $E_{\frac{1}{2}}$, the potential where $i = 0.851\ i_p$, can be measured fairly accurately, so the number of electrons can be calculated from the relationship:

$$E_{p/2} - E_{\frac{1}{2}} = 1.09\ RT/nF \qquad [5.10]$$

For a diffusion-controlled reversible charge transfer process E_p is independent of ν, the scan rate, whereas i_p, as well as the current at any other point on the wave, is proportional to $\nu^{\frac{1}{2}}$. Also used as a criterion of reversibility and diffusion control is the ratio of the anodic (i_{pa}) to the cathodic (i_{pc}) peak currents, which is calculated using the equation:

$$\frac{i_{pa}}{i_{pc}} = \frac{(i_{pa})_o}{i_{pc}} + 0.485\ \frac{(i_{sp})_o}{i_{pc}} + 0.086 \qquad [5.11]$$

where $(i_{pa})_o$ is the value of the current measured from the potential axis to the anodic peak and $(i_{sp})_o$ is the current recorded at the switching potential, where the potential scan is reversed. For a reversible process the current ratio is unity and is independent of the scan rate. Equation 5.11 is given in the form applicable to voltammograms where the initial sweep is in the cathodic direction i.e. reduction of an electroactive species is occurring. For a voltammogram where the anodic sweep is the first, the ratio i_{pc}/i_{pa} is used.

As systems deviate from reversibility so new equations become applicable. For quasi-reversible processes the current is controlled by a mixture of diffusion and charge transfer kinetics and this has to be taken into account, whilst for irreversible processes yet another set of equations relating the voltammetric parameters have to be used. For the irreversible processes the charge transfer rate constants are small, around 10^{-6} cm sec^{-1}, so the potential at which a significant extent of reaction occurs may be quite cathodic of the standard potential. At such potentials the reverse charge transfer process does not occur, and no anodic peak is seen on the reverse scan, assuming the initial sweep was in the cathodic direction. For more detailed discussions and full mathematical treatment of the cyclic voltammetric method references 136 and 137 are recommended.

The voltammetric parameters for the diffusion-controlled reduction of HCl dissolved in $ZnCl_2$-NaCl melts are listed in Table 5.8-5.13. These relate to the peaks labelled II and III in Figure 5.6. The peak potentials, E_{pc}^{II} and E_{pa}^{III}, and the potentials $E_{p/2}$ and $E_{1/2}$ were measured against the platinum q.r.e. Peak currents were measured from the potential axis, but corrections for the adsorption peaks will be mentioned later. Initially a Ag/AgCl reference electrode was to be used but problems occurred with prolonged use and the platinum q.r.e. was more durable. Interestingly, Perry et al.[83] used a $Pt/PtCl_2$ reference electrode and a Pt q.r.e. for their work on HCl in $ZnCl_2$-KCl and obtained better results with the latter electrode than with the former. Experimental values of ΔE_p and $|E_{p/2} - E_{1/2}|$ were much closer to the calculated values when the Pt q.r.e. was used. For these reasons a platinum q.r.e. was used for the rest of this work.

The values of ΔE_p and $|E_{p/2} - E_{\frac{1}{2}}|$ determined experimentally for the reduction of HCl in $ZnCl_2$-NaCl melts, listed in Table 5.8-5.13, can be seen to be fairly close to the calculated values of these functions, taking n, the number of electrons, as being equal to 1. The calculated values, found using equations 5.9 and 5.10, are given at the bottom of each set of results. Figure 5.8 shows that very little variation in the cathodic peak potential, E_{pc}^{II}, occurred as the scan rate was altered. This is a characteristic of a reversible charge transfer process.

ν (Vs^{-1})	T (K)	$-Ep^c$ (V)	$-Ep^a$ (V)	ΔEp (V)	$-E_{\frac{1}{2}}$ (V)	$-E_{p/2}$ (V)	$\lvert E_{p/2} - E_{\frac{1}{2}} \rvert$ (V)	i_p (mA)	i_{pa}/i_{pc}
0.02	620	0.540	0.415	0.125	0.478	0.420	0.058	0.017	1.09
0.05	620	0.540	0.410	0.130	0.485	0.420	0.065	0.027	1.17
0.10	620	0.536	0.405	0.130	0.475	0.410	0.065	0.040	1.18
0.20	620	0.540	0.400	0.140	0.478	0.397	0.081	0.059	1.23
0.50	620	0.535	0.375	0.160	0.485	0.380	0.105	0.101	1.27
1.00	620	0.540	0.370	0.170				0.151	1.30
calc.				0.123			0.058		

TABLE 5.8

Voltammetric Parameters for the Diffusion Controlled Reduction of HCl in Pure $ZnCl_2$
(Pt electrode, 0.151 cm^2)

ν (Vs^{-1})	T (K)	$-Ep^c$ (V)	$-Ep^a$ (V)	ΔEp (V)	$-E_{\frac{1}{2}}$ (V)	$-E_{p/2}$ (V)	$\lvert E_{p/2} - E_{\frac{1}{2}} \rvert$	i_p (mA)	i_{pa}/i_{pc}
0.02	596	0.640	0.520	0.120	0.573	0.517	0.056	0.026	1.39
0.05	596	0.690	0.550	0.140	0.592	0.530	0.062	0.045	1.12
0.10	596	0.723	0.580	0.143	0.625	0.567	0.058	0.066	1.04
0.20	596	0.710	0.570	0.140	0.625	0.558	0.067	0.090	1.15
0.50	596	0.705	0.555	0.150	0.610	0.525	0.085	0.150	1.19
1.00	596	0.705	0.550	0.155	0.600			0.230	1.21
calc.				0.118			0.056		
0.02	647	0.310	0.160	0.150	0.240	0.186	0.054	0.041	0.93
0.05	647	0.305	0.165	0.140	0.240	0.183	0.057	0.064	1.02
0.10	647	0.305	0.170	0.135	0.240	0.180	0.060	0.094	1.07
0.20	647	0.300	0.170	0.130	0.238	0.175	0.063	0.131	1.12
0.50	647	0.300	0.160	0.140	0.238	0.170	0.068	0.225	1.19
1.00	647	0.300	0.165	0.135	0.250	0.175	0.075	0.345	1.23
calc.				0.128			0.061		

TABLE 5.9

Voltammetric Parameters for the Diffusion-Controlled Reduction of HCl in 90 mol. % $ZnCl_2$-NaCl (Pt electrode, 0.143 cm^2)

$\nu(Vs^{-1})$	T (K)	$-Ep^c$(V)	$-Ep^a$(V)	ΔEp(V)	$-E_{\frac{1}{2}}$(V)	$-E_{p/2}$(V)	$\lvert E_{p/2} - E_{\frac{1}{2}} \rvert$(V)	i_p (mA)	i_{pa}/i_{pc}
0.02	590	0.525	0.414	0.111	0.465	0.415	0.050	0.039	0.87
0.05	590	0.525	0.413	0.112	0.465	0.415	0.050	0.061	0.97
0.10	590	0.530	0.410	0.120	0.465	0.417	0.048	0.086	1.05
0.20	590	0.530	0.410	0.120	0.460	0.400	0.060	0.122	1.06
0.50	590	0.534	0.415	0.121	0.462	0.405	0.057	0.200	1.17
1.00	590	0.540	0.415	0.125	0.465	0.402	0.063	0.295	1.18
calc.				0.116			0.055		
0.01	617	0.515	0.392	0.123	0.460	0.408	0.052	0.037	0.79
0.02	617	0.510	0.390	0.120	0.455	0.405	0.050	0.048	0.86
0.05	617	0.513	0.390	0.123	0.458	0.405	0.053	0.076	0.92
0.10	617	0.510	0.390	0.120	0.460	0.405	0.055	0.108	0.97
0.20	617	0.520	0.390	0.120	0.460	0.405	0.055	0.151	1.00
0.50	617	0.528	0.392	0.126	0.472	0.410	0.062	0.242	1.00
1.00	617	0.530	0.390	0.128	0.470	0.403	0.067	0.365	1.04
calc.				0.122			0.058		
0.01	649	0.455	0.315	0.140	0.410	0.365	0.045	0.043	0.81
0.02	649	0.457	0.335	0.122	0.405	0.355	0.050	0.058	0.85
0.05	649	0.460	0.335	0.125	0.405	0.350	0.055	0.085	0.99
0.10	649	0.453	0.335	0.125	0.400	0.346	0.054	0.118	1.05
0.20	649	0.455	0.335	0.120	0.400	0.340	0.060	0.167	1.09
0.50	649	0.460	0.330	0.118	0.405	0.340	0.065	0.280	1.15
1.00	649	0.460	0.330	0.130	0.400	0.335	0.065	0.420	1.16
calc.				0.129			0.061		

(continued ...)

TABLE 5.10

Voltammetric Parameters for the Diffusion-Controlled Reduction of HCl in 80 mol. % $ZnCl_2$-NaCl
(Pt electrode, 0.151 cm^2)

continuation....

$\nu(Vs^{-1})$	T (K)	$-Ep^c(V)$	$-Ep^a(V)$	$\Delta Ep(V)$	$-E_{\frac{1}{2}}(V)$	$-E_{p/2}(V)$	$\lvert E_{p/2} - E_{\frac{1}{2}} \rvert (V)$	i_p (mA)	i_{pa}/i_{pc}
0.01	682	0.548	0.410	0.138	0.460	0.404	0.056	0.053	0.85
0.02	682	0.535	0.405	0.130	0.468	0.409	0.059	0.067	0.93
0.05	682	0.542	0.410	0.132	0.465	0.407	0.058	0.103	0.99
0.10	682	0.547	0.410	0.137	0.468	0.405	0.063	0.147	1.01
0.20	682	0.540	0.405	0.135	0.470	0.409	0.061	0.206	1.04
0.50	682	0.548	0.407	0.141	0.470	0.403	0.067	0.340	1.15
1.00	682	0.547	0.400	0.147	0.473	0.404	0.069	0.502	1.21
calc.				0.135			0.064		

TABLE 5.10

Voltammetric Parameters for the Diffusion-Controlled Reduction of HCl in 80 mol. % $ZnCl_2$-NaCl
(Pt electrode, 0.151 cm^2)

ν (Vs^{-1})	T (K)	$-Ep^c$ (V)	$-Ep^a$ (V)	ΔEp (V)	$-E_{\frac{1}{2}}$ (V)	$-E_{p/2}$ (V)	$\lvert E_{p/2}-E_{\frac{1}{2}} \rvert$ (V)	i_p (mA)	i_{pa}/i_{pc}
0.01	586	0.620	0.500	0.120	0.570	0.528	0.042	0.037	0.88
0.02	586	0.640	0.530	0.110	0.590	0.545	0.045	0.051	0.91
0.05	586	0.645	0.532	0.113	0.590	0.542	0.048	0.081	0.99
0.10	586	0.645	0.525	0.120	0.585	0.532	0.053	0.112	1.04
0.20	586	0.650	0.525	0.125	0.580	0.525	0.055	0.157	1.07
0.50	586	0.645	0.520	0.125	0.575	0.515	0.060	0.246	1.13
1.00	586	0.655	0.515	0.140	0.575	0.505	0.075	0.365	1.14
calc.	586			0.116			0.055		
0.01	619	0.480	0.360	0.120	0.435	0.384	0.051	0.047	0.69
0.02	619	0.480	0.365	0.115	0.430	0.380	0.050	0.063	0.81
0.05	619	0.490	0.372	0.118	0.431	0.380	0.051	0.095	1.09
0.10	619	0.490	0.370	0.120	0.435	0.380	0.055	0.132	1.00
0.20	619	0.490	0.370	0.120	0.440	0.380	0.060	0.191	1.03
0.50	619	0.505	0.380	0.125	0.453	0.388	0.065	0.315	1.08
1.00	619	0.510	0.375	0.145	0.455	0.380	0.075	0.472	1.07
calc.	619			0.123			0.058		
0.01	654	0.695	0.535	0.160	0.657	0.595	0.062	0.049	0.79
0.02	654	0.680	0.560	0.120	0.640	0.587	0.053	0.071	0.72
0.05	654	0.690	0.572	0.118	0.644	0.585	0.059	0.103	0.88
0.10	654	0.690	0.572	0.118	0.643	0.585	0.058	0.145	0.95
0.20	654	0.700	0.570	0.130	0.643	0.585	0.058	0.210	0.98
0.50	654	0.690	0.570	0.120	0.640	0.575	0.065	0.354	1.04
1.00	654	0.685	0.570	0.130	0.645	0.575	0.070	0.523	0.98
calc.							0.061		

(continued ...)

TABLE 5.11

Reduction of HCl in 70 mol. % $ZnCl_2$-NaCl

Continuation ....

(Vs^{-1})	T (K)	$-Ep^c$(V)	$-Ep^a$(V)	ΔEp(V)	$-E_{\frac{1}{2}}$(V)	$-E_{p/2}$(V)	$\lvert E_{p/2}-E_{\frac{1}{2}}\rvert$(V)	i_p (mA)	i_{pa}/i_{pc}
0.01	680	0.602	0.460	0.142	0.548	0.490	0.058	0.055	0.74
0.02	680	0.605	0.485	0.120	0.546	0.495	0.051	0.080	0.87
0.05	680	0.605	0.490	0.115	0.555	0.500	0.055	0.118	0.99
0.10	680	0.610	0.480	0.130	0.570	0.498	0.072	0.170	1.03
0.20	680	0.617	0.480	0.137	0.565	0.500	0.065	0.238	1.01
0.50	680	0.610	0.490	0.120	0.560	0.490	0.070	0.398	1.12
1.00	680	0.620	0.480	0.140	0.572	0.490	0.082	0.570	1.16
calc.				0.135			0.064		

TABLE 5.11

Reduction of HCl in 70 mol. % $ZnCl_2$-NaCl

$\nu(Vs^{-1})$	T (K)	$-Ep^c$(V)	$-Ep^a$(V)	ΔEp(V)	$-E_{\frac{1}{2}}$(V)	$-E_{p/2}$(V)	$\lvert E_{p/2}-E_{\frac{1}{2}}\rvert$(V)	i_p (mA)	i_{pa}/i_{pc}
0.01	592	0.640	0.500	0.140	0.583	0.535	0.048	0.040	0.64
0.02	592	0.640	0.525	0.115	0.577	0.535	0.042	0.050	0.76
0.05	592	0.645	0.525	0.120	0.580	0.532	0.048	0.077	0.94
0.10	592	0.645	0.522	0.123	0.577	0.527	0.050	0.108	1.02
0.20	592	0.650	0.520	0.130	0.577	0.523	0.054	0.154	1.05
0.50	592	0.660	0.525	0.135	0.587	0.525	0.062	0.252	1.06
1.00	592	0.665	0.523	0.142	0.587	0.515	0.072	0.375	1.09
calc.				0.117			0.056		
0.01	623	0.625	0.470	0.155	0.580	0.520	0.060	0.043	
0.02	623	0.615	0.485	0.130	0.560	0.505	0.055	0.054	0.70
0.05	623	0.615	0.490	0.125	0.560	0.505	0.055	0.085	0.85
0.10	623	0.620	0.490	0.130	0.560	0.503	0.057	0.121	0.92
0.20	623	0.620	0.490	0.130	0.560	0.505	0.055	0.171	0.99
0.50	623	0.630	0.500	0.130	0.570	0.505	0.065	0.278	1.03
1.00	623	0.635	0.495	0.140	0.570	0.503	0.067	0.418	1.03
calc.				0.123			0.059		
0.02	651	0.570	0.410	0.160	0.503	0.440	0.063	0.071	0.65
0.05	651	0.570	0.450	0.120	0.510	0.455	0.055	0.101	0.86
0.10	651	0.520	0.405	0.115	0.480	0.422	0.058	0.141	0.94
0.20	651	0.520	0.402	0.118	0.480	0.417	0.063	0.202	0.95
0.50	651	0.525	0.400	0.125	0.475	0.415	0.060	0.325	1.02
1.00	651	0.520	0.395	0.125	0.473	0.405	0.068	0.480	1.02
calc.				0.129			0.061		

(continued ...)

TABLE 5.12

Reduction of HCl in 60 mol. % $ZnCl_2$-NaCl

Continuation....

$\nu(Vs^{-1})$	T (K)	$-Ep^c$(V)	$-Ep^a$(V)	ΔEp(V)	$-E_{\frac{1}{2}}$(V)	$-E_{p/2}$(V)	$\lvert E_{p/2}-E_{\frac{1}{2}} \rvert$ (V)	i_p (mA)	i_{pa}/i_{pc}
0.01	685	0.615	0.445	0.170	0.565	0.497	0.068	0.055	
0.02	685	0.610	0.485	0.125	0.555	0.503	0.052	0.074	0.64
0.05	685	0.610	0.482	0.128	0.550	0.492	0.058	0.115	0.83
0.10	685	0.605	0.487	0.118	0.560	0.495	0.065	0.163	0.99
0.20	685	0.610	0.478	0.132	0.560	0.500	0.060	0.230	1.01
0.50	685	0.605	0.465	0.140	0.560	0.490	0.070	0.368	1.04
1.00	685	0.615	0.465	0.150	0.565	0.490	0.075	0.555	1.12
calc.				0.136			0.064		

TABLE 5.12

Reduction of HCl in 60 mol. % $ZnCl_2$-NaCl

$\nu(Vs^{-1})$	T (K)	$-Ep^c$(V)	$-Ep^a$(V)	ΔEp(V)	$-E_{\frac{1}{2}}$(V)	$-E_{p/2}$(V)	$\lvert E_{p/2}-E_{\frac{1}{2}}\rvert$(V)	ip (mA)	i_{pa}/i_{pc}
0.02	604	0.630	0.505	0.125	0.570	0.520	0.050	0.050	0.72
0.05	604	0.630	0.510	0.120	0.570	0.518	0.052	0.075	0.90
0.10	604	0.635	0.512	0.123	0.570	0.518	0.052	0.106	1.00
0.20	604	0.640	0.510	0.130	0.570	0.515	0.055	0.153	1.04
0.50	604	0.652	0.510	0.142	0.587	0.520	0.057	0.245	1.05
1.00	604	0.655	0.510	0.145	0.585	0.510	0.075	0.365	1.08
calc.				0.120			0.057		
0.01	628	0.640	0.510	0.130	0.592	0.530	0.062	0.043	
0.02	628	0.635	0.515	0.120	0.590	0.530	0.060	0.056	0.67
0.05	628	0.640	0.515	0.125	0.590	0.530	0.060	0.087	0.81
0.10	628	0.650	0.515	0.135	0.600	0.535	0.065	0.122	0.86
0.20	628	0.650	0.512	0.138	0.595	0.528	0.067	0.178	0.93
0.50	628	0.650	0.510	0.140	0.600	0.532	0.068	0.305	0.96
1.00	628	0.650	0.505	0.145	0.605	0.530	0.075	0.458	0.98
calc.				0.124			0.059		
0.02	657	0.635	0.500	0.135	0.585	0.535	0.050	0.063	0.68
0.05	657	0.635	0.520	0.115	0.590	0.530	0.060	0.093	0.86
0.10	657	0.640	0.520	0.120	0.590	0.530	0.060	0.130	0.97
0.20	657	0.650	0.520	0.130	0.595	0.528	0.067	0.187	1.01
0.50	657	0.640	0.515	0.125	0.590	0.520	0.070	0.311	1.10
1.00	657	0.645	0.515	0.130	0.592	0.510	0.082	0.465	1.11
calc.				0.130			0.062		

(continued...)

TABLE 5.13

Reduction of HCl in 50 mol. % $ZnCl_2$-NaCl

Continuation...

$\nu(Vs^{-1})$	T (K)	$-Ep^c$(V)	$-Ep^a$(V)	ΔEp (V)	$-E_{\frac{1}{2}}$(V)	$-E_{p/2}$(V)	$\lvert E_{p/2}-E_{\frac{1}{2}}\rvert$(V)	ip (mA)	i_{pa}/i_{pc}
0.02	687	0.625	0.495	0.130	0.590	0.538	0.052	0.067	0.63
0.05	687	0.630	0.505	0.125	0.585	0.530	0.055	0.104	0.85
0.10	687	0.630	0.500	0.130	0.590	0.528	0.062	0.146	0.99
0.20	687	0.635	0.495	0.140	0.595	0.535	0.060	0.206	1.01
0.50	687	0.640	0.498	0.142	0.602	0.530	0.072	0.338	1.09
1.00	687	0.640	0.490	0.150	0.598	0.518	0.080	0.510	1.12
calc.				0.136			0.065		

TABLE 5.13

Reduction of HCl in 50 mol. % $ZnCl_2$-NaCl

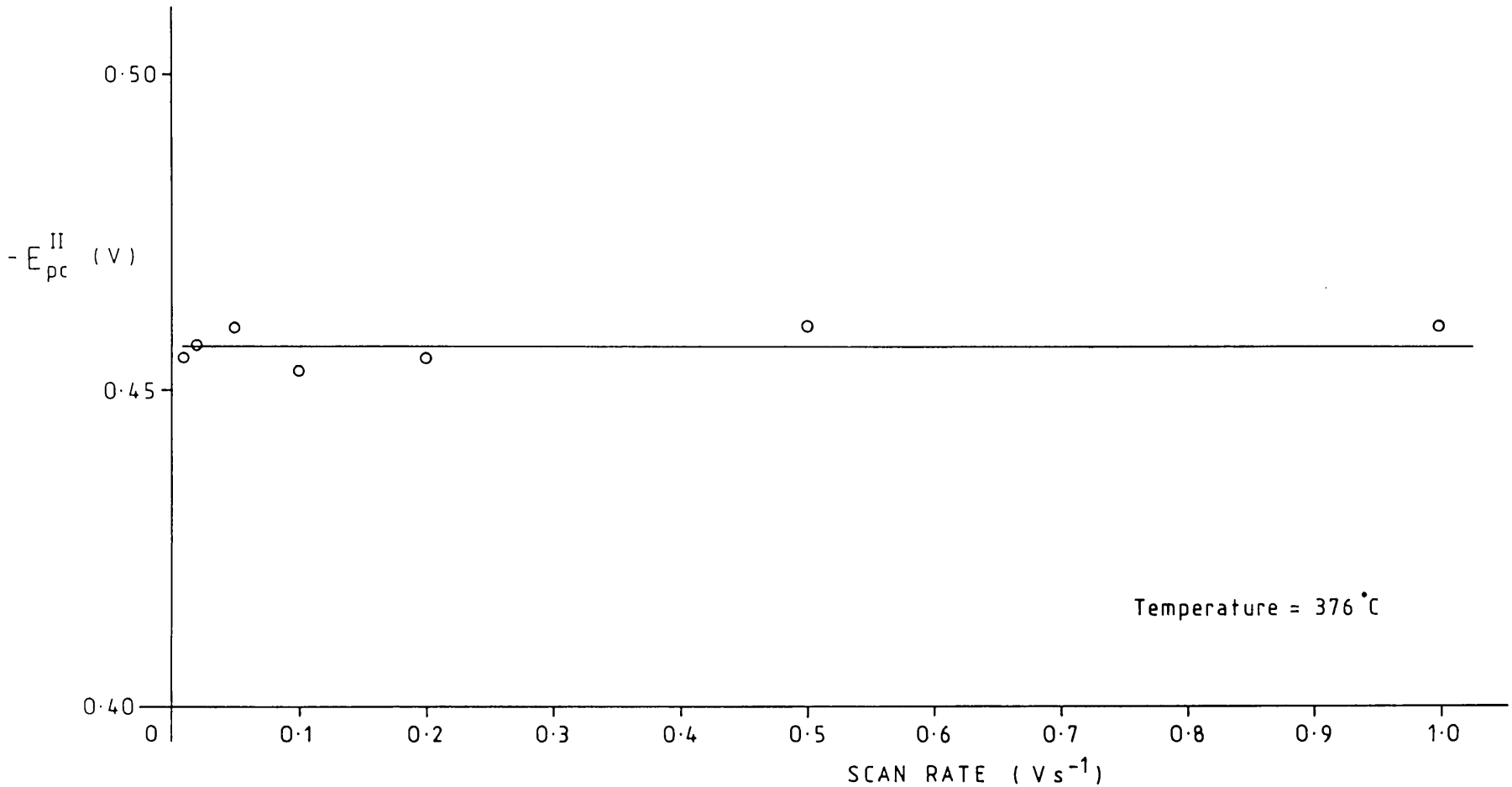


FIGURE 5.8: Variation of the Peak Potential With Scan Rate for the Reduction of HCl in 80 mol. % $ZnCl_2$-NaCl

A linear dependence of the peak current i_p on the square root of the scan rate is the criterion for a diffusion-controlled process. As is evident from the graph shown in Figure 5.9 positive deviations occur in this system at low scan rates ($< 20\ mVs^{-1}$) and at high scan rates ($> 500\ mVs^{-1}$), but linear behaviour is found for the intermediate scan rates. The deviations found at high scan rates are the result of the proximity of the adsorption peaks to the diffusion-controlled reduction peaks, which causes the voltammetric baseline to be raised above the $i_p = 0$ axis. If a correction is made for this, by substracting the current of the voltammetric wave prior to the reduction peak from the i_p value measured from the potential axis, then a deviation is still seen, but this time in the negative direction (Figure 5.10). As mentioned previously, as the scan rate increases so the adsorption peak takes over from the diffusion-controlled peak, until the latter disappears at very high scan rates. The consequence of this is that the corrected i_p against $\nu^{\frac{1}{2}}$ plots for the reduction will become almost semicircular as the scan rate increases.

It is possible that diffusion is not the only process transporting material to the working electrode, but that convection may also be playing a part in the transportation, especially in the less viscous melts. Hence the extra reducible material over and above that transported by diffusion would cause a greater i_p value than that expected if diffusion were the sole transportation process. This extra component in the i_p value would only become noticeable for low scan rates when the length of time required for the scan to be carried out allows non-negligible convection processes to occur, and cause the positive deviation in i_p values seen in Figure 5.9.

It is also noticeable that as the temperature of a particular system increases, so the peak current values increase progressively for each scan rate. This is contrary to what might be expected - at higher temperatures the solubility of HCl in these melts has been found to decrease, so in terms of concentration alone it might be expected that i_p values would decrease at higher temperatures, as reflected in equation 5.8. This was indeed found to be the case in LiCl-KCl-$ZnCl_2$ [70] but not in $ZnCl_2$-KCl [83]. It must be recalled, however, that the peak current also depends on the diffusion coefficient of the diffusing species, and this factor may well override the concentration factor, as it has in this case.

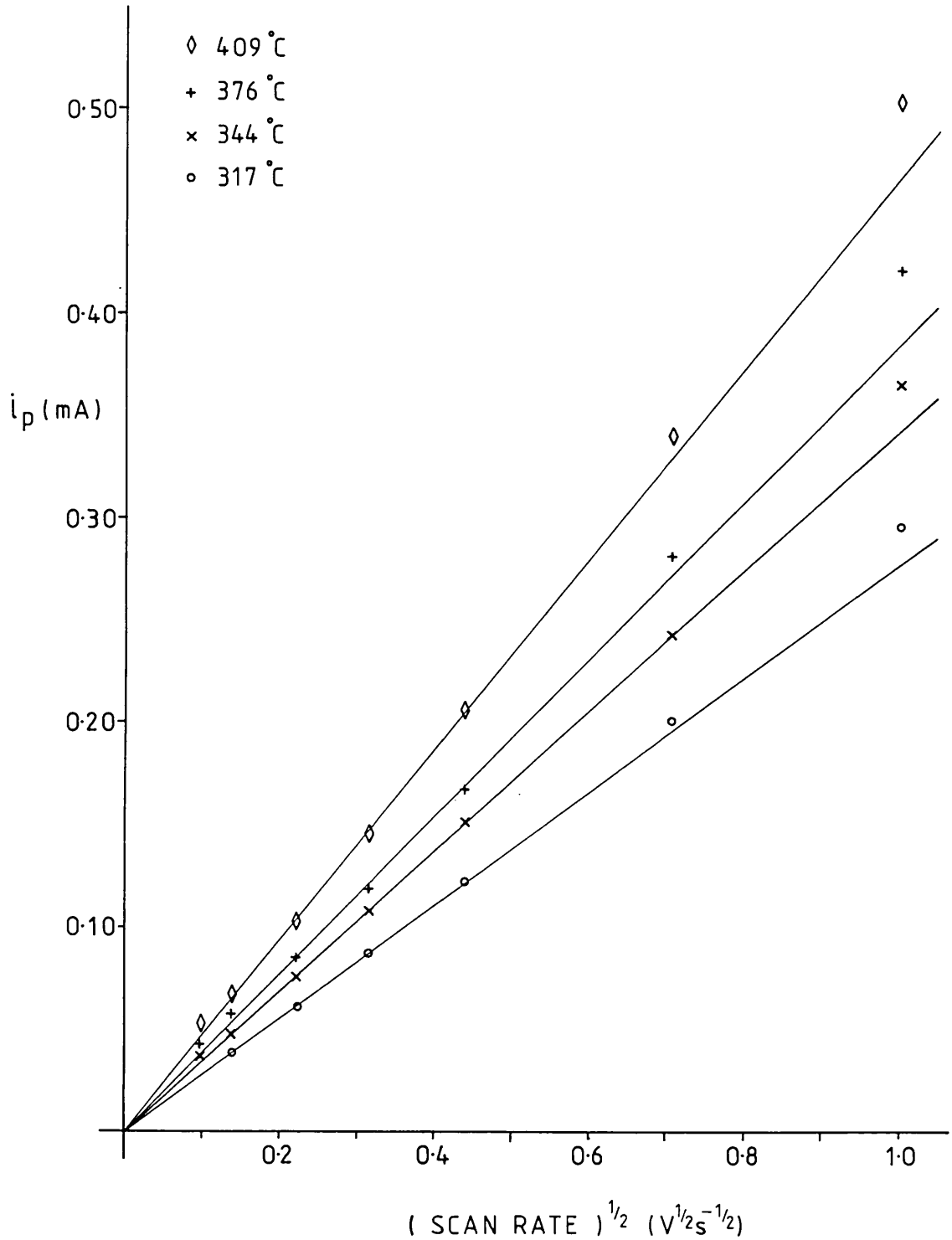


FIGURE 5.9: Variation of i_p with $\nu^{\frac{1}{2}}$ for the Reduction of HCl in 80 mol. % $ZnCl_2$-NaCl

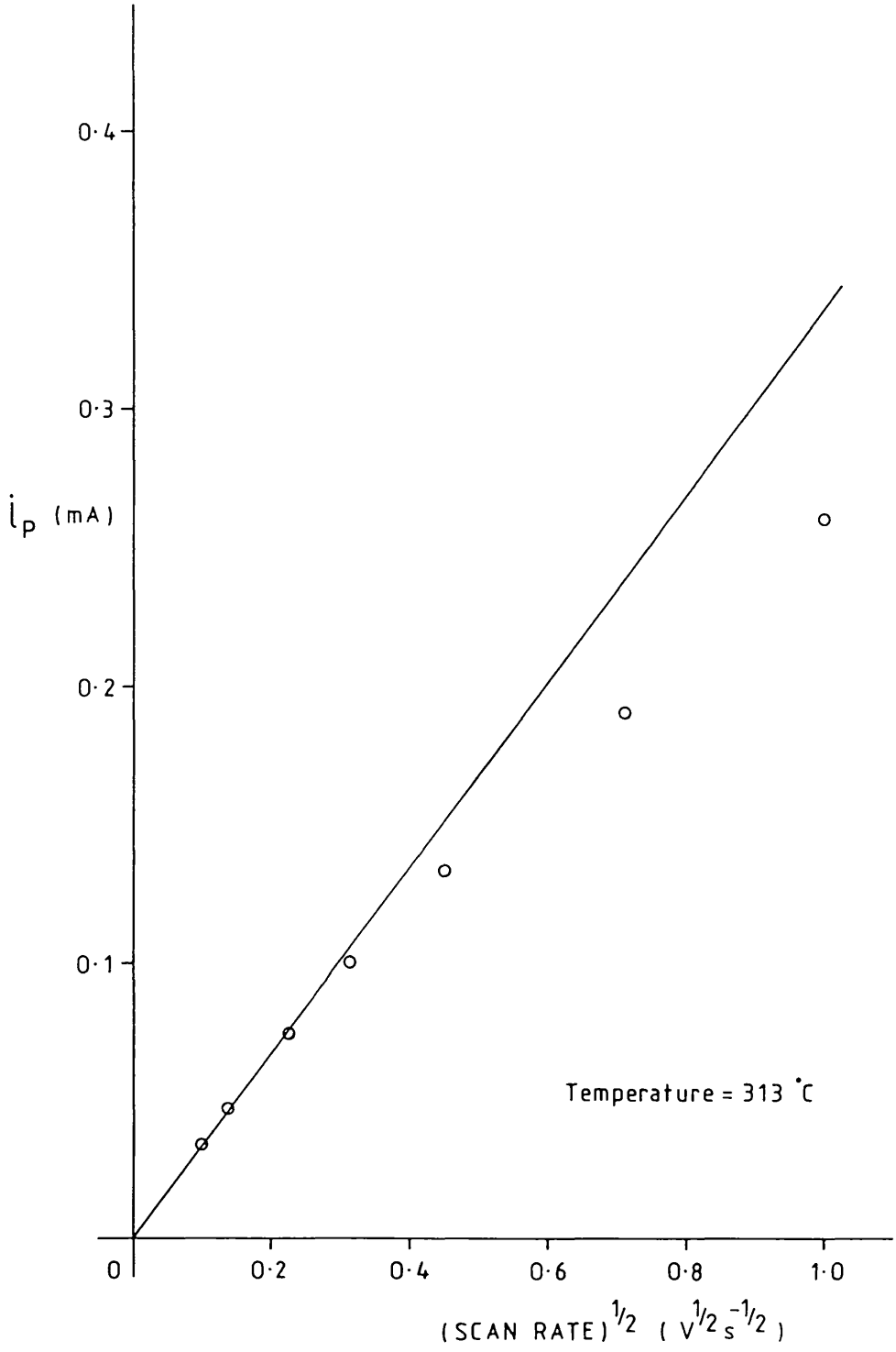


FIGURE 5.10

"Corrected" Plot of i_p against $\nu^{\frac{1}{2}}$ for the Reduction of HCl in 70 mol. % $ZnCl_2$-NaCl

The values of the peak current ratio, i_{pa}/i_{pc}, calculated using equation 5.11, are found to fall below unity at low scan rates for the less viscous melt systems (Figure 5.11). For an uncomplicated, reversible system involving a soluble product the current ratio should be unity, regardless of the scan rate. The drop in the i_{pa}/i_{pc} values, to as low as 0.63 in one case, indicates that some of the reduced material does not remain at the electrode to be oxidised back to H^+. Two explanations could account for this. The hydrogen atoms formed may well have time to travel away from the electrode at low scan rates, probably aided by convection currents that may be present. This assumes that hydrogen is soluble in $ZnCl_2$-NaCl melts. The second explanation is that an irreversible chemical reaction follows the reduction step to produce an electroinactive species. Since hydrogen atoms are being formed during the reduction it is possible that an atom-atom combination reaction may be occurring to produce H_2. This process would probably be quite slow, and so only become noticeable at low scan rates. Various reaction mechanisms can be postulated for an overall reduction which is complicated by adsorption effects and a following irreversible chemical reaction, and some are given below:

$$H^+ + e^- = H$$

$$H = H_{ads}$$

$$H_{ads} + H_{ads} \rightarrow H_2$$

$$H_{ads} + H \rightarrow H_2$$

$$H_{ads} + H^+ + e^- \rightarrow H_2$$

$$H + H^+ + e^- \rightarrow H_2$$

Using a working curve of i_{pa}/i_{pc} against $\log(k_f\tau)$, given in references 136 and 137, where k_f is the rate constant for the following chemical

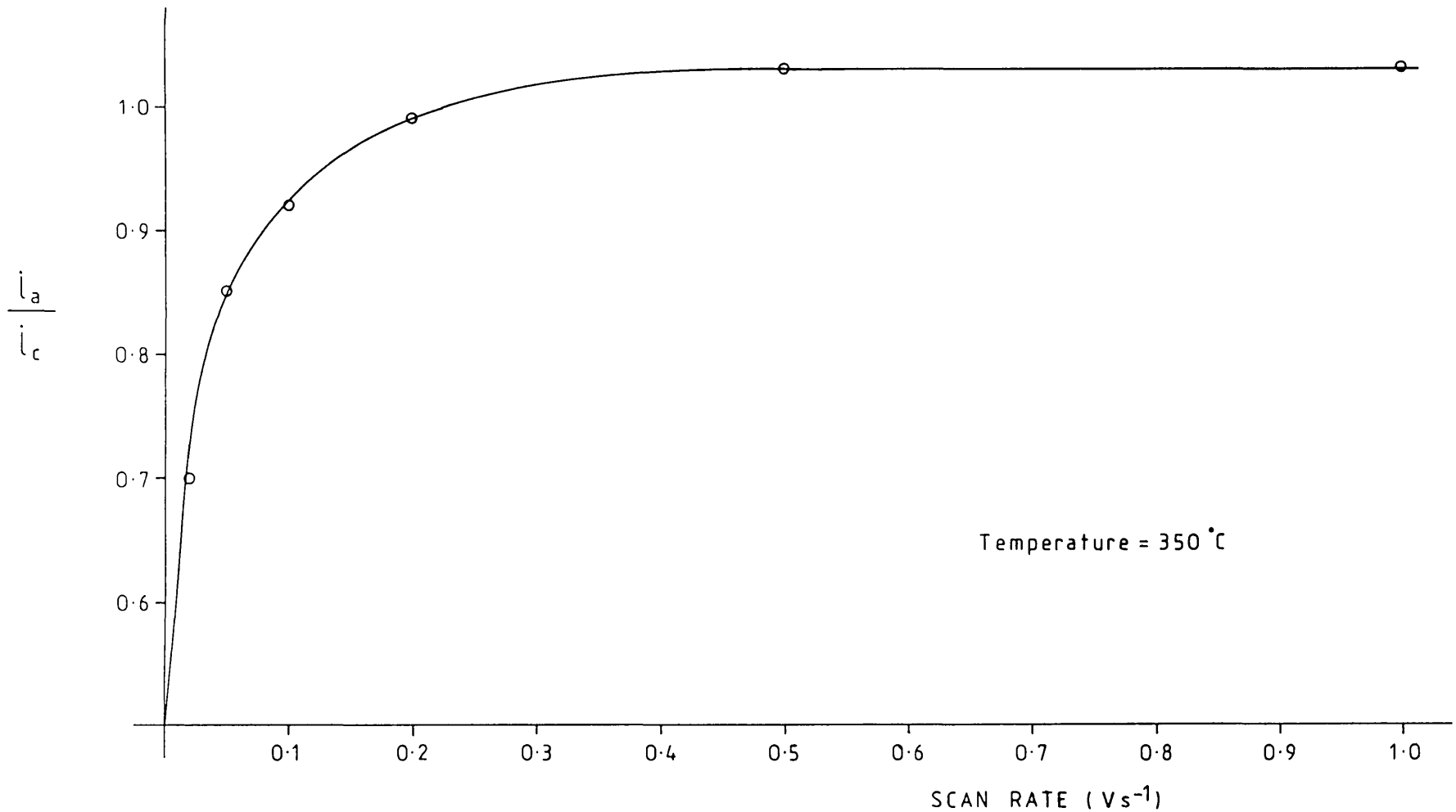


FIGURE 5.11: Variation of the Current Ratio With Scan Rate for Reduction of HCl in 60 mol. % $ZnCl_2$-NaCl

reaction and τ is the time in seconds required to scan from $E_{\frac{1}{2}}$ to the switching potential, it is possible to use the experimentally determined values of i_{pa}/i_{pc} to calculate k_f. The values so calculated are listed in Table 5.14. Two rather vague trends can be seen in the values of k_f. As the temperature of the melt system increases so the rate constant increases. Similarly, as X_{NaCl} increases so k_f is seen to increase. Two other papers were found where the same calculations had been made but for different systems. In LiCl-KCl[139] the reduction of Cr^{3+} to Cr^{2+} was said to be followed by slow precipitation of $CrCl_2$, a process which was found to have a rate constant of 0.028 $sec.^{-1}$ at 500°C. For the same system addition of moisture[91] also resulted in a chemical reaction following the reduction of Cr^{3+} to Cr^{2+} with a rate constant calculated to be around 0.013 $sec.^{-1}$ at 450°C and 0.018 $sec.^{-1}$ at 500°C, but the authors have not elaborated on the nature of this reaction.

So it can be seen that the rate constants determined for the possible reaction following the reduction of HCl in $ZnCl_2$-NaCl are larger than those found in other molten salt systems, which might be expected since the combination of hydrogen atoms is a thermodynamically and kinetically favourable reaction. However, these results do not allow a diagnostic choice to be made between a following chemical reaction and a convective transport process. If the hydrogen atoms formed are given time to move away from the electrode, by diffusion or convection,, then the i_{pa}/i_{pc} ratio will decrease from unity as the scan rate decreases. Any convection process will be enhanced in the less viscous melts or at higher temperatures, so further reducing the i_{pa}/i_{pc} ratio and increasing the apparent rate constant, as has been found. Many other authors[81,83,99,100] have almost assumed that the dimerization reaction to form H_2 occurs, albeit slowly, and the results of this work can be used to support their assumptions. However, the same results can be explained by a convection process in the melt.

5.2.3 Diffusion Coefficients of HCl in $ZnCl_2$-NaCl Melts

Using the Randles-Sevcik equation ([5.8]) it was possible to calculate the diffusion coefficients for the diffusing species. The current function, $i_p/\nu^{\frac{1}{2}}$, was found from the gradients of the plots of i_p

Melt Composition	Temp. (K)	$\nu(Vs^{-1})$	K_f (s^{-1})
80 mol. % $ZnCl_2$-NaCl	590	0.02	0.022
		0.05	0.016
	617	0.01	0.028
		0.02	0.033
		0.05	0.041
	649	0.01	0.016
		0.02	0.024
	682	0.01	0.029
		0.02	0.038
70 mol. % $ZnCl_2$-NaCl	586	0.01	0.009
		0.02	0.015
	619	0.01	0.044
		0.02	0.044
	654	0.01	0.030
		0.02	0.072
		0.05	0.068
		0.10	0.057
	680	0.01	0.091
		0.02	0.099
60 mol. % $ZnCl_2$-NaCl	592	0.01	0.045
		0.02	0.053
		0.05	0.029
	623	0.02	0.093
		0.05	0.100
	651	0.02	0.079
		0.05	0.065
		0.10	0.043
	685	0.02	0.083
		0.05	0.075
50 mol. % $ZnCl_2$-NaCl	604	0.02	0.069
		0.05	0.050
	628	0.02	0.107
		0.05	0.129
		0.10	0.258
	657	0.02	0.102
		0.05	0.097
	687	0.05	0.112

TABLE 5.14

Calculated Rate Constants for the Reaction Following the Reduction of HCl in $ZnCl_2$-NaCl Melts

against $\nu^{\frac{1}{2}}$ (Figure 5.9). The number of electrons n was found from ΔE_p, and in this case the solubilities of HCl in $ZnCl_2$-NaCl have been determined (Section 5.1). The diffusion coefficients D_{HCl} are listed in Table 5.15 for melt compositions from pure $ZnCl_2$ to 50 mol. % $ZnCl_2$-NaCl. The two compositions asterisked are those outside the range of compositions for which the HCl solubility was measured, the solubilities having been estimated by extrapolation of Figure 5.2. Linear behaviour of the solubility isotherms was assumed so that a rough value of the solubility could be obtained, but this assumption has no real foundation. It may be that the isotherms exhibit curvature at high X_{ZnCl_2} values, in which case the D_{HCl} values would be smaller than those listed.

Two trends are apparent in the values of D_{HCl}. As X_{NaCl} increases so the diffusion coefficients increase, as they do for increasing temperature within the same melt composition. Both trends are explained by the decreasing viscosity of the melts, and hence the increasing mobility of solute species, as alkali chloride is added or as the temperature is raised (Section 2.2.3). The values of D_{HCl} are of the order of 10^{-6} cm^2 $sec.^{-1}$ in melts where $X_{NaCl} > 0.20$, falling to around 10^{-8} cm^2 $sec.^{-1}$ in pure $ZnCl_2$. This contrasts with the results for $ZnCl_2$-KCl[83], where D_{HCl} was found to be around 10^{-8}-10^{-9} cm^2 $sec.^{-1}$ for melts in which X_{KCl} values were 0.28 and 0.685. However, the large difference comes from the HCl concentrations used in this work and by those workers, who used results that differed by a factor of 10^2 from those listed in Section 5.1. As a first approximation the HCl solubility data for $ZnCl_2$-NaCl were used to recalculate the D_{HCl} values for $ZnCl_2$-KCl, and values of the order of 10^{-5}-10^{-6} cm^2 $sec.^{-1}$ were obtained, which are much closer to the values found in this work. The diffusion coefficients[70] for HCl in $ZnCl_2$-LiCl-KCl ($X_{ZnCl_2} < 0.174$) are larger than those found in this work, being of the order of 10^{-4} cm^2 $sec.^{-1}$, which can be accounted for by the lower viscosity of that solvent compared to the $ZnCl_2$-rich melts used here. The diffusion coefficients of HCl in $ZnCl_2$-NaCl are of the same order as those of metal cations in the same solvent, which have been found[1] to be around 10^{-5}-10^{-6} cm^2 $sec.^{-1}$, although no values could be found for systems where pure $ZnCl_2$ had been the solvent.

Melt Composition	T (K)	$i_p/\nu^{\frac{1}{2}}$ ($\times 10^{-4}$ $AV^{-\frac{1}{2}}s^{\frac{1}{2}}$)	Concentration of HCl ($\times 10^{-6}$ mol. cm^{-3})	Diffusion Coefficient ($\times 10^{-6}$ cm^2s^{-1})
80 mol. % $ZnCl_2$-NaCl	590	2.79	12.85	0.567
	617	3.40	11.85	1.04
	649	3.74	10.73	1.61
	682	4.64	9.56	3.27
70 mol.% $ZnCl_2$-NaCl	586	3.57	10.60	1.35
	619	4.29	9.60	2.52
	654	4.73	8.35	4.28
	680	5.36	7.40	7.27
60 mol. % $ZnCl_2$-NaCl	592	3.43	7.90	2.27
	623	3.82	6.90	3.89
	651	4.47	6.05	7.24
	685	5.13	5.00	14.70
50 mol. % $ZnCl_2$-NaCl	604	3.39	4.56	6.80
	628	3.99	4.11	12.06
	657	4.19	3.55	18.65
	687	4.60	3.00	32.92
*Pure $ZnCl_2$	620	1.29	~16.5	~0.077
*90 mol. % $ZnCl_2$-NaCl	596	2.03	~15.1	~0.220
	647	2.94	~13.3	~0.644

TABLE 5.15

Diffusion Coefficients of HCl in $ZnCl_2$-NaCl Melts

The activation energy, E_A^{HCl}, for the diffusion process can be calculated if the diffusion coefficients are found to obey the Arrhenius relationship, that is, if plots of lnD against 1/T are linear, in which case the slope will be $-E_A^{HCl}/R$. This has been carried out for the melt compositions where X_{ZnCl_2} = 0.80, 0.70, 0.60 and 0.50. The Arrhenius plots are shown in Figure 5.12 and the activation energies listed in Table 5.16. The diffusion coefficients are seen to obey the Arrhenius equation reasonably well, so the values of E_A^{HCl} may be taken as valid. No discernible trend can be seen as the melt composition varies, but it is noticeable that these values are somewhat larger than those found for metal cations in chloride melts. In the LiCl-KCl[140] eutectic over the temperature range 660-900 K, the activation energies for diffusion of Cu^+, Ag^+, Au^+, Fe^{2+} and Ni^{2+} were in the range 24-30 kJ mol^{-1}, those for the divalent ions being larger than for the monovalent ions. In 50 mol. % $ZnCl_2$-KCl[1] the activation energy for diffusion of Cr^{3+} was found to be rather larger, around 45 kJ $mol.^{-1}$, over the range 530-700 K. The magnitude of E_A^{HCl} in $ZnCl_2$-NaCl melts can perhaps be accounted for by considering the high charge density surrounding H^+ ions, making them more polarizing than monovalent metal cations, and by the range of equilibria that may be present in the HCl solutions (Figure 5.4). The diffusion process almost certainly does not involve one simple species. Interestingly, the values of E_A^{HCl}, calculated from the D_{HCl} values in reference 83, for $ZnCl_2$-KCl melts and shown in Table 5.16, are larger than those found in $ZnCl_2$-NaCl melts. This is not as might be expected, since the lower viscosity of the $ZnCl_2$-KCl systems should enhance, rather than diminish, the diffusion process.

5.2.4 Stokes-Einstein Behaviour of HCl in $ZnCl_2$-NaCl Melts

The Stokes-Einstein relationship ([5.18]) connects the diffusion coefficient, D_i, and the radius, r_i, of a diffusing species i to the viscosity of the solvent liquid, η. An important feature of this equation is that it is independent of the charge of the diffusing species,

$$D_i = \frac{kT}{6\pi \eta r_i} \qquad [5.18]$$

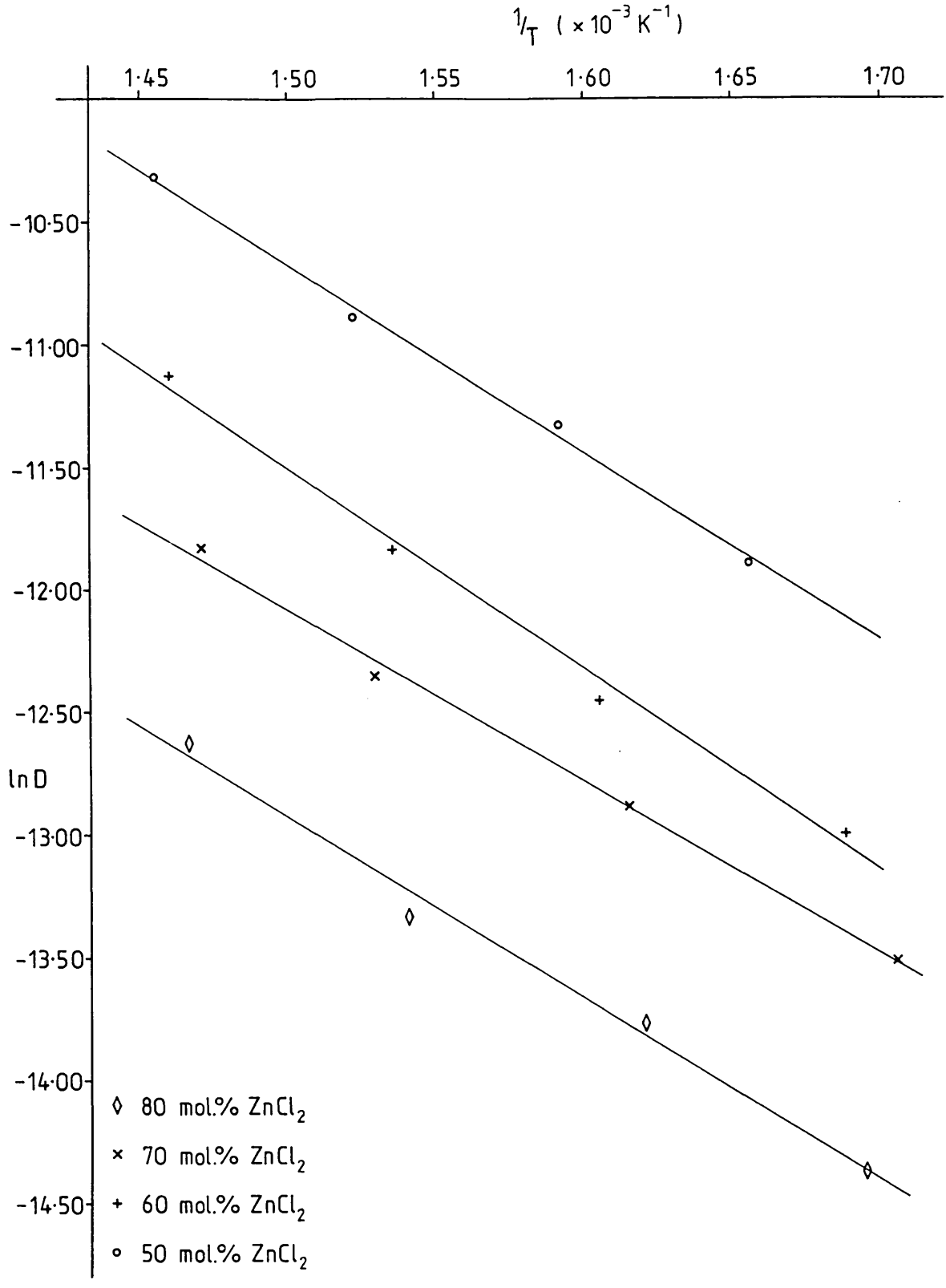


FIGURE 5.12

Arrhenius Plot for D_{HCl} in $ZnCl_2$-NaCl Melts

Melt Composition	T (K)	E_A^{HCl} (kJ mol.$^{-1}$)	Reference
80 mol. % $ZnCl_2$-NaCl	590-682	61.6	This work
70 mol. % $ZnCl_2$-NaCl	586-680	58.2	This work
60 mol. % $ZnCl_2$-NaCl	592-685	68.3	This work
50 mol. % $ZnCl_2$-NaCl	604-687	64.1	This work
72 mol. % $ZnCl_2$-KCl	637-777	91.2	83
31.5 mol. % $ZnCl_2$-KCl	753-873	79.4	83

TABLE 5.16

Activation Energies of Diffusion Processes Present in Solutions of HCl in $ZnCl_2$-MCl Melts

but it must be remembered that it is an approximation, originally derived to describe the motion of spheres thorough an infinite, incompressible liquid.

Using the viscosity data of Bloom and Weeks[51], and the diffusion coefficients listed in Table 5.15, the Stokes-Einstein radii for the diffusing species in HCl- containing $ZnCl_2$-NaCl melts have been calculated and are listed in Table 5.17. Li and Chang[141] have suggested that, for particles of the same size or larger than those of the medium, the 6π factor is applicable, but this factor should become 4π if the diffusing particles are small compared to those of the medium. The diffusing species is not known for this work so Table 5.17 lists radii calculated with both factors.

Given that the crystal radius[42] of Cl^- is 1.81 Å and of Zn^{2+} is 0.74 Å, the radii calculated can not be expressed in terms of numbers of different ions. This is not surprising since it is unlikely that the radii of ions in solution are anything like their crystal radii. In this case the calculated radii might be thought of as representing the effective radii of the diffusing species. In Figure 5.4 various species were postulated to exist in a range of equilibria, and if these are all interconverting then the radii calculated could be thought of as "time-averaged" radii. Whilst the "time-averaged" radii do not individually point to the actual diffusing species, collectively they follow an interesting pattern. It can be seen that as the melt temperature is raised, so the values of r start to decrease, a feature more noticeable in those solutions with larger X_{NaCl} values. It was suggested in Section 5.1 that dissolution of HCl in $ZnCl_2$-NaCl melts gave rise to different species, $H^+ZnCl_3^-$ and HCl_2^-, depending on the composition and temperature of the melt system. The trend seen in the r values could be explained by regarding the points where they start to decrease as being those points where the changeover in melt species starts to occur. The larger $H^+ZnCl_3^-$ could be thought of as giving way to the formation of the smaller HCl_2^- species, suggested to be more favourable in melts

Melt Composition	T (K)	Viscosity (Pa.S)	r(n=6) (Å)	r(n=4) (Å)
80 mol. % $ZnCl_2$-NaCl	590	0.0622	1.23	1.84
	617	0.0374	1.16	1.74
	649	0.0228	1.30	1.94
	682	0.0150	1.02	1.53
70 mol. % $ZnCl_2$-NaCl	586	0.0267	1.19	1.79
	619	0.0168	1.07	1.61
	654	0.0111	1.01	1.51
	680	0.0086	0.80	1.20
60 mol. % $ZnCl_2$-NaCl	592	0.0162	1.18	1.77
	623	0.0112	1.05	1.57
	651	0.0084	0.78	1.18
	685	0.0062	0.55	0.83

TABLE 5.17

Stokes-Einstein Radii for the Diffusing Species Present in Solutions of HCl in $ZnCl_2$-NaCl Melts

with larger X_{NaCl} or in those at higher temperatures. Little help could be gained by using the D_{HCl} values in $ZnCl_2$-KCl[83] to determine the radii of the diffusing species in that system. Since those D_{HCl} values were 10^2 times smaller than those found in this work, for melts of similar viscosity, the r values were found to be up to several hundred angstroms in size, which would mean the diffusing species are massive polymers moving through the solutions.

Other authors have tentatively used the Stokes-Einstein equation, and in chloroaluminate melts Osteryoung has intimated that it is obeyed reasonably well by diffusing metal cations[143]. In LiCl-KCl eutectic[140], values of r for Fe^{2+} and Ni^{2+} were found to be 2-3 times their crystal radii, and this was taken to infer that those bivalent ions are complexed by Cl^- ions in that medium.

5.2.5 Possible Alloy Formation Between Zinc and Platinum

Figure 5.6 shows typical voltammograms for the reduction of HCl in $ZnCl_2$-NaCl melts where the potential sweep has been reversed almost immediately after the reduction peak for H^+ had occurred. If, however, the potential sweep was continued almost to the cathodic limit of the melt further voltammetric peaks could been seen, as shown in Figure 5.13. Following the HCl reduction peak two waves can be seen as the scan continues in the cathodic direction, whilst on the reverse scan one wave appears before the hydrogen oxidation peak and another in between the hydrogen oxidation peak and what has been ascribed to the adsorption process. The variation of these peaks with scan rate is quite interesting. At low scan rates a very small wave, A, follows the HCl reduction peak, II, whilst B and C bear some resemblance to those of a diffusion-controlled process. As the scan rate is increased so peak A dramatically grows whilst peak B disappears, until at 1000 mVs^{-1} peak A is the only response evident. As the scan rate increases so the potential at which peak A occurs becomes progressively more cathodic. Peak C remains at the same potential, whilst peak D causes deformation of peak IV.

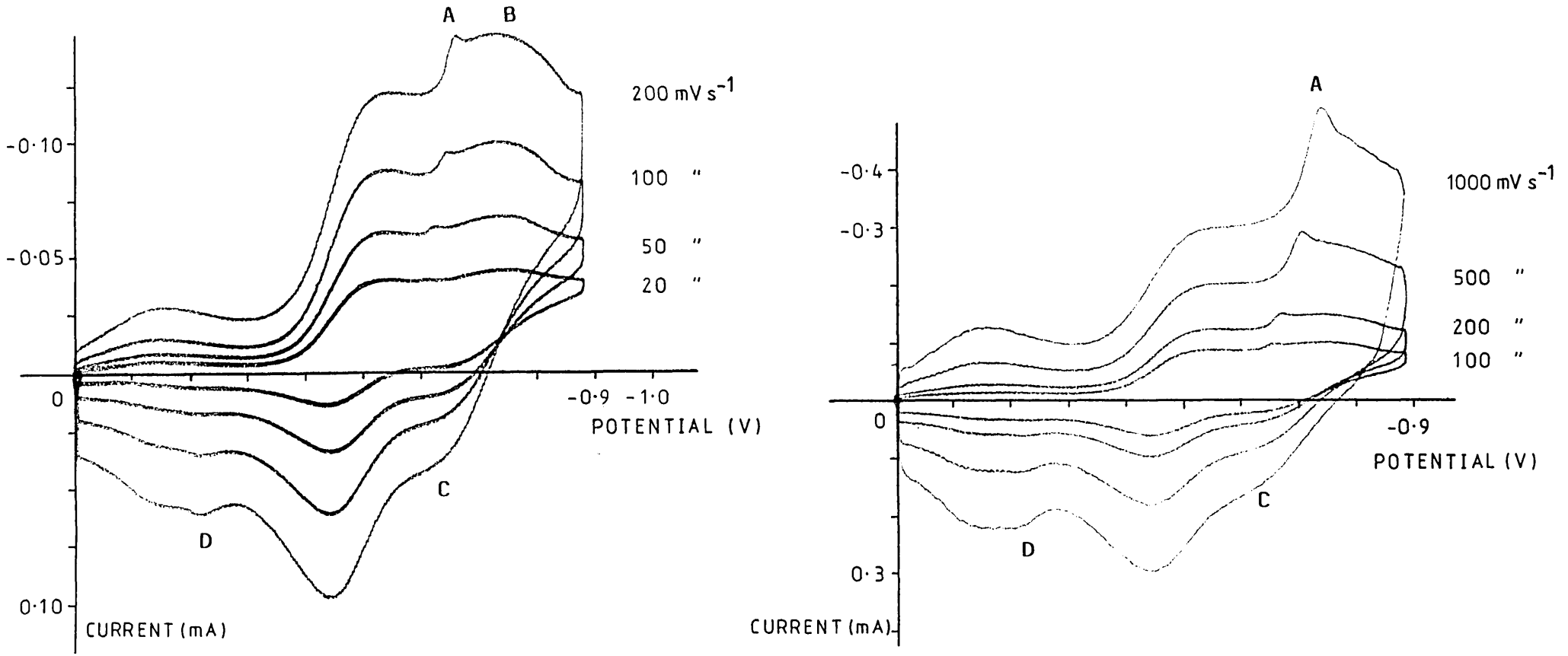


FIGURE 5.13

Voltammograms Showing Possible Zn-Pt Alloy Formation for 80 mol. % $ZnCl_2$-NaCl (317°C)

The origin of these peaks (A,B,C,D) is unclear. Perry et al.(83) observed very similar voltammetric response using platinum electrodes in HCl- containing $ZnCl_2$-KCl and tentatively ascribed them to either weak adsorption of the hydrogen formed in the HCl reduction, or to alloy formation between Zn and Pt, but went no further. This author, to see if the same waves occurred on another electrode material, tested a vitreous carbon electrode in the same melt solution but no voltammetric waves were seen. This infers that these waves (A,B,C,D,) are all a result of the electrode material, platinum, rather than of impurity species in the melt. These peaks, however, were only observed in $ZnCl_2$-NaCl melts that had HCl gas dissolved in them and when platinum electrodes were used. No such peaks were seen when platinum electrodes were used in the pure melts (Section 4). So the presence of HCl in the melts would seem to affect the Pt electrode in some way. It had originally been thought that if the HCl is present in two different chemical environments, say as $H^+ZnCl_3^-$ and HCl_2^-, then it might be reduced at different potentials. Since the products are the same, only one oxidation peak would be expected on the reverse sweep. Since the voltammograms are far more complex than this the idea is too simplistic to account for what was found.

If a metal is electrodeposited out of solution to form an alloy with the electrode material then the potential at which it deposits is found to be somewhat anodic of its usual value. Instead of forming pure metal it is forming an alloy where its activity is less than unity. The Nernst equation then describes the behaviour of the system; as the activity of the deposit drops below unity so the potential moves in a positive direction. Now, zinc and platinum are known to form a range of alloys[110], including Zn_8Pt, $Zn_{4.2}Pt$, Zn_2Pt, ZnPt, and $ZnPt_3$, so it would be entirely plausible to suspect alloy formation between electrodeposited zinc and the platinum electrode, and this has been found to occur[110]. The question remains why these alloy peaks only appear when HCl is present in the melt.

One explanation of this involves the presence of a thin oxide film on the platinum electrodes. In the pure melts zinc would be depositing on to an oxide layer so no alloy could form, and only one voltammetric response would be observed, the cathodic melt decomposition limit. If the dissolved HCl interacted with the oxide layer to strip it off, the zinc would now be depositing on bare platinum and any of the aforementioned alloys might be formed, leading to the extraneous voltammetric peaks observed. This is only a postulate, however, and no further work was carried out to determine if alloys were indeed produced.

CHAPTER 6

ELECTRICAL CONDUCTIVITY OF $ZnCl_2$-NaCl MELTS CONTAINING HCl and H_2O

6.1 Introduction

The dissolution of HCl and H_2O in $ZnCl_2$-NaCl melts is thought to result in chemical interactions between solute and solvent molecules. These interactions should cause changes in the physico-chemical properties of the melts[175], for which investigations into the nature of these changes should infer the chemical processes occurring. It was decided to measure the effect on the melt conductivity of adding H_2O and HCl as solutes using the a.c. impedance method, which provides a relatively simple method of electrical conductivity determination, with no interference from any electrolytic processes. Measurement of the cell constant, coupled with the melt resistance found by the impedance technique, allows the melt conductivity to be calculated.

6.2 The A.C. Impedance Technique

Electrode processes in high temperature molten salts tend to be much faster than those in room temperature solvents, mainly due to the higher temperatures at which they are occurring. It has been suggested by Gabrielli[174] that the impedance method should be a useful tool for systematic studies of these processes. However, few papers outlining impedance measurements in molten salts could be found in the literature[176-180]. Of those, one was concerned with the behaviour of zinc dissolved in molten $ZnCl_2$-LiCl-KCl[178], where it was found that values of the diffusion coefficients of the zinc ions determined using an impedance method were close to chronopotentiometric values. Since the impedance method is relatively unused by molten salt workers it would be useful to give a brief introduction to the technique. The complicated mathematical treatments involved are covered elsewhere[136,174,181], and this account will only give a simplified guide to the method and the theory behind it.

The impedance, Z, of an electrochemical system is a complex number which may be represented in polar or Cartesian co-ordinates:

$$Z(\omega) = |Z| e^{j\Phi} \qquad [6.1]$$

$$Z(\omega) = Z' + jZ'' \qquad [6.2]$$

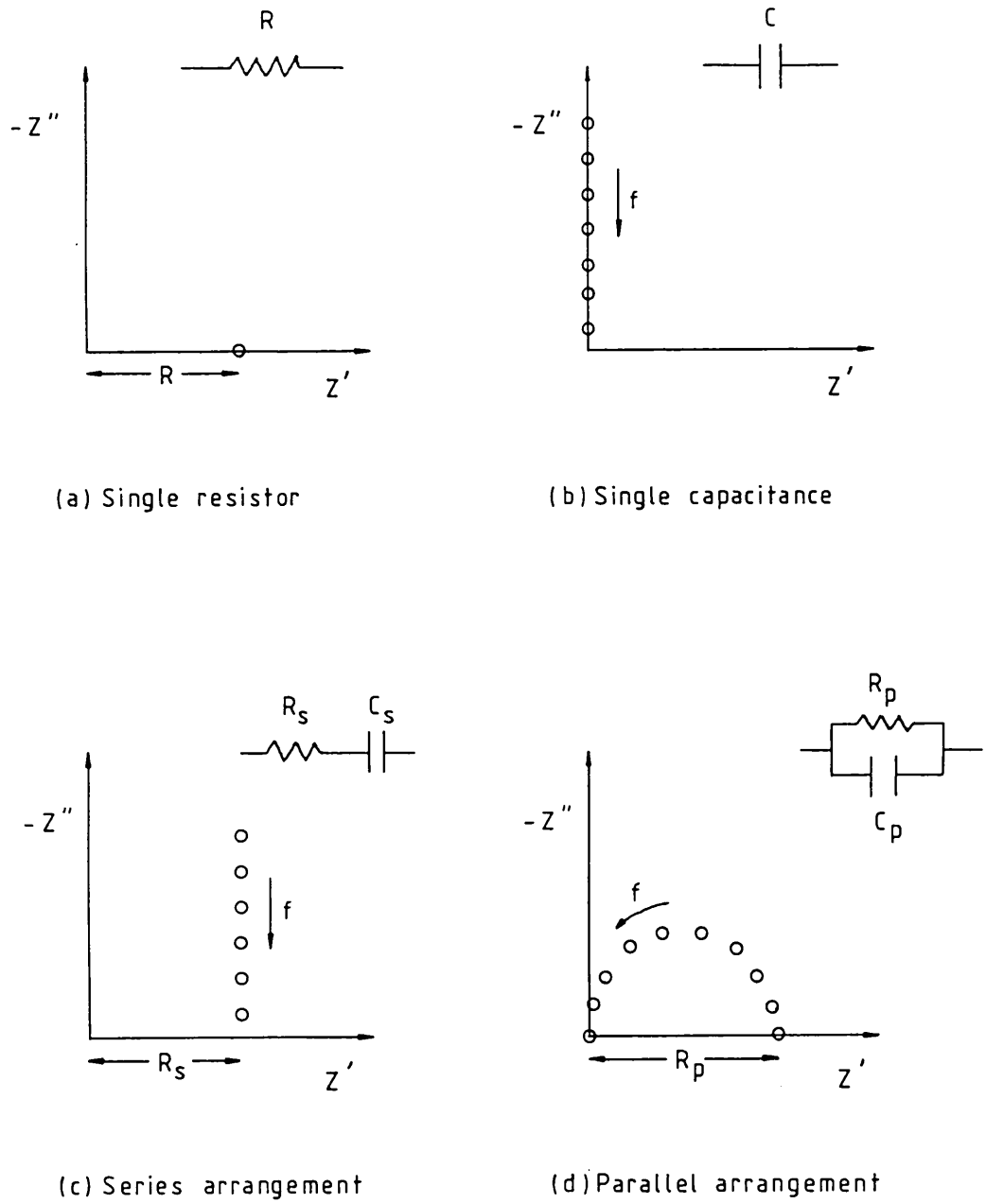
where Z' and Z'' are the real and imaginary parts of the impedance respectively, ω is the angular frequency ($= 2\pi f$) and Φ is the phase angle of the sinusoidal wave. Two types of plot can be used to show the impedance behaviour:

(i) an Argand diagram with Z' plotted against - Z'' (a Nyquist plot),

(ii) a Bode plot which allows the variation of $|Z|$ and Φ with frequency to be observed.

Before considering the response of an electrochemical cell to an a.c. perturbation, and the models used to describe the cell, it would be useful to mention the behaviour of passive electrical circuit components, such as resistors and capacitors which are used in the models, when an a.c. perturbation is applied to them. Figures 6.1 (a)-(d) show the complex plane impedance plots (Nyquist plots) for simple circuits. A single resistance R will give one point, for all frequencies of a.c., lying on the Z' axis (Figure 6.1(a)), whilst a single capacitor C will give a set of points along the Z'' axis, with the points lying closer to the origin at higher frequencies. Figures 6.1(c) and 6.1(d) show the effect of R and C in series and parallel respectively.

Expressed simply, an electrochemical cell is an impedance to a small sinusoidal excitation. Consequently, it should be possible to represent the cells behaviour by an equivalent circuit of resistors and capacitors. This circuit must take into account the behaviour of the electrode-electrolyte interface and the electrolyte resistance. The first useful equivalent circuit, suggested by Randles[136], is shown in Figure 6.2(a). The resistance R_Ω represents the uncompensated solution resistance. The



(a) Single resistor

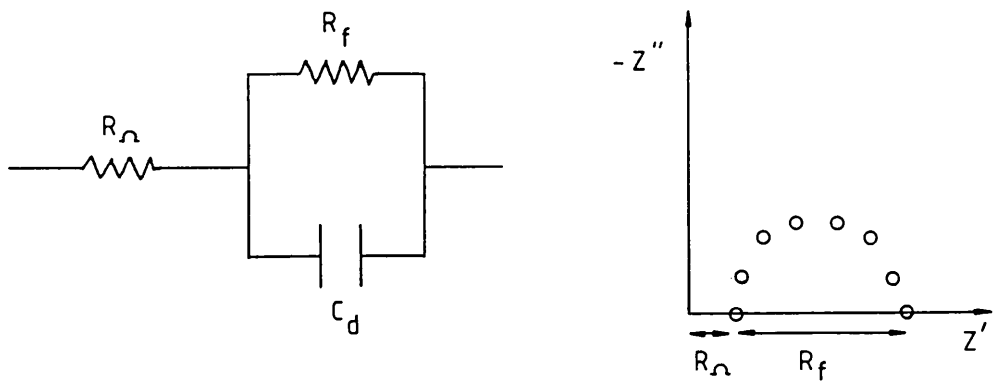
(b) Single capacitance

(c) Series arrangement

(d) Parallel arrangement

FIGURE 6.1

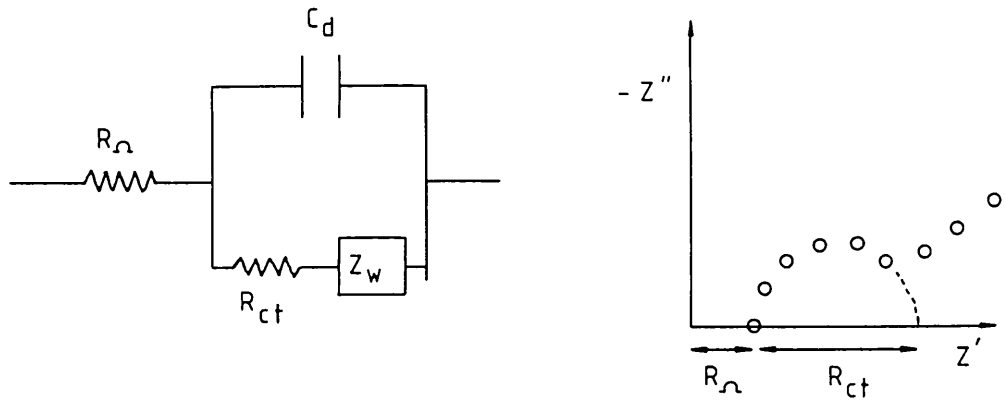
Complex Plane Impedance Spectra With Their Association Equivalent Circuits



(a) Circuit (b) Response

FIGURE 6.2

Randles - Type Equivalent Circuit and Response



(a) Circuit (b) Response

FIGURE 6.3

Modified Equivalent Circuit Incorporating the Warburg Impedance Component

parallel combination of R_f and C_d represents the interface, R_f being the Faradaic resistance and C_d the electrochemical double layer capacitance. The response of this circuit to an a.c. perturbation is shown in Figure 6.2(b). The imaginary component to the impedance in the circuit comes solely from C_d, the capacitance. At high frequencies its contribution falls to zero because it offers no impedance; the only impedance the current sees is the ohmic resistance R_Ω. As the frequency is decreased the finite impedance of C_d results in a significant Z" value, with the current passing through both C_d and R_f. As the frequency tends to zero (i.e. the a.c. tends to d.c.) the capacitance C_d offers a high impedance and the current flow passes through R_f and R_Ω. Thus the imaginary impedance component falls off again. The resulting Nyqvist plot for the range of frequencies is semicircular in shape.

This simple representation has to be modified to take into account effects caused by mass transfer. The Faradaic process, treated as a simple resistance before, may be considered as a general impedance Z_f which can be separated into two parts; R_{ct}, the charge transfer resistance, and Z_w, the Warburg impedance which takes into account mass transfer effects. In contrast to R_Ω and C_d which are nearly ideal circuit elements, the components of Z_f are not ideal because they change with frequency. Figures 6.3(a) and 6.3(b) show the modified circuit and the complete response of the modified circuit to the a.c. perturbation at various frequencies, respectively. The Warburg impedance drops out at high frequencies because the time scale is so short that diffusion cannot manifest itself as a factor influencing the current, and the semi-circular segment of the response in Figure 6.3(b) is seen, the modified circuit having been reduced to the simple Randles circuit (Figure 6.2(a)). At low frequencies, if the electrode process is diffusion controlled, a linear correlation between Z' and Z" is seen, having a slope of unity. However, both regions may not be well defined for any given system. The determining feature is the charge transfer resistance R_{ct} and its relationship to the Warburg impedance, which is controlled by the mass transfer of the system. If the chemical system is kinetically slow it will have a large value of R_{ct} and may display only a very limited frequency region where mass transfer is important. At the other extreme R_{ct} might be very small compared to R_Ω and

the Warburg impedance, in which case the system is so kinetically rapid that mass transfer always plays a role and the semicircular region is not well defined.

6.3 Measurement of the Cell Constant

The specific conductivity, $K(\Omega^{-1}\ cm^{-1})$, of a material is calculated using equation [6.3]:

$$K = 1/RA$$

where l is the distance between the electrodes (cm), A is the area of the electrodes (cm^2) and R is the measured resistance (Ω). The quotient l/A is known as the cell constant, and can be found by determining the resistance of a solution of known conductivity held in the cell to be used. In this case an aqueous solution of KCl was used (0.10 mol. dm^{-3}, 25°C; $K = 0.0129\ \Omega^{-1}\ cm^{-1}$)[142]. The cell constant was calculated to be $1.295 \pm 0.008\ cm^{-1}$, this value being assumed to be more accurate than any value found by trying to measure the actual areas of the platinum electrodes used.

6.4 Conductivity of $ZnCl_2$-NaCl Melts Containing HCl and H_2O

By varying the frequency of the applied a.c. signal to the melt system values for the real and imaginary components of the impedance, the resistance Z' and the reactance Z" respectively, were determined. These have been displayed on Nyqvist plots, where Z' is plotted against -Z", as described in Section 6.1. A typical plot is shown in Figure 6.4. At low frequencies the term Z" is quite large, decreasing as the frequency increases until at around 10 kHz the imaginary component falls to zero. At the point where the plot crosses the Z' axis the value of the real component of the impedance was taken as being the melt resistance. Using this value and the cell constant the specific conductivity of the melt was calculated.

It can be seen that none of the three lines in Figure 6.4 conform to the theoretical predictions given in Section 6.1 for ideal cells, where either

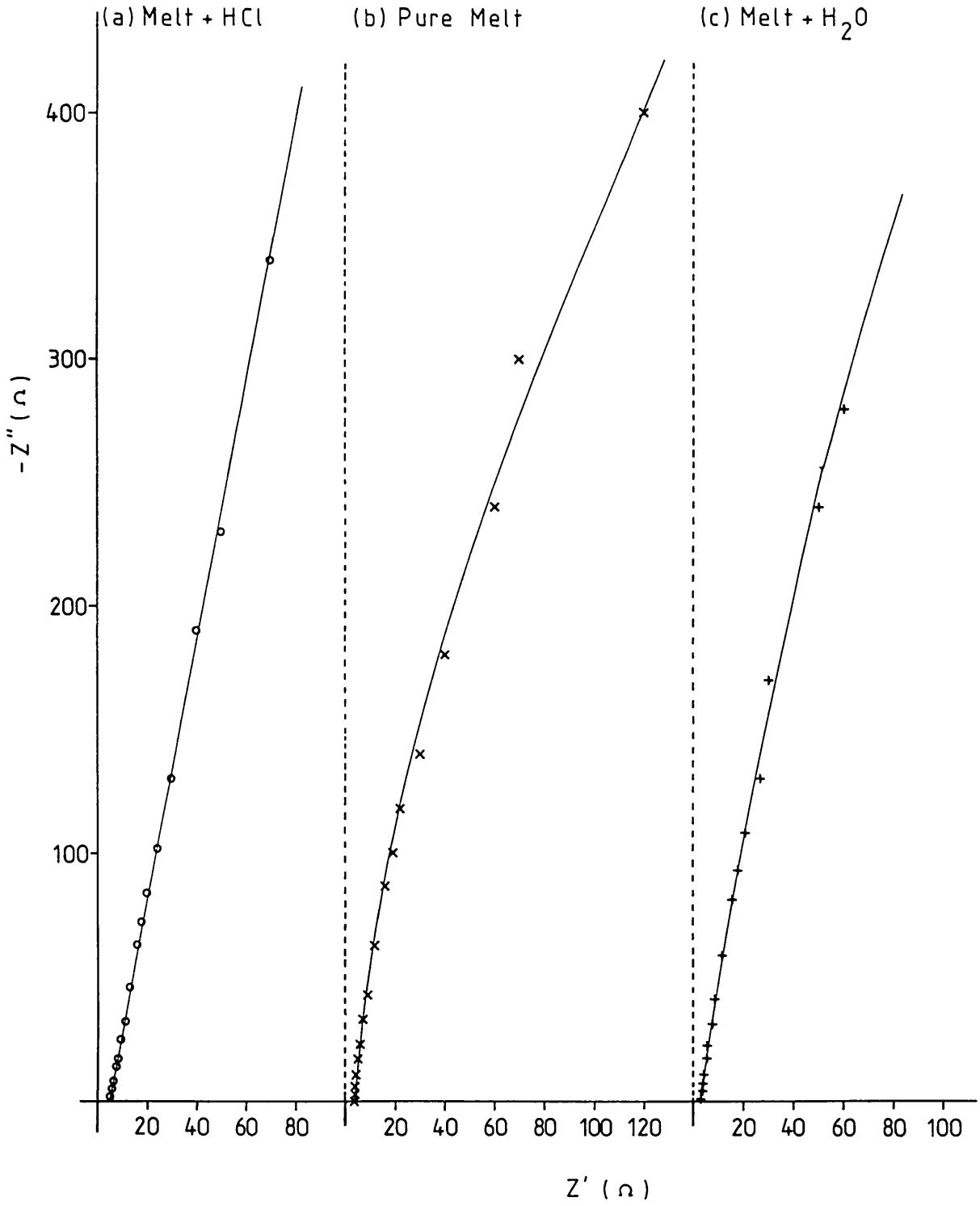


FIGURE 6.4

Complex Plane Impedance Spectra for 80 mol. % $ZnCl_2$-NaCl (357°C)

vertical lines or semicircles were the shapes obtained for the unmodified circuits, or 45^{o} lines obtained when mass transfer modifications were introduced. Rather, the plots obtained in this work were a few degrees off the vertical, but not far enough to be treated as Warburg processes. That the plots were taken as straight lines rather than semicircles or curves was because the analyzer used could not reach frequencies below 5Hz. Often the semicircular regions begin to occur at frequencies of less than 1Hz[174]. In a few of the plots some curvature was seen at low frequencies but not enough to attempt an extrapolation to try to define the whole semicircle. Lelievre et al.[179] obtained similar straight line plots when they carried out a.c. impedance measurements on pure $PbCl_2$-KCl melts using vitreous carbon electrodes. One cause of these deviations might be the presence of impurities within the melt systems.

It was found during this work that Nyqvist plots obtained for melts with water dissolved in them had smaller slopes i.e. suffered greater deviation from the vertical, than those with HCl or the pure melts. The melts with HCl dissolved in them also had greater slopes than the supposedly pure melts, which was thought to be caused by the presence of oxygen in the argon used to purge the melts. This oxygen would be absent after the melts had been saturated with HCl. These results would seem to confirm the idea that the presence of impurities in the melts causes the Nyqvist plots to deviate from ideality, since small Faradaic processes interfere with the pure double layer[179]. As the amount of impurity increases so the system tends towards the behaviour noted for diffusion-controlled electrochemical reactions, where the plot is a line at 45^{o} and the Warburg modifications are introduced. It was also noticed that as the amplitude of the applied a.c. signal was increased so the extent of deviation increased, especially in the melt + H_2O systems, as shown in Figure 6.5.

Hence, one possible use of the a.c. impedance method would be to assess the purity levels of melt systems, in much the same manner as cyclic voltammetry has been used (Chapter 4).

Having determined the melt resistances from the Nyqvist plots the melt conductivities (K) were calculated, and are listed in Table 6.1. The

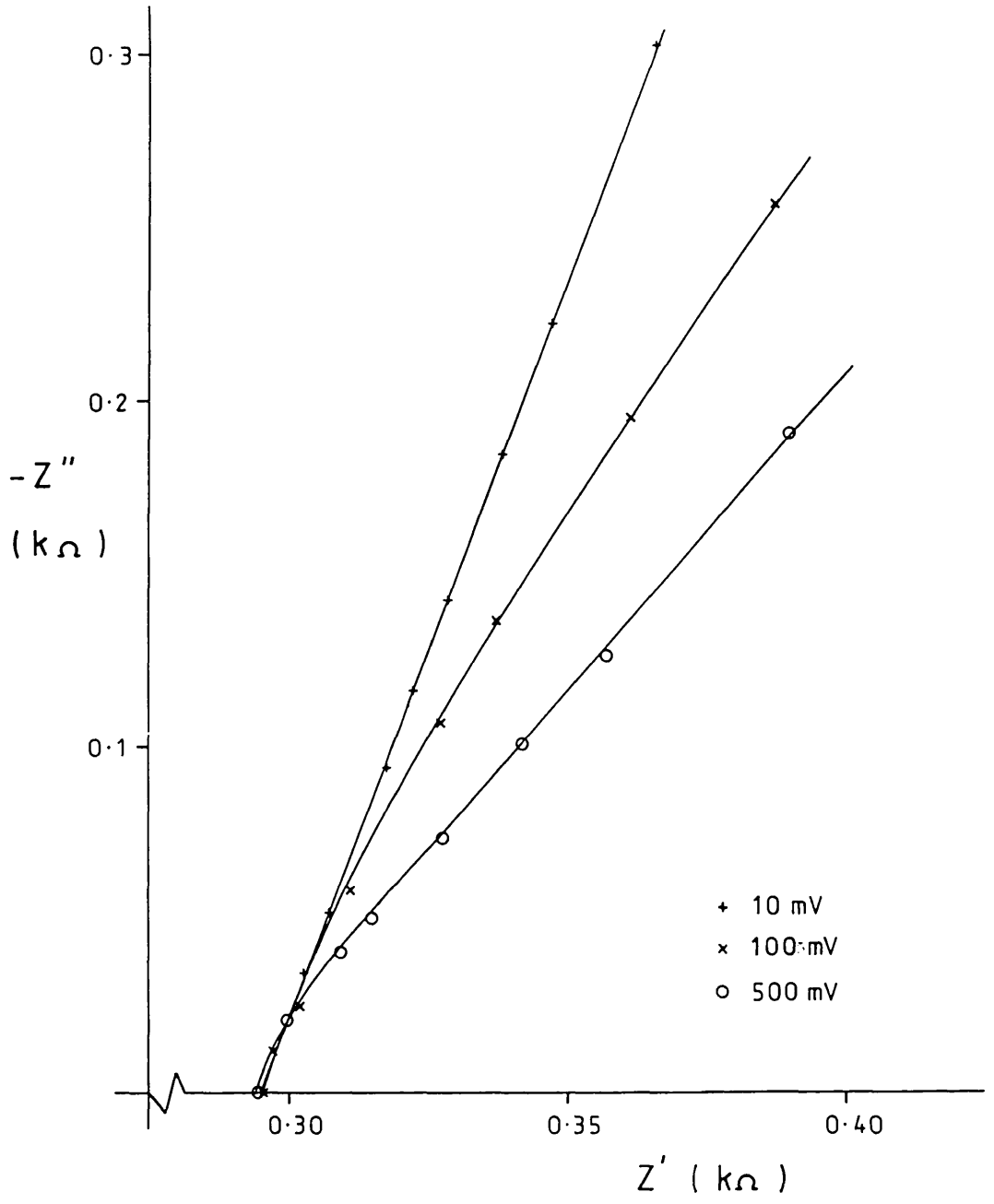


FIGURE 6.5

Complex Plane Impedance Spectra for Molten $ZnCl_2$+H_2O (355°C) Showing the Effect of Varying the A.C. Amplitude

Melt Composition	Temp (^{o}C)	$K_{HCl}(\Omega^{-1}cm^{-1})$	$K_{Ar}(\Omega^{-1}cm^{-1})$	$K_{H_2O/Ar}(\Omega^{-1}cm^{-1})$
50 mol% $ZnCl_2$-NaCl	358	0.539 ± 0.023	0.616 ± 0.028	0.647 ± 0.031
70 mol% $ZnCl_2$-NaCl	355	0.308 ± 0.016	0.370 ± 0.010	0.392 ± 0.012
80 mol% $ZnCl_2$-NaCl	357	0.184 ± 0.004	0.190 ± 0.005	0.193 ± 0.003
90 mol% $ZnCl_2$-NaCl	353	$(6.38\pm0.10)\times10^{-2}$	$(6.78\pm0.07)\times10^{-2}$	$(6.85\pm0.04)\times10^{-2}$
100 mol% $ZnCl_2$	355	$(3.78\pm0.14)\times10^{-3}$	$(3.92\pm0.12)\times10^{-3}$	$(4.46\pm0.24)\times10^{-3}$

TABLE 6.1

Specific Conductivities of $ZnCl_2$-NaCl Melts Containing HCl and H_2O and of the Pure Melts

trends in these results are rather surprising in that the conductivities of melts containing HCl are lower than those of the pure melt and of those containing H_2O. It was thought that HCl might affect $ZnCl_2$ melts in the same way as alkali chlorides, by enhancing the break-up of the melt structure and lowering the melt resistance. Instead it seems to have had the opposite effect and increased the melt resistance, so lowering the conductivity. Water, however, was found to increase the melt conductivity, which would imply that the HCl and H_2O are interacting in different ways with the $ZnCl_2$ melts.

The species thought to be formed by the interaction of water with $ZnCl_2$ melts are $[H^+ZnCl_2OH]$ and similar hydroxy- or oxy-chloro entities (Chapter 7, Appendix 1). Formation of these species should break down the polymeric $ZnCl_2$ melt structure and increase melt conductivity, as has been found. However, HCl would appear to be, if anything, reforming that structure. This could be occurring if HCl is a stronger Lewis acid than $ZnCl_2$, and is complexing available Cl^- ions to form $HCl_n^{(n-1)-}$. This explanation was put forward to account for the solubility behaviour of HCl in $ZnCl_2$-NaCl melts (Section 5.1) in NaCl-rich melts, but in the very $ZnCl_2$- rich melts it had been assumed that $H^+ZnCl_3^-$ or similar species were formed, there being a changeover in which species was formed as the melt compositions were altered. It might be possible that the HCl is acting as a bridging agent, with two $ZnCl_4^{2-}$ tetrahedra linked via a hydrogen ion, as shown below.

$$^{(2-\delta)-}Cl_3ZnCl^{\delta-}....H^{\delta+}.....^{\delta-}ClZnCl_3^{(2-\delta)-}$$

In this case the reduced mobilities of the species might cause a reduction in conductivity, and the bridging would also help account for the solubility behaviour.

Another possible effect could be some interaction between the platinum electrodes and the HCl. It was noticed during the voltammetric study of HCl in $ZnCl_2$-NaCl melts (Section 5.2) that extraneous peaks appeared on the voltammograms, that were not seen when pure melts were used. It was suggested there that perhaps the HCl was stripping an oxide layer from the

platinum so allowing alloying between deposited zinc and the platinum to occur. If this is indeed occurring then this might alter the electrode area in some way, which would cause a change in the cell constant, and could be responsible for the conductivity effects observed. In order to verify this explanation the experiment would need to be repeated using vitreous carbon electrodes which would not suffer interference from oxide layers.

By plotting the conductivities of the pure $ZnCl_2$-NaCl melts obtained in this work with those obtained by Bloom and Weeks[47] over the same composition range it was possible to compare the two sets of results (Figure 6.6). Taking the average temperature of the results from this work as 628K, it can be seen that all the values are slightly higher than those of Bloom, the isotherm at 628K lying almost on top of their 640K isotherm. However, the general shapes of the isotherms match fairly well, indicating that the simple impedance method used here provided reasonably good results, and that use of a purpose-built cell would lead to accurate values should the technique be used in the future for other melt systems.

6.5 Double Layer Capacitances Measured by A.C. Impedance

The application of the equation valid in the absence of an electrochemical reaction (equation [6.2]), which can be rewritten in the form:

$$Z = R_m + \frac{1}{j \omega C_d} \qquad [6.4]$$

Where R_m is the melt resistance and C_d the double layer capacitance, allowed values of C_d to be estimated.

However, the values obtained from this work were in the range 200-300 $\mu F\ cm^{-2}$, which is a factor of 10 larger than those obtained by workers using other methods[182]. This effect seems to be common to the a.c. impedance technique used in molten salts, since Lelievre et al.[179] also noticed it. Having calculated a capacitance from a value of Z" by equation [6.4], the effect of dividing that value ($\sim$ 50-80 μF) by the estimated area of the Pt wire electrode ($\sim 0.14\ cm^2$) was to obtain the large values mentioned. If,

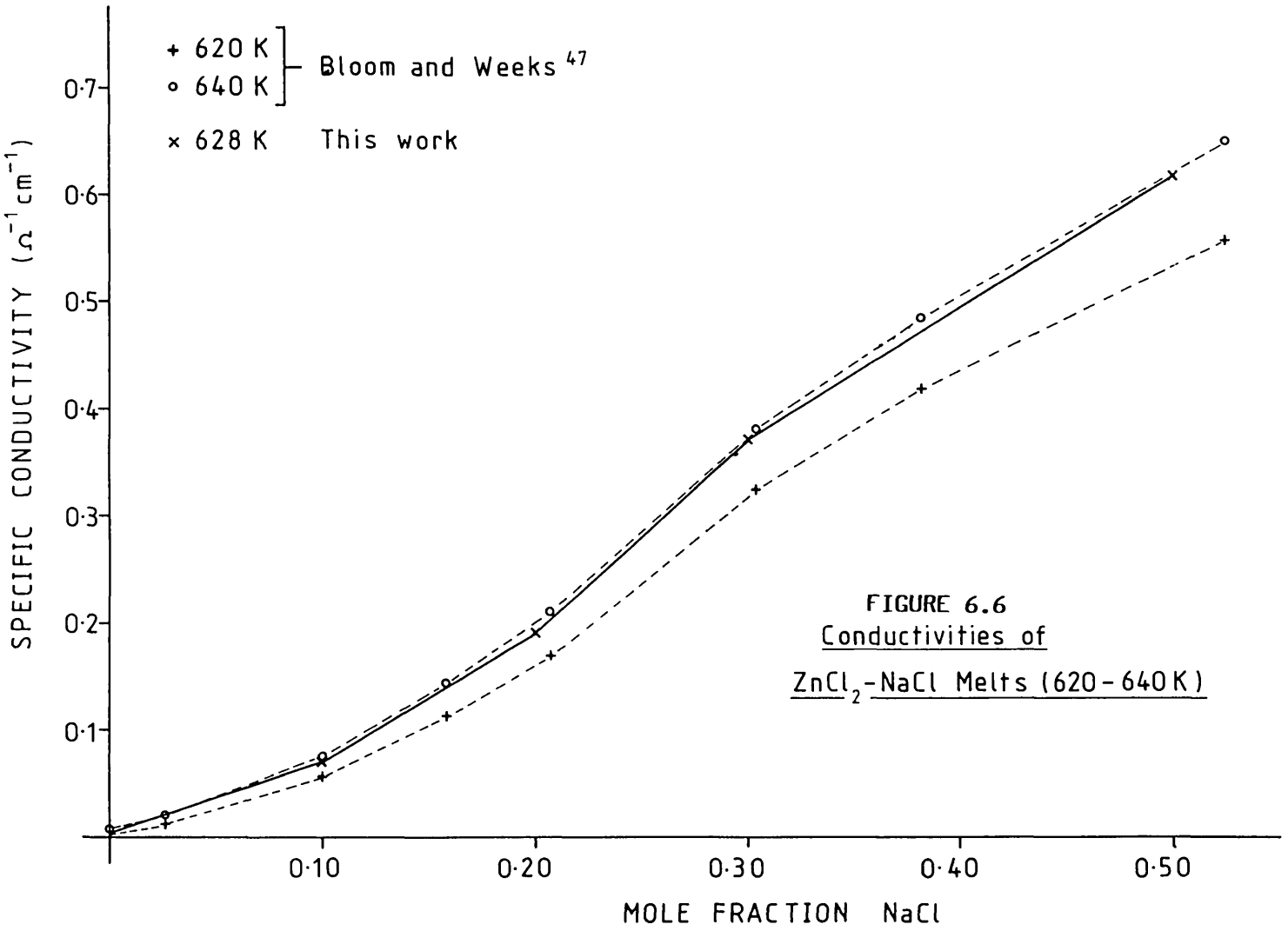


FIGURE 6.6
Conductivities of
$ZnCl_2$-NaCl Melts (620 - 640 K)

however, the total area of the two electrodes was used (~ 2.2 cm^2) then values of the same size as those of other workers were obtained.

The idea of using a small area working electrode and a larger area flag counter electrode was that any effect on the flag electrode would become negligible since the area was much greater. This may not be the case. Another reason might be that the active surface area of the Pt wire electrode may not be the simple geometric area calculated from the dimensions of the wire, but that surface roughness could lead to a much larger area. This, it might be expected, should have shown up in the cell constant. As mentioned before, any effect the HCl has on the Pt might cause some alteration in the C_d values. Until this effect is resolved the impedance technique will be treated with scepticism by some workers in the area of C_d determination.

CHAPTER 7

BEHAVIOUR OF H_2O IN $ZnCl_2$-NaCl MELTS

7.1 Introduction

Studies of the behaviour of water in zinc chloride melts are very few in number[101-103], as shown in Section 2.6, but the available results all indicate that the degree of hydrolysis of the melts on introduction of moisture is low. The two reactions thought to occur upon the addition of water to chloride melts are:

$$2OH^- = O^{2-} + H_2O \qquad [7.1]$$

$$H_2O + 2Cl^- = O^{2-} + 2HCl \qquad [7.2]$$

Ito et al.[101] found that the equilibrium constant for the hydrolysis reaction, [7.2], had a value of 1.91×10^{-7} atm in $ZnCl_2$-NaCl at 360^oC, showing the relative lack of reactivity of these melts in the presence of water. No published voltammetric results for water in $ZnCl_2$ melts were available, but the presence of the ubiquitous "water wave" in voltammograms obtained from impure $ZnCl_2$ at 369^oC has been claimed[183]. This "water wave" is thought to arise from the reduction process [7.3], and takes the form of a broad, ill-defined wave rather than a sharp peak.

$$H_2O + e^- \rightarrow OH^- + \tfrac{1}{2}H_2 \qquad [7.3]$$

Its presence in voltammograms of other chloride melts containing water has been noticed[144], along with "hydroxide waves", believed to arise from the reduction of OH^- to O^{2-} (equation [7.4]).

$$OH^- + e^- \rightarrow O^{2-} + \tfrac{1}{2}H_2 \qquad [7.4]$$

Oxide formed by chemical (equation [7.1]) or electrochemical (equation [7.4]) means in LiCl-KCl melts has been shown[88] to undergo two electron

oxidation to $\frac{1}{2}O_2$, but such a process was not noted in the results for $ZnCl_2$ melts[183].

Other processes claimed to occur upon the addition of water to chloride melts include the quantitative formation of HCl in $AlCl_3$-BuPyCl[99] and $AlCl_3$-NaCl[100], the formation of stable peroxy-species in $CaCl_2$-KCl[98] and hydroxychloro-species of Cr^{3+} in LiCl-KCl[90,91]. Given the lack of published work on the behaviour of water in $ZnCl_2$ melts, and the uncertainty as to the species present, it was felt that a close look at the area would be useful. Workers in the hydrocracking field have suggested that hydroxychlorozinc species may exist in melts (Appendix 1) but offered little proof other than that this supposition would account for the observed products of their hydrocracking processes. The results of the a.c. impedance study (Chapter 6) indicate that water does have an effect upon the physical properties of the $ZnCl_2$-NaCl system but offered little information as the species present. Voltammograms seen in Chapter 4 for the impure melts also showed that some degree of reaction occurs in water-contaminated $ZnCl_2$ melts.

7.2 Solubility of H_2O in $ZnCl_2$-NaCl melts

In much the same way as the solubility of HCl in $ZnCl_2$-NaCl melts was determined (Section 5.1) for use with the voltammetric results (Section 5.2) so attempts were made to measure the solubility of water in $ZnCl_2$ melts. The experimental details are given in Section 3.8; dissolved water was purged from the melts with HCl and absorbed on a drying column packed with AW500 molecular sieve. It was hoped to discover the effect, if any, of the water vapour pressure on the solubility in melts held at different temperatures and to correlate it with the voltammetric results.

However, it was found that as the HCl carried over the purged water onto the drying column it also carried over non-negligible amounts of ZnCl2 which condensed on the column and interfered with the weighings. The weight of the column never became steady; the longer the purging went on the heavier the column became. Putting a trap between the melt and the column resulted in moisture condensing in the trap along with the $ZnCl_2$. This had

worked for the HCl solubility determination since the HCl would not condense and would be carried through the trap into the distilled water.

Initially, the weight increase of the column was due to the absorption/condensation of both water and $ZnCl_2$ on the column, whilst after a time the increase was due only to $ZnCl_2$. It was thought that by monitoring the rate of weight increase it would be possible to separate the two stages, so long as the melt temperature, and hence the $ZnCl_2$ vapour pressure, remained constant. The rate should have decreased when all the water had come out of the melt, and a point seen where the weight increase became solely due to the $ZnCl_2$. However, no such distinction could be made since the weight increases were actually quite erratic and could not be split into two regions. Consequently, it was not possible to even estimate the solubility of water in the $ZnCl_2$ melts, but the method may work better for melts which do not contain such a volatile component.

7.3 Extent of the hydrolysis reaction in $ZnCl_2$-NaCl melts

It had been thought that addition of water to these melts might cause zinc oxide to precipitate out of solution. The solubility of ZnO in $ZnCl_2$ melts is thought to be very low (Chapter 9), and given the equilibria set up in chloride melts by the presence of water (equations [7.1] and [7.2]) such a precipitation seemed likely. The O^{2-} formed by the decomposition of H_2O molecules could combine with Zn^{2+} to form ZnO as a white precipitate, but even prolonged saturation of the $ZnCl_2$ melts with water vapour left the melts clear with no sign of any precipitate.

The presence of water in chloride melts has been found to cause the evolution of HCl (equation [7.2]). An attempt was made to determine the amount of HCl evolved from $ZnCl_2$ melts by passing water vapour through melts and on through distilled water. Any HCl formed should have been dissolved in the water, which was then titrated against standard NaOH solution (0.02M) using phenolphthalein as the indicator. That the distilled water was made acidic by the experiment could be seen by using pH indicator paper, but the presence of $ZnCl_2$ in the distilled water, carried over by the gas stream, may have affected the phenolphthalein indicator.

The amount of $ZnCl_2$ in the solution was determined by analysing for Zn using atomic absorption analysis (Section 3.14). The results for pure molten $ZnCl_2$ are given in Table 7.1.

Temp (^oC)	HCl evolved (mol. g^{-1})	Total Zn content of solutions (g)	Calculated [$ZnCl_2$] (M)
341	2.3×10^{-6}	0.008	7.6×10^{-4}
372	4.1×10^{-6}	0.036	3.7×10^{-3}

TABLE 7.1

Evolution of HCl by addition of water to pure molten $ZnCl_2$

The amount of HCl evolved, determined directly from the titrations, is given in the units moles of HCl per gram of melt, and in the next column is the amount of zinc found in total in the distilled water solutions (volume = 160 cm^3). The last column gives the calculated concentration of $ZnCl_2$ in the solutions. To what extent the $ZnCl_2$ affected the phenolpthalein indicator is not known, so the figures for HCl evolution should be treated with caution, but that HCl was formed is certain. Those small amounts of $ZnCl_2$ would not affect the pH paper.

Interestingly, the amounts of HCl formed were of the same magnitude as the HCl solubilities in the $ZnCl_2$ melts (Section 5.1). Since the HCl was formed by reaction [7.2], where one molecule of water causes the evolution of two molecules of HCl, some idea of the water solubility may be obtained from the data in Table 7.1. It appears that the hydrolysis reaction is enhanced by rise in melt temperature, but so is the volatility of $ZnCl_2$. The 30^oC rise in melt temperature caused a four-fold increase in the amount of $ZnCl_2$ dissolved in the distilled water, which will increase

the error in the titration results. The situation in aluminium chloride melts is rather different[99,152]. Prolonged passage of water vapour through those melts results in the formation of a precipitate which eventually engulfs the melts. In $ZnCl_2$ melts, though, the hydrolysis reaction appears to reach a limit and continued addition of moisture does not appear to push equilibrium [7.2] beyond that limit. Accepting that the hydrolysis reaction occurs to some extent implies that some melt-soluble species, perhaps a hydroxychlorozinc entity, is formed. Some ZnO may also be formed but the solubility product is not exceeded, otherwise it would precipitate out of solution.

As discussed in Chapter 8, a solid was formed on the inside of the Pyrex gas bubbler used to introduce water vapour into the melts. This was identified as being zinc oxide; yellow at high temperatures and remaining yellow as the cell temperature decreased, since the atmosphere was oxygen deficient. The formation of the oxide appears to have been catalysed by the glass surface, but why only on the inside of the bubbler is unknown.

7.4 Voltammetric study of H_2O in $ZnCl_2$-NaCl melts

The behaviour of water in $ZnCl_2$ melts was studied voltammetrically using the Pt working and quasi-reference electrodes. As discussed in Chapter 4, no voltammetric waves were observed with vitreous carbon electrodes for water-contaminated melts, but several peaks were seen with platinum electrodes. The experimental details for the equilibration of the melts with water vapour were given in Section 3.9; four different vapour pressures were used, supplied by distilled water and saturated solutions of various salts. These were introduced into pure molten $ZnCl_2$ and two $ZnCl_2$-NaCl mixtures (80 and 50 mol. % $ZnCl_2$-NaCl) and voltammograms recorded at different melt temperatures. Results for each melt composition are given in turn, and then will be discussed as a whole, with reference to the results of other workers.

For water in pure molten $ZnCl_2$ the voltammograms show six (I-VI) reasonably well-defined peaks between the melt limits (Figure 7.1), which have been split into three pairs, each pair comprising a cathodic and

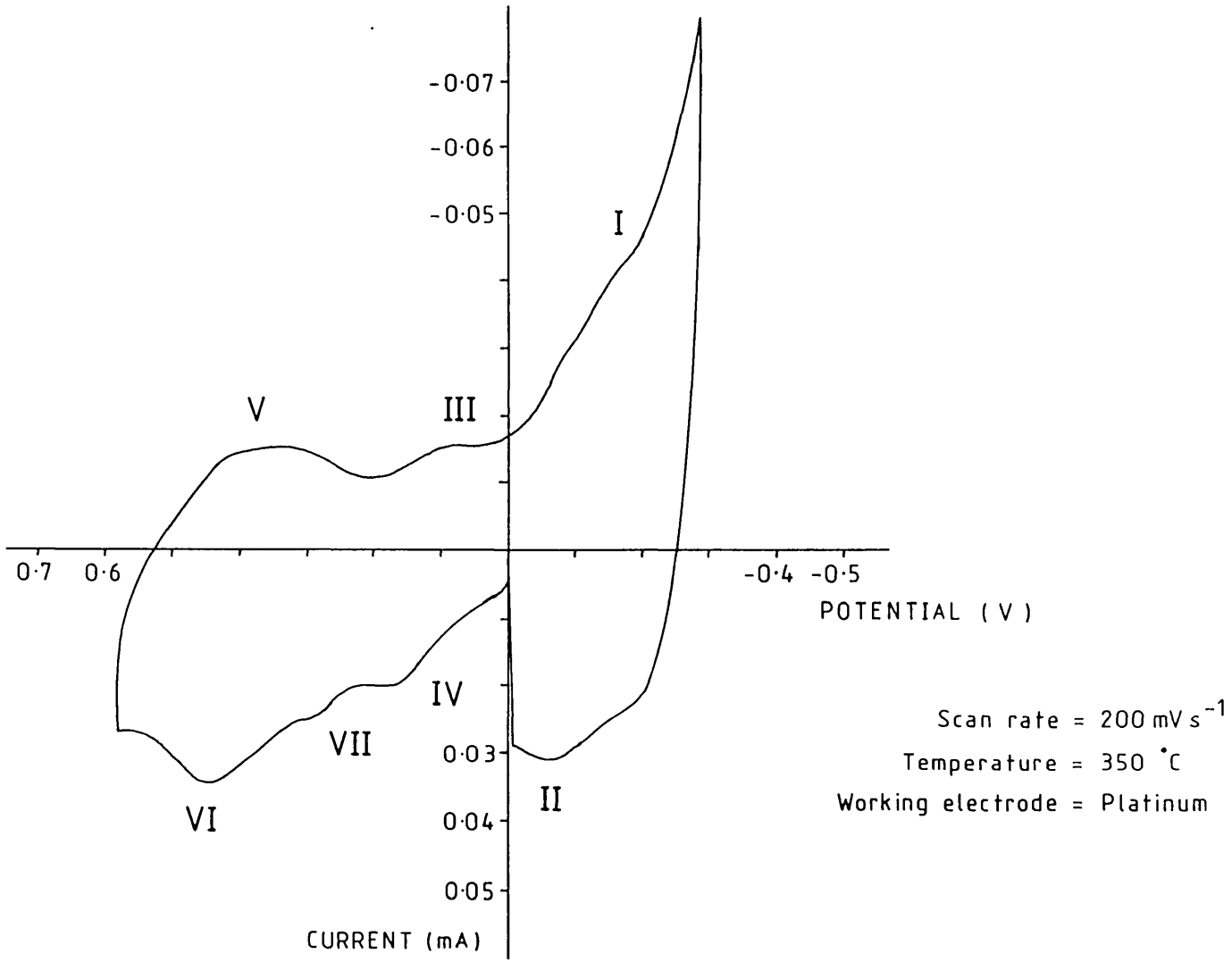


FIGURE 7.1

Voltammogram for Water in Pure Molten Zinc Chloride

anodic response. Between the anodic peaks IV and VI would sometimes be seen a small peak, labelled VII here. The voltammetric parameters of the peaks are listed in Tables 7.2 (peaks I and II), 7.3 (peaks III and IV) and 7.4 (peaks V and VI). All the measurements were taken from voltammograms recorded with water at a vapour pressure of 19.8 torr (distilled water at room temperature 22^{o}C) having been equilibrated with the melt. It was noticed that although the initial voltage sweeps gave voltammograms like the one shown in Figure 7.1, subsequent scans resulted in a change of position for peak IV, which moved slightly cathodic of its initial position. This shift is shown in Figure 7.2 where three successive sweeps have been carried out. The parameters for both positions of peak IV have been included in Table 7.3. At low scan rates the high resistance of the melt caused the voltammograms to be twisted away from the horizontal and assume a shape like that shown in Figure 7.3, where at a scan rate of 50 mVs^{-1} the parts of the waves at cathodic potentials did not drop below the potential axis. It was also noticed that as the melt temperature was raised, so the voltammetric responses became less well-defined, a phenomenon that had also been noticed during the voltammetric study of HCl in these melts (Section 5.2).

Analysis of the six peaks in turn revealed that I and II were the result of a one-electron transfer process, the peak separation being reasonably close to the calculated value for a reversible one-electron process (equation [5.9]). Figure 7.4 shows plots of the height of the reduction peak I, i_p^I, against the square root of the scan rate, $\nu^{\frac{1}{2}}$. All can be seen to be linear and passing through the origin, indicating the diffusion control of the process. The plot at 642K lies below those for lower temperatures, which will be discussed later.

On the initial scan the peak separation of III and IV was characteristic of a one electron process, but the change in position by peak IV for subsequent scans altered the peak separation to that for a two electron process (Table 7.3 (a) and (b)). On the initial scan peak IV can be seen to be quite well-defined but on subsequent scans became very broad, making exact measurement of the peak position difficult. Nevertheless, the change from a one- to a two- electron process following the first scan

ν (Vs^{-1})	T (K)	$-Ep^{I}$(V)	$-Ep^{II}$(V)	ΔEp(V)	$i_p{}^{I}$ (mA)	$i_p{}^{II}$ (mA)
0.02	615	0.240	0.080	0.160	0.012	--
0.05	615	0.260	0.110	0.150	0.020	0.003
0.10	615	0.460	0.300	0.160	0.029	0.008
0.20	615	0.510	0.340	0.170	0.041	0.012
0.50	615	0.400	0.210	0.190	0.062	0.021
1.00	615	0.270	0.110	0.160	0.080	0.043
calc. (n=1)				0.123		
0.05	623	0.190	0.050	0.140	0.020	--
0.10	623	0.250	0.130	0.120	0.028	0.019
0.20	623	0.190	0.060	0.130	0.040	0.031
0.50	623	0.210	0.090	0.120	0.065	0.053
calc. (n=1)				0.123		
0.05	642	0.190	0.070	0.120	0.013	--
0.10	642	0.195	0.080	0.115	0.018	--
0.20	642	0.170	0.040	0.130	0.023	0.007
0.50	642	0.170	0.035	0.135	0.038	0.012
1.00	642	0.165	0.045	0.120	0.055	0.025
2.00	642	0.135	-0.010	0.140	0.085	0.041
calc. (n=1)				0.127		

TABLE 7.2

Voltammetric Parameters of Peaks I and II

for H_2O (v.p. = 19.8 torr) in $ZnCl_2$

$\nu(Vs^{-1})$	T (K)	$-Ep^{III}$ (V)	$Ep^{(IV)}$(V)	Δ Ep(V)	i_p^{III} (mA)	i_p^{IV} (mA)
(a) Initial scan						
0.05	623	0.060	0.190	0.130	0.005	0.005
0.10	623	0.065	0.190	0.125	0.009	0.011
0.20	623	0.070	0.185	0.115	0.016	0.020
0.50	623	0.050	0.170	0.120	0.036	0.040
calc. (n=1)				0.123		
0.05	642	0.010	0.130	0.120	0.006	~ 0.001
0.10	642	0.020	0.140	0.120	0.010	0.001
0.20	642	0.060	0.190	0.130	0.012	0.005
0.50	642	0.085	0.190	0.105	0.018	0.013
1.00	642	0.090	0.215	0.125	0.025	0.026
2.00	642	0.130	0.250	0.120	0.038	0.039
calc. (n=1)				0.127		
(b) Subsequent scans						
0.05	623	0.060	0.130	0.070	0.005	0.010
0.10	623	0.065	0.125	0.060	0.009	0.017
0.20	623	0.070	0.140	0.070	0.016	0.029
0.50	623	0.050	0.125	0.075	0.036	0.052
calc. (n=2)				0.062		
0.05	642	0.010	0.080	0.070	0.006	~ 0.002
0.10	642	0.020	0.090	0.070	0.010	0.002
0.20	642	0.060	0.125	0.065	0.012	0.007
0.50	642	0.085	--	--	0.018	--
1.00	642	0.090	0.160	0.070	0.025	0.029
2.00	642	0.130	0.210	0.080	0.038	0.040
calc. (n=2)				0.064		

TABLE 7.3

Voltammetric Parameters of Peaks III and IV for H_2O (v.p. = 19.8 torr) in $ZnCl_2$; (a) Initial scan (b) Subsequent Scans

$\nu(Vs^{-1})$	T (K)	$Ep^{V}(V)$	$Ep^{VI}(V)$	$\Delta Ep(V)$	$i_p{}^{V}$ (mA)	$i_p{}^{VI}$ (mA)
0.05	623	0.330	0.410	0.080	0.003	0.011
0.10	623	0.335	0.405	0.070	0.007	0.022
0.20	623	0.340	0.405	0.065	0.016	0.028
0.50	623	0.320	0.408	0.088	0.041	0.057
calc.	(n=1)			0.123		
	(n=2)			0.064		
0.05	642	0.330	0.400	0.070	0.004	0.003
0.10	642	0.330	0.390	0.060	0.005	0.005
0.20	642	0.340	0.420	0.080	0.007	0.011
0.50	642	0.375	0.400	0.065	0.012	0.020
1.00	642	0.380	0.450	0.070	0.018	0.035
2.00	642	0.445	0.510	0.065	0.030	0.060
calc.	(n=1)			0.123		
	(n=2)			0.064		

TABLE 7.4

Voltammetric Parameters of Peaks V and VI
for H_2O (v.p. = 19.8 torr) in $ZnCl_2$

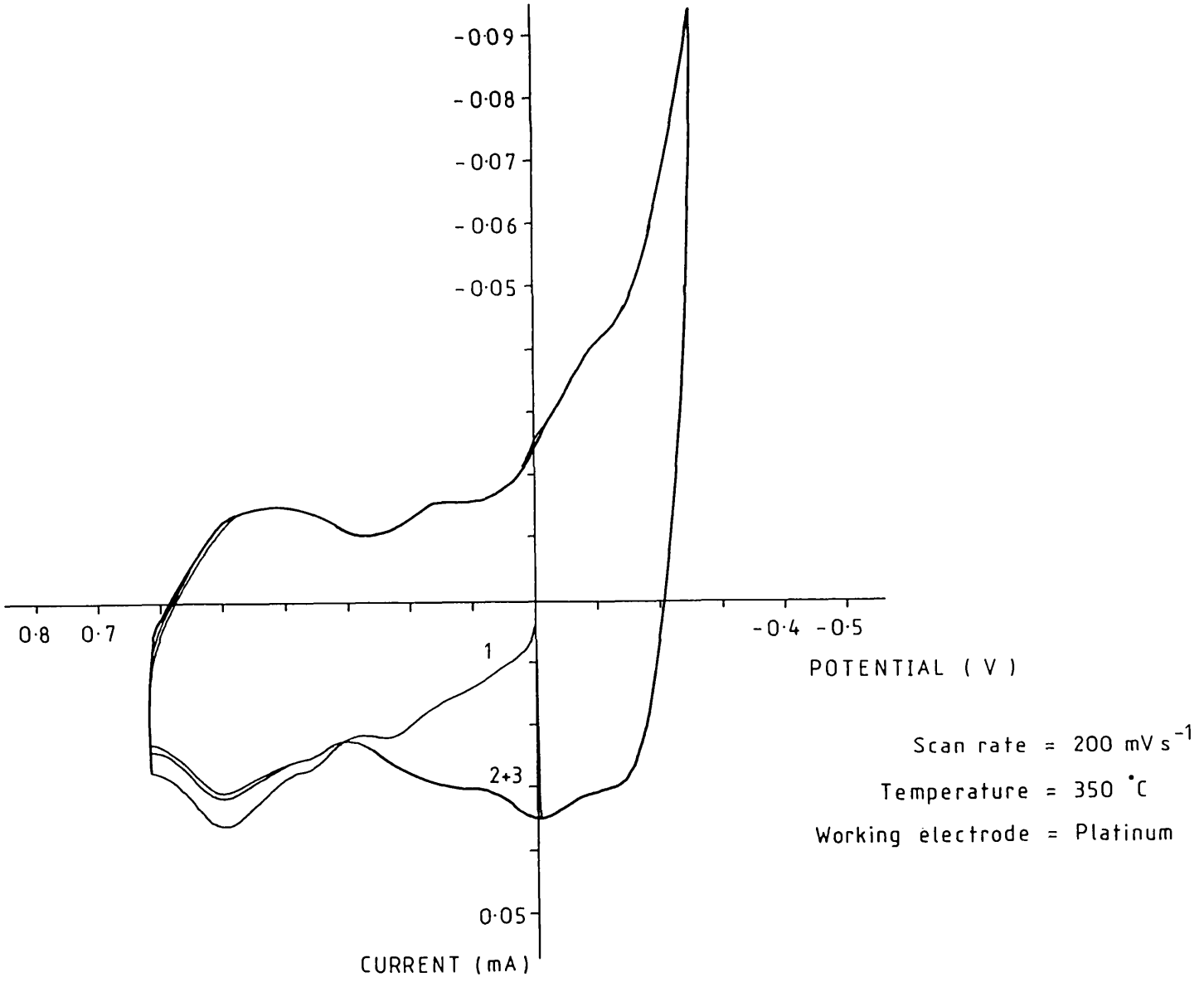


FIGURE 7.2: Voltammogram Showing the Effect of Three Successive Scans for Water in Molten Zinc Chloride

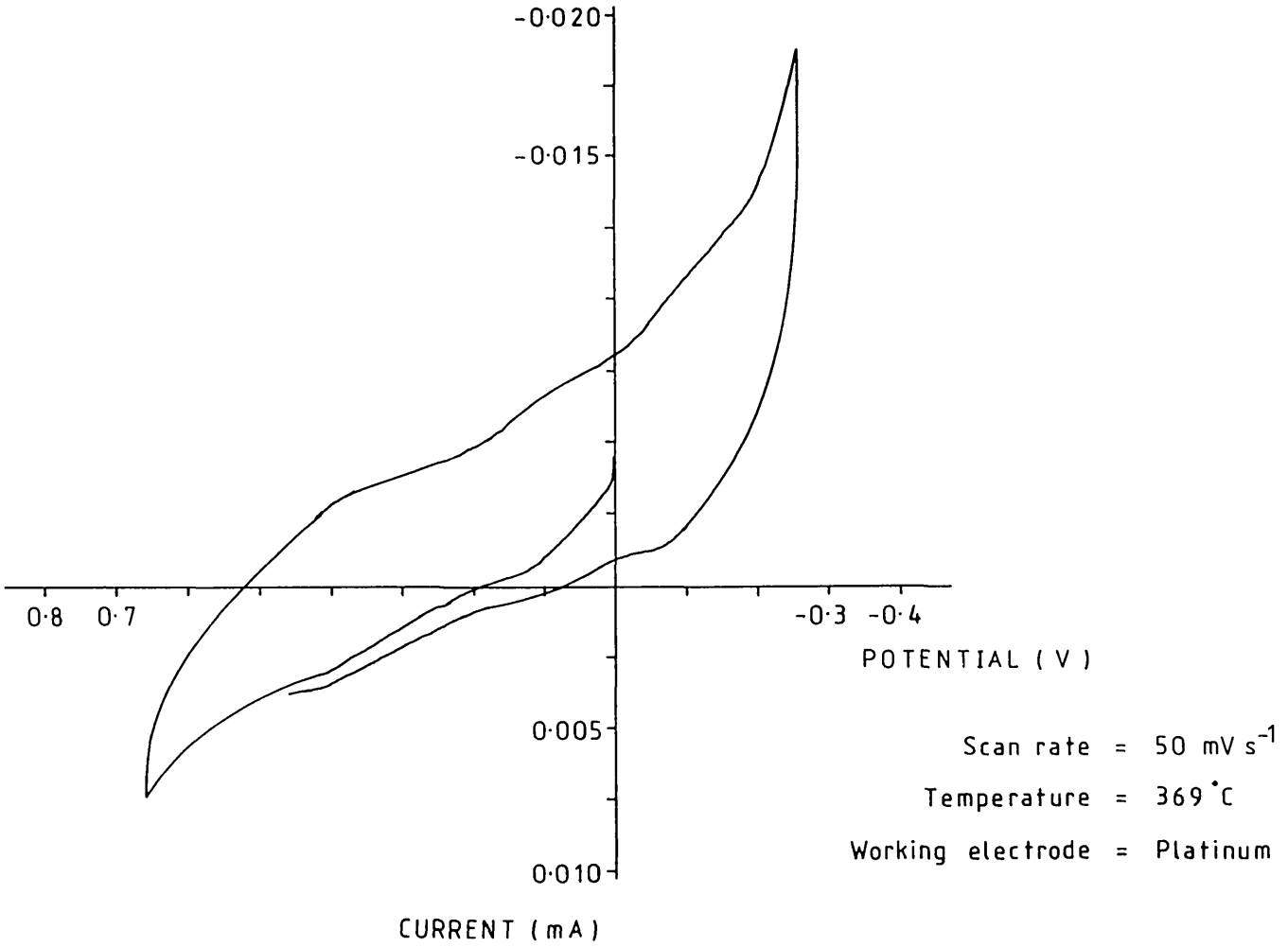


FIGURE 7.3

Voltammogram Recorded at a Low Scan Rate for Water in Molten Zinc Chloride

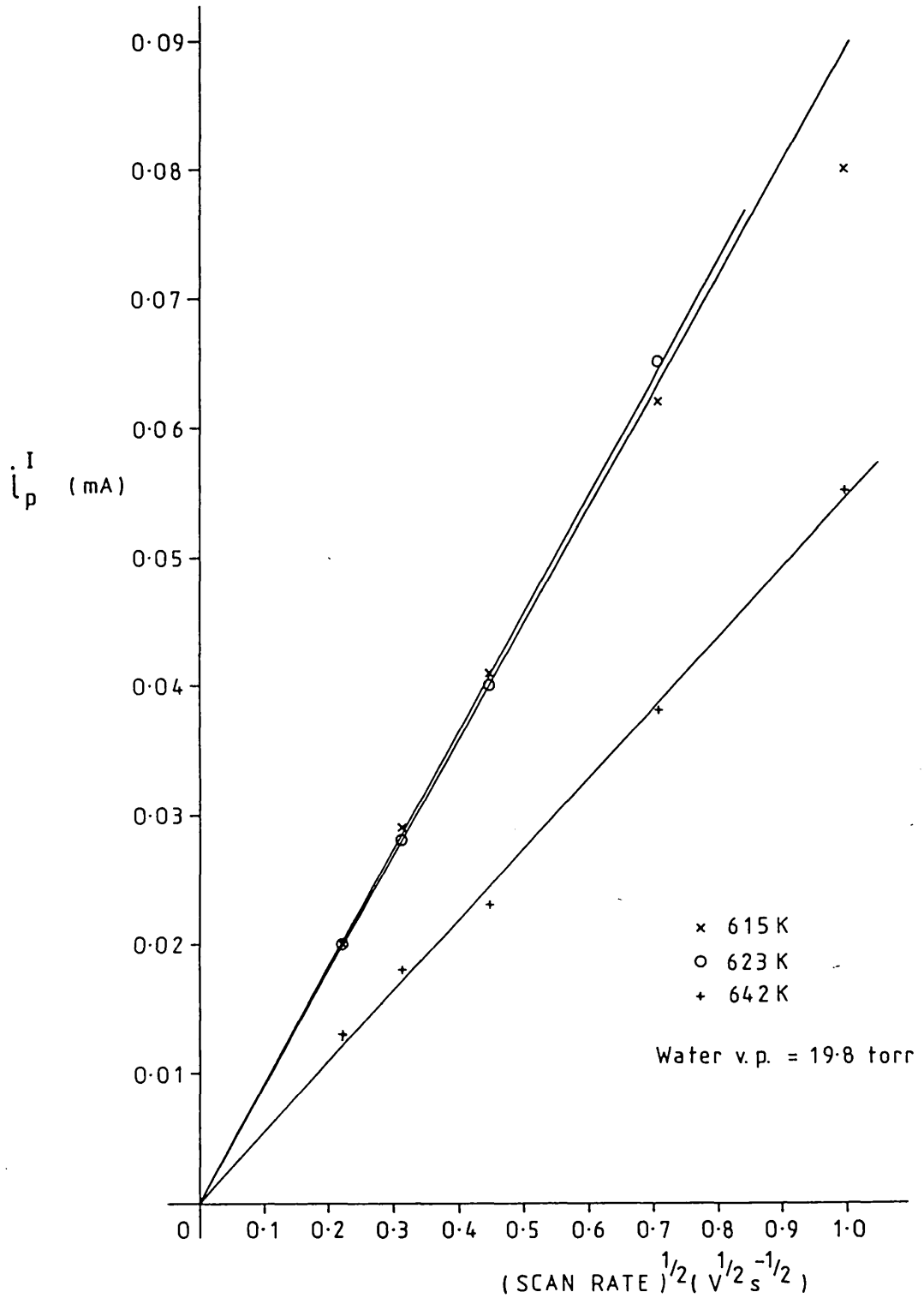


FIGURE 7.4

Variation of i_p^I with $\nu^{\frac{1}{2}}$ for Water in Zinc Chloride

was noticed on every occasion and did not appear to be a freak result. Plots of i_p vs. $\nu^{\frac{1}{2}}$ for peaks III and IV are shown in Figures 7.5(a) and (b), the graphs displaying data for initial and subsequent scans, respectively. The i_p^{III} values can be seen to be linear with respect to $\nu^{\frac{1}{2}}$ with the plot passing through the origin. However, although the values of i_p^{IV} provide linear plots with respect to $\nu^{\frac{1}{2}}$, in no instance did they pass through the origin. Even though the values of i_p^{IV} alter on subsequent scans, the plots do not come any closer to passing through the origin (Figure 7.5 (b)), indicating the lack of diffusion control of the electrochemical process.

Similar behaviour was seen for peaks V and VI. The ΔE_p values indicated that the peaks arose from a two-electron transfer process, and the independence of E_p^V and E_p^{VI} with scan rate demonstrated the reversibility of the process (Table 7.4). However, the variation of i_p with $\nu^{\frac{1}{2}}$ (Figure 7.6), although linear for both peaks, was only found to go through the origin for peak V. The peak currents of peak VI, like those of peak IV, deviated a long way from a path through the origin.

The fact that peak VII did not consistently appear on voltammograms made monitoring its behaviour very difficult. Visually, it appeared between peaks IV and VI as a slight hump. However, the effect of holding the voltage sweep at the most cathodic end of the voltammogram can be seen in Figure 7.7 and this might provide an idea of the origin of peak VII. Holding the sweep for 30 seconds at the cathodic limit resulted in a large peak appearing on the return anodic sweep, at roughly the same potential as peak VII on the earlier voltammograms (Figure 7.1). The origin of this peak will be discussed during the discussion of the other peaks later in this section.

The effect of adding NaCl to the $ZnCl_2$ melts containing H_2O can be seen in Figure 7.8, which shows a voltammogram recorded from 80 mol. % $ZnCl_2$-NaCl with water vapour (12.35 torr) having been bubbled through the melt for several hours. On comparing this with Figure 7.1 the differences can be seen immediately. The reasonably well-defined peaks seen for water in pure $ZnCl_2$ have given way to a broad "envelope" for water in 80 mol.% $ZnCl_2$-NaCl, where only peaks I and II are clearly visible. Although

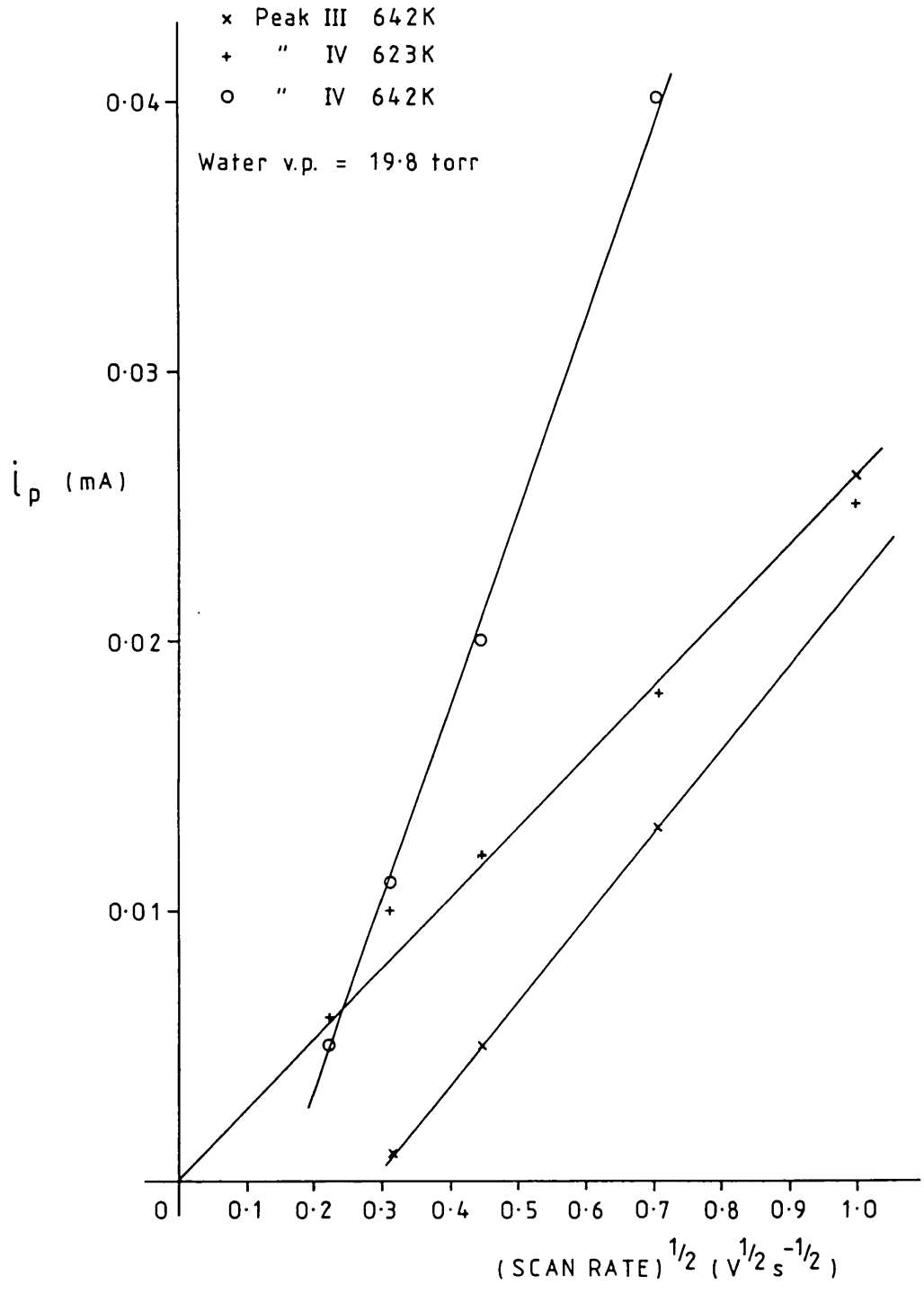


FIGURE 7.5 (a) Variation of i_p with $\nu^{\frac{1}{2}}$ for Peaks III and IV for Water in Zinc Chloride (Initial Scan)

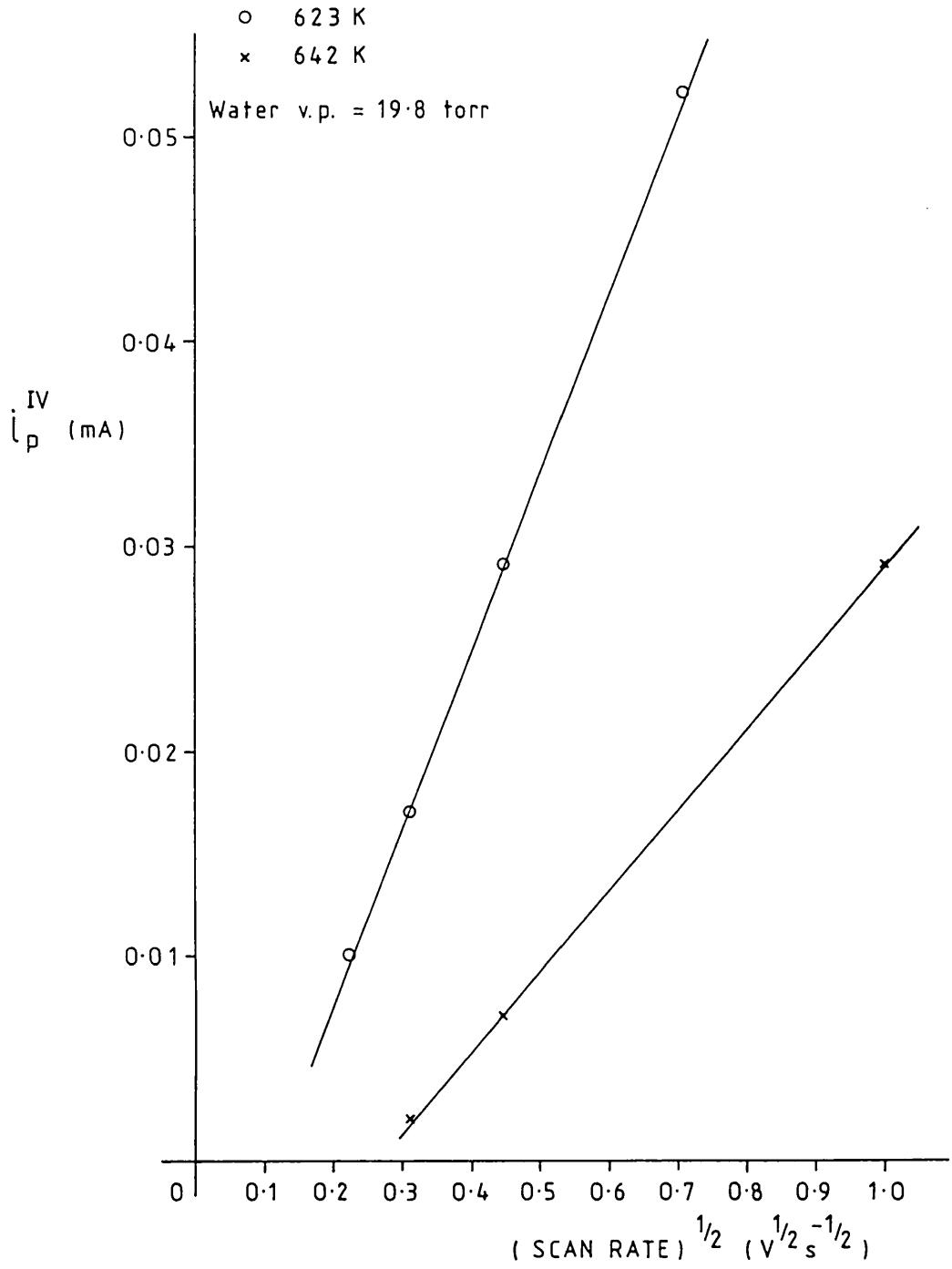


FIGURE 7.5 (b) Variation of i_p^{IV} with $\nu^{\frac{1}{2}}$ for Water in Zinc Chloride (Subsequent Scans)

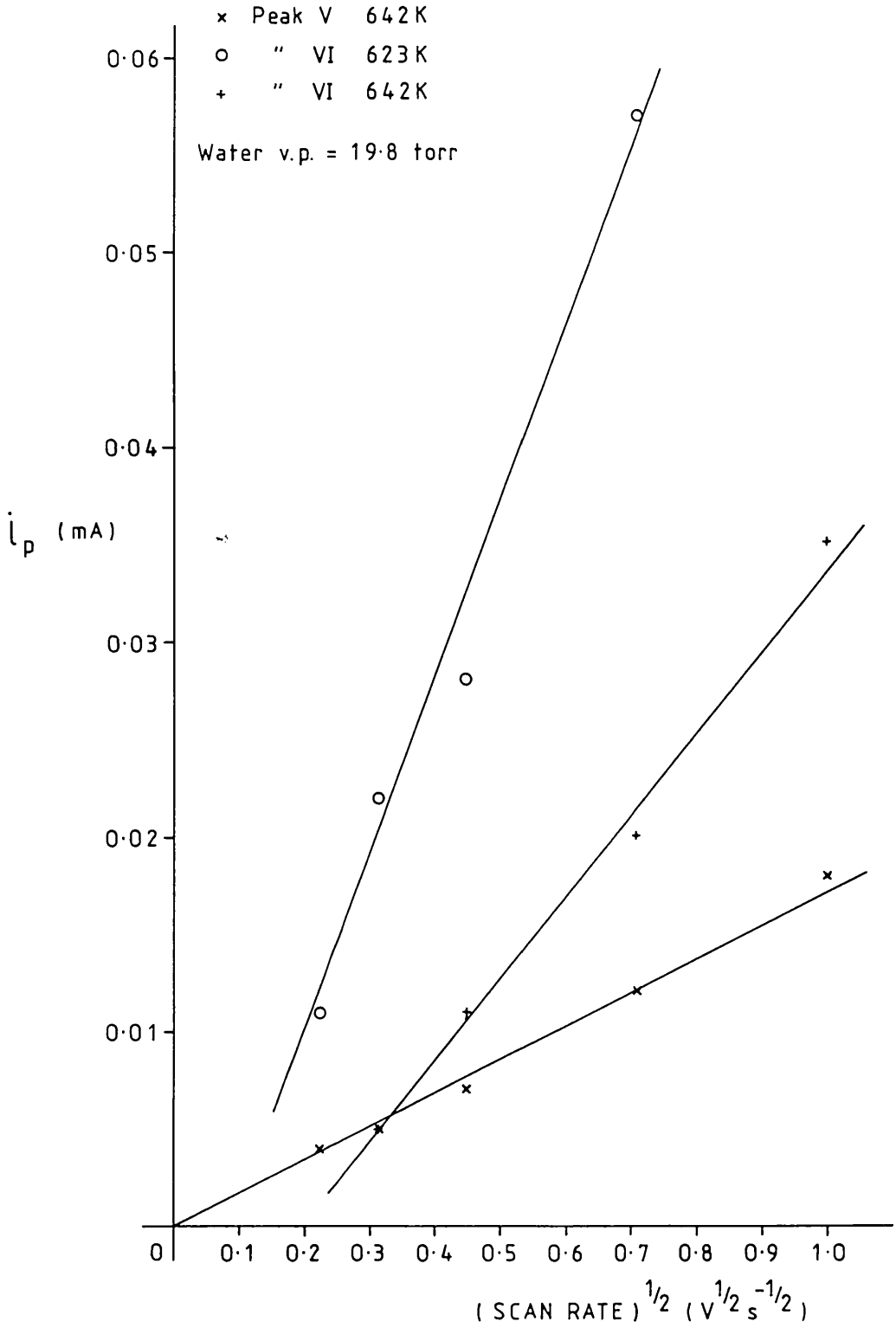


FIGURE 7.6

Variation of i_p With $\nu^{\frac{1}{2}}$ for Peaks V and VI for Water in Zinc Chloride

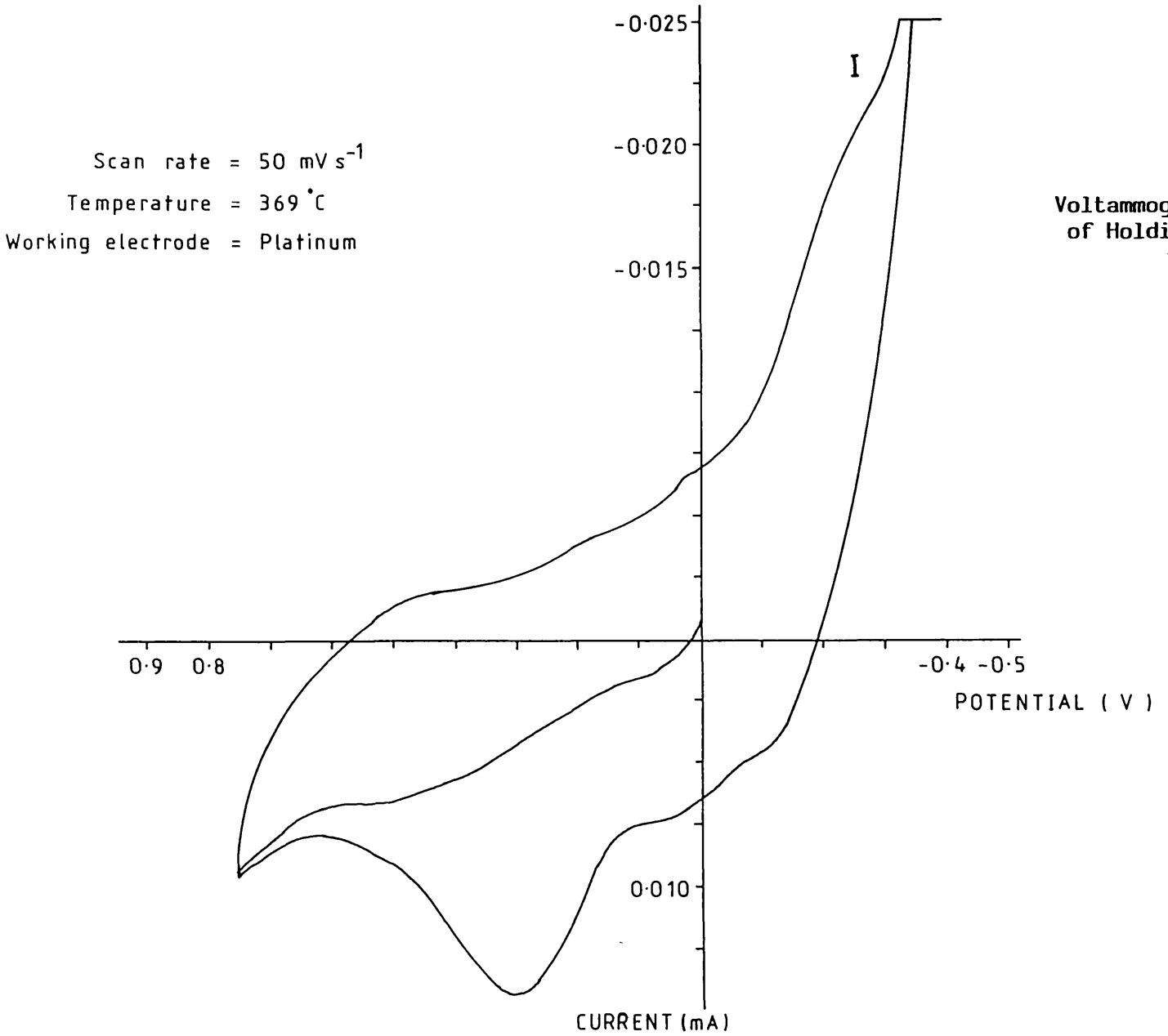


FIGURE 7.7

Voltammogram Showing the Effect of Holding the Scan at Peak I for 30 Seconds

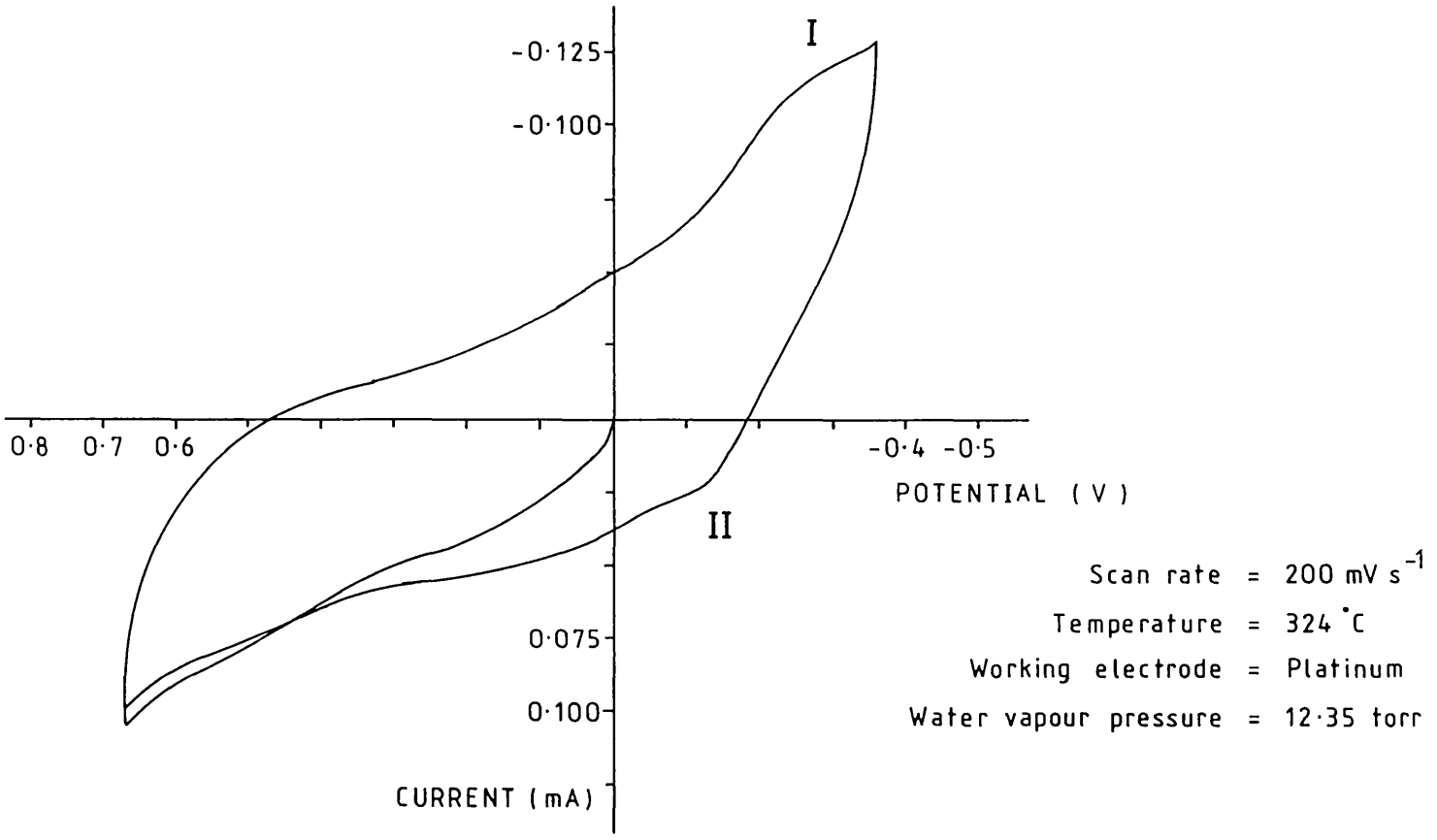


FIGURE 7.8

Voltammograms Obtained for Water in 80 mol. % $ZnCl_2$-NaCl

slight humps can be seen where peaks III-VI were expected to appear, it was almost impossible to attempt to measure the parameters of these peaks since on many of the voltammograms there was no sign of any response other than peaks I and II.

Tables 7.5-7.8 give the voltammetric parameters for peaks I and II measured for water at four different vapour pressures in 80 mol. % $ZnCl_2$-NaCl at various temperatures. The values of ΔE_p for all melt temperatures and water vapour pressures indicated that the peaks were due to a one electron transfer process , as found for the same peaks in pure molten $ZnCl_2$. As the melt temperatures were raised for each water vapour pressure so peaks I and II became less distinguishable, and at higher temperatures became unnoticeable, especially when lower water vapour pressures were being used. For the system using 2.61 torr water vapour only a few measurements of peak I were possible at 324^{o}C. All i_p^I values were found to be linearly dependent on $\nu^{\frac{1}{2}}$, and as can be seen in Figure 7.9. the plots passed through the origin, again as seen for the pure molten $ZnCl_2$ (Figure 7.4). The effect of melt temperature on the peak currents was very inconsistent: in some cases i_p^I decreased with increase in temperature whereas in others it rose. In all aspects though the behaviour of peaks I and II in 80 mol. % $ZnCl_2$-NaCl mirrored that of the same peaks for water in molten $ZnCl_2$.

The dependence of the peak current, i_p^I, on the water vapour pressure is shown in Figure 7.10 for the 80 mol. % $ZnCl_2$-NaCl system at 324^{o}C, where it can be seen that a linear relationship exists between the two. The values were taken from voltammograms recorded at the low melt temperature of 324^{o}C since at higher temperatures peak I was sometimes not visible.

Voltammograms recorded in 50 mol. % $ZnCl_2$-NaCl that had been saturated with water vapour showed no voltammetric peaks other than the anodic and cathodic melt limits. The only difference between them and the voltammograms recorded for the pure melts (Chapter 4) was that the residual currents were slightly larger for the water-contaminated melts. Consequently, no voltammetric data is available for water in the equimolar melts.

$\nu(Vs^{-1})$	T (K)	$-Ep^{I}(V)$	$-Ep^{II}(V)$	$\Delta Ep(V)$	$i_p{}^{I}$ (mA)
0.02	599	0.335	0.190	0.145	0.054
0.05	599	0.320	0.210	0.110	0.073
0.10	599	0.345	0.215	0.130	0.092
0.20	599	0.350	0.200	0.150	0.125
0.50	599	0.335	0.185	0.150	0.191
1.00	599	0.650	0.490	0.160	0.296
calc.				0.119	
0.05	618	0.360	0.220	0.140	0.090
0.10	618	0.370	0.240	0.130	0.115
0.20	618	0.360	0.225	0.135	0.150
0.50	618	0.355	0.220	0.135	0.200
calc.				0.122	

TABLE 7.5

Voltammetric Parameters of Peaks I and II for H_2O (v.p. = 19.1 torr) in 80 mol. % $ZnCl_2$-NaCl

$\nu(Vs^{-1})$	T (K)	$-Ep^{I}(V)$	$-Ep^{II}(V)$	$\Delta Ep(V)$	$i_p{}^{I}$ (mA)	$i_p{}^{I}/i_p{}^{II}$
0.01	597	0.620	0.430	0.190	0.029	0.81
0.02	597	0.620	0.410	0.210	0.039	0.83
0.05	597	0.610	0.435	0.175	0.058	0.84
0.10	597	0.300	0.130	0.170	0.082	0.77
0.20	597	0.620	0.440	0.180	0.110	0.86
0.50	597	0.630	0.420	0.210	0.171	0.91
1.00	597	0.320	0.110	0.210	0.240	0.90
calc.				0.118		
0.02	616	0.550	--	--	0.035	
0.05	616	0.530	--	--	0.055	
0.10	616	0.530	--	--	0.078	
0.20	616	0.540	0.360	0.180	0.105	
0.50	616	0.510	0.380	0.130	0.160	
				0.122		
0.02	640	0.260	~0.070	~0.190	0.028	
0.05	640	0.230	~0.050	~0.180	0.042	
0.10	640	0.250	--	--	0.065	
0.20	640	0.260	~0.060	~0.200	0.091	
0.50	640	0.260	--	--	0.153	
				0.127		

TABLE 7.6

Voltammetric Parameters of Peaks I and II
for H_2O (v.p. = 12.35 torr) in 80 mol. % $ZnCl_2$-NaCl

ν (Vs^{-1})	T (K)	$-Ep^{I}$(V)	$-Ep^{II}$(V)	Δ Ep(V)	i_p^{I} (mA)
0.01	597	0.580	0.420	0.160	0.027
0.02	597	0.590	0.440	0.150	0.035
0.05	597	0.600	0.480	0.120	0.055
0.10	597	0.600	0.460	0.140	0.079
0.20	597	0.595	0.470	0.125	0.115
0.50	597	0.600	0.440	0.160	0.185
1.00	597	0.607	0.520	0.150	0.274
calc.				0.118	
0.02	618	0.550	0.420	0.130	0.046
0.05	618	0.565	0.425	0.140	0.068
0.10	618	0.570	0.420	0.150	0.096
0.20	618	0.560	0.410	0.150	0.140
0.50	618	0.545	0.400	0.145	0.231
calc.				0.122	

TABLE 7.7

Voltammetric Parameters of Peaks I and II for H_2O (v.p. = 7.84 torr) in 80 mol. % $ZnCl_2$-NaCl

$\nu(Vs^{-1})$	T (K)	$-Ep^{I}$ (V)	$i_p{}^{I}$ (mA)
0.05	598	0.530	0.052
0.10	598	0.540	0.071
0.20	598	0.535	0.103
0.50	598	0.540	0.161
1.00	598	0.550	0.240

TABLE 7.8

Voltammetric Parameters of Peak I
for H_2O (v.p. 2.61 torr) in
80 mol. % $ZnCl_2$-NaCl

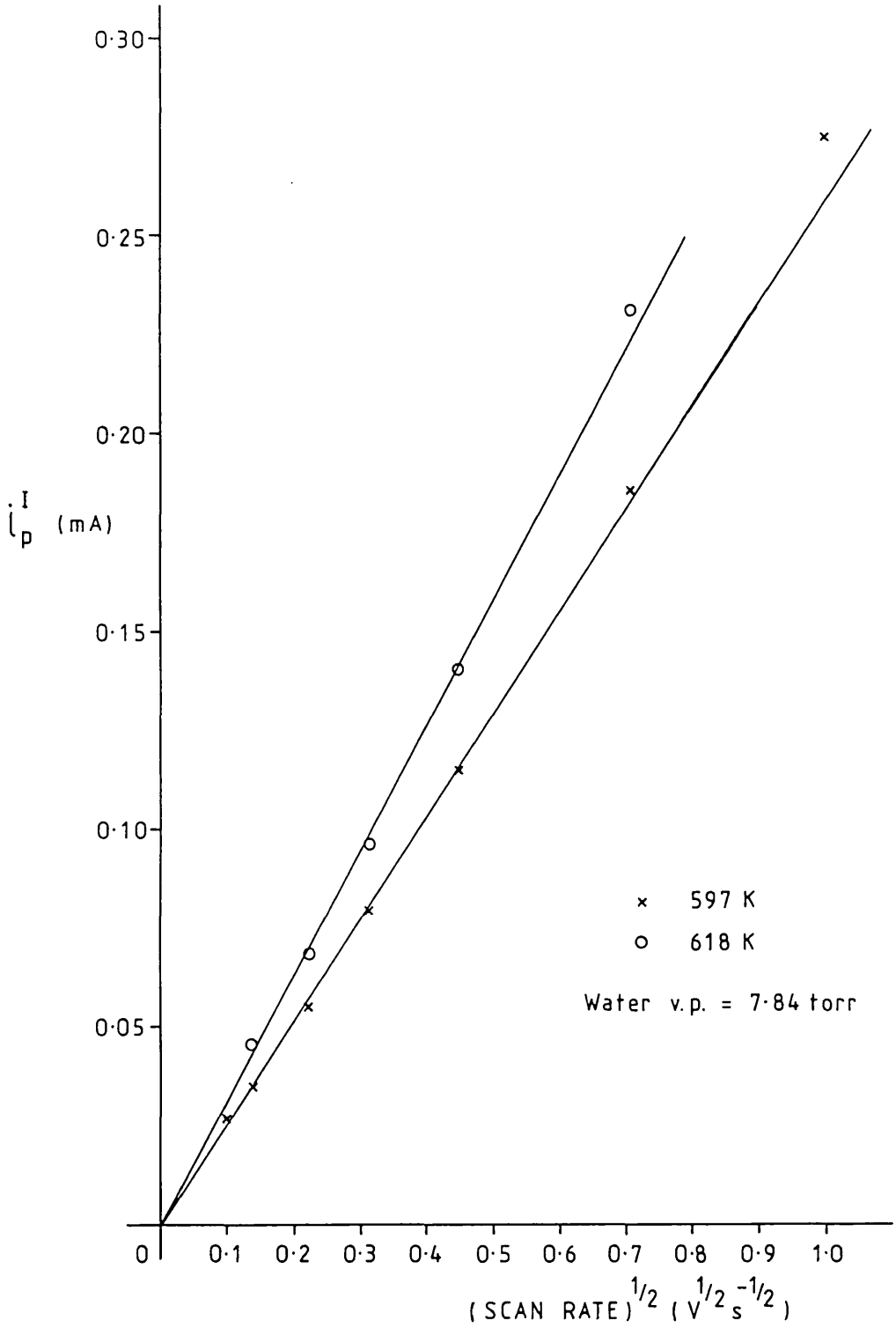


FIGURE 7.9

Variation of i_p^I with $\nu^{\frac{1}{2}}$ for Water in 80 mol. % $ZnCl_2$-NaCl

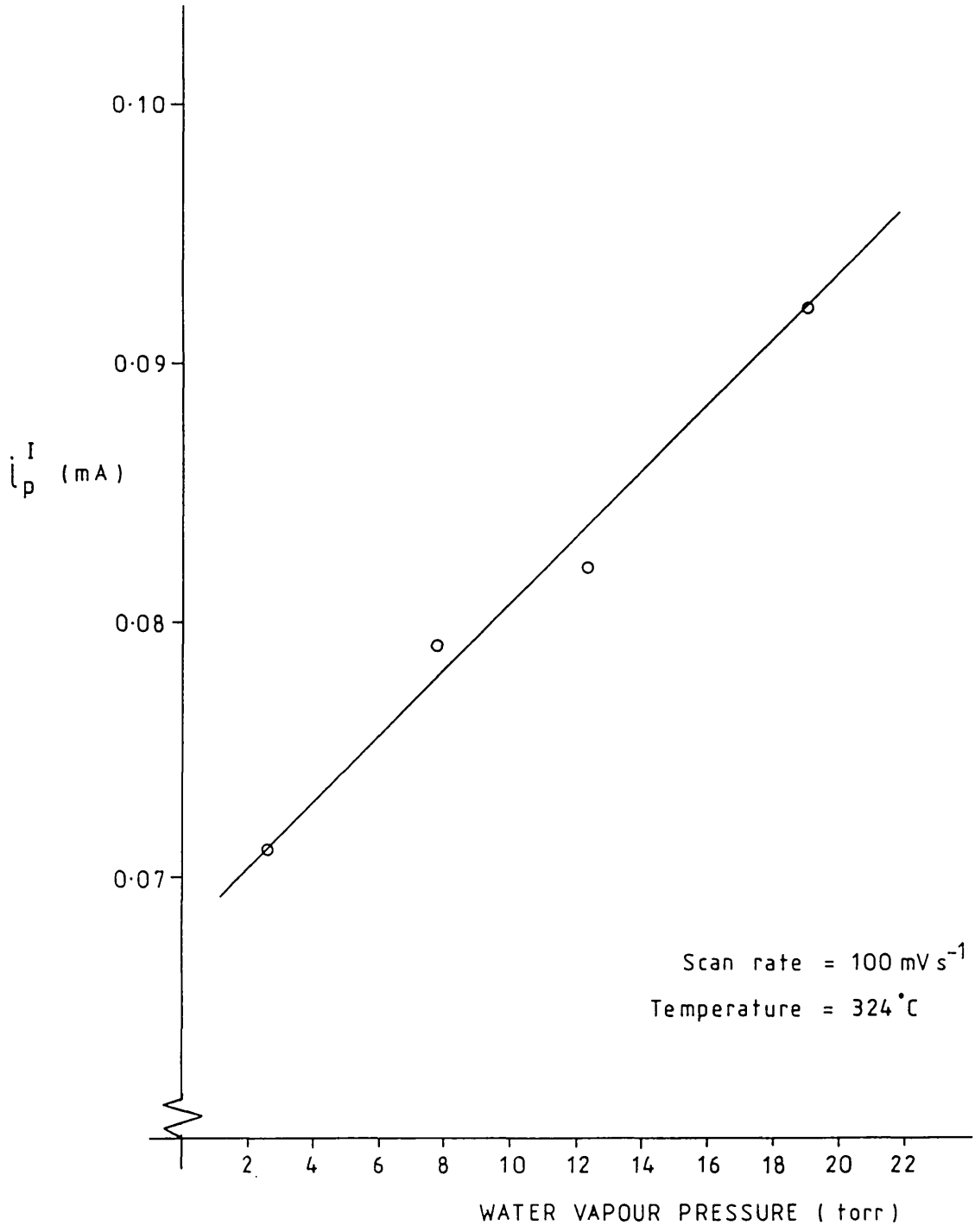


FIGURE 7.10

Variation of Peak I With Water Vapour Pressure for 80 mol. % $ZnCl_2$-NaCl

Having summarized the voltammetric results obtained during this work, the next stage is to try to assign those results to species or processes that may exist in the water-contaminated melts. Three electrode reactions have been intimated[82,88,92] to occur in chloride melts containing water, with [7.4] occurring at the most cathodic

$$OH^- + e^- = O^{2-} + \tfrac{1}{2}H_2 \qquad [7.4]$$

$$H_2O + e^- = OH^- + \tfrac{1}{2}H_2 \qquad [7.3]$$

$$O^{2-} - 2e^- = \tfrac{1}{2}O_2 \qquad [7.5]$$

potentials and [7.5] just prior to the chlorine evolution potential. This would match well with the results obtained here if the shift observed in peak IV had not occurred. In that case the six voltammetric peaks could have been easily assigned as the "hydroxide wave" (I, II); the "water wave" (III, IV) and the oxide/oxygen couple (V/VI). However, the change of peaks III/IV from a one-to a two-electron process after the initial scan could not be accounted for by such a simplistic explanation.

The existence of peroxide ions has been put forward to explain the behaviour of H_2O in $CaCl_2$-KCl melts[98]. Three pairs of voltammetric peaks were observed on gold electrodes, the most cathodic being designated the "hydroxide wave" [7.4] as previously, but the other two being ascribed to peroxy-species. In place of the "water wave" the process [7.6] was

$$O_2^{2-} + 2e^- = 2O^{2-} \qquad [7.6]$$

$$O_2 + 2e^- = O_2^{2-} \qquad [7.7]$$

claimed to occur, whilst the most anodic pair was said to be due to oxidation of the peroxy-species [7.7] rather than oxidation of oxide ions [7.5].

Three chemical equilibria were said to be dominant in the melt at

700°C, with all three ([7.1], [7.8], and [7.9]) being rapidly displaced to the right on introduction of water or oxy-species to the melt. The concept

$$2OH^- = O^{2-} + H_2O \qquad [7.1]$$

$$Cl^- + H_2O = HCl + OH^- \qquad [7.8]$$

$$O_2 + 2O^{2-} = 2O_2^{2-} \qquad [7.9]$$

of a peroxide/oxide conversion [7.6] would explain the two-electron process occurring on subsequent scans (Figure 7.2). During the initial scan it seemed something happened either on the electrode surface or in the melt that altered the process causing peak IV to arise. One possible mechanism is as follows. Oxygen could be produced at oxidation peak VI and then remain in the vicinity of the electrode to combine with oxide ions formed on the reduction step (V) or with oxide ions formed on the reduction of OH^- (I/II; [7.4]). In this way some peroxide ions could conceivably be formed ([7.9]) and perhaps affect peak IV. However, the direct oxidation of oxide ions could also form peroxide ions[98], as indicated in [7.6], the oxide ions having been produced by the reduction of OH^-. The width of peak IV on subsequent scans could then be explained as being caused by the proximity of the "water wave" oxidation process to the peroxide formation process [7.6] on the potential scale. However, peak III was found to be reproducible over any number of scans, which might not be expected to occur since its reverse response was varying.

The effect of holding the potential sweep at the cathodic limit (Figure 7.7) caused a large peak to appear on the reverse scan in the anodic direction. The most cathodic process (I,II) is believed to be reduction of OH^- to O^{2-} and H, as agreed by other workers[82,88,92,98]. In this case the presence of O^{2-} in the vicinity of the electrode could cause an oxide film to form on the surface, either of ZnO or perhaps a platinum oxide. If zinc were being deposited to some extent at the same time as the OH^- ions were being reduced then such a film could indeed form. Zinc oxide is very insoluble in these melts (Chapter 9) and might not be expected to dissolve into the melt. At times, after extended use, the surface of the platinum

disc electrode was tarnished by a film that could be scraped off but not washed off with distilled water. The decomposition of this film on the reverse sweep could cause the large peak observed. Thus the origin of the small peak VII (Figure 7.1) may have been uncovered: on the rapid continuous sweeps very little oxide film could form and peak VII would be small, as observed. Similar films have been said to form in $MgCl_2$-KCl melts under the same conditions[184]. These surface films may also be part of the cause of the inconsistent $i_p/\nu^{\frac{1}{2}}$ plots where in some cases the plots for higher melt temperatures lay below those for lower melt temperatures.

The addition of sodium chloride to the molten zinc chloride caused a marked change in the voltammograms recorded in the H_2O-saturated melts. From the reasonably well-defined peaks seen for water in molten $ZnCl_2$ (Figure 7.1) the presence of 20 mol. % NaCl resulted in fewer, very vague peaks (Figure 7.8) whilst for the equimolar melt the voltammograms exhibited no peaks other than the melt limits. Obviously the presence of NaCl was having an effect on the species being formed upon the dissolution of water in the melts, the voltammetric evidence inferring that fewer species were being formed since the peaks disappeared as more NaCl was added. From the results of the a.c. impedance study (Chapter 6) it was found that water lowered the melt resistance, and notions of hydroxychlorozinc species were put forward, the water thought to be causing a break-up of the polymeric $ZnCl_2$ structure. There the effect was most marked in the pure $ZnCl_2$ melt, just as the voltammetric peaks were most marked for the same melt. That the extent of hydrolysis was low was shown by the Raman spectra of H_2O in $ZnCl_2$ (Chapter 8) where no vibrations characteristic of OH^- groups were noticed.

Assuming that hydrolysis does occur to some extent then perhaps it is not surprising that the effect was most noticeable in pure molten $ZnCl_2$. In the $ZnCl_2$-NaCl melts, especially where $X_{NaCl} > 0.2$, much of the polymeric structure of the $ZnCl_2$ has been broken up to form $ZnCl_4^{2-}$ complexes, which are assumed to be quite stable. Any hydrolytic process would involve the replacement of Cl^- ligands with OH^-, which may not be a favourable reaction. In the pure molten $ZnCl_2$, especially at lower

temperatures, much of the liquid is thought to have a polymeric structure (Section 2.1) which would be more susceptible to break-up and formation of four-coordinate zinc species (e.g. $H^+[ZnCl_2OH]^-$, $[H^+]_2[ZnCl_2(OH)_2]^{2-}$). As discussed in Section 7.3, the presence of water in these melts did not result in precipitation as is seen in chloroaluminate melts, implying that the hydrolytic/water dissolution process reaches an equilibrium limit. From Figure 7.10 the height of peak I was seen to be dependent on water vapour pressure, so perhaps if more and more water could be pumped into the melts then eventually some precipitate might form. Peak I is believed to arise from the OH^- reduction process, showing that the water dissolution, and hence hydrolysis, increase with water vapour pressure.

In much the same way as a whole series of equilibria were postulated for the dissolution of HCl in these melts (Section 5.1), so an even larger series may be postulated for water, involving a range of complexes and species as well as possibly water dissolving as H_2O molecules without splitting to H^+ and OH^-. The last process may be occurring in the alkali chloride-rich melts where hydrolysis appeared to minimal.

In conclusion, the investigation of the behaviour of H_2O in $ZnCl_2$-NaCl melts has shown that hydrolytic reactions do occur in these melts. The extent of hydrolysis appears to be greatest in the pure $ZnCl_2$ melt, falling as NaCl is added until at equimolar melt compositions where the hydrolytic reaction appears to be virtually non-existent. Definite assignment of all the voltammetric responses was not possible, but suggestions have been made as to the origins of those that were not identifiable.

CHAPTER 8

SPECTROSCOPIC INVESTIGATION OF $ZnCl_2$ CONTAINING PROTONIC AND OXY-SPECIES

8.1 Introduction

The Raman spectra of zinc chloride in various states are well documented; molten $ZnCl_2(+MCl_x)$[21,23,24,26-28,122], glassy $ZnCl_2$[21,23,156-158], aqueous glassy $ZnCl_2$[159], crystalline $ZnCl_2$[160] and saturated aqueous solutions of $ZnCl_2$[25,161,162]. It was decided that Raman spectroscopy would be a suitable method for studying the behaviour of water and HCl in molten $ZnCl_2$. Unfortunately, no heated cell was available for work to be carried out with molten samples. By saturating the melt with solute, quenching the solution and grinding the solid to a powder, it was hoped that the solute would be trapped within the solid matrix. One advantage of Raman spectroscopy over infra-red, say, is that samples can be held in Pyrex tubes which may be sealed to prevent contamination by moisture, whereas absorption of infra-red by Pyrex masks the sample absorption and other sample-holding materials must be used. However, a penalty is paid in that Raman spectroscopy lacks the sensitivity of the infra-red technique.

8.2 Raman Spectrum of Pure $ZnCl_2$

In order to ascertain the purity of the starting material a Raman spectrum of purified $ZnCl_2$ was recorded, using the method outlined in Section 3.11. Since quenching of the melt, carried out by lifting the melt container out of the furnace whilst hot, would leave the sample as a lump of part crystalline, part vitreous material, the solid was ground for 20 minutes to devitrify the sample. The Raman spectrum of the resulting white powder is shown in Figure 8.1.

Two sharp peaks can be observed, at 86.5 cm^{-1} and 249 cm^{-1}, and a broad "wave" at around 470 cm^{-1}. Small shoulders can be seen on either side of the base of the peak at 249 cm^{-1}, centred around 230 cm^{-1}

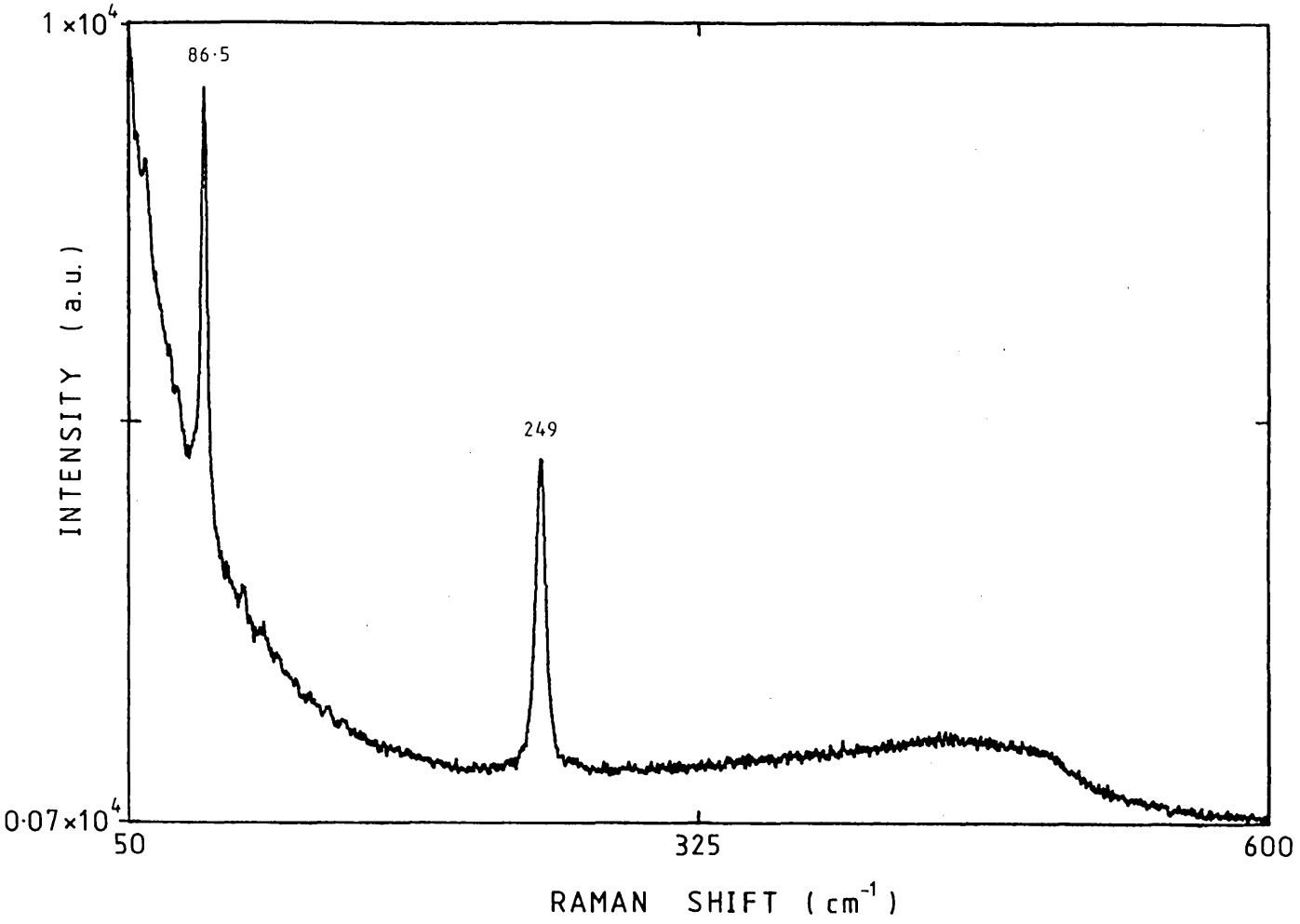


FIGURE 8.1: Raman Spectrum of Pure Zinc Chloride

and 265 cm^{-1}. The peak at 249 cm^{-1} may be assigned to the symmetric stretching mode of vibration (ν_1) of the $ZnCl_4$ tetrahedra in the crystal[160], a mode otherwise called the "breathing" mode. This mode of vibration is often used when a first approximation is required in comparing spectra since it is usually the most intense of the vibrational modes and is not infra-red active. The shoulder at 268 cm^{-1} has elsewhere[158] been attributed to the antisymmetric stretching mode ν_3, whilst the sharp peak at 86.5 cm^{-1} can be tentatively attributed[160] to the antisymmetric bending mode ν_4. The fourth Raman active mode of vibration, the symmetric bending mode (ν_2) could not be observed on these spectra and may well be masked by the rapidly rising spectrum intensity at lower Raman shifts, since other workers have identified it at lower Raman shifts than that of ν_4. The shoulder at 230 cm^{-1} may well be due to residual glass within the sample, which was not totally removed by the grinding of the quenched sample. The Raman shift is the same as that measured for vitreous $ZnCl_2$ samples by other workers[21,156] but since the shoulder is so small it was felt that 20 minutes vigorous grinding would be sufficient to remove any glassy $ZnCl_2$ from future samples.

Continuing the Raman scan on to 4000 cm^{-1} confirmed the absence of impurity water, since the characteristic peaks attributable to the vibrations of water molecules at around 3400 cm^{-1} were not observed. The broad wave centred around 470 cm^{-1} can be attributed to a vibration within the Pyrex tube[163] used as a sample holder, and was seen in all the spectra recorded.

8.3 Raman Spectrum of $ZnCl_2$ Containing HCl

Pure $ZnCl_2$ was saturated with HCl by bubbling the gas through the melt (~ 330°C) for 6 hours, and then air-quenching the solution. Vigorous grinding of the solid gave a white powder which was sealed into a 6mm Pyrex tube. The Raman spectrum recorded for the sample is shown in Figure 8.2.

It can immediately be seen that this spectrum has a much "noisier" baseline than that of the pure $ZnCl_2$, and this noise can be seen in

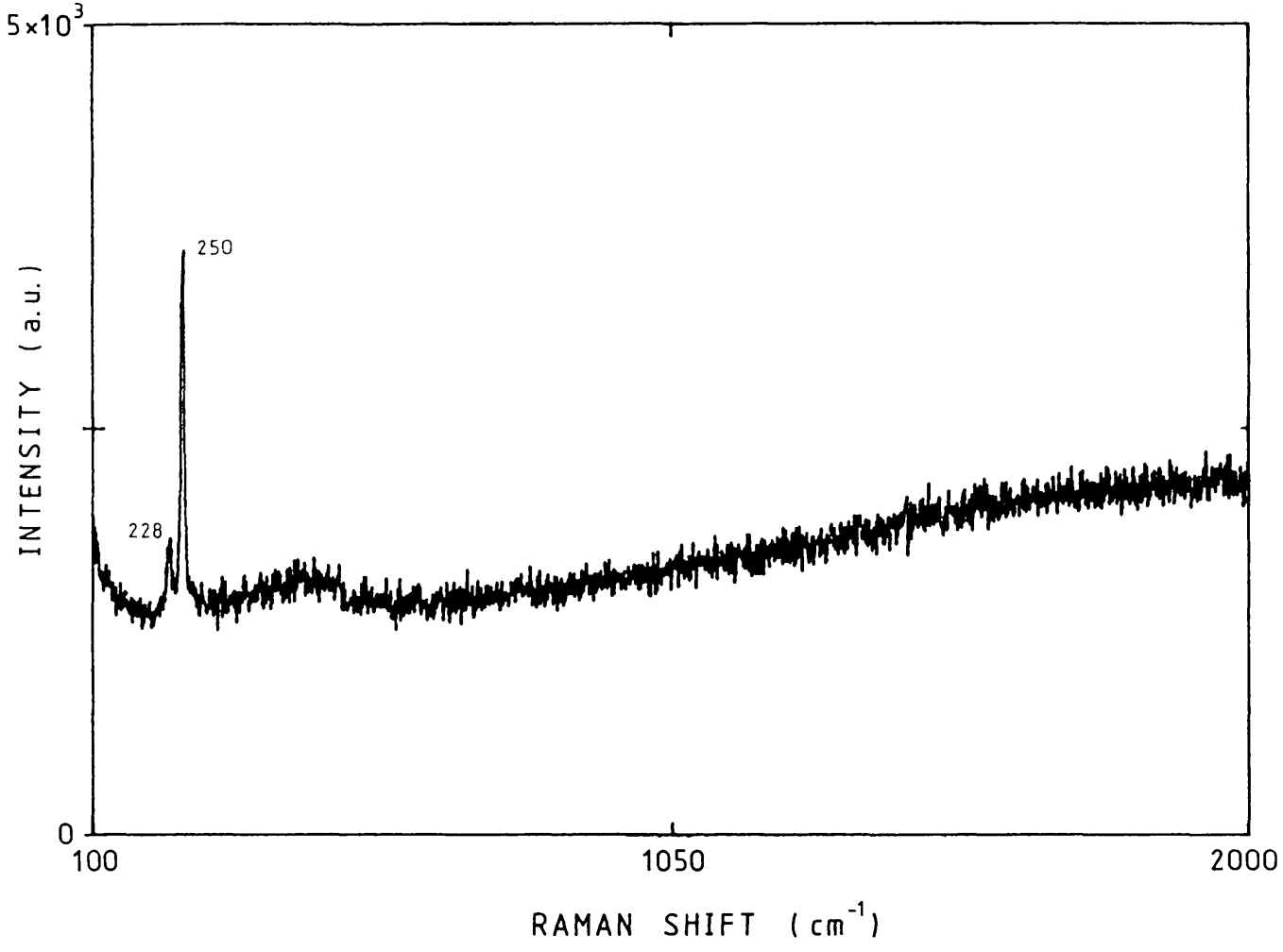


FIGURE 8.2: Raman Spectrum of $ZnCl_2$ Containing HCl

some of the other spectra. It is thought to have been caused by having too much sample in the path of the laser causing excessive dispersion of the radiation. As a result of this noise only two sharp, discernable peaks could be seen on the spectrum between the range 100-4000 cm^{-1}, and the broad wave caused by Pyrex appears at around 460 cm^{-1}. The largest peak, at 250 cm^{-1}, is assigned to the ν_1 symmetric stretching mode of vibration; the same as that seen for pure $ZnCl_2$ at 249 cm^{-1}. The smaller peak at 228 cm^{-1} can be attributed to residual glass in the ground powder. Since the solid material had been ground for as long as the pure $ZnCl_2$, it would appear that the vitreous phase is stabilized by the presence of HCl in the matrix, since the intensity of the 228 cm^{-1} peak is greater than that of the 230 cm^{-1} shoulder seen for pure $ZnCl_2$. A small shoulder at around 265 cm^{-1} is just discernable which as before can be attributed to the antisymmetric stretching mode, ν_3.

The mechanism by which HCl might stabilise the vitreous $ZnCl_2$ phase could be as follows. Upon devitrification the disordered glassy solid is rearranged to form a regular ordered crystal structure. If an impurity is present within the glass then presumably it would need to be removed before recrystallization could be completed or incorporated into the crystal structure, and if that impurity were chemically bound to the substrate material, as HCl is thought to bind to $ZnCl_2$, then more energy would be required to effect crystallisation.

8.4 Raman Spectrum of $ZnCl_2$ Containing H_2O

Pure molten $ZnCl_2$ (~ 340^{o}C) was saturated with water vapour by the passage of moist argon for 6 hours, then air-quenched and vigorously ground for 20 minutes. The Raman spectrum of the resulting white powder is shown in Figure 8.3. Only two sharp peaks are discernable, at 225 cm^{-1} and 248 cm^{-1}, as well as the wave due to the Pyrex tube at 470 cm^{-1}. No other peaks were observed within the range 100-4000 cm^{-1}. Rather surprisingly, no peaks due to the vibrations of water molecules could be seen in the region 3400-3600 cm^{-1},

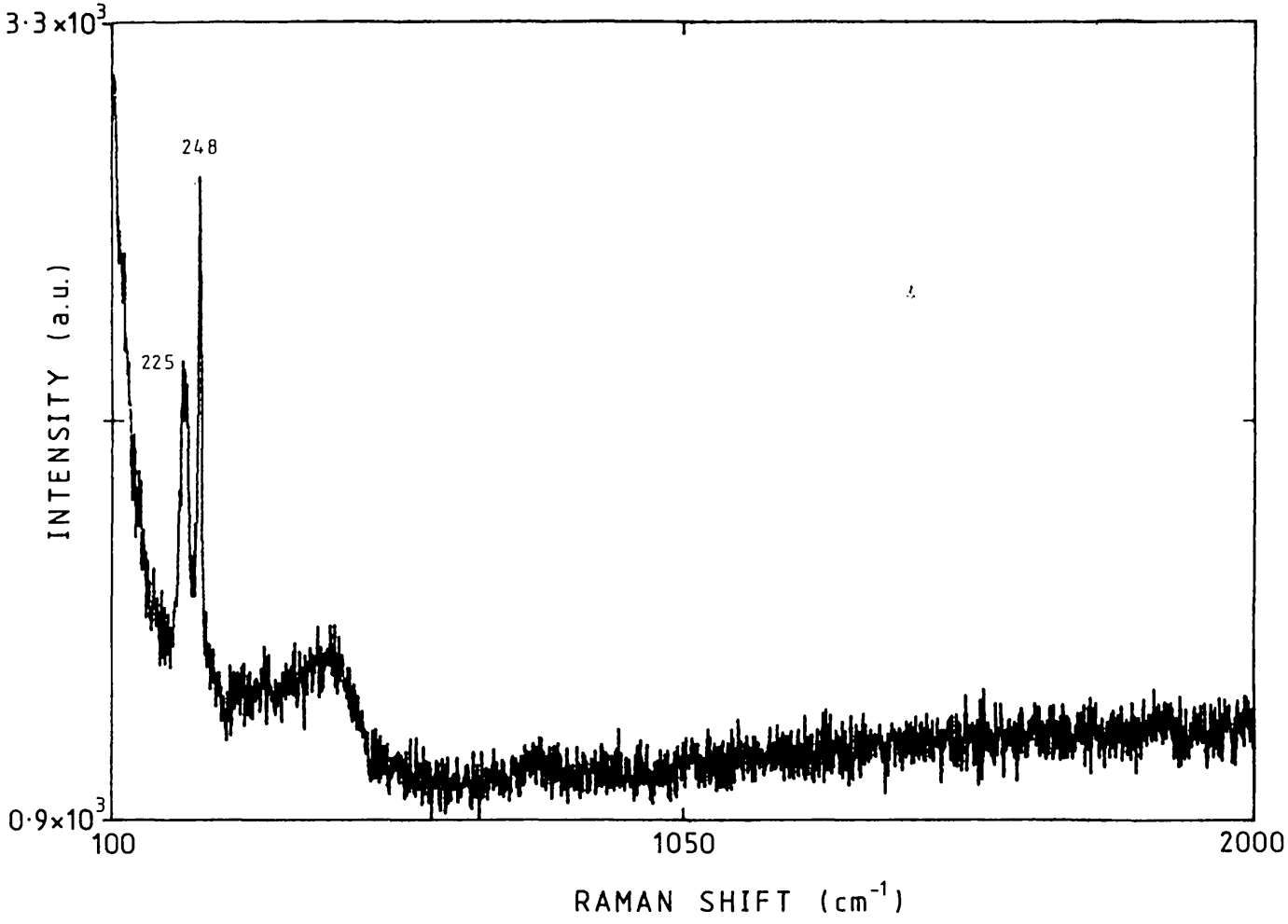


FIGURE 8.3: Raman Spectrum of $ZnCl_2$ Containing H_2O
20 Minutes Grinding

indicating that if water were present within the matrix it was in quantities too small for detection by Raman spectroscopy. However, Raman spectroscopy is a rather poor detector of water[163], especially impurity water. Water of crystallization will be detected but that present in ppm levels will not be. Infra-red spectroscopy has been found to be much more sensitive to the presence of moisture within the sample[163,164].

The peak at 248 cm^{-1} can be assigned to the ν_1 symmetric stretching mode of vibration of crystalline $ZnCl_2$, while that at 225 cm^{-1} is the same mode seen in the glassy form. The behaviour is analogous to that caused by the presence of HCl in $ZnCl_2$. By comparing the peak intensities it can be seen that the glassy form containing H_2O is even more durable than that containing HCl; even after 20 minutes grinding the devitrification process is a long way from completion. Figure 8.4 shows the Raman spectrum of the same sample after only 5 minutes grinding - the peak at 248 cm^{-1} is barely discernible whilst that at 227 cm^{-1} is very prominent. This stabilization of $ZnCl_2$ glass by water has been noticed by other workers[9,151,159]. The mechanism by which this stabilization is occurring can be thought of as being the same as that put forward to explain the stabilization by HCl (Section 8.3), but the extent of any hydrolytic reactions cannot be estimated since no other peaks are discernible. That the peak at 227 cm^{-1} is a result of formation of some oxy- or hydroxy-chloride species seems unlikely since the same peak occurred with the HCl-containing powder.

8.5 Raman Spectrum of Ar/H_2O Bubbler Deposit

It was noticed that as moist argon was bubbled through $ZnCl_2$(+NaCl) melts a yellow deposit formed on the inside wall of the Pyrex bubbler. The Raman spectrum of the deposit whilst still in the bubbler is shown in Figure 8.5. Peak assignments that could be made on the basis of other published work dealing with Raman spectroscopic studies of aqueous zinc chloride solutions are listed in Table 8.1. It was not possible to assign all the peaks, but most of them were due

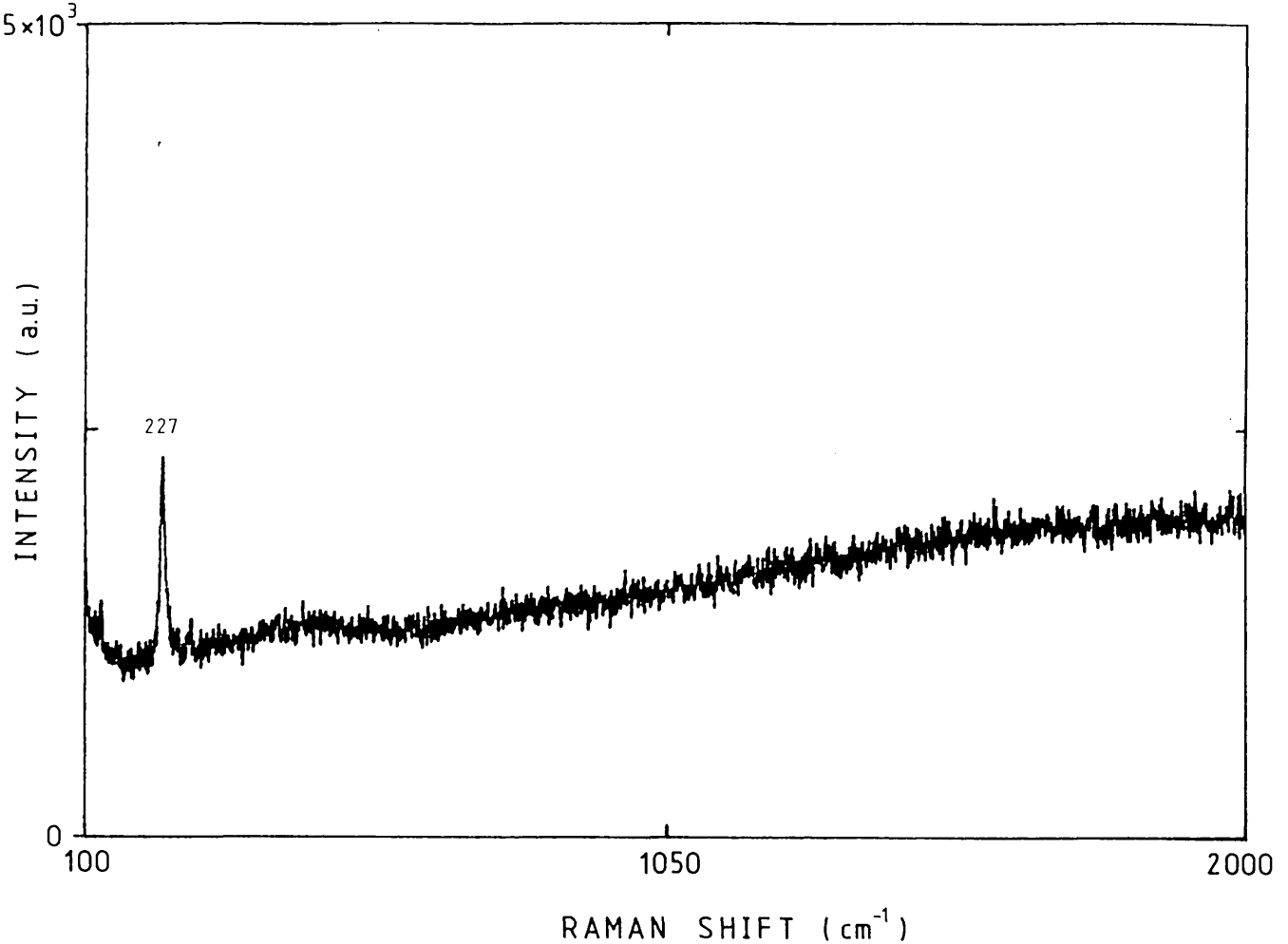


FIGURE 8.4: Raman Spectrum of $ZnCl_2$ Containing H_2O
5 Minutes Grinding

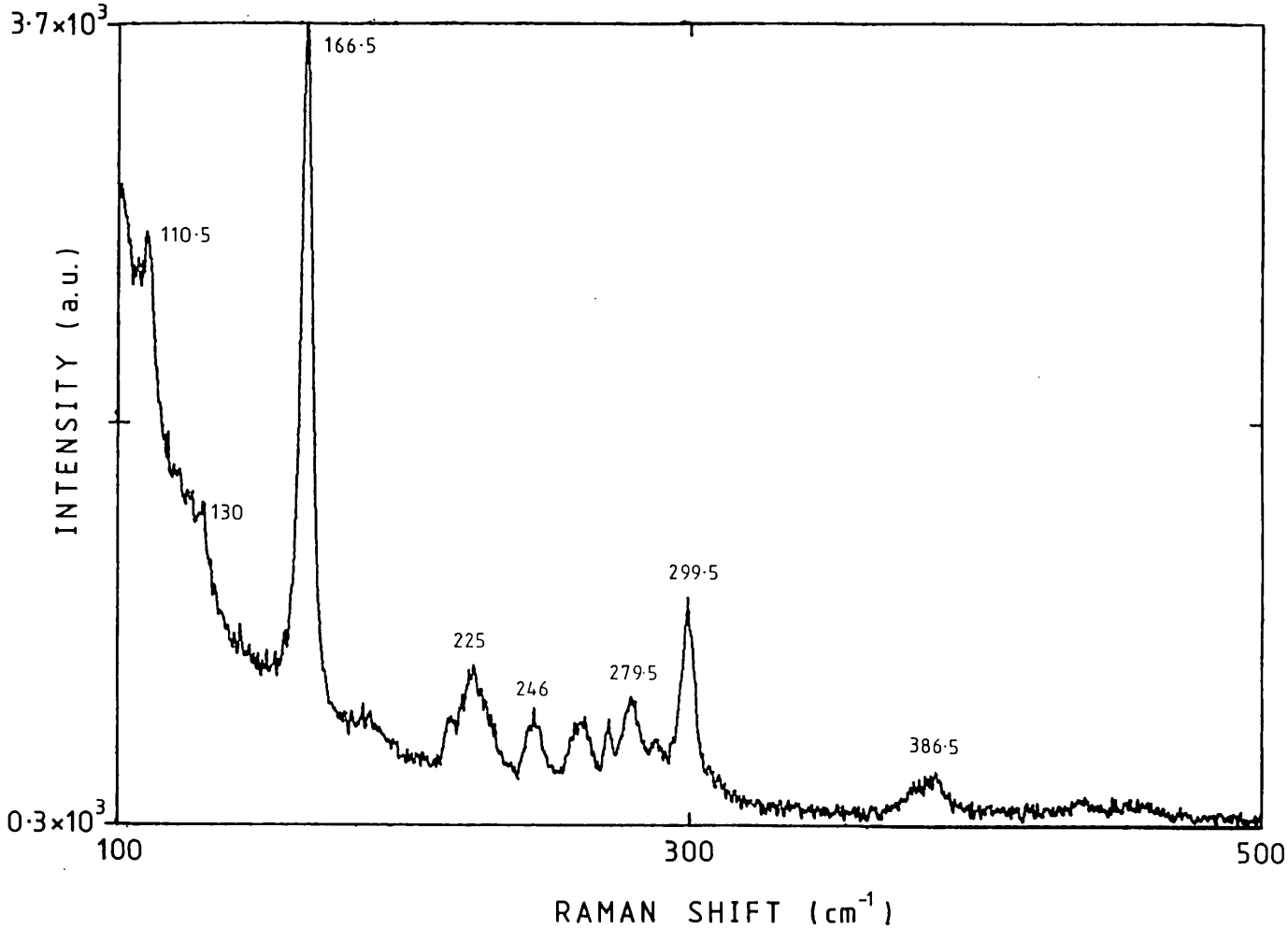


FIGURE 8.5: Raman Spectrum of the Ar/H_2O Bubbler Deposit

(continued...)

(Continuation...)

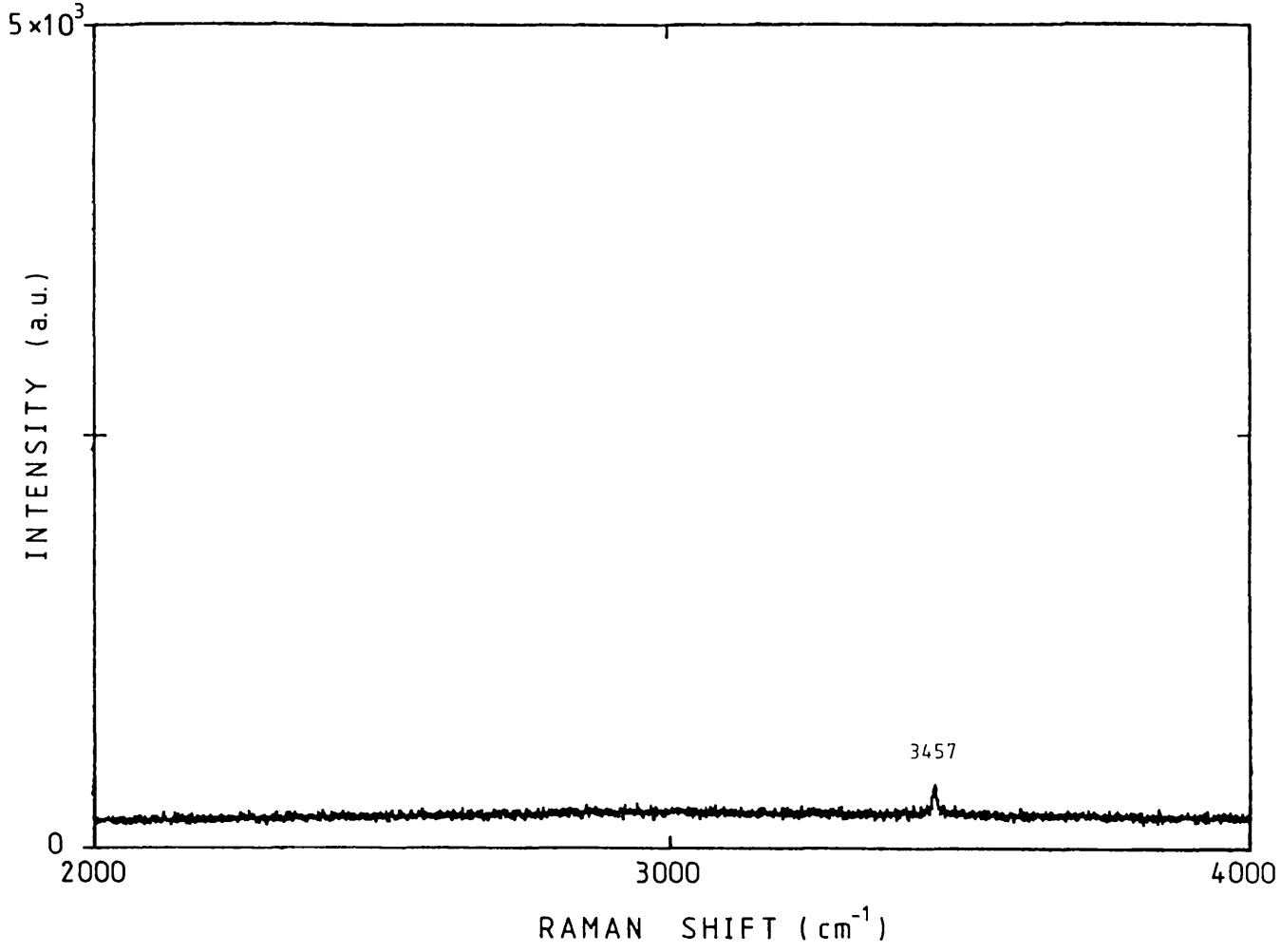


FIGURE 8.5: Raman Spectrum of the Ar/H_2O Bubbler Deposit

Raman shift (cm^{-1})	Description /	Assignment	Reference
101		ZnO	166
110.5	sharp	$ZnCl_4(H_2O)_2^{2-}(\nu_2)$	25
130	shoulder		
166.5	v.strong, sharp	Water structure (?)	25
186.5	broad		
212	shoulder	ZnO	165
225			
246		$ZnCl_2$ (ν_1)	
263.5			
272			
279.5		$ZnCl_4(H_2O)_2^{2-}(\nu_1)$	25
289			
299.5	sharp	$Zn(OH)_4^{2-}$	164
386.5	broad	$Zn(H_2O)_6^{2+}(\nu_1)$	25,159
3457	small	H_2O, OH^-	

TABLE 8.1

Peak Assignments for the Raman Spectrum of the Deposit formed in the Ar/H_2O Bubbler

to the formation of various aquo-, hydroxy-, and oxy- species on the inside of the bubbler.

The yellow colour, found to become more intense as the melt temperature was increased, is thought to be due to the formation of non-stoichiometric zinc oxide. Since it was being formed in a virtually oxygen-free atmosphere at high temperatures this seems to be a reasonable explanation. The colour was found to persist even as the cell was cooled to room temperature, and if the bubbler was held in the open air the yellow colour would often remain for at least 30 minutes. In due course the yellow would fade to white. In an argon dry-box the colour would persist for days. Not enough solid could be produced to carry out a powder X-ray diffraction investigation.

The small peak at 3457 cm^{-1} can be assigned to H_2O/OH^- group vibrations. Considering the number of water molecules and hydroxyl groups incorporated into the various products it is surprising how small this peak is, confirming the lack of sensitivity of Raman spectroscopy for detecting moisture. Galeener et al.[156] used Raman to confirm the purity of their $ZnCl_2$ glasses, but these results demonstrate the unsuitability of the method.

8.6 Raman Spectrum of $ZnCl_2$ Containing O_2

It was noticed that the passage of O_2 gas through pure molten $ZnCl_2$ and molten $ZnCl_2$-NaCl mixtures resulted in an amber colouration of the melt. Prolonged bubbling, for many hours, resulted in the bright amber colour slowly becoming duller, this occurring more rapidly in NaCl-rich melts. Oxygen was bubbled through molten $ZnCl_2$ ($\sim 360^oC$) for 4 hours, after which the melt was air-quenched and the sample ground for 20 minutes. Although the lump of quenched $ZnCl_2$ had an orange tinge to it the powder looked white. The Raman spectrum is shown in Figure 8.6.

The $ZnCl_2$ glass peak at 227 cm^{-1} is the prominent peak, with the characteristic crystal peak at 249 cm^{-1} barely visible in the

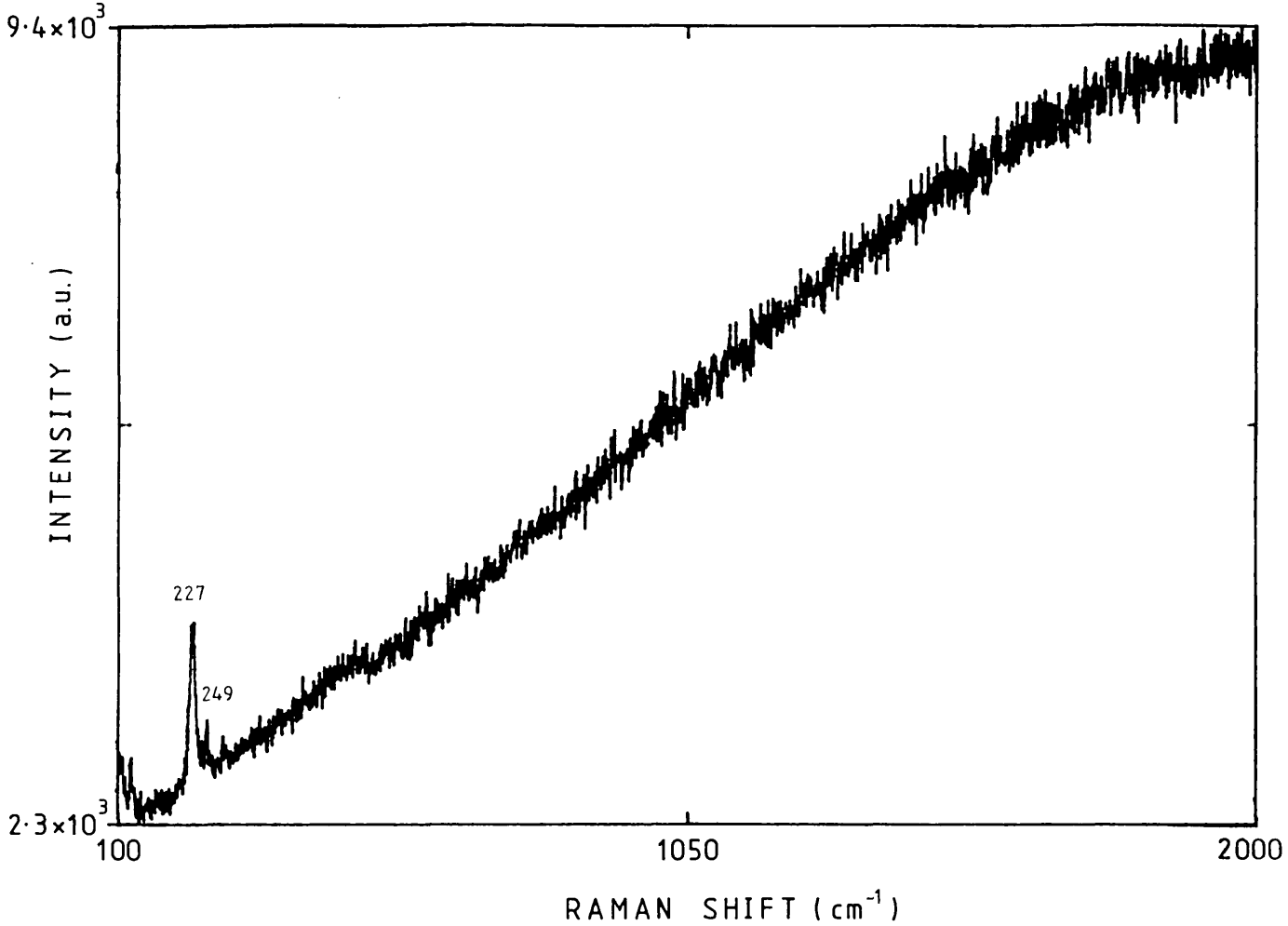


FIGURE 8.6: Raman Spectrum of $ZnCl_2$ Containing O_2

(Continued...)

(Continuation...)

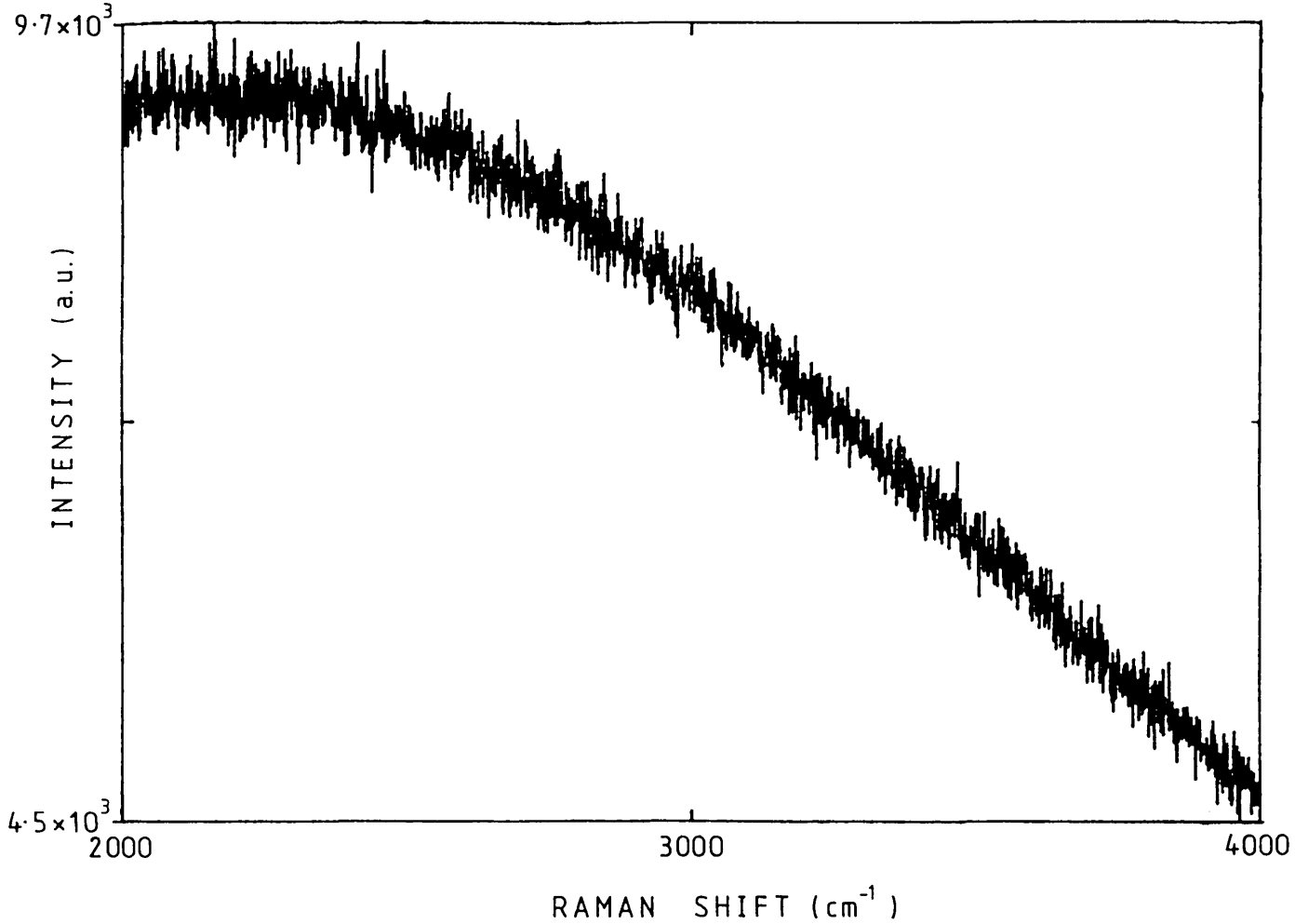


FIGURE 8.6: Raman Spectrum of $ZnCl_2$ Containing O_2

background noise. Comparison of this spectrum with that of $ZnCl_2/H_2O$ after 20 minutes grinding (Figure 8.3) shows that O_2 has stabilised the vitreous $ZnCl_2$ phase to an even greater extent than H_2O. It had been thought that a possible oxychloro-species might show up on the Raman spectrum, but if such a species was present its Raman peaks could not be observed.

Most noticeable is the massive hump starting at 100 cm^{-1} and stretching all the way to 4000 cm^{-1}. This was a result of the sample undergoing a fluorescence process caused by the presence of impurities in the sample. Since the same batch of $ZnCl_2$ was used to provide each sample and no fluorescence had been observed in those other samples, it was assumed that the dissolved O_2 had caused the fluorescence. In fluorescence, radiation must be absorbed by the molecule and an excited electronic state formed. In Raman spectroscopy energy is transferred from radiation to molecule, or vice versa, but no excited electronic state is formed, only changes in the rotational or vibrational levels. The top of the hump occurs in the orange region of the spectrum, as might have been expected since the melt had been an amber colour.

Several suggestions as to the species responsible for the fluorescence included iron impurities[150], peroxide or superoxide ions[152], oxychlorides or some organic contaminant. The iron impurity was virtually ruled out since it would have been present in other samples where no fluorescence was observed, nor was it observed during the voltammetric experiments. Unlike acetylene, where acetone is used to increase the amount of gas in the cylinder, no organic is used for the same purpose in oxygen-containing cylinders[167]. Besides, the gas was passed through drying columns (molecular sieves and activated charcoal) which should have removed organics along with moisture. Addition of sodium peroxide to $ZnCl_2$-NaCl melts did not produce the orange colour (Chapter 9). However, alkali metal superoxides, MO_2, are orange in colour and a process could be occurring whereby O_2 molecules abstract electrons from Cl^- in the melt to form O_2^- species, so conferring the orange colour on the

melt, If O_2^- species were indeed formed then, being free radical species, their single electron should show up on an electron spin resonance spectrum of the same material.

8.7 Electron Spin Resonance Spectrum of $ZnCl_2$ Containing O_2

The e.s.r. spectrum of the O_2-containing sample is shown in Figure 8.7. The spectrum obtained with the empty tube is also shown. It can be seen that all but one of the peaks and troughs are in both spectra showing that they are background noise due to the glass tube. One extra, sharp signal could be seen upon introduction of the sample, showing the presence of an unpaired electron- containing species within the sample. Using equation [8.1] where h is the Planck constant, ν is the frequency, g is the Lande splitting factor, β is the Bohr magneton and B is the applied magnetic field, the g-value may be calculated. Resonance was observed at 9.487 GHz in a field of 3375 Gauss

$$h\nu = g \beta B \qquad [8.1]$$

(0.3375 Tesla), and from this the value of g was found to be 2.008. Since different spectrometers operate under different conditions it is customary to report resonance at a certain g-value, allowing direct comparison between samples. Virtually all free radicals and some ionic crystals have g-values of around 2 since their unpaired electrons can move about more or less freely over an orbital encompassing the whole molecule, rather than being held by particular atoms when orbital angular momentum effects are noticed, as in some ionic crystals. Then g-values can vary between 0.2 and 8.

It is unlikely that this unpaired electron was a result of iron impurities since Fe^{3+} species either exhibit very broad signals or more than one peak on their e.s.r. spectra[168]. The only e.s.r. spectrum of a transition metal in the $ZnCl_2$ matrix available in the literature was that of Mn^{2+} at 25°C, which contains many peaks[169]. It seems unlikely that any organic radicals would still be present in the samples - if being held at 360°C had not decomposed any organic

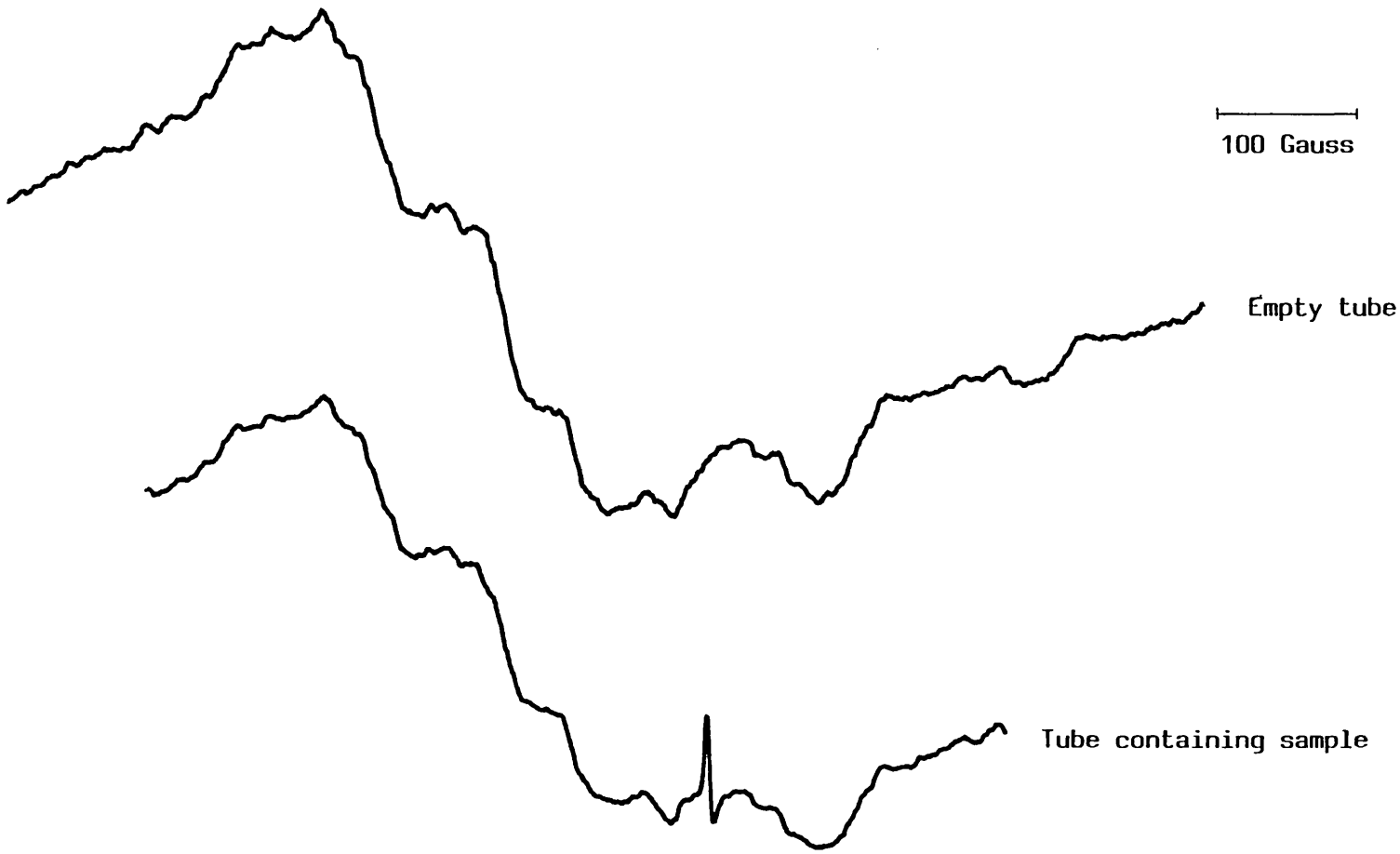


FIGURE 8.7

E.s.r. Spectrum of $ZnCl_2$ Containing O_2

molecules then the presence of O_2 would have oxidised them to CO_2 at those temperatures. The black flecks of carbon were found to disappear as O_2 was bubbled through the melts. The formation of an O_2^- superoxide species seems most likely to account for the colour, the fluorescence noted in the Raman spectrum and the signal on the e.s.r. spectrum. Voltammetric results are given in Chapter 9. A reaction such as [8.2] could be envisaged, the oxygen oxidising the Cl^- ions to form the superoxide.

$$O_2 + Cl^- \rightarrow O_2^- + \tfrac{1}{2}Cl_2 \qquad [8.2]$$

Superoxides have been postulated to exist in a variety of other systems: in NaOH-KOH melts[170], in $NaNO_3$-KNO_3 melts[171], in LiCl-KCl melts[172], and a general account of their behaviour has been given by El Hosary et al.[173].

So, by use of Raman and e.s.r. spectroscopy the existence of superoxide ions in $ZnCl_2$ melts has been inferred, although a more exhaustive study would be needed for confirmation.

CHAPTER 9

BEHAVIOUR OF OXY-SPECIES IN $ZnCl_2$-NaCl MELTS

Investigation of the behaviour of oxy-species in chloride melts is a widely covered area, as shown by the extensive reviews given in various publications on the subject of molten salts[84]. Having studied the behaviour of water in molten zinc chloride (Chapter 7) it was of interest to look at the behaviour of hydroxide- and oxide-containing compounds in these melts. Consequently the effects of individually adding sodium hydroxide, zinc oxide, oxygen, sodium peroxide and sodium carbonate to $ZnCl_2$-NaCl melts were investigated and have been described in turn in the following sections.

9.1 Behaviour of NaOH in $ZnCl_2$-NaCl melts

The addition of hydroxides to molten chlorides has been widely studied since OH^- ions are thought to be one of the dissociation products of water in these melts. The presence of the "hydroxide" wave [7.4] in the voltammograms of hydroxide solutions has been used to assign the same peaks in voltammograms of water in molten chlorides[87,88,98,144,173,186].

The visible effects of adding a small pellet of NaOH to a $ZnCl_2$-NaCl melt were vigorous effervescence on the melt surface around the pellet, evolution of water which condensed on the cell cap and a pale yellow/white powder on the melt surface which collected on the bottom of the melt container. In the viscous pure $ZnCl_2$ melt the powder would remain on the surface. The yellow colour arose from the non-stoichiometry of the ZnO formed, with the colour becoming more intense at higher melt temperatures. Delarue[193] found that addition of a small amount of KOH to $ZnCl_2$-LiCl-KCl melts resulted in the precipitation of yellow ZnO which redissolved, but further KOH caused the permanent precipitation of ZnO. However, no accurate figures for the amounts of KOH were given. No precipitate formation was mentioned by workers using LiCl-KCl melts[87,88,186], implying that hydroxides are more stable in those melts, whilst the higher

temperature melts tend to be held in ceramic containers which preclude sight of any precipitate[98].

No voltammetric responses other than the melt limits were observed using vitreous carbon electrodes, but on platinum electrodes the voltammograms were very similar to those recorded for water in $ZnCl_2$-NaCl melts (Figure 7.8). Figure 9.1 shows a voltammogram recorded for NaOH in 80 mol. % $ZnCl_2$-NaCl at 330°C, where the "hydroxide" wave [7.4] can be seen just prior to the zinc deposition peak.

$$OH^- + e^- = O^{2-} + \tfrac{1}{2}H_2 \qquad [7.4]$$

The poor quality of the voltammograms prevented a thorough study; Figure 9.1 was one of the best obtained but it did serve as confirmation of the presence of OH^- ions in the melts. Vague humps could be seen prior to the anodic limit that could be due to the oxidation of oxide ions to oxygen, and the reverse process [7.5], given that ZnO precipitated out of solution but would be present to some degree in the melt.

$$O^{2-} - 2e^- = \tfrac{1}{2}O_2 \qquad [7.5]$$

Occasionally noticed on the voltammograms were prepeaks prior to those humps, shown in Figure 9.2. These prepeaks had peak currents linearly dependent on the scan rate ν, rather than $\nu^{\frac{1}{2}}$, and the anodic and cathodic responses had identical peak potentials. These facts infer some adsorption process, which could be oxygen atoms adsorbing on platinum, known to occur in other systems[136]. However, no trend could be found to account for the occurrence of these prepeaks.

The effect of bubbling HCl gas through the solutions was to evolve a lot of water and to eventually leave clear, colourless melts, as expected from equilibrium [4.2].

It had been assumed that the precipitate was ZnO, but experimental evidence was required. It was discovered that dissolving the solidified melts in pre-dried acetone would remove the $ZnCl_2$ but leave a white powder

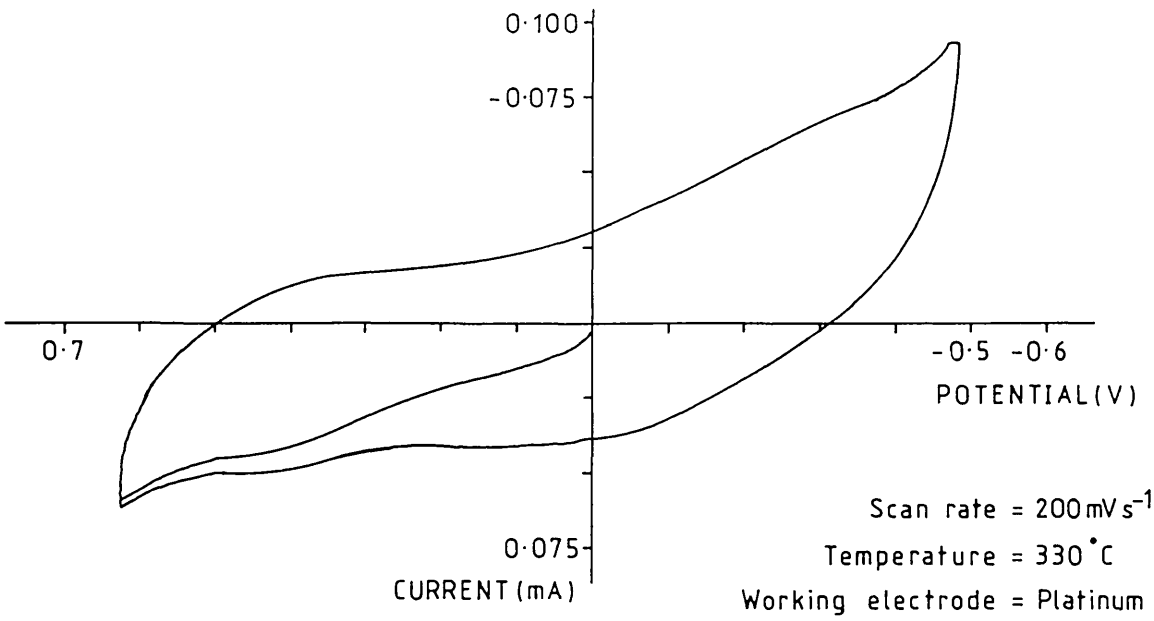


FIGURE 9.1

Voltammogram Obtained for NaOH in 80 mol. % $ZnCl_2$-NaCl

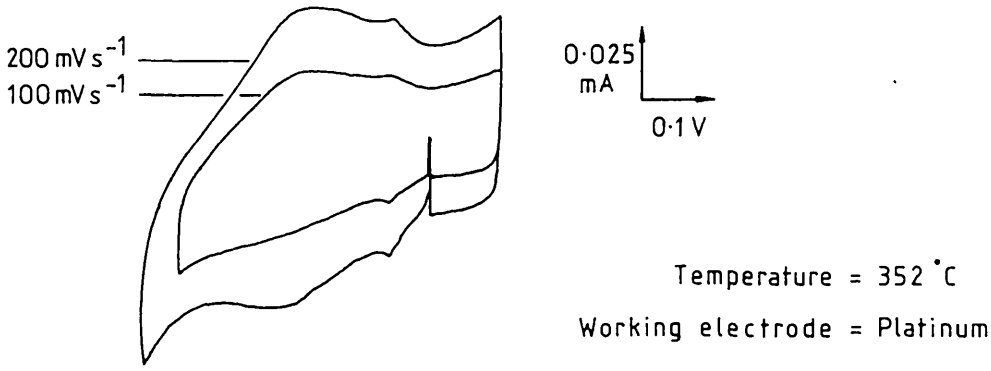


FIGURE 9.2

Voltammograms Showing Prepeaks Obtained for NaOH in 80 mol. % $ZnCl_2$-NaCl

behind. NaCl and ZnO are insoluble in acetone and analysis of the powder by X-ray powder diffraction showed both to be present. However, the diffraction patterns also unexpectedly showed the presence of another compound. Comparison of the calculated d-spacings with the standards from the literature[18] showed the compound to be a hydroxychloride of zinc, $Zn_5(OH)_8Cl_2$. This was found for powders prepared from pure molten $ZnCl_2$ as well as 80 and 50 mol. % $ZnCl_2$-NaCl melts. Table 9.1 lists the d-spacings obtained from the diffraction of a powder produced from 80 mol. % $ZnCl_2$-NaCl, and it can be seen that most of the peaks were due to the hydroxychloride.

Infra-red spectra of the mixtures ($ZnO/NaCl/Zn_5(OH)_8Cl_2$) (Figure 9.3) confirmed the presence of hydroxy-groups within the powders, with vibrational frequencies characteristic of such groups at 3450-3480 cm^{-1}. This was in agreement with published results[198] where the OH^- vibrations occurred at 3470 cm^{-1}.

Investigation of previous work on zinc hydroxychlorides showed that several have been isolated, some of which are listed in Table 9.2. Also listed for comparison are several oxychlorides of zinc. These have all been produced from aqueous solutions, either of $ZnCl_2$ or ZnO-$ZnCl_2$[194], although some metal hydroxychlorides have been prepared from fused salts[195]. It was thought that perhaps water in the acetone was responsible for the hydroxychloride rather than the NaOH in the melt, so some small experiments were carried out to check this. Dissolving large amounts of $ZnCl_2$ in acetone left no precipitate, whilst $ZnCl_2$ and NaCl together only left NaCl. Addition of ZnO to a $ZnCl_2$-NaCl melt, then cooling and dissolving the solid in acetone left a powder analysed as only ZnO and NaCl.

The discovery of the hydroxychloride prompted another look at the water-saturated melts. An 80 mol. % $ZnCl_2$-NaCl melt was saturated with water vapour (dist. water 21.2°C), cooled and dissolved in acetone. The white powder recovered was found to be NaCl and $Zn_5(OH)_8Cl_2$. No ZnO appeared to be present. This was found to be reproducible for the $ZnCl_2$-NaCl melts, but was not tried for pure molten $ZnCl_2$. The fact that NaOH had

d-spacing	intensity	NaCl	ZnO	Other
7.900	VS			$Zn_5(OH)_8Cl_2$
5.340	M			"
4.022	M			"
3.952	W			"
3.583	M			"
3.164	M			"
2.940	M			"
2.876	M			"
2.814	VS	NaCl	ZnO	
2.722	S			$Zn_5(OH)_8Cl_2$
2.675	VS			"
2.600	VS		ZnO	"
2.475	VS		ZnO	"
2.374	M			"
2.171	VW			"
2.067	VW			"
2.019	M	NaCl		"
1.961	W			"
1.910	S		ZnO	
1.831	VW			$Zn_5(OH)_8Cl_2$
1.784	W			"
1.768	W			"
1.694	M	NaCl		"
1.661	VW			"
1.623	VS	NaCl	ZnO	
1.585	M			$Zn_5(OH)_8Cl_2$
1.554	W			"
1.517	W			"
1.503	VW			"
1.478	VS		ZnO	"
1.447	VW			"
1.437	VW			"
1.407	W	NaCl	ZnO	
1.379	S		ZnO	

(continued ...)

TABLE 9.1

d-spacing	intensity	NaCl	ZnO	Other
1.359	M		ZnO	
1.316	VW			
1.302	W	NaCl	ZnO	
1.238	W		ZnO	
1.182	VW		ZnO	
1.168	VW	NaCl		
1.148	VW	NaCl		

VS - very strong S - strong M - Medium
W - weak VW - very weak

TABLE 9.1

Assignment and d-spacings of X-ray diffraction pattern for precipitate from NaOH in 80 mol. % $ZnCl_2$-NaCl at $330^{o}C$

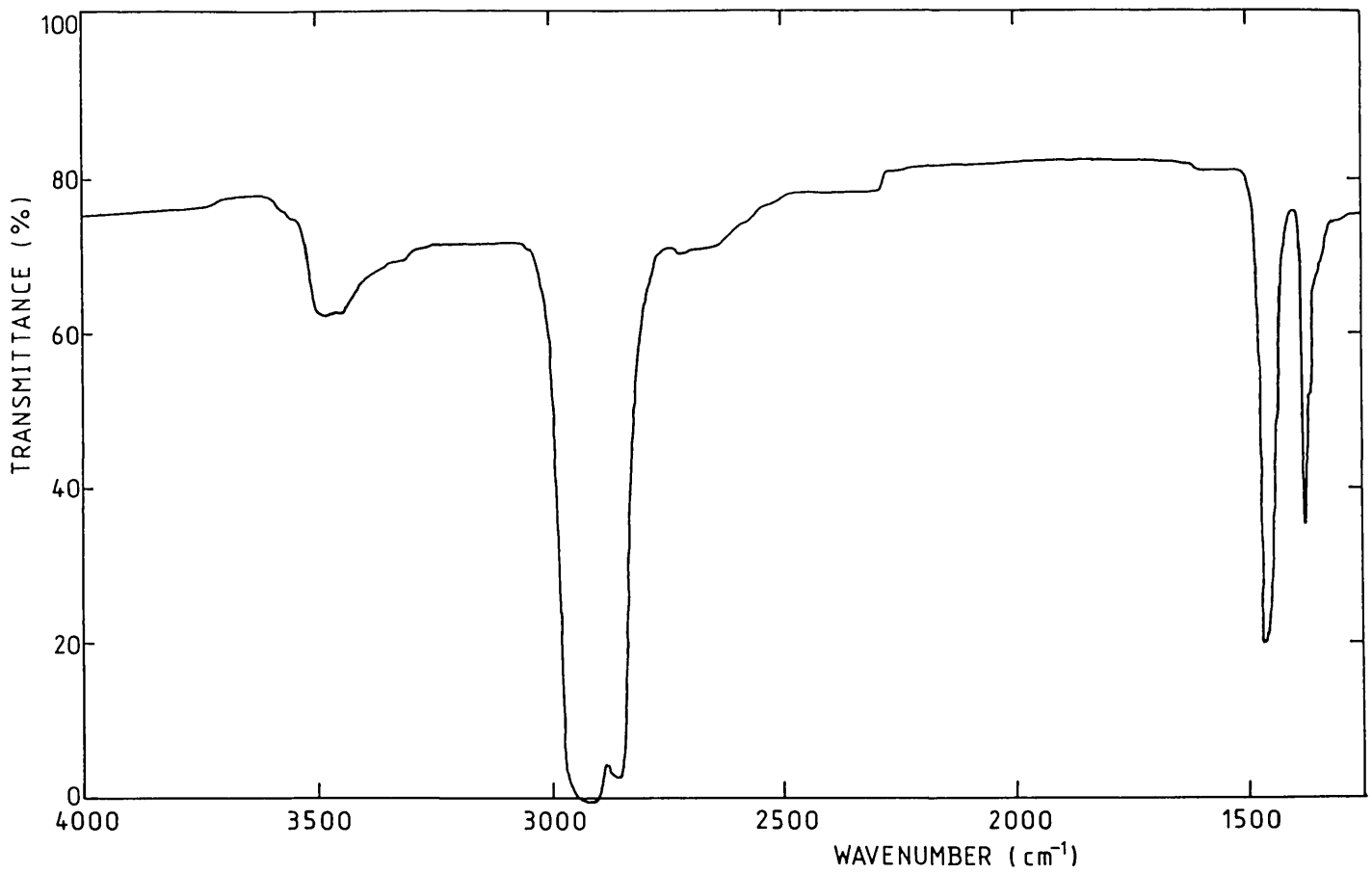


FIGURE 9.3

I.R. Spectrum of NaCl-ZnO-$Zn_5(OH)_8Cl_2$ Mixture (as a Nujol Mull)

Zinc Hydroxychlorides	Zinc Oxychlorides	Zinc Chloride Oxide Peroxide
$Zn(OH)Cl$	$ZnOCl_2$	$Zn_{10}O_3Cl_2(O_2)_6$
$Zn_2(OH)_3Cl$	Zn_2OCl_2	$.3H_2O$
$Zn_5(OH)_8Cl_2$	$Zn_3O_2Cl_2$	
$Zn_5(OH)_9Cl$	$Zn_5O_4Cl_2$	
$Zn_7(OH)_{12}Cl_2$	$Zn_6O_5Cl_2$	

TABLE 9.2

Hydroxy- and Oxychlorides of Zinc

produced a precipitate in these melts but water had not had supported the idea that the dissociation of H_2O molecules in the melts was minimal. However, the isolation of the hydroxychloride demonstrated that some hydrolysis did indeed occur, as inferred by the voltammetric work (Section 7.4). It was not possible to ascertain whether the $Zn_5(OH)_8Cl_2$ exists as a distinct species in the melt, but its formula is similar to $LiZn_5Cl_{11}$, postulated to exist in 83 mol. % $ZnCl_2$-LiCl melts[58]. It is possible that OH^- ions present in the melts cause the formation of a soluble hydroxychloride complex which when cooled forms $Zn_5(OH)_8Cl_2$. The hydrocracking researchers have postulated the existence of $H^+[ZnCl_2OH]^-$ species (Appendix 1) which may exist too. Rather surprisingly, although ZnOHCl is more thermally stable[196] than $Zn_5(OH)_8Cl_2$ and so might have been expected to be the preferred product, no evidence of its formation was obtained.

The concept of hydroxychloro-species existing in divalent metal chloride melts is not new. Addition of hydroxide, either as $Mg(OH)_2$ or NaOH, to $MgCl_2$ melts has been said to form MgOHCl although very little evidence other than a few voltammograms was put forward[131,132]. However, in $CaCl_2$-KCl melts OH^- ions were thought to rapidly form O^{2-} anions and water, but enough hydroxide remained to be observed voltammetrically and could be existing as a calcium hydroxychloride in the melt[98].

Some controversy existed as to how $Zn_5(OH)_8Cl_2$ decomposed on heating[197]. Two decomposition pathways are possible, [9.1] and [9.2]. Differential thermal analyses and thermo-gravimetric studies showed that the material underwent two weight losses, but the nature of the losses

$$Zn_5(OH)_8Cl_2 \rightarrow 4ZnO + ZnCl_2 + 4H_2O \qquad [9.1]$$

$$Zn_5(OH)_8Cl_2 \rightarrow 5ZnO + 2HCl + 3H_2O \qquad [9.2]$$

was in question[196-198]. Samples of the powders produced during this work were analysed by simultaneous D.T.A./T.G.A. under conditions

outlined in Section 3.15. Two endotherms were seen on the thermograms (Figure 9.4), occurring at around 150 $\pm$ 2^{o}C and 205 $\pm$ 4^{o}C. A two-stage weight loss was observed to occur concurrently with the endotherms (Figure 9.5). The weight losses were approximately in the ratio of 1.9:1, the first stage being the greater of the two.

Two groups[196,197] claimed that the decomposition occurred via [9.1] whilst another claimed that [9.2] was occurring with the $ZnCl_2$ being hydrolysed during the heating of the samples. However, at that time the melting point of $ZnCl_2$ was thought to be 275^{o}C[196], and weight losses observed at 262^{o}C were thought to be due to volatilization of $ZnCl_2$. If $ZnCl_2$ molecules were being given off during the second endothermic process then the corresponding weight loss should be the larger ($4H_2O:ZnCl_2$ = 1:1.9), which was not the case here. If the smaller of the two weight losses obtained in this work had occurred first then [9.1] would have been inferred. However, the fact that the larger weight loss occurred first pointed to [9.2]. A possible decomposition pathway could be [9.3], with the $ZnCl_2$ evolved being partially hydrolysed during the first stage, forming ZnOHCl which has been found to be thermally stable to about 227^{o}C[196]. Supporting this mechanism was the fact that on completion

$$Zn_5(OH)_8Cl_2 \xrightarrow[150^{o}C]{\Delta} 4ZnO + 3H_2O_{(g)} + ZnCl_2 \qquad [9.3]$$

$$ZnCl_2 \xrightarrow{H_2O} ZnOHCl + HCl$$

$$ZnO + HCl_{(g)} \xleftarrow[205^{o}C]{\Delta} ZnOHCl + HCl$$

of the thermal analyses a white powder remained that did not undergo a weight increase. If $ZnCl_2$ had been present then its deliquescent nature would have caused an increase in weight of the powder as water was absorbed.

So, it has been found that the addition of hydroxide ions, as either NaOH or water, to $ZnCl_2$-NaCl melts does result in some hydrolysis of the melts, confirming the voltammetric results from Section 7.4. As an interesting sideline, $Zn_5(OH)_8Cl_2$ was found to decompose on heating to form ZnO, HCl and H_2O.

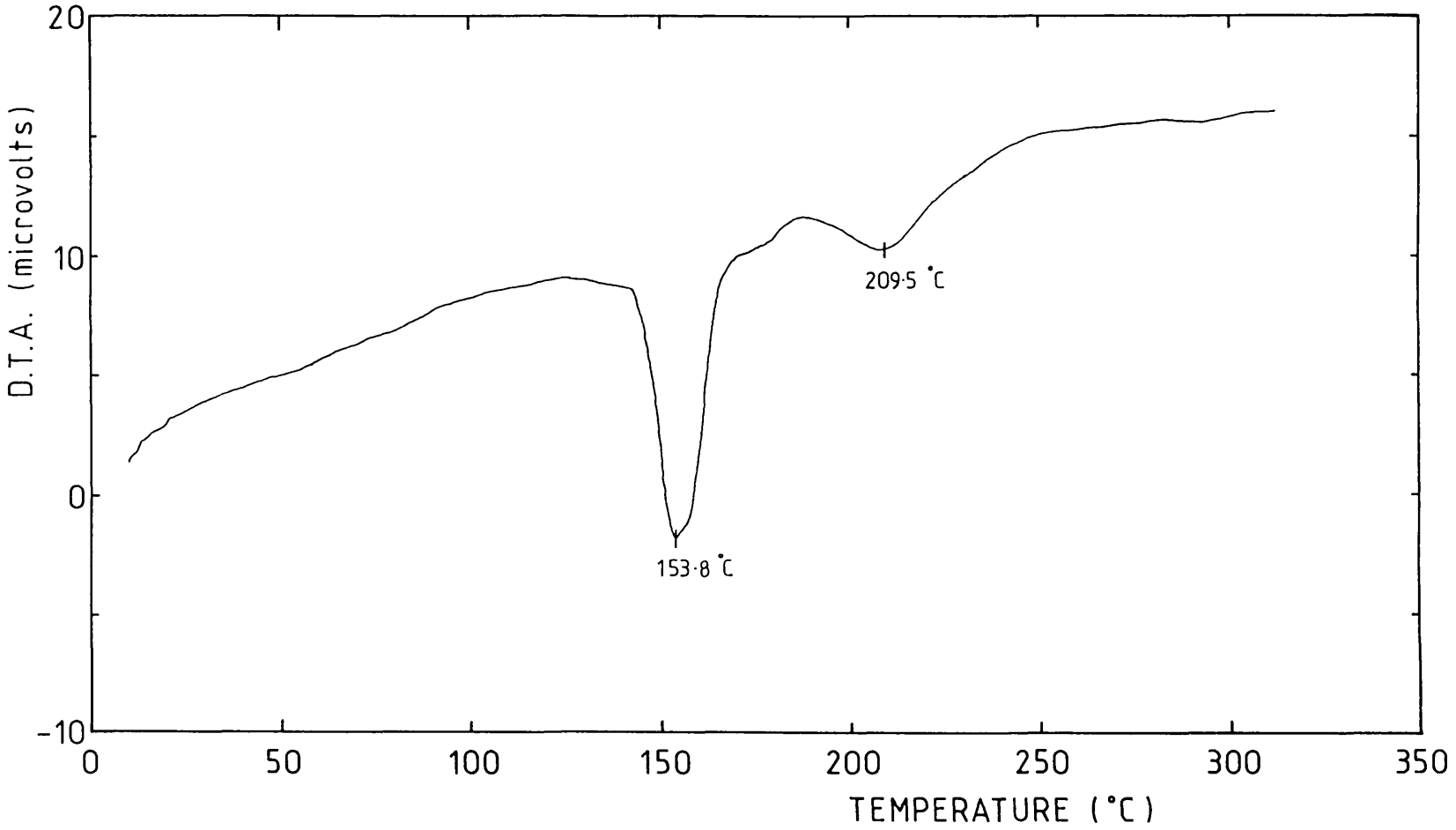


FIGURE 9.4: Thermogram for NaCl-ZnO-$Zn_5(OH)_8Cl_2$ Mixture

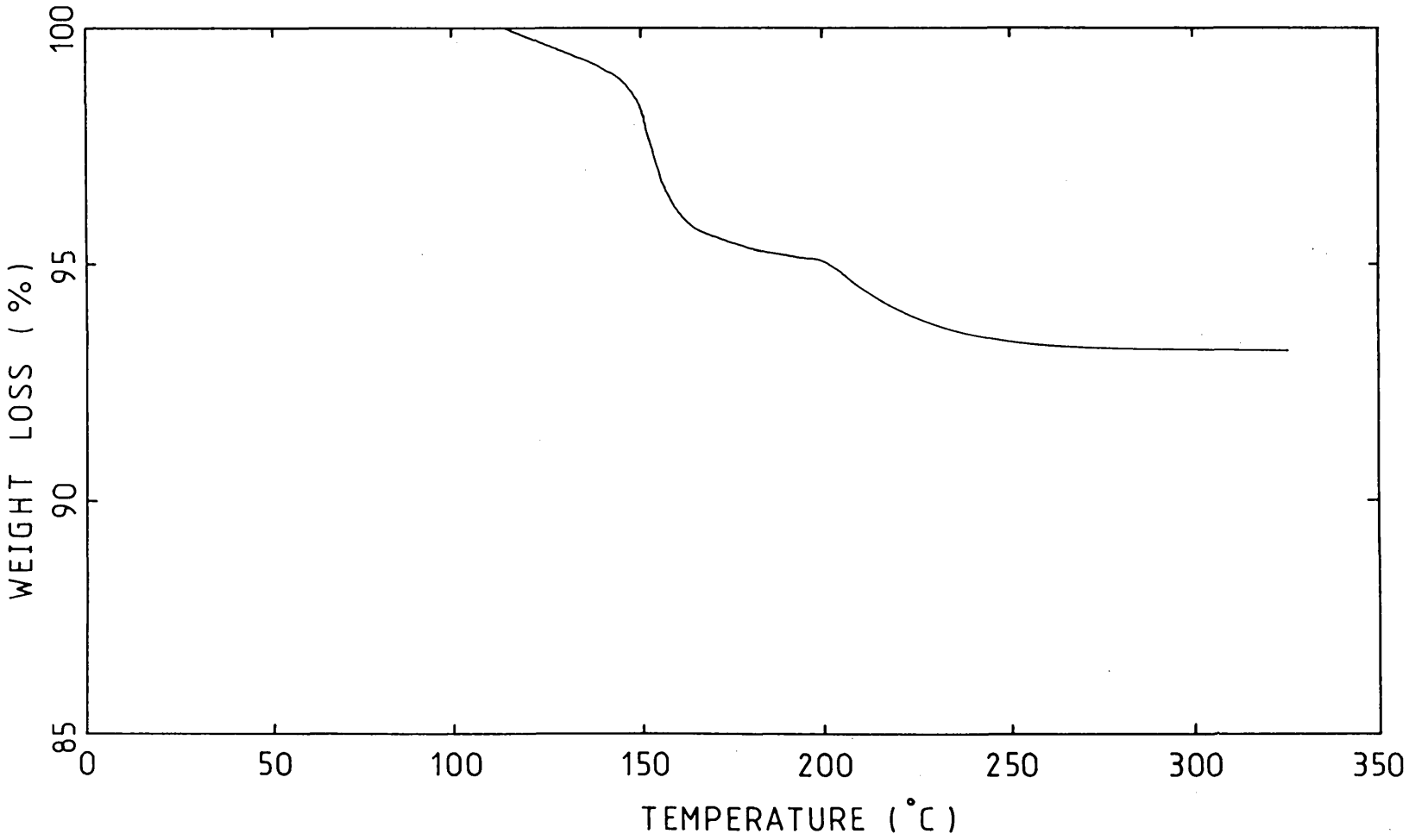


FIGURE 9.5: Temperature - Dependent Weight Loss of NaCl-ZnO-$Zn_5(OH)_8Cl_2$ Mixture

9.2 Behaviour of ZnO in $ZnCl_2$-NaCl melts

As with hydroxide ions, the behaviour of oxide ions in molten chlorides has been the subject of many investigations, since O^{2-} ions are also thought to be one of the dissociation products of water in these melts. Delarue[87,193] investigated the behaviour of a wide range of metallic oxides in LiCl-KCl eutectic melt and found that ZnO was only slightly soluble. Tremillon et al.[93-96] have formulated an oxoacidity scale, using oxide-ion conducting materials such as stabilized zirconia to make electrodes, to describe the effect of adding oxide ions to molten alkali chlorides. These stabilized zirconia electrodes have also been used to monitor the effect of adding oxide ions, as BaO and ZnO, to $ZnCl_2$-NaCl melts[101], where it was found that the presence of oxide ions prolonged the life of metallic anodes used during sodium extraction processes. The presence of oxide ions in $AlCl_3$ melts has been said to result in the formation of $AlOCl_2^-$ (basic melts) or AlOCl (acidic or neutral melts) species, as well as $Al_2OCl_6^{2-}$ and $Al_3O_2Cl_6^{2-}$ species. The use of $TiCl_4$[199] and $TaCl_5$[200] as probe solutes allowed the behaviour of oxide ions to be investigated in the $AlCl_3$ melts since those metal chlorides form oxychlorides such as $TiOCl_4^{2-}$ and $TaOCl_4^-$ which can be detected voltammetrically. In $ZnCl_2$-$AlCl_3$ melts, where $Zn(AlCl_4)_2$ complexes were also found, the addition of O^{2-} ions caused formation of the oxychloroaluminates rather than oxychlorozincates[201].

Given the wide range of zinc oxychlorides formed from aqueous solutions (Table 9.2) and the oxychloroaluminates that are assumed to exist, it was thought that introduction of ZnO into $ZnCl_2$-NaCl melts could result in such species. The addition of ZnO to melts of various compositions resulted in the initially white powder becoming a pale yellow on the melt surface, caused by the non-stoichiometry of the oxide at higher temperatures. Argon stirring of the mixtures produced light grey liquids that became clear upon standing as the ZnO settled. In pure molten $ZnCl_2$ the addition of oxide resulted in a slightly cloudy liquid caused by the formation of a suspension of fine ZnO particles. The effect of filtering the solutions through the apparatus outlined in Section 3.8 was to produce clear solutions, with seemingly all of the ZnO trapped in the filter.

Attempts were made to determine how much, if any, ZnO would dissolve in the molten $ZnCl_2$-NaCl mixtures. The simplest was to dissolve a filtered, cooled solution in water, which would leave any ZnO as a solid since it is virtually insoluble in water (0.00016g in 100g water at 25^oC[142]). However, no such powder was observed. Dissolving the filtered, cooled solutions in acetone and analysing the remaining solid by X-ray diffraction revealed that only NaCl was present. Passage of HCl gas through the filtered molten solutions, which would convert O^{2-} ions to H_2O (equilibrium [4.2]), did not result in the visible formation of water.

Solubility measurements of oxides in the binary melts MCl_2-NaCl (M = Mg, Ca, Sr, Ba) were explained as being due to the formation of oxychlorides such as Mg_2OCl_2, $Ca_4O_2Cl_4$ and $Ba_3O_2Cl_2$[202], but the few simple tests carried out here showed that ZnO was virtually insoluble. Supporting this conclusion are data from Kerridge[203] for the solubility of ZnO in pure $ZnCl_2$. At around 650^oC ZnO could be dissolved to about 2 mol. % of the total, but at 490^oC this had fallen to about 0.4 mol. %. At 450^oC it was down to 0.07 mol. %, so at the temperatures used in this study ($< 380^oC$) the ZnO was essentially insoluble. The presence of NaCl would probably not enhance the oxide solubility markedly.

A voltammetric study was attempted, using platinum quasi-reference and graphite counter electrodes. No voltammetric response other than the melt limits was observed on vitreous carbon electrodes for $ZnCl_2$-NaCl melts with excess ZnO present. Very little response could be obtained on platinum electrodes either, as shown in Figure 9.6. Two broad humps were observed prior to the anodic limit, which have been assumed to be the oxidation of oxide to oxygen and the reverse process ([7.5]). Apart from

$$O^{2-} - 2e^- = \tfrac{1}{2}O_2 \qquad [7.5]$$

that very little else could be obtained; the voltammograms were too ill-defined to permit detailed measurements.

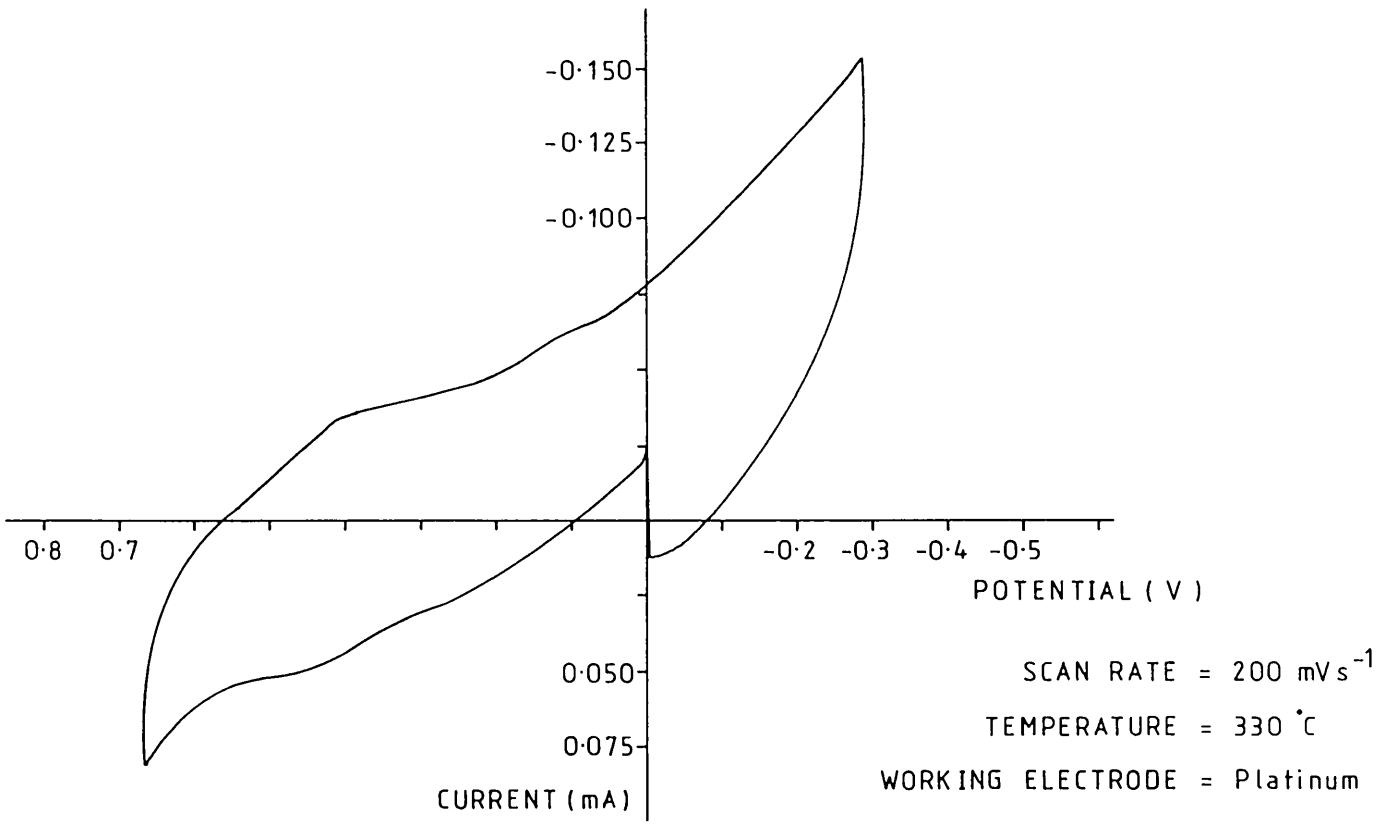


FIGURE 9.6

Voltammogram Obtained for ZnO in 80 mol. % $ZnCl_2$-NaCl

9.3 Behaviour of oxygen in $ZnCl_2$-NaCl melts

As discussed in Section 8.6 the effect of passing pure oxygen gas through these melts was to convert originally clear, colourless liquids to a bright amber colour. Prolonged passage of the gas eventually resulted in the bright amber becoming rather dull, this occurring more quickly in the alkali chloride rich melts. However, no evidence of a precipitate was seen. It had been half-expected that the oxygen would cause the formation of ZnO which would precipitate out of solution. The passage of HCl gas through the amber melts resulted in the evolution of water and the melts resuming their initial colourless state. Purging the HCl with argon, followed by passage of more oxygen through the melts saw the return of the amber colour. For the reasons outlined in Section 8.6 the idea of impurities causing the colouration was ruled out.

The results of the Raman and e.s.r. spectroscopic work (Sections 8.6 and 8.7 respectively) on quenched samples inferred the existence of superoxide species within the melt matrix, thought to be formed by the O_2 molecules abstracting electrons from the chloride ions, although as discussed in Section 7.4 they could also form via a chain of chemical reactions. This accounted for the fluorescence process observed in the Raman spectrum, the orange/amber colour and the single peak seen in the e.s.r. spectrum.

The behaviour of oxygen in other chloride melts has been investigated[98,172,173,186,187] but no such amber colouration was reported by those workers, although it apparently has been noticed, but ignored, by another group working with $ZnCl_2$ melts[150]. Mignonsin et al.[172] inferred the existence of O_2^{2-} and O_2^- species in alkali chloride melts, which have been said to interfere with attempts to produce a reversible oxygen electrode in those melts[185]. The existence of O_2^{2-} species was also put forward to account for the behaviour of water and O_2 in $CaCl_2$-KCl melts[98].

Voltammograms were recorded for oxygen-saturated 80 mol. % $ZnCl_2$-NaCl melts using platinum working and quasi-reference electrodes and typical examples are shown in Figure 9.7 (a) and (b) with the voltammetric

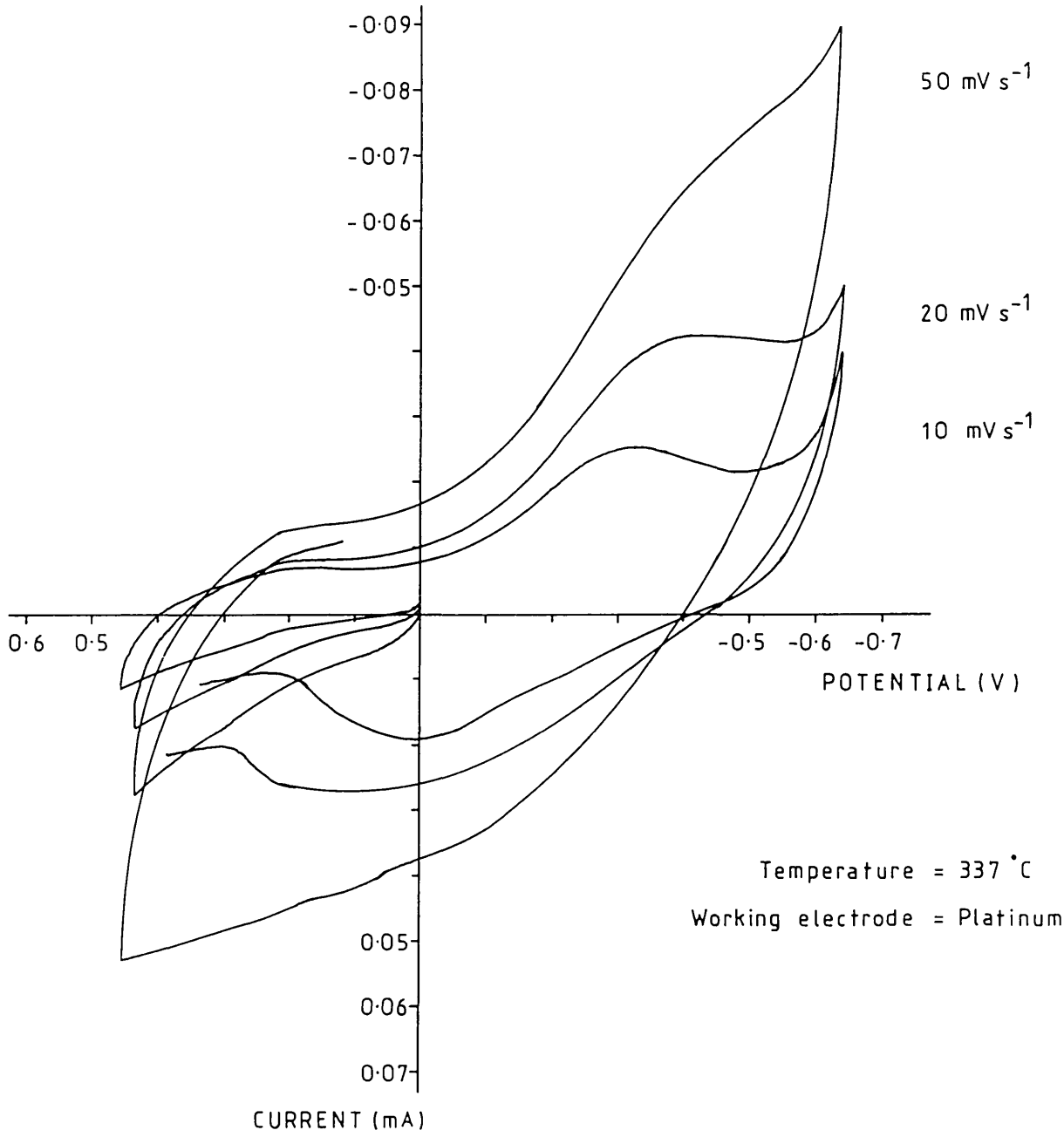


FIGURE 9.7: Voltammogram Obtained for O_2 in 80 mol. % $ZnCl_2$-NaCl
(a) Scan rate > 10 mVs^{-1}

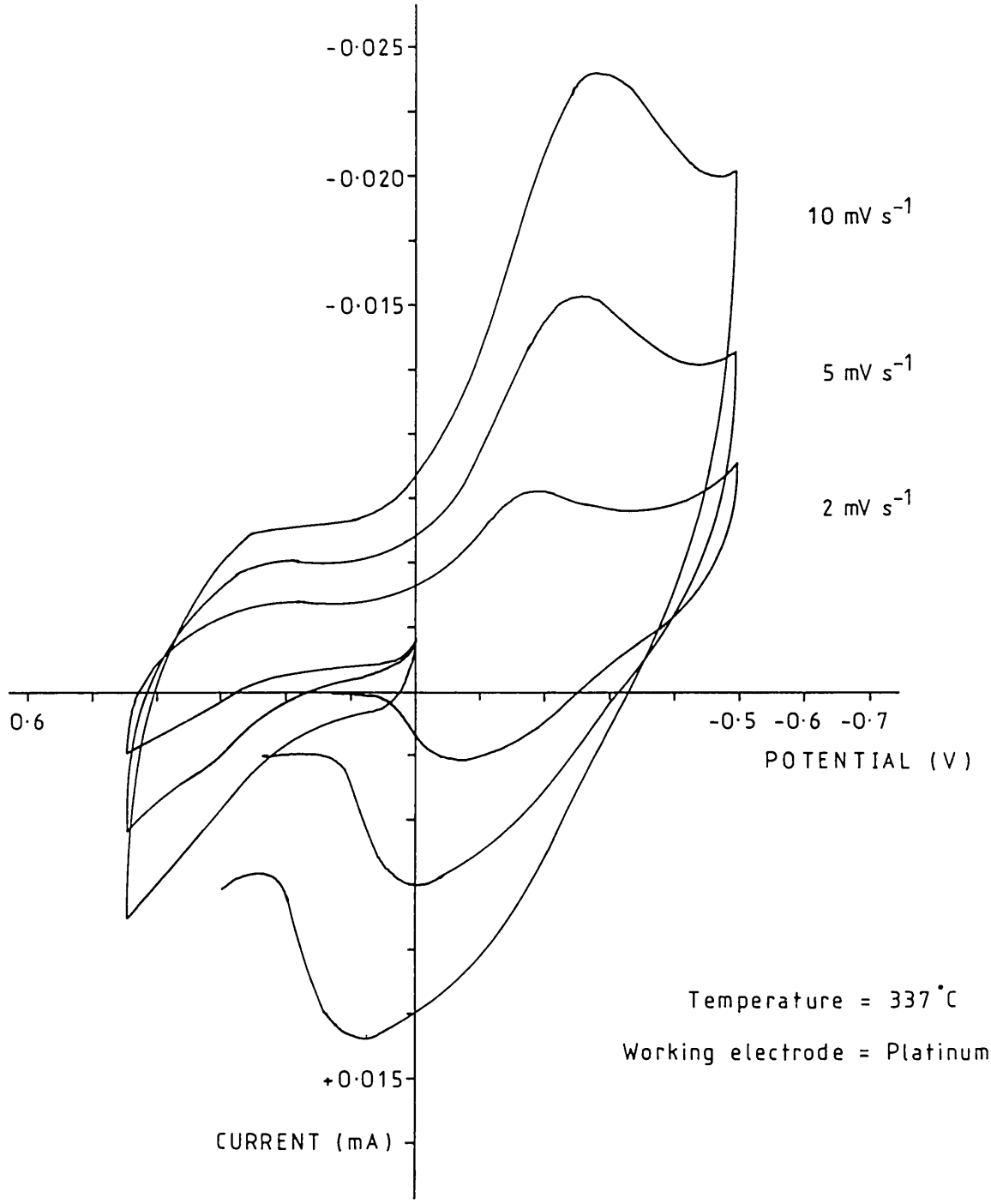


FIGURE 9.7: Voltammograms Obtained for O_2 in 80 mol. % $ZnCl_2$-NaCl
(b) Scan rate < 10 mVs^{-1}

parameters listed in Table 9.3. At high scan rates (>50 mVs^{-1}) the voltammograms were seen to have a "boomerang" shape, with the current at cathodic potentials continuously climbing to the zinc deposition potential, in much the same manner as that observed for $CaCl_2$-KCl melts[98]. Also, as the melt temperature was raised so this shape became more pronounced, although no visible change in the melt occurred.

However, as the scan rate was lowered so the voltammograms took on the appearance of a typical pair of reduction/oxidation responses. At 2 mVs^{-1} the value of ΔE_p was the same as that calculated for a one electron process (equation [5.9]), with it rapidly increasing with increase in scan rate. Figure 9.8 shows that $i_p/\nu^{\frac{1}{2}}$ values are relatively independent of ν, the scan rate, but that the plot does not pass through the origin. The values of i_{pc}/i_{pa} are, however, seen to be unity for all scan rates.

This behaviour resembles that characteristic of a quasi-reversible electrode process, in which the electrode reaction is not solely governed by the rate of diffusion of the electroactive species but also by the charge transfer kinetics of that process. Purely reversible processes are governed by rates of diffusion, their charge transfer rates being very fast (>0.3 $\nu^{\frac{1}{2}}$ cm s^{-1}) whilst irreversible processes have very small charge transfer rate constants ($<10^{-5}$ $\nu^{\frac{1}{2}}$ cm s^{-1}) and consequently the reverse process is not seen on voltammetric sweeps. With quasi-reversible systems at low scan rates the charge transfer processes are fast enough to be observed in both forward and reverse sweeps, but as the scan rate is increased so they tend to behaviour characteristic of irreversible processes[136].

Given that at 2 mVs^{-1} the voltammograms yield ΔE_p values matching the theoretical value for a single electron process, and that the results from Sections 8.6 and 8.7 inferred the existence of superoxide species in the melts, then a possible electrode reaction is:

$$O_2^- + e^- = O_2^{2-} \qquad [9.4]$$

This has also been put forward as occurring in alkali chloride melts, the superoxide having been formed during addition of peroxide ions[172], and

ν (Vs^{-1})	T (K)	-Epc(V)	Epa(V)	Δ Ep(V)	i_{pc} (mA)	i_{pa} (mA)	i_{pa}/i_{pc}
0.002	610	0.185	-0.070	0.115	0.008	0.003	0.99
0.005	610	0.255	0.000	0.255	0.015	0.008	0.99
0.010	610	0.280	0.080	0.360	0.025	0.014	1.01
0.020	610	0.420	0.100	0.520	0.042	0.019	1.08
0.050	610	0.510	--	--	0.074	--	--

TABLE 9.3

Voltammetric Parameters of O_2 in 80 mol. % $ZnCl_2$-NaCl

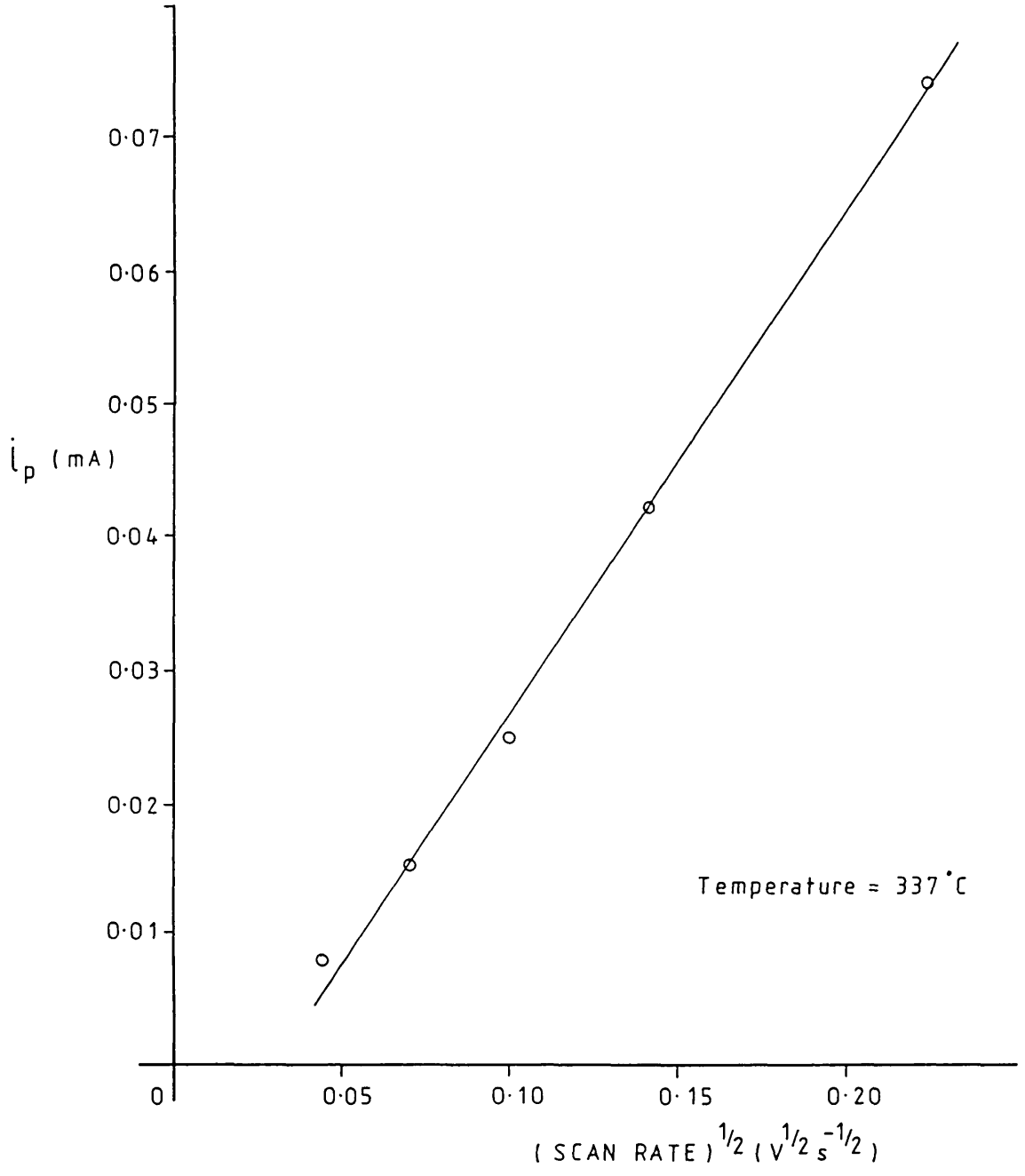


FIGURE 9.8

Variation of i_p With $\nu^{\frac{1}{2}}$ for O_2 in 80 mol. % $ZnCl_2$-NaCl

being reduced back to the peroxide. The same process has also been found to occur in molten hydroxides and nitrates where the behaviour of the various oxide anions has been much more widely investigated[173]. However, superoxide ions were found to be decomposed to peroxide ions upon addition of NaO_2 to LiF-BeF_2-Zr/ThF_4 melts, although they were more stable in LiF-NaF-KF eutectic[188]. The stabilising influence of the large K^+ cations was invoked to account for the difference in behaviour.

9.4 Behaviour of Na_2O_2 in $ZnCl_2$-NaCl melts

Having intimated the existence of superoxide species during work on oxygen-saturated melts (Sections 8.6 and 9.3), the stability of peroxide species was also of interest. Their existence has been claimed in various halide melts such as $CaCl_2$-KCl[98], LiCl-KCl[172,185] and LiF-BeF_2-Th/ZrF_4[188] as well as nitrate, hydroxide and carbonate melts[173]. In the alkali halide melts the following equilibria were assumed to be present ([9.5] and [9.6]), describing the interconversion of oxygen with oxide, peroxide and superoxide species[172]. The formation of superoxides

$$\begin{array}{rcl} O_2 + Cl^- & = & O_2^- + \tfrac{1}{2}Cl_2 \\ & & \| \; O_2 \end{array} \qquad [9.5]$$

$$O_2 + 2Cl^- = O_2^{2-} + Cl_2$$

$$2O_2^{2-} = 2O^{2-} + O_2 \qquad [9.6]$$

during the addition of oxygen gas to $ZnCl_2$-NaCl melts in this work has been thought to follow the first equilibrium, the oxygen molecules abstracting electrons from chloride ions in the melts (Section 8.6). From the same equation it can be seen that peroxide species could be formed at the same time, although they were not directly detected.

Sodium peroxide, as purchased from the suppliers (Section 3.17), had an orange tinge caused by the presence of around 5% sodium superoxide (NaO_2). The peroxide is slightly deliquescent so was stored in the argon dry-box and taken out immediately prior to use. Sodium peroxide was added

to 80 mol. % $ZnCl_2$-NaCl melts (0.1 molal) at around 350^{o}C, and its behaviour investigated by use of voltammetry with platinum electrodes. No voltammetric response was observed with vitreous carbon electrodes other than the melt decomposition limits. No moisture was evolved as the peroxide was added, showing the dryness of the powder. Initially, the powder underwent a vigorous reaction with the melt surface causing it to bubble violently, eventually leaving a pale yellow powder which sank to the bottom of the melt container. No orange colour could be discerned amongst the murky grey of the melt. Stirring the mixture with argon served to enhance the mixing.

The voltammograms obtained depended on the length of time allowed to pass between the introduction of the peroxide into the melt and the instant at which the voltammograms were recorded. On the voltammograms recorded immediately after the Na_2O_2 addition (Figure 9.9) very little could be seen apart from some vague humps. However, after three minutes of vigorous stirring the voltammograms contained six reasonably well-defined responses (Figure 9.10). To distinguish the peaks they have been labelled and analysed as three pairs; F-G, H-J and K-L. The voltammetric parameters measured have been listed in Table 9.4.

Initially, the peaks were thought to be due to aqueous contamination of the melt, given the similarity of Figure 9.10 to the voltammograms recorded for water in pure $ZnCl_2$ (Figure 7.1) and the deliquescent nature of Na_2O_2. However, the voltammograms obtained for H_2O in 80 mol. % $ZnCl_2$-NaCl, the melt used with Na_2O_2, did not show the same sharpness of response (Figure 7.8) as those recorded for Na_2O_2, and no water was observed on the cell cap on addition of the peroxide.

Closer analysis of the voltammograms revealed, moreover, that the parameters of peaks F-L were quite different to those of the voltammograms recorded for water in these melts. Peaks F and G had a separation comparable to that calculated for a one-electron process at low scan rates but with increase in scan rate ΔE_p became larger, similar to the behaviour observed with the oxygen-saturated melts (Section 9.3). A feature common to nearly all the voltammograms recorded during this work was the width of

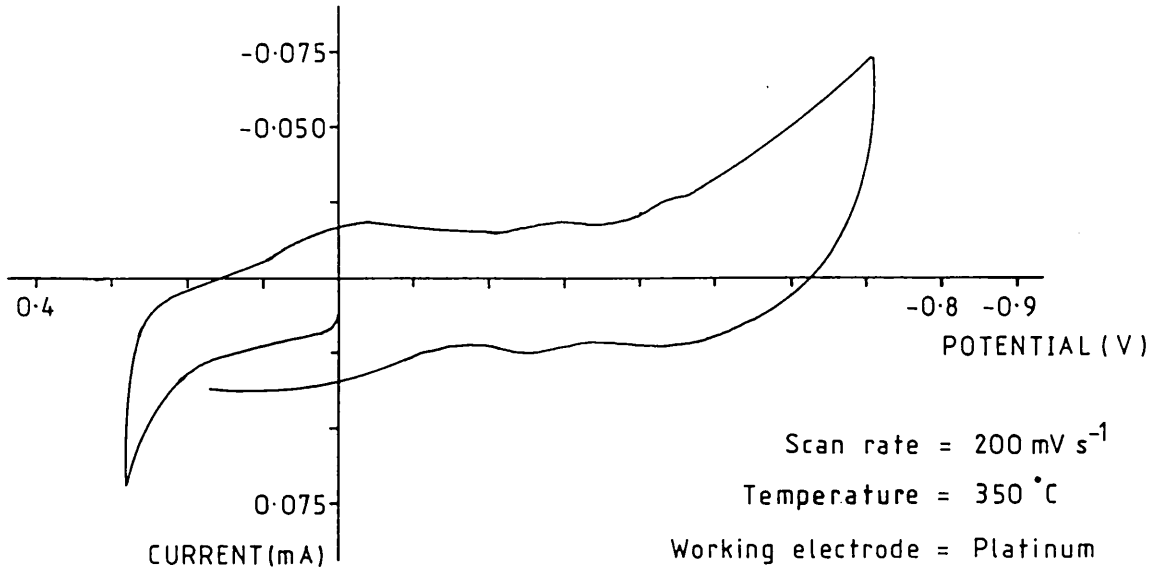


FIGURE 9.9: Voltammogram Obtained for Na_2O_2 in 80 mol. % $ZnCl_2$-NaCl Immediately After Solute Addition

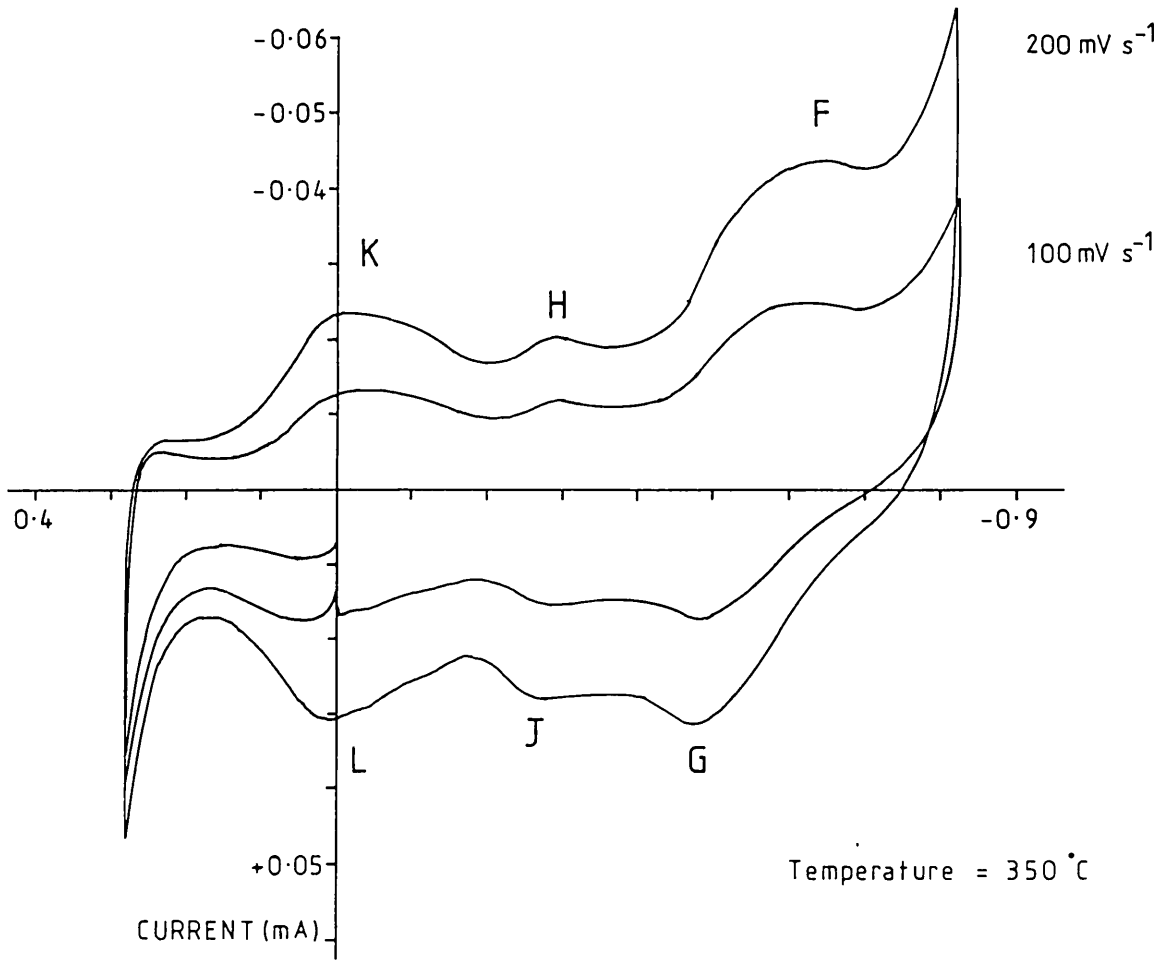


FIGURE 9.10: Voltammograms Obtained for Na_2O_2 in 80 mol. % $ZnCl_2$-NaCl Three Minutes After Solute Addition

the responses, making exact determination of the peak potentials difficult, and this factor must be remembered when drawing conclusions from the results. Peaks K and L, the most anodic pair, had a separation characteristic of a two-electron process, as found for the voltammograms of water in molten $ZnCl_2$ (Chapter 7). Interestingly, the anodic responses G and L consistently had almost identical peak current values (Table 9.4) but whether any significance can be attached to this is uncertain.

At low scan rates the peak potentials of H and J were identical, only slowly changing with scan rate until at 500 mVs^{-1} the ΔE_p value was about that for a two-electron process. Plots of i_p, the peak currents, against $\nu^{\frac{1}{2}}$, the root of the scan rate, were curved (Figure 9.11) for all six peaks, demonstrating that the electrode processes were only partially diffusion-controlled.

It was not possible to make definite assignments of the voltammetric peaks, but suggestions of their origins can be outlined. The behaviour of peaks F and G mirrors the behaviour of the voltammograms of oxygen-saturated melts, thought to be due to the reduction of the superoxide and its reverse process. Given the equilibria thought to be present in alkali chloride melts ([9.5] and [9.6]) it may be that the peroxide is unstable in $ZnCl_2$ melts and forms the more stable superoxide. Two electrode processes have been suggested to account for peaks K and L ([7.5] and [7.7]), but it was not possible to discern which was occurring here.

$$O^{2-} - 2e^- = \tfrac{1}{2}O_2 \qquad [7.5]$$

$$O_2 + 2e^- = O_2^{2-} \qquad [7.7]$$

The most remarkable behaviour, and the most difficult to assign, was that of peaks H and J. The fact that the peak potentials were almost identical suggested an adsorption process, for example oxygen on platinum, and the peak currents exhibited greater linearity with ν than with $\nu^{\frac{1}{2}}$. Brookes[98] has stated that the process [7.6] may occur if peroxides are present in $CaCl_2$-KCl melts, with peroxide and oxide species being interconverted via a two electron process, and at higher scan rates the

$\nu(mVs^{-1})$	Temp (K)	-Epc(V)	-Epa(V)	ΔEp(V)	i_{pc} (mA)	i_{pa} (mA)
Peaks F/G						
50	623	0.600	0.475	0.125	0.0145	0.0095
100	623	0.630	0.475	0.155	0.0245	0.0180
200	623	0.660	0.475	0.185	0.0430	0.0315
500	623	~ 0.650	0.460	~0.190	0.0913	0.0675
Peaks H/J						
50	623	0.300	0.300	0.000	0.0070	0.0085
100	623	0.300	0.295	0.005	0.0110	0.0155
200	623	0.300	0.280	0.020	0.0200	0.0280
500	623	0.305	0.255	0.050	0.0413	0.0625
Peaks K/L						
50	623	0.030	-0.015	0.045	0.0070	0.0095
100	623	0.035	-0.020	0.055	0.0120	0.0175
200	623	0.035	-0.015	0.050	0.0233	0.0315
500	623	0.030	-0.025	0.055	0.0500	0.0675
calc.(n=2)				0.061		

TABLE 9.4

Voltametric Parameters for Na_2O_2 (0.1 molal) in 80 mol. % $ZnCl_2$-NaCl

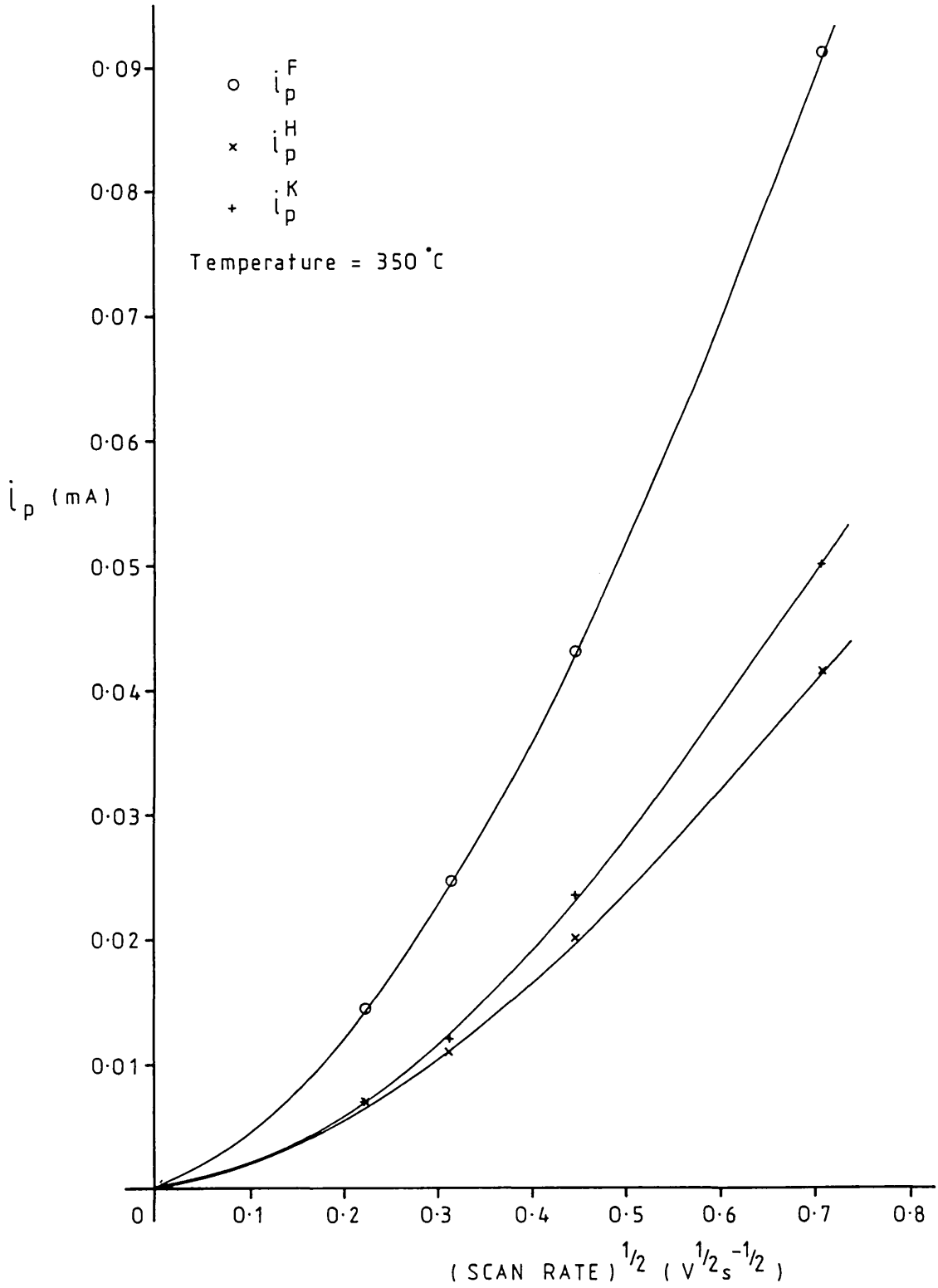


FIGURE 9.11

Variation of i_p with $\nu^{\frac{1}{2}}$ for Na_2O_2 in 80 mol. % $ZnCl_2$-NaCl

value of ΔE_p of peaks H and J tended towards calculated values for such a

$$O_2^{2-} + 2e^- = 2O^{2-} \qquad [7.6]$$

process. Another possibility was that one of the charge transfer products underwent a chemical reaction to yield an unstable, electrochemically active species responsible for H and J.

One scheme that could be envisaged is that where the peroxide ions decompose to form superoxide and oxide species ([9.5] and [9.6]), with excess zinc oxide precipitating out of solution, as observed. A similar decomposition process has been found in molten nitrates and hydroxides, and was thought to follow equation [9.7][173]. The electroactive superoxide ions could be responsible for peaks F and G, with reduction of O_2^- to O_2^{2-} and the reverse process. Conversion of the oxide ions to oxygen, and vice versa, via [7.5] could account for peaks K and L. Either a chemical reaction of oxygen atoms with oxide ions, say, or some electrochemical process (e.g. [7.6]) could produce peroxide species for a short period which are responsible for peaks H and J.

$$3O_2^{2-} = 2O^{2-} + 2O_2^- \qquad [9.7]$$

This, however, is only a suggested reaction scheme, based upon the observation of ZnO precipitated out of solution, the stability of O_2^- species in these melts (Sections 8.6 and 9.3) and the voltammograms obtained. More work, such as an e.s.r. investigation of the melt to determine the presence of O_2^-, would be required to positively describe the system. It could be that the presence of around 5% superoxide in the supplied sodium peroxide was in some way catalysing the breakdown of the peroxide species, and that a pure peroxide would not decompose.

Interestingly, the existence of zinc chloride oxide peroxide ($Zn_{10}O_3Cl_2(O_2)_6.3H_2O$) has been claimed[191]. Apparently this compound can be isolated in the solid phase but decomposes on heating. However, a patent by Ito et al.[192] gives details for the preparation of divalent metal peroxides including ZnO_2, said to be stable to 150°C. If these materials can be isolated in the solid phase, then their existence in zinc chloride melts is not so unlikely.

9.5 Behaviour of Na_2CO_3 in $ZnCl_2$-NaCl melts

In an attempt to increase the oxide ion content of a 80 mol % $ZnCl_2$-NaCl melt above that achievable by adding zinc oxide, sodium carbonate was added to the melt. At elevated temperatures carbonate ions dissociate into CO_2 and O^{2-} ions (equation [9.8]) and this has been found to occur in various chloride melts[198]. Under fixed carbon dioxide pressures equilibrium [9.8] is maintained, the CO_3^{2-} acting as a buffer for pO^{2-}. However,

$$CO_3^{2-} = CO_2(g) + O^{2-} \qquad [9.8]$$

under inert atmospheres CO_3^{2-} has been found to act as a reasonable source of oxide ions.

The introduction of powdered Na_2CO_3 into a 80 mol % $ZnCl_2$-NaCl melt at around 350°C resulted in a vigorous reaction on the melt surface, the carbonate causing the melt surface to bubble as a gas was evolved. A pale yellow powder formed on the surface of the melt and slowly sank to the cell bottom. That CO_2 was formed could be seen by passing the gas through lime water which turned faintly cloudy.

Cyclic voltammograms were recorded using platinum and vitreous carbon working electrodes, but no peaks other than the melt limits were observable on the voltammograms recorded with the latter electrode. The voltammograms recorded with the platinum working electrode were rather irreproducible, sometimes containing no peaks other than the melt limits, but other times vaguely resembling those recorded upon addition of ZnO to the melts (Section 9.2), with slight humps appearing that were not well-defined. Analysis by X-ray diffraction of the white powder formed as a precipitate confirmed that it was ZnO, the yellow colour having arisen as a result of the non-stoichiometric nature of ZnO at high temperatures. Thus the attempt to increase the oxide ion concentration of the melt was not successful since zinc oxide was almost immediately formed.

The solubility of carbon dioxide in zinc chloride melts has been determined[190], and a more thorough study of the behaviour of equilibrium [9.8] in these melts might prove interesting.

A problematic source of oxide impurities can often be the glass melt containers[173]. Silicate formation [9.9] between added oxide ions and

$$O^{2-} + xSiO_2 = (SiO)_x.O^{2-} \qquad [9.9]$$

silica in the glass can result in spurious electrochemical results, but no sign of such a process was ever observed during the work outlined here.

CHAPTER 10

CONCLUSIONS

a) It has been shown that several diverse uses exist for molten zinc chloride, ranging from hydrocracking catalyst to chemical reaction medium to stable glass former.

b) The review of previous work carried out on molten zinc chloride has shown that the structure of the melt, and of mixtures with alkali metal chlorides, has been investigated many times using a wide range of experimental techniques, but that groups of workers are still in disagreement over how to most accurately describe the systems. Investigation of the physico-chemical and transport properties of the melts has been carried out for most melt compositions and a degree of agreement is seen between the various sets of results.

c) In contrast, the solvent properties of the melts have not been so widely investigated, with only a small amount having been done on the behaviour of gases, water and transition metal compounds within these molten systems. However, a variety of complex species are postulated to exist in these media and the scope for further work is large.

d) A wide range of experimental techniques have been used during this project, both to utilise available equipment and to obtain as much information as possible. Small scale electrochemical glassware was found to perform as well as the cumbersome large cells used for electroplating.

e) Various melt purifications steps have been summarized and some were used here to produce melts that were colourless and voltammetrically featureless, but that were subject to carbon contamination.

f) Water absorption studies showed that the presence of alkali metal chloride in the solid phase reduced the deliquescent nature of the zinc chloride.

g) Platinum has been shown to be a suitable electrode material for voltammetric investigations of oxide and protonic species in the zinc chloride melt systems. Vitreous carbon electrodes failed to exhibit any voltammetric response other than the melt decomposition limits.

h) The solubility data for HCl in molten $ZnCl_2$-NaCl binary mixtures were found to exhibit trends characteristic of a chemical dissolution process, implying the formation of complex species. It was postulated that as the melt basicity increased so the species formed changed from $H^+ZnCl_3^-$ to HCl_2^-, with the more basic melts tending towards behaviour exhibited by HCl in pure molten alkali metal chlorides.

i) The platinum quasi-reference electrode has been shown to remain stable in HCl-saturated $ZnCl_2$-NaCl melts.

j) The reduction of HCl dissolved in $ZnCl_2$-NaCl melts of various compositions followed a one electron diffusion-controlled reversible charge transfer process complicated by adsorption of hydrogen, formed as the reduction product, onto the platinum electrode. Peak current ratios of less than unity could be interpreted either as being due to the dimerization of the hydrogen atoms evolved or to convection effects within the melts.

k) Coupling the solubility data with the voltammetric results, the diffusion coefficients of HCl so calculated were found to increase with increasing melt temperature and basicity. The activation energies of the diffusion process in the various melt compositions were larger than those for metal cations implying that more complex diffusion processes occur with HCl as the solute.

l) The Stokes-Einstein equation was obeyed for the more acidic melt systems but not for those at high temperatures or with $X_{NaCl} > 0.3$. The calculated radii of the diffusing species were assumed to be "effective" radii rather than actual values, and taken to infer the changeover in species present in the melts, from $H^+ZnCl_3^-$ to HCl_2^- with increasing melt basicity.

m) Extraneous voltammetric responses were taken to imply the formation of Zn-Pt alloys, of which at least five are known.

n) Values of the electrical conductivity of $ZnCl_2$-NaCl melts of various compositions, determined using the novel a.c. impedance technique, correlated favourably with results of previous studies. Individually adding HCl and water to the melts was found to cause differences in the conductivity values but the solutes had opposite effects, the HCl lowering the conductivity whilst water increased the conductivity. This was interpreted in terms of possible melt species.

o) The volatility of zinc chloride melts disrupted attempts to measure the water solubility in these media, but the hydrolysis reaction was shown to occur to a limited extent, and was at its greatest in pure molten zinc chloride.

p) The presence of hydroxide ions in water-saturated melts was confirmed by voltammetric means but definite assignment of other voltammetric responses was not possible. Most workers have stated that the reduction of water and the oxidation of oxide ions, and the reverse steps, are the voltammetric processes observed and this seemed most likely here. However, the existence of peroxide ions has also been put forward to account for the same observed voltammetric responses. The addition of peroxide ions to the zinc chloride melts resulted in different voltammetric responses, which was taken to infer that these ions were not present in water-containing zinc chloride melts.

q) The formation of zinc oxide films on the working electrodes was shown to occur upon holding the electrodes at suitably cathodic potentials in the water-containing melts.

r) The presence of HCl or water in pure molten zinc chloride has been shown to stabilize the amorphous phase formed upon quenching the melt. However, no Raman peaks characteristic of vibrations of those molecules were observed, emphasising the unsuitability of the technique for studying trace materials. A deposit formed in the gas bubbler during passage of water vapour into the melts was found to be zinc oxide and various hydroxides.

s) The saturation of $ZnCl_2$-NaCl melts with oxygen resulted in an amber colouration. Raman, electron spin resonance and voltammetric studies all inferred the presence of superoxide ions within the melt matrix, thought to be formed by abstraction of electrons from chloride ions by the oxygen molecules.

t) Peroxide ions were thought to decompose on contact with the melts to form superoxide and oxide ions, and mechanisms for this process have been put forward, with interconversion between all three oxide species suggested.

u) The white precipitate isolated following addition of sodium hydroxide to zinc chloride melts was found to be sodium chloride, zinc oxide and $Zn_5(OH)_8Cl_2$. The hydroxychlorozincate was also isolated following saturation of $ZnCl_2$-NaCl melts with water, confirming the existence of the hydrolysis reaction. The decomposition pathway of the hydroxychlorozincate was confirmed as being via formation of HCl, water and zinc oxide and a possible mechanism has been put forward.

v) The solubility of zinc oxide in the zinc chloride melts is so low that only very poor voltammograms were obtained. However, evidence of the oxidation of oxide ions, and the reverse process, was obtained.

w) Carbonate ions were thought to decompose to form carbon dioxide and oxide ions on contact with the melts, the oxide ions being precipitated as zinc oxide.

Suggestions for further work

As mentioned earlier, the scope for further work in the use of molten zinc chloride as a reaction medium is quite large. Relatively little work has been carried out on the behaviour of solutes in these melt systems, compared to the chloroaluminate melts, for example. The diverse uses of molten zinc chloride systems demonstrate that they have great potential.

As a continuation of the work carried out with HCl and water being individually added to the melts, the effect of adding the two together should be investigated. The possible existence of more than one oxide species in the $ZnCl_2$-NaCl binary systems is something that also needs further work. Maintaining an oxygen atmosphere over melts into which oxide, peroxide or superoxide ions have been added could have a marked effect on the species present. Similarly, the addition of carbonate ions was not fully investigated, and there exists scope for holding a carbon dioxide atmosphere over the melts to see if carbonate ions can be stabilised. The use of an oxide-ion conducting indicating electrode, such as one of yttria-stabilised zirconia which has proved reliable elsewhere, to monitor the effects of addition of oxy-species to the melts would allow further information to be obtained.

Given that alloys are thought to be formed following the deposition of zinc onto platinum, gold or tungsten, the use of these melts for such an industrial purpose might be explored. Similarly, the apparent stabilization of the amorphous zinc chloride phase by the introduction of water or hydrogen chloride could be studied with a view to its use as optical components.

REFERENCES

1) **N.A. Carthey:** Ph.D. Thesis, University of London, (1988)

2) "Molten Salt Techniques", eds. D.G. Lovering, R.J. Gale, (Plenum), vol. 1, (1983); vol. 2 (1984)

3) **G.S. Perry, L.G. MacDonald, S.D. Wilcox:** HCTD Technical Memo. no. 3/84 (A.W.R.E.)

4) **Y.K. Delimarskii, S.V. Volkov:** Ukr. Khim. Zh., 53(1), 3, (1987)

5) **G.P. Pez, R.T. Trotter:** Eur. Pat. Appl. EP 194, 483

6) **V.I. Skudaev, A.B. Solomonov, P.P. Gertsen:** Zh. Prikl, Khim., 59(4), 839, (1986)

7) **J.D. Mackenzie, W.K. Murphy:** J. Chem. Phys., 33(2), 366, (1960)

8) **A.J. Easteal, C.A. Angell:** J. Phys. Chem., 74(22), 3987,(1970)

9) **I.A. Kirilenko:** Zh. Neorg. Khim., 32(4), 1047, (1987)

10) **P.M. Stokes:** M.Phil. Transfer Report, Imperial College, (1987)

11) **W. Sundermeyer:** Pure Appl. Chem., 13(1-2), 93, (1966)

12) **D. Inman, A.D. Graves, R.S. Sethi:** "Electrochemistry - Vol 1", Specialist Periodical Reports: Chemical Society, London, p.190, (1970)

13) **J. Jordan, W.B. McCarthy, P.G. Zambonin:** "Molten Salts - Characterization and Analysis" ed. G. Mamantov, (Dekker, 1969)

14) **R.G. Pearson:** J.A.C.S., 85, 3533, (1963)

15) **S.N. Flengas, A.S. Kucharski:** Can. J. Chem., 49, 3971, (1971)

16) **D. Inman, D.G. Lovering:** "Comp. Treat. Electrochem., vol 7", ed. B. Conway et al p.593, (1983), Plenum

17) "Comprehensive Inorganic Chemistry": ed. J.C. Bailar et al., p.212, (1973)

18) Powder Diffraction File - Inorganic Phases: J.C.P.D.S., (1984)

19) **J. Brynestad, H.L. Yakel:** Inorg. Chem., 17(5), 1376, (1978)

20) **H.L. Yakel, J. Brynestad:** Inorg. Chem., 17(11), 3291, (1978)

21) **C.A. Angell, J. Wong:** J. Chem. Phys., 53(5), 2053, (1970)

22) **J.K. Wilmshurst:** J. Chem. Phys., 39(7), 1779, (1963)

23) **C.A. Angell, J. Wong, W.F. Edgell:** J. Chem. Phys., 51(10), 4519, (1969)

24) **D.E. Irish, T.F. Young:** J. Chem. Phys., 43(5), 1765, (1965)

25) **D.E. Irish, B. McCarroll, T.F. Young:** J. Chem. Phys., 39(12), 3436 (1963)

26) **R.B. Ellis:** J. Electrochem. Soc., 113(5), 485, (1966)

27) **J.R. Moyer, J.C. Evans, G. Y-S Lo:** J. Electrochem. Soc., 113 (2), 158, (1966)

28) **M. Itoh, K. Sakai, T. Nakamura:** Inorg. Chem., 21, 3552, (1982)

29) **R. Triolo, A.H. Narten:** J. Chem. Phys., 74 (1), 703, (1981)

30) **Y. Takagi, T. Nakamura:** J. Chem. Soc., Faraday Trans. 1, 81, 1901, (1985)

31) **M.V. Susic, S.V. Mentus:** J. Chem. Phys., 62(2), 744, (1975)

32) **S. Biggin, J.E. Enderby:** J. Phys., C: Solid State Phys., 14, 3129, (1981)

33) **J.E. Enderby:** "Molten Salt Chemistry" eds. G. Mamantov, R. Marassi, NATO ASI Series C, p.8 (1987)

34) **L.V. Woodcock, C.A. Angell, P. Cheeseman:** J. Chem. Phys., 65, 1565, (1976)

35) **P.J. Gardner, D.M. Heyes:** Physica, 131B, 227, (1985)

36) **P. Ballone, G. Pastore, J.S. Thakur, M.P. Tosi:** Physica, 142B, 294, (1986)

37) **G.J. Janz, R.P.T. Tomkins et al:** J. Phys. Chem. Ref. Data, 4 (4), 871, (1975)

38) **T. Ejima, T. Yoko, G. Sato, Y. Kato:** Nippon Kinzoko Gakkaishi, 43(10), 929, 1978

39) **T. Ejima, T. Yoko, K. Nakashima:** Nippon Kinzoko Gakkasishi, 41(1), 86, (1977)

40) **T. Yoko, R. Crescent, Y. Tsukagoshi, T. Ejima:** Nippon Kinzoko Gakkaishi, 42(12), 1179, (1978)

41) **F.R. Duke, R.A. Fleming:** J. Electrochem. Soc., 104(4), 251, (1957)

42) **H. Bloom, I.A. Weeks:** Trans. Faraday Soc., 67, 1410, (1971)

43) **Y. Takagi, K. Sakai, T. Nakamura:** Rep. Res. Lab. Eng. Mat., Tokyo Inst. Tech., 11, 103, (1986)

44) **Y. Takagi, H. Hayashi, T. Nakamura:** Rep. Res. Lab. Eng. Mat., Tokyo Inst. Tech., 8, 73, (1983)

45) **L.F. Grantham, S.J. Yosim:** J. Chem. Phys., 45(4), 1192, (1966)

46) **H. Bloom, I.A. Weeks:** J. Chem. Soc. (A), 2028, (1969)

47) **H. Bloom, I.A. Weeks:** Trans. Faraday Soc., 67, 1416, (1971)

48) **H. Bloom, E. Heymann:** Proc. Royal Soc. (London), A188, 392, (1946)

49) **G.J. Gruber, T.A. Litovitz:** J. Chem. Phys., 40(1), 13, (1964)

50) **A.J. Easteal, C.A. Angell:** J. Chem. Phys., 56(8), 4231, (1972)

51) **H. Bloom, I.A. Weeks:** Trans. Faraday Soc., 67, 1420, (1971)

52) **F.J. Keneshea, D. Cubicciotti:** J. Chem. Phys., 40(1), 191, (1964)

53) **D.W. Rice, N.W. Gregory:** J. Phys. Chem., 72(13), 4524, (1968)

54) **H. Bloom, T.H. Spurling, J. Wong:** Aust. J. Chem., 23, 501, (1970)

55) **L. Topor:** Revue Roumaine de Chimie, 17(9), 1503, (1972)

56) "Phase Diagrams for Ceramists", American Chem. Soc.

57) **G.S. Perry, S.J. Shaw:** (1) Proc. M.S.D.G., Imperial College, (1987) (2) A.W.R.E., report no O 17/87

58) **L.G. MacDonald, G.S. Perry, J.R. Smith, S.D. Wilcox:** Thermochim. Acta, 97, 29, (1986)

59) **E.A. Ukshe, V.N. Devyatkin:** Russ. J. Phys. Chem., 39(9), 1222, (1965)

60) **V.N. Devyatkin, E.A. Ukshe:** Russ. Met., 3, 42, (1966)

61) **A.L. Novozhilov, V.N. Devyatkin, E.I. Gribova:** Russ. J. Phys. Chem., 46(9), 1398, (1972)

62) **A.L. Novozhilov, V.N. Devyatkin, E.I. Gribova:** Russ. J. Phys. Chem., 46(7), 1066, (1972)

63) **P.E. Field:** "Adv. in Molten Salt Chem. III", eds. J. Braunstein. G. Mamantov, G.P. Smith, p.89, (1971)

64) **A.L. Novozhilov, E.I. Gribova, V.N. Devyatkin:** Russ. J. Inorg. Chem., 17(9), 1345, (1972)

65) **J.D. Van Norman, R.J. Tivers:** J. Electrochem. Soc., 118, 259, (1971)

66) **N.Q. Minh, B.J. Welch:** Aust. J. Chem., 28, 965, (1975)

67) **E.A. Ukshe, V.N. Devyatkin:** Russ. J. Phys. Chem., 39, 1641, (1965)

68) **V.G. Ryabov, A.B. Solomonov:** Zh. Prikl. Khim., 54(8), 1821, (1981)

69) **Y.G. Prasolov, L.P. Kostin, A.N. Ketov:** Izv. Vyssh. Ucheb. Zareb., Khim., Khim Tekhnol., 17, 162, (1964), (A.W.R.E. Translation)

70) **N.Q. Minh, B.J. Welch:** J. Electroanal. Chem., 92, 179, (1978)

71) **P.F. Claes, C.R. Coppe, L.A. Simonis, J.E. Glibert:** J. Chem. Eng. Data, 32, 70, (1987)

72) **R. Combes:** "Ionic Liquids" eds. D. Inman, D.G. Lovering, p.305, (1981), Plenum.

73) **W.J. Burkhard, J.D. Corbett:** J.A.C.S., 79, 6361, (1957)

74) **H.A. Laitinen, W.S. Ferguson, R.A. Osteryoung:** J. Electrochem. Soc., 104, 516, (1957)

75) **D.L. Maricle, D.N. Hume:** J. Electrochem. Soc., 107, 354, (1960)

76) **A.L. Novozhilov, E.I. Gribova, V.N. Devyatkin:** Russ. J. Inorg. Chem., 17(8), 1081, (1972)

77) **E.P. Mignonsin, G. Duyckaerts:** Anal. Chim. Acta, 47, 71, (1969)

78) **A.L. Novozhilov, E.I. Pchelina:** Russ. J. Inorg. Chem., 22(4), 494, (1977)

79) **A.L. Novozhilov, E.I. Pchelina:** Russ. J. Inorg. Chem., 22(4), 1115, (1977)

80) **J.D. Van Norman, R.J. Tivers:** "Molten Salts - Characterization and Analysis" ed. G. Mamantov, p.509, (1969), Dekker

81) **N.Q. Minh, B.J. Welch:** Aust. J. Chem., 28, 2579, (1975)

82) **Y. Kanzaki, M. Takahashi:** J. Electroanal. Chem., 58, 349, (1975)

83) **G.S. Perry, L.G. MacDonald:** J. Electroanal. Chem., 144, 251, (1983)

84) "Ionic Liquids", eds. D. Inman, D.G. Lovering, Plenum (1981)

85) **F. Clews, H. Thompson:** J. Chem. Soc., 1442, (1922)

86) **J.A. Duffy, M.D. Ingram:** "Ionic Liquids" eds. D. Inman, D.G. Lovering, p.127, (1981), Plenum

87) **G. Delarue:** J. Electroanal. Chem., 1, 13, (1959)

88) **C.A. Melendres, J.P. Ackerman, R.K. Steunenberg:** Proc. Int. Symp. Molten Salts, p.575, (1976)

89) **R. Lysy, R. Combes:** J. Electroanal. Chem., 83, 287, (1977)

90) **I. Uchida, H.A. Laitinen:** J. Electrochem. Soc., 123(6), 829, (1976)

91) **H.A. Laitinen, Y. Yamamura, I. Uchida:** J. Electrochem. Soc., 125(9), 1450, (1978)

92) **S.H. White, U.M. Twardoch:** Electrochim. Acta, 32(1), 191, (1987)

93) **R. Combes, J. Vedel, B. Tremillon:** C.R. Acad. Sc. Paris, t. 275, Serie-C, 199, (1972)

94) **R. Combes, J. Vedel, B. Tremillon:** Electrochim. Acta, 20, 191, (1975)

95) **R. Combes, M.N. Levelut, B. Tremillon:** Electrochim. Acta, 23, 1291, (1978)

96) **R. Combes, B. Tremillon, D. de Andrade, M. Lopes, H. Ferreira:** Anal. Lett., 15(A20), 1585, (1982)

97) **R. Littlewood, E.J. Argent:** Electrochim. Acta, 4, 114, (1961)

98) **H.C. Brookes, D. Inman:** J. Electrochem. Soc., 135(2), 373, (1988)

99) **S. Sahami, R.A. Osteryoung:** Anal. Chem., 55, 1970, (1983)

100) **B. Tremillon, A. Bermond, R.J. Molina:** J. Electroanal. Chem., 74, 53, (1976)

101) **Y. Ito, H. Kotohda, J. Vuhida, S. Yoshizawa:** Nippon Kagaku Kaishi, 6, 1034, (1982)

102) **L.E. Gorre, R.C. Pastor:** Mat. Res. Bull., 18, 1391, (1983)

103) **S. Biggin, J.E. Enderby:** J. Phys. Chem., 88, 3637, (1984)

104) **J.D. Van Norman, J.S. Bookless, J.J. Egan:** J. Phys. Chem., 70, 1276, (1966)

105) **M.M. Vetyukov, A. Fransis:** Elektrokhimiya, 5(3), 362, (1969)

106) **G.G. Bombi, G.A. Sacchetto, M. Fiorani:** Chem. Comm., 563, (1966)

107) **H.A. Laitinen, C.H. Liu, W.S. Ferguson:** Anal. Chem., 30(7), 1266, (1958)

108) **M. Taoumi, J. Bouteillon, M.J. Barbier:** Electrochim. Acta, 31(7), 837, (1986)

109) **J.K. Koziol, D.R. Sadoway:** Energy Red. Tech. in Metal Electrochem. Processes, p.433, (Feb. 1985, NY)

110) **S.V. Mentus, M.V. Susic:** J. Serb. Chem. Soc., 50 (11-12), 563, (1985)

111) **G. Rubel, M. Gross:** Corr. Science, 15, 261, (1975)

112) **H.E. Bartlett, P. Crowther:** Electrochim. Acta, 15, 681, (1970)

113) **C.A. Angell, D.M. Gruen:** J. Inorg. Nucl. Chem., 29, 2243, (1967)

114) **D.M. Gruen, R.L. McBeth:** Pure Appl. Chem., 6, 23, (1963)

115) **H.A. Oye, D.M. Gruen:** Inorg. Chem., 3, 836, (1964)

116) **C.A. Angell, D.M. Gruen:** J. Phys. Chem., 70 1601, (1966)

117) **W.E. Smith, J. Brynestad, G.P. Smith:**
(1) J.A.C.S., 89(23), 5983, (1967)
(2) J. Chem. Phys., 52, 3890, (1970)

118) **G.P. Smith, C.R. Boston, J. Brynestad:** J. Chem. Phys., 45(3), 829, (1966)

119) **J. Brynestad, C.R. Boston, G.P. Smith:** J. Chem. Phys., 47(9), 3179, (1967)

120) **J. Brynestad, G.P. Smith:** J. Chem. Phys., 47(9), 3190, (1967)

121) **C. Mazanek, G. Radjiejowska:** Proc. III Int. Conf. on Molten Salt Chem., (Wroclaw, Poland), p.226, (1979)

122) **G.M. Begun, J. Brynestad, K.W. Fung, G. Mamantov:** Inorg. Chem. Nucl. Lett., 8, 79, (1972)

123) **J.A. Duffy, G.L. Wood:** J. Chem. Soc., Faraday Trans., 1, 81, 265, (1985)

124) **J.A. Duffy, G.L. Wood:** J. Chem. Soc., Dalton Trans., 1485, (1987)

125) **M.L. Deanhardt, K.W. Hanck:**
(1) Ph.D. Thesis, N.C. State University, (1975)
(2) J. Electrochem. Soc., 122, 1627, (1975)
(3) Diss. Abstr. Int., 37, 179-B, (1976)

126) **L.E. Topol, W.A. McCollum, S.J. Yosim:** Final Report N.A.S.A. CR-72791, North American Rockwell Corp., Canoga Park, Calif., (1970)

127) **M. Matsunaga, K. Hosokawa:** Rep. Asahi Glass Found. Ind. Technol., 41, 255, (1982)

128) **N.J. Bjerrum, C.R. Boston, G.P. Smith:** Inorg. Chem., 6(6), 1162. (1967)

129) **N.J. Bjerrum, G.P. Smith:** Inorg. Chem., 6(11), 1968, (1967)

130) **R.E. Andresen, T. Ostvold, H.A. Oye:** Proc. Int. Symp. Molten Salts ed. J. Braunstein et al., p.111, (1976)

131) **A. Bjorgum, M. Eie, G.M. Haarberg, K.S. Osen, R. Tunold:** Poster Presentation, Euchem Conf., (1986), Geiranger, Norway

132) **U. Erikson, G.M. Haarberg, K.S. Osen, R. Tunold:** Poster Presentation, Euchem Conf., (1988), St. Andrews, U.K.

133) **J. Stenzel, W. Sundermeyer:** Chem. Ber., 100(10), 3368, (1967)

134) **W. Lutz, W. Sundermeyer, W. Towae:** Z. Anorg. Allg. Chem., 444, 21, (1978)

135) **H.J. Klockner, W. Sundermeyer:** Z. Anorg. Allg. Chem., 509, 76, (1984)

136) "Electrochemical Methods, Fundamentals and Applications"; A.J. Bard, L.R. Faulkner, Wiley, (1980)

137) "Techniques of Chemistry, Vol 1; Physical Methods of Chemistry, Part IIA: Electrochemical Methods"; eds. A. Weissberger and B.W. Rossiter, Wiley-Interscience, (1971)

138) **R.H. Wopschall, I. Shain:** Anal. Chem., 39(13), 1514, (1967)

139) **S.C. Levy, F.W. Reinhardt:** J. Electrochem. Soc., 122, 200, (1975)

140) **J.C. Poignet, M.J. Barbier:** Electrochim. Acta, 17(7), 1227, (1972)

141) **J.C.M. Li, P. Chang:** J. Chem. Phys., 23, 518, (1955)

142) "Handbook of Chemistry and Physics", editor R.C. Weast, C.R.C. Press, (1974-75)

143) **R.A. Osteryoung:** "Molten Salt Chemistry", eds, G. Mamantov and R. Marassi, N.A.T.O., A.S.I. Series C, p.341, (1987)

144) **S.H. White:** "Ionic Liquids" eds. D. Inman, D.G. Lovering, p.185, (1981), Plenum

145) **H. Monk, D.J. Fray:** Trans. Instn. Min. Metall. (Sect. C: Mineral Process Extr. Metall.) 82, 161, (1973)

146) **H. Monk, D.J. Fray:** Trans. Instn. Min. Metall. (Sect. C: Mineral Process Extr. Metall.), 82, 240, (1973)

147) **H. Monk, D.J. Fray:** Trans. Instn. Min. Metall. (Sect. C: Mineral Process Extr. Metall.), 83, 118, (1974)

148) **J.P. Hager, J.F. Lemons:** Recycle and Secondary Recovery of Metal - Int. Symp. Fort Lauderdale, p.203, (Dec. 1985).

149) **A.K. Abdul-Sada, A.G. Avent, M.J. Parkington, T.A. Ryan, K.R. Seddon, T. Welton:** J. Chem. Soc., Chem. Commun., 1643, (1987)

150) **K. Holder:** Private communication, (1987)

151) **D. Quitmann:** Private communication, (1988)

152) **K.R. Seddon:** Private communication, (1988)

153) **G.S. Perry, L.G. MacDonald, S.D. Wilcox:** A.W.R.E, H.C.T.D. Technical Memorandum, No 3/84, (1984)

154) **P.G. Dudley:** D.I.C. Thesis, Imperial College, London (1979)

155) Smithells Metal Refernce Book 6th edn; ed. E.A. Brandes, Butterworths, London, (1983)

156) **F.L. Galeener, J.C. Mikkelsen, A.C. Wright, R.N. Sinclair, J.A.E. Desa, J. Wong:** J. Non-Cryst. Solids, 42, 23, (1980)

157) **F. Aliotta, G. Maisano, P. Migliardo, C. Vasi, F. Wanderlingh, G. Pedro Smith, R. Triolo:** J. Chem. Phys., 75(2), 613, (1981)

158) **M.L. Cacciola, S. Magazu, P. Migliardo, F. Aliotta, C. Vasi:** Solid State Comm., 57(7), 513, (1986)

159) **H. Kanno, J. Hiraishi:** J. Raman Spec., 9(2), 85, (1980)

160) **D.W. James, R.M. Parry, W.H. Leong:** J. Raman Spec., 7(2), 71, (1978)

161) **A.L. Bortnichuk, N.A. Bushuev, N.N. Kornilova, A.D. Stepukhovich:** Russ. J. Inorg. Chem., 24(2), 157, (1979)

162) **M.P. Fontana, G. Maisano, P. Migliardo, F. Wanderlingh:** J. Chem. Phys., 69(2), 676, (1978)

163) **M.L. Brooker:** Private communication (1988)

164) "Infra-red and Raman Spectra of Inorganic and Co-ordination Compounds - 4th Edition", K. Nakamoto, (1986), Wiley

165) **E.A. Vinogradov, N.N. Mel'nik, A.E. Tsurkan, L.V. Kicherman:** Russ. J. Phys. Chem., 26, 764, (1977)

166) **C.A. Arguello, D.L. Rousseau, S.P.S. Porto:** Phys. Rev., 181 (3), 1351, (1969)

167) B.O.C. Technical Services Dept., Private communication, (1988)

168) **B.A. Goodman, J.B. Raynor:** Adv. Inorg. Chem. Radiochem., 13, 135, (1970)

169) **A. Chatelain, R.A. Weeks:** J. Chem. Phys., 52(7), 3758, (1970)

170) **S. Zecchin, G. Schiavon, G.G. Bombi:** J. Electroanal. Chem., 50, 261, (1974)

171) **D.R. Flinn, K.H. Stern:** J. Electroanal. Chem., 63, 39, (1975)

172) **E.P. Mignonsin, L. Martinot, G. Duyckaerts:** Inorg. Nucl. Chem. Lett, 3, 511, (1967)

173) **A.A. El Hosary, D.H. Kerridge, A.M. Shams El Din:** "Ionic Liquids" ed. D. Inman, D.G. Lovering, p.339, (1981), Plenum

174) **C. Gabrielli:** "Identification of Electrochemical Processes by Frequency Response Analysis", Technical Report no. 004/83. Solartron Instruments Publishers, (1984)

175) **B.R. Hubble:**
(1) Ph.D. Thesis, Kansas State University (1971)
(2) Diss. Abstr. Int. B, 32(6), 3283, (1971)

176) **H.A. Laitinen, R.A. Osteryoung:** J. Electrochem. Soc., 102(10), 598, (1955)

177) **L.S. Leonova, E.A. Ukshe, N.G. Bukun:** Elektrokhimiya, 6(2), 249, (1970)

178) **R. Yu. Bek, A.S. Lifshits:** Izv. Sibirsk. Otd. Akad. Nauk. SSSR, Ser. Khim. Nauk, 6, 120, (1969)

179) **D. Lelievre, A. de Guibert, V. Plichon:** Electrochim. Acta, 24, 1243, (1979)

180) **D.M. Ferry, G.S. Picard, B.L. Tremillon:** Proc. Electrochem. Soc. (1987), 87-7 (Proc. It. Int. Symp. Molten Salts), p.517-26

181) **W.I. Archer, R.D. Armstrong:** Specialist Periodical Report, The Chemical Society, London. Electrochemistry 7, 157, (1980)

182) **A.D. Graves, D. Inman:** J. Electroanal. Chem., 25, 357, (1970)

183) **P. Pang, P.J. Gardner:** Unpublished Results (1984)

184) **A. Komura, H. Imanaga, N. Watanabe:** Denki Kagaku, 10, 762, (1972)

185) **N.S. Wrench, D. Inman:** J. Electroanal. Chem., 17, 319, (1968)

186) **Y. Kanzaki, M. Takahashi:** J. Electroanal. Chem., 58, 339, (1975)

187) **I. Uchida, H.A. Laitinen:** Proc. First Int. Symp. Molten Salt Chem. Tech. (Kyoto), I-208, p.219, (1983)

188) **D.L. Manning, G. Mamantov:** J. Electrochem. Soc., 124, 480, (1977)

189) **R. Combes, R. Feys, B. Tremillon:** J. Electroanal. Chem., 83, 383, (1977)

190) **A. Borodzinski, A. Sokolowski, L. Suski:** J. Chem. Thermodynamics, 7, 655, (1975)

191) **V.F. Boiko:** Obshch. Prikl. Khim, 3, 58, (1970)

192) **Y. Ito, H. Kikuchi, K. Togashi:** Jpn. Kokai Tokkyo Koho, JP 62 65908 (Cl. C01 B15/04) (March 1987)

193) **G. Delarue:** J. Electroanal. Chem., 1, 285, (1959)

194) **I. Suzuki, S. Wada:** Corr. Science, 27(5), 475, (1987)

195) **H.R. Oswald, W. Feitknecht:** Helv. Chim. Acta, 44, 847, (1961)

196) **O.K. Srivastava, E.A. Secco:** Can. J. Chem., 45, 579, (1967)

197) **J.W. Hoffman, I. Lauder:** Aust. J. Chem., 21, 1439, (1968)

198) **O. Garcia Martinez, J. Cano Ruiz:** An. Fis. Quim., 63-B, 325, (1967)

199) **H. Linga, Z. Stojek, R.A. Osteryoung:** J.A.C.S., 103, 3754, (1981)

200) **T.M. Laher, L.E. McCurry, G. Mamantov:** Anal. Chem., 57, 500, (1985)

201) **M.A. Einarsrud:** Ph.D. Thesis, University of Trondheim (1987)

202) **A. Godo:** Poster Presentation, Euchem Conf. (1988), St. Andrews, UK

203) **D.H. Kerridge, I.A. Sturton:** Inorg. Chim. Acta, 8, 27 (1974)

204) **H. Bloom:** "Chemistry of Molten Salts", p.105, (1967), publ. W.A. Benjamin Inc.

205) **C.R. Boston:** "Adv. Molten Salt Chem. Vol.1", ed. J. Braunstein, G. Mamantov, G.P. Smith, p.151, (1971), Plenum

APPENDIX 1

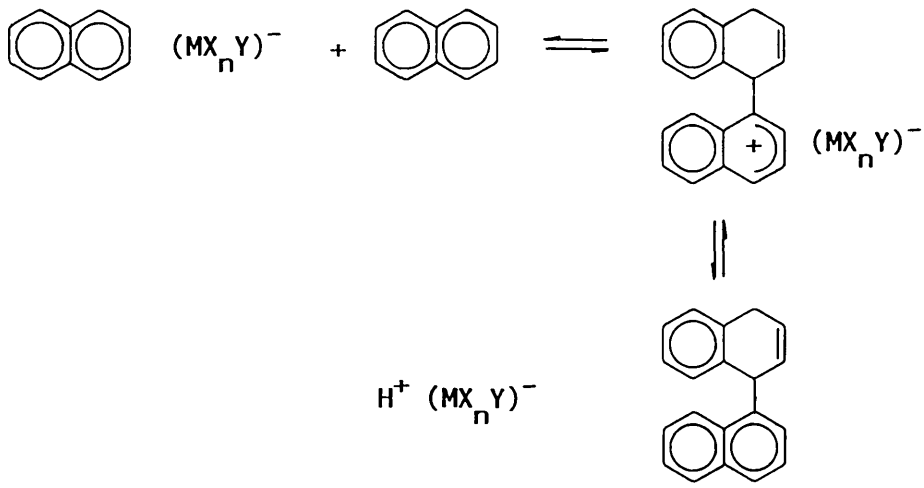
METAL HALIDES IN THE HYDROCRACKING PROCESS

A1.1 General

The use of various metal halides as catalysts for the hydrocracking of polynuclear hydrocarbons had been initiated before World War II but it was not until the 1960's that detailed, large scale investigations of their properties began. The key discovery was that molten metal halides that are relatively weak Lewis acids are much more active and selective in hydrocracking processes than conventional sulphur-resistant catalysts, but the metal halides must be used in large amounts. Since that time much work has been done on perfecting the hydrocracking process, with a wide range of metal halides being tested.

Tin (II) chloride and nickel chloride[1] were found to behave as very weak Friedel-Crafts type catalysts with very little cracking activity compared to zinc chloride. Neither are well known as active Lewis acids, although $SnCl_2$ does have electron-accepting properties (e.g. $SnCl_2.NH_3$). Aluminium bromide was rejected by Gorin et al.[1,2] since it was destroyed by the steam produced, and the products included a large amount of tar and low molecular weight paraffins. Buchanan et al.[3] have outlined work done with $SbCl_3$ and $SbCl_3$-$AlCl_3$ mixtures as catalysts, considering both the Friedel-Crafts behaviour and the redox properties of the $SbCl_3$. Under aprotic low-temperature reaction conditions the redox properties of $SbCl_3$ are believed to play a key role in the catalytic process, the effect of the $AlCl_3$ being to enhance the oxidizing power of the $SbCl_3$ in addition to increasing the Lewis acidity.

Work by Salim and Bell[4] indicated that whereas $AlCl_3$ is significantly more active in promoting the hydrogenation and cracking of fused-ring aromatic structures than $ZnCl_2$, it also promotes extensive tar formation via Scholl condensation, as seen overleaf for napthalene:



Of the halides tested $ZnCl_2$ was considered as the best catalyst. It is sufficiently active to readily hydrocrack polynuclear aromatic compounds, but will not crack single-ring aromatics. $ZnCl_2$ hydrocracking also produces a fairly high ratio of iso-to-normal paraffins, indicating that the $ZnCl_2$ is acting as a catalyst, and not merely facilitating good gas-liquid or gas-solid contact.

A1.2 Zinc chloride hydrocracking process

The process consists of two main steps. The first step is the hydrocracking of the polyaromatic hydrocarbon, conducted in a pool of molten $ZnCl_2$ with typical conditions being temperatures of 413-427^{o}C and pressures of 17.3 MPa[5]. The amount of zinc chloride used is high - $ZnCl_2$: coal feed ratios of 1.0 are the usual values.

The second stage is the catalyst regeneration[6,7]. The spent melt is contaminated with hydrocarbonaceous residue, coal ash and sulphur (ZnS), oxygen (ZnO) and nitrogen ($ZnCl_2.NH_3$) impurities, which do not settle out of the molten catalyst. Regeneration is carried out in a fluidized-bed combustor, the $ZnCl_2$ being vaporized, and impurities converted to N_2, CO_2, H_2O and SO_2 at temperatures of around 930^{o}C and pressures of 0.1-0.5 MPa.

A1.3 Process chemistry

The feed coal is rich in hetero-atoms[2]: 1.5% N, 5-8% O and 1.1-2.2% S, and during the hydrocracking process the $ZnCl_2$ is partially

consumed by its interaction with these, which are released from the coal substrate as NH_3, H_2O and H_2S. The following reactions then occur:

$$ZnCl_2 + H_2S = ZnS + 2HCl \qquad [A1.1]$$

$$ZnCl_2 + NH_3 = ZnCl_2.NH_3 \qquad [A1.2]$$

$$ZnCl_2 + H_2O = ZnO + 2HCl \qquad [A1.3]$$

The ammonia complex formed in [A1.2] can react with the HCl produced to form a double salt, as in equation [A1.4], the extent of reaction depending on the relative amounts of sulphur, oxygen and nitrogen present.

$$ZnCl_2.\ NH_3 + HCl = ZnCl_2.NH_4Cl \qquad [A1.4]$$

Equilibrium data for [A1.1] and [A1.2] predict nearly quantitative absorption of NH_3 and H_2S, and this has been shown experimentally to occur. However, $ZnCl_2$ is quite resistant to hydrolysis at high temperatures[5] and reaction [A1.3] will not proceed to completion. Addition of small amounts of ZnO prevents the formation of NH_4Cl by absorbing the HCl produced in [A1.1] by reversal of [A1.3], but in large amounts ZnO has a marked inhibiting effect[2]. As with more conventional cracking catalysts NH_3 tends to deactivate the cracking activity of $ZnCl_2$, but this effect is minimised by the use of massive amounts of the catalyst.

In the regeneration process zinc sulphide is roasted to zinc oxide, the HCl added to the feed air causing reversal of [A1.3] to yield zinc chloride. The ammonia complex is oxidised giving H_2O and N_2.

The main reactions are:

$$ZnS + 3/2\ O_2 \rightarrow ZnO + SO_2 \qquad [A1.5]$$

$$ZnO + 2HCl \rightarrow ZnCl_2 + H_2O \qquad [A1.6]$$

$$ZnCl_2.NH_4Cl \rightarrow ZnCl_2.NH_3 + HCl \qquad [A1.7]$$

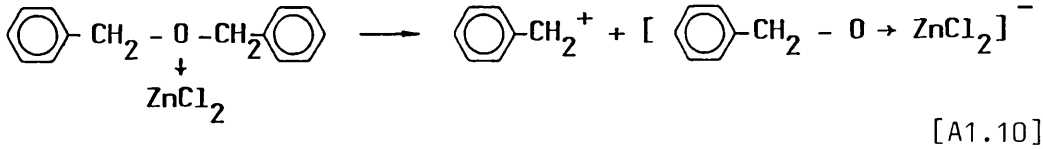
$$2ZnCl_2.NH_3 + 3/2\ O_2 \rightarrow 2ZnCl_2 + N_2 + 3H_2O \qquad [A1.8]$$

$$CH_x + (1 + x/4)O_2 \rightarrow CO_2 + x/2\ H_2O \qquad [A1.9]$$

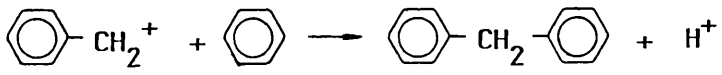
To conduct the regeneration adiabatically the heats of combustion of the organic NH_3 and ZnS impurities in the spent melt must be large enough to vaporize the melt and to achieve the desired bed temperature of around 930^oC.

A1.4 Structure of the active catalyst and mechanistic considerations

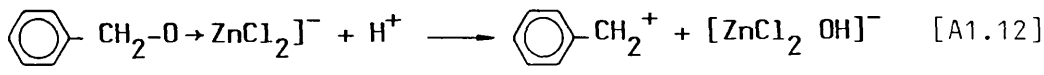
The mechanism by which molten Lewis acids, such as $ZnCl_2$, promote or catalyse the hydrocracking of polynuclear hydrocarbons is not well understood, despite much work to determine the reaction path. Using model compounds containing oxygen[8], sulphur[9], and aliphatic-aromatic[10] linkages like those found in oil and coal, workers have attempted to distinguish which of a few possible routes is operating. One possibility is that $ZnCl_2$ is acting as a classic Friedel-Crafts Lewis acid, and initiating the reaction through the formation and subsequent decomposition of an adduct between $ZnCl_2$ and hetero-atoms in the feed present as oxygen or sulphur linkages, the $ZnCl_2$ acting as an electron acceptor. The example reaction pathway below indicates the manner in which this would occur:



[A1.10]



[A1.11]



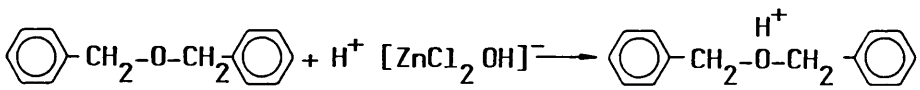
[A1.12]

$$[ZnCl_2OH]^- + H^+ \rightarrow H_2O + ZnCl_2 \qquad [A1.13]$$

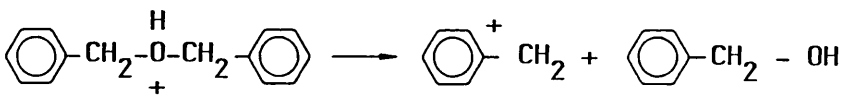
The benzyl carbonium ion, formed by the decomposition of the addition product formed between $ZnCl_2$ and dibenzyl ether, attacks an aromatic centre to yield the benzylation product. The remaining fragment of the addition product proceeds to form a second carbonium ion (reaction [A1.12]) and finally the catalyst is regenerated in reaction [A1.13].

The second mechanism similarly relies upon the formation of a carbonium ion, but now by a different route. A popular view is that Lewis acids become active catalysts when converted to their Bronsted acid form, a conversion thought to occur via a reaction of the Lewis acid with hydrogen halide or water, the latter often being present in $ZnCl_2$ as an impurity due to the hygroscopic nature of $ZnCl_2$. The protonic acids so formed would be $H^+[ZnCl_3]^-$ and $H^+[ZnCl_2OH]^-$ respectively, although the $(H^+)_2[ZnCl_2(OH)_2]^{2-}$ entity has also been postulated[5]. The mechanism here, using the earlier example compounds, involves protonation of the ether to form the oxonium ion before it decomposes to the carbonium ion:

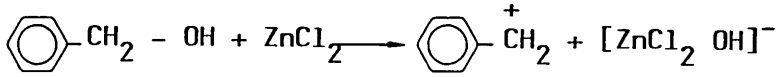
$$ZnCl_2 + H_2O \rightarrow H^+ [ZnCl_2OH]^- \qquad [A1.14]$$



$$+ [ZnCl_2\ OH]^- \qquad [A1.15]$$



[A1.16]



[A1.17]

The alcohol generated by the oxonium ion decomposition forms a second carbonium ion as in reaction [A1.17]. The carbonium ions again form products, by attack on an aromatic centre, as earlier.

It is possible that both mechanisms could operate simultaneously, and as yet there is little evidence to allow distinguishability. The second mechanism could be promoted by the formation of water as a product of the first mechanism, which does not require water as an initiator. The activity of $ZnCl_2$ is enhanced by the presence of water[4]. In Figure A1.1 the conversion route for n-butyl benzene is shown, and it can be seen that hydride ions are required. Two possible sources of hydride ions are either hydride abstraction during the condensation reactions or from molecular hydrogen. In 1979 Mobley and Bell[8] stated that H_2 does not participate, whereas in 1982 Salim and Bell[4] stated that "H_2 is the primary source of hydride ions when $ZnCl_2$ is used as the catalyst".

A third postulated mechanism is that proposed by Greene[5], who suggested that the active species may involve a Zn^{2+}/Zn^{+} redox couple, which sets up a radical-cation mechanism. Stating that the Zn^{+} ion has been observed in molten $ZnCl_2$, he agreed with work by Vetyukov and Fransis[11] who in chronopotentiometric work inferred the existence of Zn_2^{2+} species. Such a $ZnCl_2/ZnCl$ couple is analogous to the Sb^{3+}/Sb^{o} redox couple proposed by Smith et al.[3] in their work on $SbCl_3$.

A1.5 Effect of addition of transition metal and alkali metal chlorides to zinc chloride

The catalytic properties of the transition metals are well known, so it was thought that use of a binary melt of zinc chloride-transition metal chloride might enhance the hydrocracking properties exhibited by pure zinc chloride. Several transition metal chlorides were tested in this role and the results are outlined later (Section A1.5.2).

Similarly, the addition of alkali metal chlorides, with the consequent lowering of the melt viscosity and acidity, coupled with high hydrogen solubility, was expected to be an improvement on the pure zinc chloride.

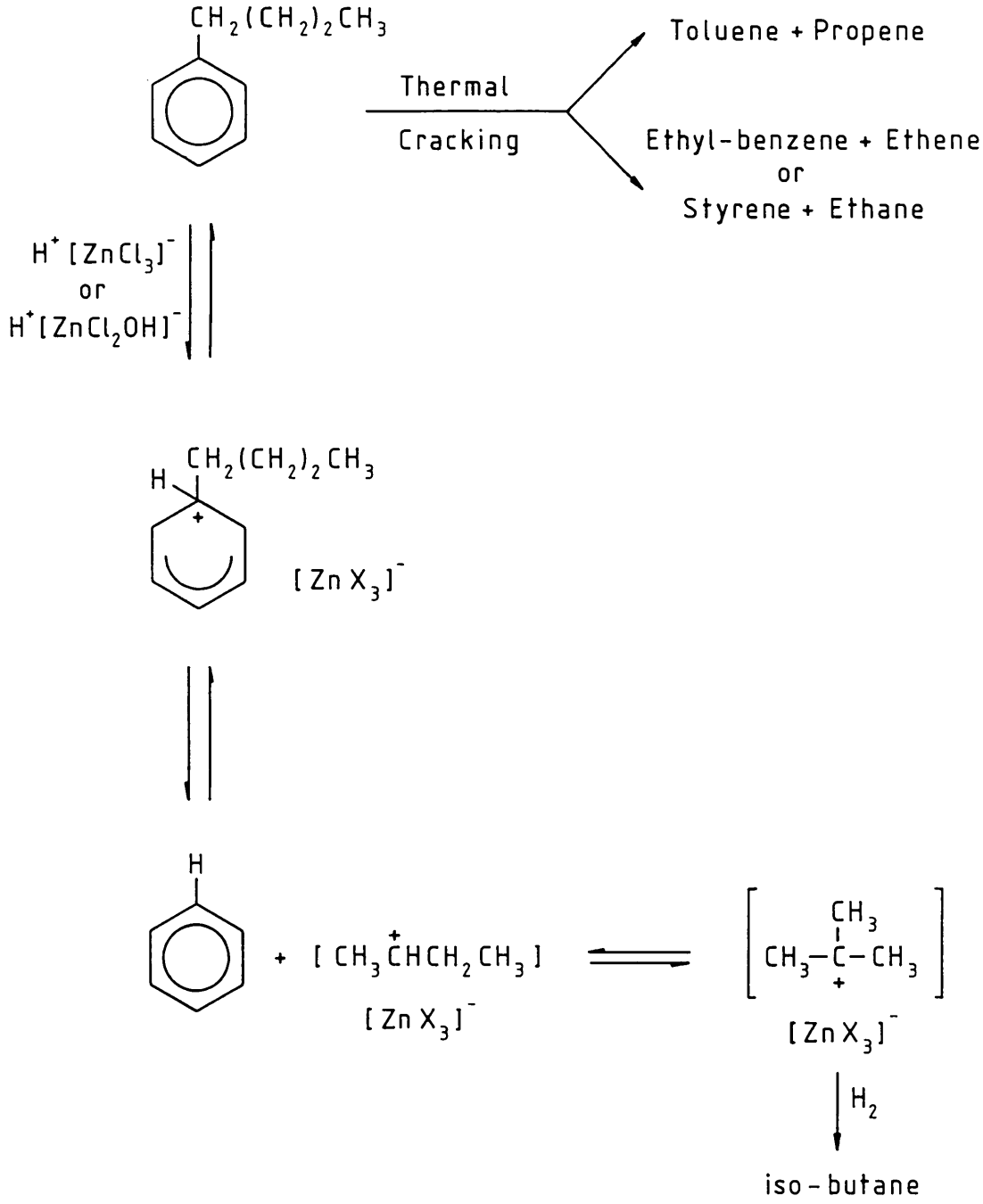


FIGURE A1.1

Conversion of n-butyl Benzene

A1.5.1 Zinc chloride-alkali metal chloride ($ZnCl_2$-MCl) catalysts

Addition of alkali metal halide (often KCl) results in a break-up of the polymeric $ZnCl_2$ melt. Raman spectroscopy (Section 2.1) has indicated that the Cl^- ion from KCl is consumed largely in the depolymerization of $(ZnCl_2)_n$ up to the molar ratio of $ZnCl_2$ to KCl of about 0.2, and the addition of more than 50 mol. % KCl causes predominance of complex ions $[(K^+)_2ZnCl_4^{2-}]$. This lowers the melt viscosity and raises the hydrogen solubility of $ZnCl_2$-KCl to above that of molten $ZnCl_2$. Hydrogen molecules dissolved in $ZnCl_2$-KCl are thought to be more polarized by the ionic character of the melt, and so KCl-containing melts assist more effectively the hydride abstraction of the carbonium ion intermediates derived from hydrocracking.

$ZnCl_2$-KCl melts have a lower Lewis acidity than pure $ZnCl_2$, and although it is difficult to evaluate said quantity, Zielke et al.[1,2] have put forward one scale. The ratio of i-butane/n-butane in the products can represent an approximate acid strength of the catalysts. Values given include:

$ZnCl_2$	(1.5-2.5)	$SnCl_2$	(0.5-0.6)
$ZnCl_2$-$SnCl_2$	(0.7-1.1)	$ZnCl_2$-$SnCl_2$-KCl	(0.3-0.5)
$ZnCl_2$-KCl	(0.6-0.9)	$SnCl_2$-KCl	(0.3-0.4)

It has been suggested[12-16] that the Lewis acidity of the molten salt can play an important role in the catalytic process. Various studies[14-16] have shown that the $ZnCl_2$-KCl system yields a much greater percentage of hexane soluble (HS) and benzene soluble (BS) fractions than pure $ZnCl_2$, and at the same time suppresses gas yield, with consumption of less hydrogen. However, disadvantages of the $ZnCl_2$-KCl system are the incomplete elimination of hetero-atoms from the feedstock and higher molecular weight HS products than those of the $ZnCl_2$ system. Weaker acid strength of the melt decreases both retrogressive reaction of BS to benzene insolubles (BI) and cracking of HS to C_1-C_4 hydrocarbons[14].

A1.5.2 Zinc chloride - transition metal chloride ($ZnCl_2$-ACl_n) catalysts

The addition of transition metal chlorides to zinc chloride to form binary melts was another area investigated in the attempt to enhance the hydrocracking ability of $ZnCl_2$. A lot of work has been carried out in this field using coal and oil, as well as model coal compounds like asphaltene[17] and phenanthrene[12], to determine how the presence of ACl_n might affect the products formed.

When using binary melts all showed superior catalytic activities to pure $ZnCl_2$. Among them the systems with $CrCl_3$, CuCl and $MoCl_5$ showed particularly high activities. The activities of the systems decreased in the order: $MoCl_5$ > CuCl > $CrCl_3$ > $NiCl_2$ > $PdCl_2$ > $CoCl_2$ > $MnCl_2$ > Sn > Cu > $SnCl_2$ > pure $ZnCl_2$, the results being taken for the phenanthrene conversions. By heating them with H_2 and D_2 and measuring the exchange reaction, it was found that the binary salts promoted hydrogen activation but that the order was reversed in that $ZnCl_2$-$PdCl_2$ was the most active. When investigating the acid catalysis the isomerization of cyclohexene was adopted as a standard. The yields of isomerized products increased in the order $ZnCl_2$ < $ZnCl_2$-$CoCl_2$ < $ZnCl_2$-$NiCl_2$ < $ZnCl_2$-CuCl, suggesting that binary melts show superior acid catalysis to pure $ZnCl_2$.

When the amounts of salts were reduced to half that of the coal or model compounds, the activity decreased considerably for the systems with CuCl and $CrCl_3$, whilst that of the $MoCl_5$ system remained high. Nomura et al.[12] suggested that hydrocracking activity is dependent upon the amount of catalyst, similar to pure $ZnCl_2$, but that $MoCl_5$ is, for some reason, anomalous. No explanation of this anomaly was given, but it must be recalled that these ACl_n are good catalysts on their own and may well be acting independently of the $ZnCl_2$.

Similar results were obtained in work on $ZnCl_2$-KCl-NaCl[13] and $ZnCl_2$-KCl-NaCl-ACl_n[17] melts, with the cracking activity increasing with the number of melt components. Again, the $MoCl_5$ system was found to be the most active in tests on various coals.

APPENDIX 1

REFERENCES

1) **C.W. Zielke, R.T. Struck, J.M. Evans, C.P. Costanza, E. Gorin:** I.E.C. Proc. Des. Dev., 5, 151, (1966)

2) **C.W. Zielke, R.T. Struck, J.M. Evans, C.P. Costanza, E. Gorin:** I.E.C. Proc. Des. Dev., 5, 158, (1966)

3) **A.C. Buchanan III, A.S. Dworkin, G.P. Smith, M.V. Buchanan, G. Olerich:** Fuel, 60, 694, (1981)

4) **S.S. Salim, A.T. Bell:** Fuel, 61, 745, (1982)

5) **R.T. Struck, C.W. Zielke:** Fuel, 60, 795, (1981)

6) **C.W. Zielke, R.T. Struck, E. Gorin:** I.E.C. Proc. Des. Dev., 8, 552, (1969)

7) **C.W. Zielke, W.A. Rosenhoover, R.T. Struck:** I.E.C. Proc. Des. Dev., 21, 61, (1982)

8) **D.P. Mobley, A.T. Bell:** Fuel, 58, 661, (1979)

9) **D.P. Mobley, A.T. Bell:** Fuel, 59, 507, (1980)

10) **N.D. Taylor, A.T. Bell:** Fuel, 59, 499, (1980)

11) **M.M. Vetyukov, A. Fransis:** Elektrokhimiya, 5, 362, (1969)

12) **M. Miyake, H. Sakashita, M. Nomura, S. Kikkawa:** Fuel, 61, 124, (1982)

13) **M. Nomura, H. Sakashita, S. Kikkawa:** Tech. Rep. Osaka Univ., 32, 439, (1982)

14) **M. Nomura, T. Yoshida, Z. Morita:** I.E.C. Prod. Res. Dev., 23, 215, (1984)

15) **M. Nomura, M. Nishimura, S. Kikkawa:** J. Japan. Petrol. Inst., 25, 364, (1982)

16) **M. Nomura:** Yoyuen, 27, 165, (1984)

17) **M. Nomura, K. Terao, S. Kikkawa:** Fuel, 60, 699, (1981)